KU LEUVEN

ARENBERG DOCTORAL SCHOOL
Faculty of Engineering Science

# Electric vehicle charging integration in buildings

## Local charging coordination and DC grids

**Juan Van Roy**

Supervisor:
Prof. dr. ir. J. Driesen

Dissertation presented in partial fulfillment of the requirements for the degree of PhD in Engineering Science: Electrical Engineering

May 2015

# Electric vehicle charging integration in buildings

Local charging coordination and DC grids

**Juan VAN ROY**

Examination committee:
Prof. dr. ir. H. Hens, chair
Prof. dr. ir. J. Driesen, supervisor
Prof. dr. ir. G. Deconinck
Prof. dr. ir. D. Saelens
Prof. dr. ir. L. Helsen
Prof. dr. G.J. Schaeffer
(VITO)
Prof. dr. A. Keane
(University College Dublin)

Dissertation presented in partial fulfillment of the requirements for the degree of PhD in Engineering Science: Electrical Engineering

May 2015

# Voorwoord

Ongeveer 5 jaren geleden viel de keuze om te gaan doctoreren, en sindsdien is het een boeiende en plezante periode geweest, met dit boekje als eindresultaat. Tijd om hier enkele mensen te bedanken zonder wie het niet mogelijk zou geweest zijn om dit werk tot een goed einde te brengen.

Eerst en vooral wil ik mijn promotor prof. Johan Driesen bedanken voor de mogelijkheid om dit doctoraatswerk te starten. Via verscheidene projecten rond de integratie van EVs in netten, en projecten rond energie-efficiëntie in gebouwen, heb ik de vrijheid gekregen mijn doctoraatswerk zelfstandig verder uit te diepen en vorm te geven. Bedankt voor de samenwerking en de vele mogelijkheden gedurende de laatste jaren.

Verder bedank ik graag de leden van de begeleidingscommissie en de examencommissie, met name prof. Geert Deconinck, prof. Dirk Saelens, prof. Lieve Helsen, prof. Gerrit Jan Schaeffer en prof. Andrew Keane, en prof. Hugo Hens als voorzitter. Dank voor het nalezen, de kritische evaluatie en de waardevolle suggesties tot het verbeteren van mijn tekst.

Tevens werd dit onderzoek mede mogelijk gemaakt door een tweejarige doctoraatsbeurs van de *Vlaamse Instelling voor Technologisch Onderzoek* (VITO). Dank aan Robbe voor de begeleiding gedurende de voorbije jaren, en voor het nauwgezet nalezen van mijn tekst.

Ook bedankt aan alle Electa-collega's voor de toffe en collegiale sfeer op en naast het werk! De aangename sfeer tijdens de koffiepauzes, Alma-lunches, uitstapjes, IEEE-trips,... zullen me steeds bijblijven. In het bijzonder bedank ik graag Frederik, Niels en Jeroen voor de samenwerking rond al het EV-gerelateerde werk. Ook dank aan Bart, Ruben en Roel voor de samenwerking en om me in te leiden in het Modelica-wereldje. Bedankt aan het Electa-secretariaat voor alle praktische regelingen.

I also would like to thank EIT for financing my two research visits abroad in

Berkeley and Dublin. I would like to thank Michael Wetter and Marco Bonvini for hosting me at *Lawrence Berkeley National Lab*, and Andrew Keane, Peter Richardson and James O'Donnell for hosting me at *University College Dublin*.

Mijn familie dank ik voor hun steun en vertrouwen. Speciale dank aan mijn ouders voor al hun steun de voorbije jaren en alle kansen die ze mij gegeven hebben. Mijn vrienden bedank ik graag voor alle leuke momenten buiten het werkleven.

Tot slot nog een welgemeende dankjewel aan Katrien, voor alle steun en voor alles wat je voor mij gedaan hebt. Dank je om er steevast voor mij te zijn!

Juan Van Roy
Leuven, Mei 2015

# Abstract

Electric vehicle (EV) charging in buildings has a non-negligible impact on the in-building and low-voltage (LV) distribution grid. It is widely accepted that the coordination of EV charging may reduce this grid impact, allowing more EVs to be charged through the power system, without grid infrastructure investments. The literature mainly focuses on (large-scale) optimization coordination for a certain objective (technical and/or economical), which requires a relative high penetration rate of EVs to be beneficial. However, local clustering of EVs in buildings or LV distribution grids might already occur in the near-future, requiring local charging solutions. Therefore, in order to reduce this EV charging grid impact, this dissertation focuses on the following local EV charging solutions:

- Local EV charging strategies (rule-based control) in large buildings (multiple EVs charging), which require minimal local or EV internal knowledge, and minimal or no communication in and outside the building.
- The use of DC grids to connect and charge the EVs in buildings.

The objective is to assess how these solutions can already limit the grid impact, in order to allow a higher penetration rate of EVs and others, such as a heat pumps and PV systems, in the system.

The following local EV charging strategies have been assessed:

- **EV based peak shaving**, which reduces the EV charging power in order to maximally use the available charging time, i.e. load shifting and load reduction.
- **Delayed charging** delays the charging as long as possible.
- **Renewable self-consumption**, i.e. matching local electricity demand and production.

- A **voltage droop mechanism** adapts the EV charging power as a function of the grid voltage.
- A **building peak shaving mechanism** reduces the EV charging power as a function of the total building load.

All local EV charging strategies succeed in their objectives, i.e. reducing the demand and/or injection peak powers, increasing the local self-consumption, and/or reducing the voltage deviations. The results show that these local EV charging strategies, which do not require any optimizations and any communication outside the building, decrease the grid impact and allow to charge more EVs in the building, postponing or avoiding the needs to invest in grid infrastructure reinforcements.

The use of DC grids also reduces the grid impact of EV charging in buildings. The results show that DC grids are primarily interesting regarding the voltage unbalance and voltage deviations in the AC grid. Both the voltage unbalance and voltage deviations are reduced. For the coordination strategies, which anticipate on the local self-consumption maximization, DC grids are a good solution to reduce the energy exchange with the LV distribution grid to which the building is connected.

In order to assess the grid impact of EV charging, two simulation tools have been developed:

- The **mobility behavior simulation tool**, that creates realistic driving profiles for individual vehicles in the fleet, based on available statistical data for mobility behavior in Flanders.
- A **Modelica library for electrical modeling**, which can be used for the integration of different multidisciplinary energy systems in buildings and districts.

# Beknopte samenvatting

Het laden van elektrische voertuigen (EVs) in gebouwen heeft een niet-verwaarloosbare impact op het elektriciteitsnet in het gebouw en het laagspanningsnet. Het wordt algemeen aangenomen dat de laadcoördinatie van EVs deze netimpact kan verlagen, hetgeen toelaat om meer elektrische voertuigen op te laden in hetzelfde net. De literatuur focust voornamelijk op (grootschalige) optimalisatietechnieken voor de coördinatie van het laden van EVs voor een bepaald objectief (technisch en/of economisch). Echter, om voordelen te kunnen bieden, is er een grote vloot van EVs noodzakelijk. Niettemin, verwacht wordt dat in de nabije toekomst reeds een lokale clustering van EVs in gebouwen of laagspanningsnetten kan optreden. Daarom zijn lokale laadoplossingen nodig. Dit proefschrift focust daarom op de volgende lokale laadoplossingen voor EVs:

- Lokale laadstrategieën (rule-based controle) voor EVs in grote gebouwen (waar meerdere EVs opladen). Deze vereisen een minimale kennis van andere lastprofielen, het mobiliteitsgedrag, en lokale of interne kennis van de EV. Er is een minimale tot geen communicatie in en buiten het gebouw.
- Het gebruik van DC-netten voor het connecteren en laden van EVs in gebouwen.

Het doel van dit proefschrift is om na te gaan in hoeverre deze oplossingen de netimpact van EVs reeds kunnen minimaliseren, zodat een hogere penetratiegraad van EVs en andere systemen, zoals warmtepompen en PV-systemen, mogelijk wordt.

De volgende lokale laadstrategieën voor EVs worden besproken:

- ***EV based peak shaving*** reduceert het laadvermogen, opdat de maximaal mogelijke laadtijd benut wordt (verschuiven en reduceren van de belasting).

- ***Delayed charging*** stelt het laden zolang mogelijk uit.
- **Zelfconsumptie van hernieuwbare energie**, oftewel het matchen van de lokale elektriciteitsvraag en -productie.
- Een ***voltage droop*** **mechanisme** past het laadvermogen aan in functie van de netspanning.
- Een ***peak shaving*** **mechanisme op gebouwniveau** past het laadvermogen aan in functie van de totale gebouwbelasting.

Alle lokale laadstrategieën voor EVs slagen in hun objectieven, namelijk het reduceren van de vraag- en/of injectiepiekvermogens, het verhogen van de lokale zelfconsumptie, en/of het reduceren van spanningsafwijkingen. De resultaten tonen aan dat deze lokale laadstrategieën, die geen optimalisaties en communicatie buiten het gebouw vereisen, de netimpact verlagen. Dit laat toe om meer EVs op te laden in het gebouw, waardoor mogelijk vereiste versterkingen van de netinfrastructuur uitgesteld of vermeden kunnen worden.

Het gebruik van DC-netten reduceert eveneens de netimpact van het laden van EVs in gebouwen. De resultaten tonen met name aan dat de spanningsonbalans en spanningsafwijkingen in het AC-net gereduceerd worden. Voor de lokale laadstrategieën die anticiperen op de zelfconsumptie van lokale hernieuwbare elektriciteitsproductie, reduceert het gebruik van DC-netten de elektriciteitsuitwisselingen met het laagspanningsnet.

Om de impact van het laden van EVs te onderzoeken, zijn twee simulatietools ontwikkeld:

- De **simulatietool voor het mobiliteitsgedrag** creëert realistische rijprofielen voor individuele voertuigen in de vloot. Deze tool is gebaseerd op beschikbare statistische data voor het mobiliteitsgedrag in Vlaanderen.
- De **Modelica bibliotheek voor elektrische modellering** kan gebruikt worden voor de integratie van verschillende multi-disciplinaire energiesystemen in gebouwen en wijken.

# Abbreviations

| | |
|---|---|
| AC | Alternating current |
| AER | All-electric range |
| | |
| BC | Boundary conditions |
| BEV | Battery electric vehicle |
| BIPV | Building integrated photovoltaic system |
| BMS | Building management system |
| BPS | Building peak shaving |
| BUF | Battery utility function |
| | |
| CCGT | Combined cycle gas turbine |
| CHP | Combined heat and power |
| CNG | Compressed natural gas |
| conv | Converter |
| COP | Coefficient of performance |
| CV | Conventional vehicle |
| | |
| DC | Direct current |
| DER | Distributed energy resources |
| DHW | Domestic hot water |
| DOD | Depth of discharge |
| DR | Demand response |
| DSM | Demand side management |
| DSO | Distribution system operator |
| | |
| EPB | Energy performance regulations |
| EREV | Extended range electric vehicle |
| ESI | Energy system integration |
| ETC | European Transient Cycle |
| EV | Electric vehicle |

| | |
|---|---|
| EVSE | Electric vehicle supply equipment |
| Febiac | Belgische federatie van de auto- en tweewielerindustrie (Belgian automotive and cycle federation) |
| FPS | Federal public service |
| FTP | Federal Test Procedure |
| GHG | Greenhouse gase |
| HEV | Hybrid electric vehicle |
| HL | Houseload |
| HP | Heat pump |
| HWFET | Highway Fuel Economy Driving Schedule |
| ICE | Internal combustion engine |
| ICT | Information and communications technology |
| LED | Light-emitting diode |
| Li-ion | Lithium-ion |
| LPG | Liquefied petroleum gas |
| LV | Low-voltage |
| MiD | Mobilität in Deutschland (Mobility in Germany) |
| MON | Mobiliteitsonderzoek Nederland (Dutch mobility study) |
| MPC | Model predictive control |
| MPP | Maximum power point |
| MSL | Modelica Standard Library |
| MV | Medium-voltage |
| NHTS | National Household Travel Survey |
| NREL | National Renewable Energy Laboratory |
| NYCC | New York City Cycle |
| nZEB | Nearly zero energy building |
| OVG | Onderzoek verplaatsingsgedrag (Research on travel behavior) |
| PCC | Point of common coupling |
| PHEV | Plug-in hybrid electric vehicle |
| POV | Point of view |

| | |
|---|---|
| PUR | Polyurethane foam |
| PV | Photovoltaic |
| PWM | Pulse width modulation |
| RES | Renewable energy sources |
| SLP | Synthetic load profile |
| SoC | State of charge |
| STC | Standard testing conditions |
| TES | Thermal energy storage |
| TSDC | Transportation Secure Data Center |
| TSO | Transmission system operator |
| TT | Terra-Terra (earthing) |
| UF | Utility function |
| UKTUS | United Kingdom Time of Use Survey |
| V2B | Vehicle-to-building |
| V2G | Vehicle-to-grid |
| VUF | Voltage unbalance factor |
| w/ | With |
| w/o | Without |
| XPS | Extruded polystyrene |
| ZEB | Zero energy building |

# Contents

# List of Figures

# List of Tables

# Chapter 1

# Introduction

## 1.1 Context and motivation

Globally, approximately 31 % of the global final energy use is in residential and commercial buildings [1]. In Flanders, buildings account for 36 to 40 % of the total primary energy use [2]. The residential and commercial buildings are responsible for about one-third of the global total end-use energy-related $CO_2$ emissions, if the indirect upstream emissions are considered [1]. On the other hand, transport keeps its status of being the most dependent on oil (about 95 %), of which road vehicles account for about 35 % of the global energy use for transport [1]. In the EU, passenger cars are responsible for about 12 % of the total $CO_2$ emissions [3].

### Climate and energy targets for buildings and passenger vehicles

Different climate and energy targets have been set on the global, European, national and regional levels in order to increase the energy efficiency and the share of renewable energy use. As a follow-up of the Kyoto protocol, e.g., the 20/20/20 targets have been set by the European Commission [4]: a 20 % reduction in greenhouse gas (GHG) emissions compared to 1990, a 20 % improvement in the EU's energy efficiency compared to a business-as-usual scenario, and a 20 % share of renewable energy in the total energy use. Recently, a framework has been set up for the 2030 EU targets, reducing the GHG emissions by 40 % in Europe [5]. Also the United States and China recently agreed on new carbon emission limits, e.g., −25 % for the US [6].

Europe has set energy performance targets at the level of individual buildings in the European Directive 2002/91/EC [7]. As per recent European Directive (2010/31/EU), by 2020 nearly zero energy buildings (nZEB) are required for new buildings and buildings undergoing large renovations. An nZEB requires very low energy requirements, which is covered by an increasing penetration rate of renewable sources. However, the definition of a nearly zero energy building is not clearly defined [8]. The literature mentions multiple definitions for zero energy buildings (ZEBs) [9–13]. On a regional level, the Flemish targets are available in the *energy performance regulations* (EPB) [14] regarding thermal insulation, energy performance, renewable energy and the climate within the building. For instance, since the start of 2014, every new building or building undergoing large renovations needs to get a minimum amount of energy from renewable sources, such as solar thermal and photovoltaic systems, or a heat pump.

Emission limits have also been set for road transport by the European Commission [3]. For instance, for passenger vehicles, legislation requires that the $CO_2$ emissions of new cars (fleet average) decrease to an average of 130 g/km by 2015, and 95 g/km by 2021. The latter corresponds to an average fuel consumption of 4.1 l/100 km and 3.6 l/100 km for gasoline and diesel cars, respectively. Besides, the European emission standards apply for road transport [15]. Since 2014, the EURO 6 standard is valid for passenger vehicles and commercial vehicles. These standards put a limit on the emissions of several pollutants. Therefore, traditional vehicles with an internal combustion engine (ICE) keep on improving their energy efficiency, but these regulations also increase the interest in alternative fuels for vehicles, such as bio-fuels and electricity.

### Increasing electrification (in buildings)

According to [1], the share of electricity consumption in the total energy demand increased from 9 % to 17 % since 1970. A further increase in electrification is expected. However, the decarbonisation, which is also required in the electricity generation sector, puts some challenges to the sector, requiring an increase in share of clean electricity production possibilities, such as renewable energy sources (RES). In buildings, an increase in electrification is also expected. The different energy performance targets for buildings and vehicles, as mentioned before, require an increase in energy efficiency and the integration of local RES.

Energy efficiency can be achieved, e.g., through proper thermal insulation. On the other hand, more energy efficient technologies have been brought to the market, such as electric vehicles (EVs) and heat pumps. These technologies

are more energy efficient, resulting in significant reductions in the consumption of GHG emitting fuels, decreasing the oil and gas dependency, and reducing the local pollutant emission concentrations [1, 16]. However, these technologies result in an increased electrification, but have an inherent flexibility in their energy use pattern [17–20].

Local integration of RES in buildings may include, e.g., photovoltaic (PV) systems and combined heat and power (CHP) units. In general, PV and wind power production are seen as intermittent renewable energy sources, for which the production depends on the availability of solar irradiation or wind with a limited predictability. Their production profile is not controllable if no loss of electricity generation is allowed. On the other hand, the production of heat and electricity by means of a CHP can be coordinated [21].

### Evolution to smart buildings and grids

The integration of these technologies and the increasing electrification has a certain impact on the electricity grid. The intermittent character of RES and the non-simultaneity of generation and consumption of electricity based on RES have an impact on the electricity grid, such as an increased demand or injection peak power and bidirectional power flows. This increased grid impact is discussed in more detail in Section 2.5. To limit the increased grid impact, a proper synchronization of consumption and production of both electricity and heat, through demand side management (DSM) or demand response (DR), electrical and thermal energy storage, and minimizing the energy use is required [22].

Therefore, a building or a district is no longer a passive electricity consumer, but buildings are evolving to buildings which also produce electricity locally, and have controllable loads, such as EVs and heat pumps. In this way, these controllable loads can be coordinated to better match the production and consumption profiles by using their flexibility in operation, in order to limit the grid impact of the building and to allow a higher penetration rate of EVs and others, such as a heat pumps and PV systems, in the system. For instance, the flexibility of EVs is determined by the mobility behavior of the EV user, the available charging power, the battery state of charge and battery limitations. EVs can be seen as one of the smart grid technologies to support an increased energy system integration, as also stated in [1].

As will be discussed in Section 2.6, EV charging coordination can take place on several levels. The charging can be coordinated by, e.g., a central controller or a distributed aggregator. On the other hand, there is a lack of research on local control of the EVs, which can be used as short-term solutions (before widespread coordination mechanisms are available) for local high EV penetration

rates or as additional backup systems to higher-order coordination systems, which for instance optimize the charging process.

Therefore, this dissertation will focus on the local coordination (within buildings) of EVs, which uses minimal local (e.g., grid topology, or building load and generation profiles) or EV internal knowledge, which requires limited communication within the building, and which does not require any optimization process. The charging strategies under consideration, are developed from a technical objective (DSO and grid point of view), taking into account the flexibility offered by the EV owners.

### DC electricity distribution

There is a growing interest in DC electricity distribution, which is already becoming a standard practice for some applications in high voltage grids [23]. But the literature also focuses more and more on DC electricity distribution in LV distribution feeders, and in buildings, as different initiatives have been set up for DC distribution standardization: EMerge Alliance [24], the *DC in the Home* initiative of the IEEE Standards Association [25], or the IET code of practice for DC distribution in buildings [26].

Traditionally, AC grids in buildings are designed to feed both AC and DC loads. Currently, almost all electric loads are equipped with power electronics, such as DC loads (e.g., computers and LED lighting) and inverter driven AC loads (e.g., variable speed motors). There is also an increasing interest in DC grids due to the DC interface of PV systems, battery storage, EVs, etc.

Therefore, this dissertation will discuss the impact of DC grids in combination with EV charging in an apartment building. This dissertation assumes an extension of the AC in-building grid with a local DC in-building grid to interconnect the EV charging infrastructure, PV system and heat pump. Therefore, this can be seen as a possible short-term solution for the use of DC grids in existing buildings.

## 1.2 Scope and objectives of the work

The objective of this doctoral research is the development of an applicable, scalable and flexible approach for the integration of EV charging in large buildings with different energy systems, and the possibility for upscaling to districts/neighbourhoods. Therefore, this dissertation is split into two parts: (i) a modeling part, and (ii) case studies of EV charging integration in buildings.

### 1.2.1 Mobility behavior modeling and electrical modeling in Modelica

#### Mobility behavior simulation tool

In order to assess the impact of EV charging and different EV charging strategies, realistic EV driving profiles are required. Therefore, in the scope of this dissertation and the Linear project [27], a simulation tool is developed, to create unique driving behavior profiles for individual vehicles in a fleet.

#### IDEAS sublibrary – Electrical modeling in Modelica

In order to meet the requirements for integrated modeling tools, which are used for the integration of different (multidisciplinary) energy systems in buildings and districts, a library for electrical modeling in Modelica is developed. Specific for this dissertation, the following models have been developed within the IDEAS framework: single/three-phase (unbalanced) AC grids and unipolar DC grids, and a battery and EV model.

### 1.2.2 EV charging integration in buildings

EV charging has a non-negligible grid impact. It is widely accepted that the coordination of EV charging may reduce this impact, allowing more EVs to be charged through the power system. Despite, the literature mainly focuses on (large-scale) optimization coordination for a certain objective (technical and/or economical), which requires a relative high penetration rate of EVs to be beneficial. However, local clustering (in buildings or LV distribution grids) of EVs might already occur in the near-future, requiring local charging solutions.

Therefore, in order to reduce this EV charging grid impact, this dissertation focuses on:

- local rule-based EV charging strategies in large buildings (multiple EVs charging), which require minimal local or EV internal knowledge, and minimal or no communication in and outside the building, respectively;
- the use of DC grids to interconnect the EV charging infrastructure, PV system and heat pump, and to charge the EVs in the building.

The objective is to assess how these solutions can already limit the grid impact, in order to allow a higher penetration rate of EVs and others, such as a heat

pumps and PV systems, in the system under consideration, i.e. an apartment and office building, respectively. For EV charging integration in residential districts, the considered local solutions can also be applied for EV charging integration in residential single dwellings. As equal impact trends may be expected [28], the assessment of the complete low-voltage distribution grid is out of the scope in this dissertation.

## 1.3 Thesis outline and contributions

Chapter 2 gives a brief background on the EV charging principles. The EV charging infrastructure standards will be discussed, including a discussion on the possibilities for local EV charging control. The EV charging flexibility, grid impact and coordination will be discussed. The chapter ends with a brief introduction to DC electricity distribution.

Chapter 3 introduces the EV mobility behavior simulation tool, which is developed in the scope of this dissertation and the Linear project [27]. An overview is given on the different use cases, for which this simulation tool is used within the research topics of EnergyVille[1].

Chapter 4 introduces the IDEAS library which can be used for energy system integration assessments. Specifically, the developed electrical models within the IDEAS library, in the scope of this dissertation and [29], will be discussed.

Chapter 5 focuses on the EV charging flexibility which is available in a fleet of vehicles, based on the results of the mobility behavior simulation tool (see Chapter 3). The general residential grid impact is discussed, including the impact of additional EV charging locations (besides the charging opportunities at home). To conclude, the EV charging power requirements at home will be discussed.

Chapter 6 discusses the residential case study scenario. The scenario description of EV charging in an apartment building is given. This chapter also defines the different local EV charging strategies, including their objective, that will be assessed in this dissertation. Three EV charging strategies (uncoordinated charging, EV based peak shaving and delayed charging) have been used to set an EV charging power set-point. Other charging strategies have been introduced to deviate from this set-point based on the charging timing, the local electricity production or grid conditions.

[1] `http://www.energyville.be`

Chapter 7 assesses the grid and fleet impact trends of the different EV charging strategies in the apartment building. The objective is to assess how these strategies can already limit the grid impact, in order to allow a higher penetration rate of EVs in the building.

Chapter 8 introduces a hybrid AC-DC grid in the apartment building. The DC grid is used to interconnect the EVs, the PV system and heat pump. This chapter focuses on the possibilities for DC networks to support an increased integration of EV charging in buildings.

Chapter 9 assesses the EV charging integration in an existing office building. Different local EV charging strategies will be examined for their grid impact, in order to assess how a higher EV penetration rate can be achieved. Besides, it is examined how many EVs can charge at the office building with a fixed number of dedicated charging infrastructures.

To conclude, Chapter 10 presents the general conclusions and recommendations for future research.

# Chapter 2

# Charging of electric vehicles

In recent years, a new wave of EVs is introduced into the market and the share of EVs in total number of vehicle sales is increasing [30]. On August 1, 2014, the share of plug-in electric vehicles still amounts to less than 0.1 % of the total Belgian passenger vehicle fleet. The fleet of plug-in hybrid electric vehicles (PHEVs) and electric vehicles (EVs) doubled compared to the previous year [31].

Moving to alternative fuels in transport reduces its oil dependency, which is 95 % nowadays [1]. Using electricity for propulsion offers opportunities to shift the power consumption in time [18] and it significantly reduces the consumption of GHG emitting fuels, such as gasoline and diesel, and local harmful pollutant emissions [22, 32]. Also, electric motors are more efficient compared to thermal combustion engines. Since the $CO_2$ emissions are moved to the electricity production, there is an inherent reduction of $CO_2$ emissions due to the EU Emissions Trading System, which sets a limit to the total $CO_2$ emissions [33].

Besides batteries as storage units for EVs, also supercapacitors may be used. Other alternative vehicles or fuels are for instance fuel cell vehicles, and vehicles driving on liquefied petroleum gas (LPG), biofuels, hydrogen or compressed natural gas (CNG).

For EVs, a distinction can be made between different types of vehicles. Section 2.1 gives a short overview of the classification of EVs. In Section 2.2, the available battery types for EVs are shortly discussed, including the battery charging profile. The electric vehicle charging infrastructure and standardization is discussed in Section 2.3. Charging an EV requires a large amount of electricity

to be charged[1], indicating a certain impact on the power system (Section 2.5). Nevertheless, as a result of the mobility behavior and long standstill times (e.g., at home), there is a certain EV charging flexibility available, both in time and charging power (Section 2.4).

Two solutions have been investigated to limit the grid impact. First, coordinated EV charging has been assessed. Compared to the main research in the literature (Section 2.6), this dissertation focuses on local EV charging strategies, which can be implemented in the EV or EV charging infrastructure. Second, the use of DC grids (Section 2.7) in combination with the coordinated charging of EVs is assessed. To conclude, Section 2.8 discusses the different grid and fleet impact indicators, which will be used to compare the different solutions.

## 2.1 Types of electric vehicles

There are different vehicle drivetrain technologies available on the market [34,35]: (plug-in) hybrid electric vehicles and full electric vehicles. In general, EVs distinguish themselves from conventional vehicles[2] (CV) with at least one electric motor that is used for, or to support propulsion[3]. An important advantage of EVs is the possibility for regenerative braking. Kinetic energy is no longer dissipated as heat, but is recovered through regenerative braking, by using the electric motor in generator mode. Plug-in EVs charge their battery through an electrical socket.

An EV is powered by an electric motor supplied with electric energy from, e.g., a battery. Electricity can be produced in different power plants, such as a nuclear power plant, a combined cycle gas turbine (CCGT) plant, photovoltaic systems and wind turbines. The flexibility in primary fuels and types of power plants increases the security of supply of energy resources.

An overview of electric vehicles on the market, both (plug-in) hybrid and plug-in electric vehicles, is available at [36].

### 2.1.1 Battery electric vehicles

A full electric vehicle uses only an electric motor for propulsion. In this dissertation, the energy is drawn from batteries. Therefore, it is called a battery

[1] Both in energy and power. For instance, the household electricity consumption is nearly doubled, while the charging power is large compared to the connection capacity.

[2] Conventional vehicles only have an internal combustion engine (ICE).

[3] The electric motor is not always used for propulsion, as shown in Section 2.1.2.

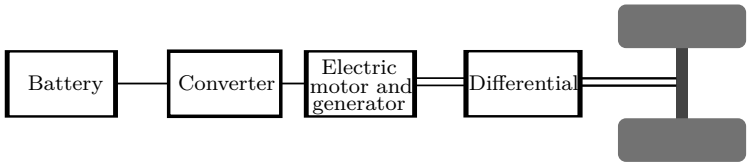


Figure 2.1: Topology of an EV drivetrain [37].

electric vehicle (BEV). In general, an EV does not have a gearbox. There is only a differential between the motor and the wheels, which is shown in Fig. 2.1. The energy management for this drivetrain is very straightforward. In normal conditions the power flow goes from the battery through the electric motor to the wheels. If the EV brakes regeneratively, then the power flow goes from the wheels to the battery. The batteries are mainly charged by plugging the car in an electrical socket. A converter (conv) is required as an interface between the battery and electric motor.

### 2.1.2 (Plug-in) Hybrid electric vehicles

Hybrid electric vehicles (HEVs) combine a conventional ICE with an electric motor, which allows to downsize the ICE without impacting the user comfort. Besides, the energy management system of the drivetrains can take into account the efficiency maps of the engines to make sure that for instance the ICE operates in more efficient working points. (P)HEVs can be classified according to a technical and functional classification.

#### Functional classification

Hybrid electric vehicles are classified according to the degree of hybridization [38]:

- **Micro hybrid**, i.e. a conventional vehicle with a start/stop function. No electric driving is possible.
- **Mild hybrid**, i.e. a conventional vehicle with a start/stop function and regenerative braking. No electric driving is possible.
- **Medium hybrid,** i.e. extra power can be delivered during acceleration of the vehicle to allow downsizing of the ICE.
- **Strong hybrid,** i.e. a short distance, depending on the battery size, can be driven electrically. As the batteries are charged by regenerative braking, the battery size is limited.

- **Plug-in hybrid,** i.e. a short distance, depending on the battery size, can be driven electrically. Batteries are charged by regenerative braking and by plugging into a socket.

### Technical classification

Different hybrid drivetrains are available. First, a **series HEV** is powered by an electric motor, which can be supplied by both the electricity from a battery or generated by a combustion engine. A generator converts the mechanical energy of the combustion engine into electricity. The combustion engine is typically smaller and operates more efficiently, compared to the engine in an ICE vehicle. The surplus of generated electricity is stored in the batteries. The series (P)HEV is shown schematically in Fig. 2.2. The advantage is that the ICE can be downsized and the combustion engine works near its optimum working point. Due to the series topology, the reliability is reduced. Also, the electric motor has to be sized large enough.

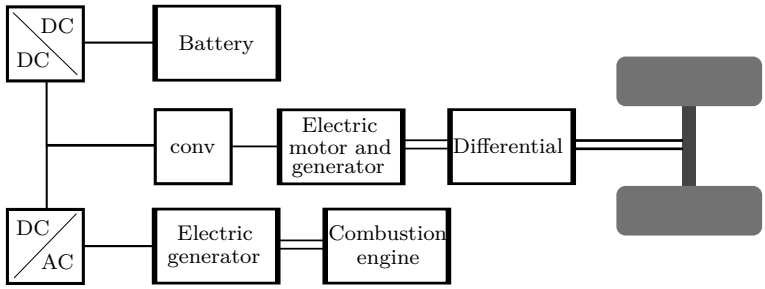


Figure 2.2: Topology of a series (P)HEV drivetrain [37].

An electric motor or ICE can power the **parallel HEV** separately or together. Again, the ICE can be downsized and it can work more efficiently to achieve minimal fuel consumption. Compared to a series HEV, the ICE and electric motor can be sized smaller, and the system is more reliable. However, the mechanical coupling is more difficult. The parallel (P)HEV is shown schematically in Fig. 2.3.

Different control strategies for series and parallel HEVs are available in the literature, such as in [39, 40]. Other topologies exist, such as the mixed series-parallel topology in a Toyota Prius [41], using the advantages of both topologies for specific situations. For instance, for city driving, the series topology is preferred to drive fully electrically, as the frequent accelerating and braking would result in a very low efficiency for an ICE. The parallel topology is preferred for highway driving.

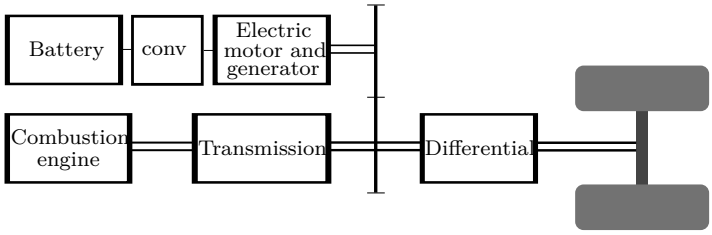


Figure 2.3: Topology of a parallel (P)HEV drivetrain [37].

Plug-in hybrid electric vehicles (PHEVs) are HEVs which have the possibility to recharge their battery from the grid. They can drive in full electric mode and have a larger battery pack compared to HEVs. Typically, the battery capacity varies between 4.4 and 20 kWh. Regular PHEVs are capable of driving fully electrically, even at high speeds. Other PHEVs, so-called blended-mode PHEVs, switch to hybrid mode at higher speeds.

In this dissertation, the EVs have been modeled as extended range electric vehicles (EREVs) in order to meet all mobility requirements, even if the battery is depleted. Therefore, no mobility behavior adaptations have been assumed in this dissertation[4]. EREVs drive fully electrically until the battery is depleted. At that moment, the internal combustion engine is engaged.

## 2.2 Batteries for electric vehicles

Current EVs on the market make in general use of batteries as energy storage units, with different battery sizes. For instance, current PHEVs on the market have a battery capacity between 4.4 and 20 kWh[5]. On the other hand, full electric vehicles have a larger battery capacity, typically ranging between 16 and 24 kWh, resulting in a range of 100 up to 200 km[6]. Others, such as the Tesla Model S, have a battery pack up to 60–85 kWh (range of 330 up to 430 km) [57]. Both PHEVs and BEVs are available in different vehicle segments, ranging from small city cars up to full-size high-end cars and sports cars.

[4]For a BEV, which drives purely on electricity, the average battery size would be considerably larger in order to meet all mobility requirements without adaptations to the mobility behavior [42].

[5]Chevrolet Volt [43], Fisker Karma [44], Ford C-Max Energi [45], Mitsubishi Outlander [46], Toyota Prius PHV [41], Volvo V60 Plug-in Hybrid [47], and others.

[6]BMW i3 [48], Ford Focus Electric [49], Kia Soul EV [50], Mitsubishi i-MiEV [51], Nissan Leaf [52], Renault Zoe [53], Volkswagen e-Up [54], Volkswagen eGolf [55], Volvo C30 eDrive [56], and others.

### 2.2.1 Battery types

Nowadays, lithium-ion (Li-ion) is generally used in EVs. Li-ion refers to a group of different battery chemistries. Different cathode and anode materials are used. These determine the properties[7] of the battery cells and their application. In current EVs, different positive electrode materials are used [58].

LCO batteries ($LiCoO_2$) were used in the past, which are identical to battery cell types used in consumer electronics. LCO batteries have a high specific energy density, but low power density and limited cycle life. A higher power density is delivered by LMO batteries ($LiMn_2O_4$). It also allows fast charging of the batteries (e.g., in the Nissan Leaf). However, the energy density is lower compared to LCO. NMC ($LiNiMnCoO_2$) combines the advantages of both LCO and LMO at a reduced cost (fewer cobalt present). For high power and energy density requirements, NCA batteries are used ($LiNiCoAlO_2$), which have a higher cost and require more attention to safety. On the other hand, LFP ($LiFePO_4$) guarantee a very low internal resistance, thermal stability, robustness, high current rating and a long cycle life, but a lower energy density, which is extremely suitable for fleets that can regularly make use of fast charging.

#### Battery lifetime

Degradation processes limit the lifetime of batteries. There are two sources of capacity losses, i.e. calendar and cycling losses [59]. A battery pack is characterized by a nominal capacity $E_{\text{nom}}$. As the battery ages, capacity is lost due to irreversible chemical reactions, which increase the battery cell resistance. In the literature, the cycle life of a battery is typically defined as the number of cycles until the remaining battery capacity drops below 80 %, i.e. a remaining nominal capacity of 80 % of its original value [60]. A battery is typically nor fully discharged (0 % SoC), nor fully charged (100 % SoC), as very low or high SoC values are to be avoided [61]. The usable battery capacity $E_{\text{eff}}$ is limited to extend the battery cycle life [60], e.g., a 65 % SoC window for the Chevrolet Volt [43]. The State of Charge (SoC) defines the amount of energy stored in the battery while cycling, compared to the nominal capacity.

The battery lifetime is a function of the chosen battery chemistry and various other parameters, which makes it difficult to predict the life expectancy, especially for variable operating conditions [60, 62], which is the case for EVs. The lifetime is a function of parameters, such as the charging and discharging powers, the average SoC, the cell temperature, the end-of-charge voltage, the discharge voltage, the depth of discharge (DOD) of cycles, etc. [60, 63].

[7] Energy and power density, power-to-energy ratio, efficiencies, cycle life time, etc.

In general, it can be concluded that lower currents or charging powers increase the battery lifetime [59, 60, 62]. On the other hand, partially discharging the battery, i.e. lower cycle DODs, results in a lower battery degradation compared to high DODs during a single discharging cycle [60]. Therefore, it may be concluded that low power charging and maximizing the number of charging opportunities (besides home charging) is preferred.

### 2.2.2 Battery charging profile

A battery management system controls the charging process of batteries to guarantee safe operation. Therefore, the power profile varies in function of the SoC while charging. A typical charging profile for a Li-ion cell contains a constant voltage and constant current profile. An example profile is shown in Fig. 2.4. The charging power decreases in the constant voltage region. These end-of-charge behaviors may be different for different EVs on the market, as for instance measured in [64] for slow and fast charging of multiple EVs. Besides, depending on the used battery balancing method, the charging profiles vary for different EV models. The end-of-charge behavior is not taken into account in this dissertation. Thus, a constant power profile during charging is assumed, resulting in a slightly shorter charging duration.

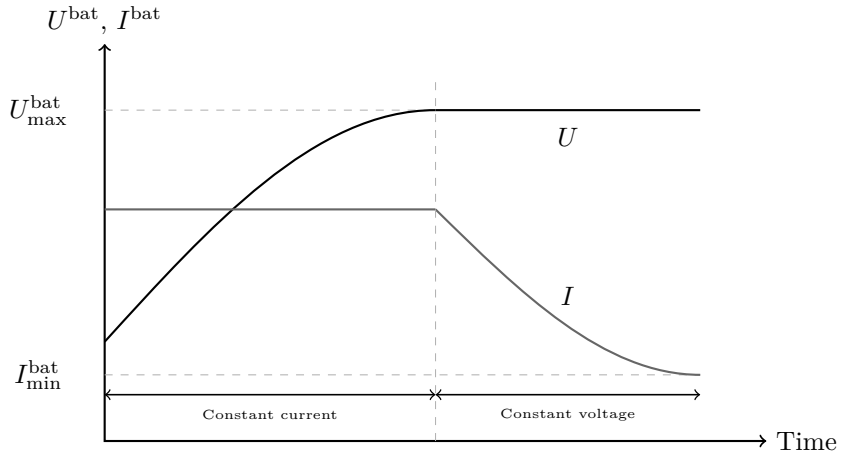


Figure 2.4: Typical Li-ion battery charging voltage $U^{\mathrm{bat}}$ and current $I^{\mathrm{bat}}$ in function of time.

## 2.3 Electric vehicle charging infrastructure

EVs can be charged in multiple ways:

- conductive charging, both AC and DC;
- inductive charging;
- battery swap.

Here, the focus lies on conductive EV charging. For conductive charging, the EV is connected to the electricity grid through a so-called electric vehicle supply equipment (EVSE), i.e. the off board charging infrastructure. In its most simple form, an EVSE is a simple socket. EV charging can occur both through AC and DC charging. However, for DC charging, the charger is located in the EVSE, resulting in a DC power flow to the EV. As shown in Fig. 2.5, an EV is connected to the EVSE with a cable. A cable has a connector on the EV side and a plug on the EVSE side. According to the international standard IEC 61851-1 [65], the connection between the EV and EVSE can be realized by three different connection cases. The cable can be attached to the EV or EVSE, or a loose cable can be used.

Different overviews on the standardization, and requirements for standardization, are available [66–70]. For instance, the European Commission set up a mandate in 2010 regarding the standardization of EV charging [71]. The standardization of the EV charging infrastructure may help to overcome some important obstacles for the rollout of EVs [70, 72]:

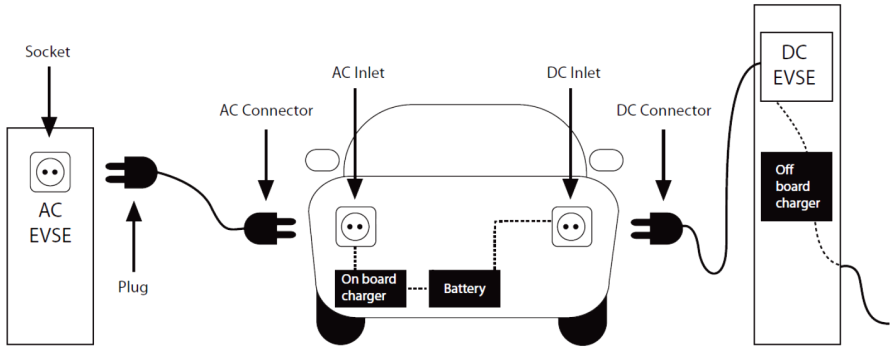


Figure 2.5: EVSE infrastructure for AC or DC charging [58].

- a rollout of standardized EVSEs increases the number of charging opportunities, i.e. it reduces range anxiety.
- a standardized interaction between the EV and EVSE allows to optimize the charging process, given the battery and grid connection constraints.
- a standardized interaction between the EVSE and the power system allows to coordinate the EV charging.

The IEC 61851-1 standard defines four different charging modes [65]:

- **Mode 1:** Single/three-phase AC charging, up to 16 A, through a standard socket. To communicate the available grid connection power to the EV, resistive coding is used.
- **Mode 2:** Single/three-phase AC charging, up to 32 A, through a standard socket, including an in-cable protection device. This protection device also provides the control pilot signal to communicate the available grid connection power to the EV.
- **Mode 3:** Dedicated AC charging infrastructure, up to 32 A (loose cable) and 63 A (EVSE fixed cable). The EVSE provides the control pilot signal.
- **Mode 4:** DC off board charging, up to 400 A.

Every domestic socket can be considered as a charging infrastructure. EVs are usually equipped with a mode 2 charging cable to be connected to a domestic socket. Mode 1 cables are rarely used due to the absence of the in-cable protection. Therefore, the latter ones are not allowed in some countries, e.g., in the United States. The current rating of mode 2 charging is typically limited to avoid overloading of the domestic electric installation and fuse tripping, e.g., 10 A in Europe [73].

Mode 3 charging has the disadvantage of requiring a dedicated charging infrastructure. However, mode 3 charging allows to adapt the charging current through a variation of the control pilot signal. This can be used to coordinate the EV charging, e.g., by adapting the charging current taking into account grid constraints, or anticipating on local electricity generation, as demonstrated for instance in [74, 75][8]. Depending on the location, mode 3 charging results in a power rating of 3.3 kW (single-phase, 16 A) up to about 40 kW (three-phase, 63 A). For higher charging rates, typically DC charging is used.

As mentioned before, communication is possible to communicate the available grid connection power[9] to the EV. This is done through the resistive coding

[8] However, this PWM is not intended to be used for coordination purposes [76]. IEC 15118 addresses this use case [77].

[9] Or charging power set-point from a higher level coordination system (e.g., an aggregator).

for mode 1 charging, and the control pilot signal for mode 2 and mode 3 charging [78]. For the control pilot signal, a 1 kHz PWM signal is used, according to IEC 61851-1 [65], to set the maximum current the EV can draw from the grid. The standard allows currents from 6 A (duty cycle of 10 %) up to 80 A (duty cycle of 95 %). An EV has to comply within 5 s to a current change.

However, the charger located within the EV defines the current it will draw from the grid, depending on the charging limitations of the vehicle. For instance, the charging power is reduced when the vehicle reaches its maximum SoC, i.e. end-of-charge behavior (see Section 2.2.2).

Besides the domestic type plug/socket (the *Schuko* plug), different types of plugs/connectors for AC charging have been defined in IEC 62196-2 [79], which allow communication between the EV and EVSE. For DC (fast) charging, the CHAdeMO standard [80], the Tesla charging infrastructure [81], and a combo AC-DC charging connector [82] are available.

## 2.4 EV charging flexibility

As a result of the mobility behavior (see Chapter 3 and 5), there is an opportunity to adapt the EV charging process, both in time and in charging power. Coordination mechanisms on different levels (see Section 2.6) can use this flexibility for different objective functions, such as charging cost minimization, grid impact minimization, RES integration maximization, etc.

In the power system, there are several sources of flexibility, both on the consumer (e.g., EVs and heat pumps) and the production side (e.g., conventional power plants), including storage possibilities. Typically for conventional power plants, different metrics are available in the literature to characterize flexibility [83]: the power capability for up/down regulation (MW), the energy storage capability (MWh), the power ramping capability (MW/min) and the power ramping duration (min). Using this flexibility offers both an economic value, and related costs (e.g., a reduction in user comfort).

For EVs, mainly the power and energy storage capabilities are of an importance. EV charging flexibility during a charging opportunity can be defined as the flexibility in (i) time and (ii) charging power, or a combination of both. Fig. 2.6 represents the definition of flexibility in time and charging power.

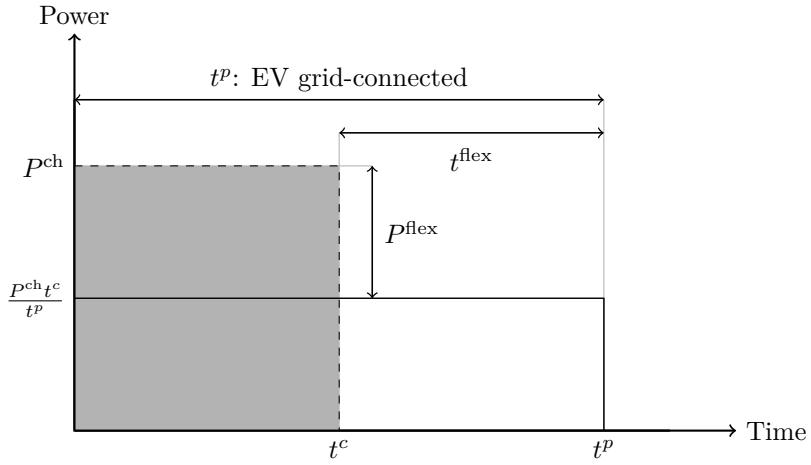


Figure 2.6: Definition of EV charging flexibility in time $t^{\text{flex}}$ and charging power $P^{\text{flex}}$, during a charging opportunity with standstill time $t^p$.

**Flexibility in time** The flexibility in time, $t^{\text{flex}}$, is the available time to shift the EV charging process. $t^{\text{flex}}$ is equal to:

$$t^{\text{flex}} = t^p - t^c, \tag{2.1}$$

with $t^p$ the total standstill (grid-connected) time, and $t^c$ the required time to charge the required electricity at maximum power, i.e. the charging rate $P^{\text{ch}}$.

**Flexibility in charging power** The flexibility in power, $P^{\text{flex}}$, is the power reduction availability to charge the same amount of electricity during $t^p$, as during $t^c$ at $P^{\text{ch}}$:

$$P^{\text{flex}} = P^{\text{ch}} - \frac{P^{\text{ch}}t^c}{t^p}. \tag{2.2}$$

The charging flexibility of EVs is limited by the mobility objective, the available charging power rates, battery SoC and battery limitations (e.g., maximum charging power). This flexibility can be represented by a flexibility curve[10]. A sample flexibility curve for a fleet of EVs is shown in Fig. 2.7. This graph defines a solution set of possible charging paths to charge the required amount of energy, limited by an upper and lower bound curve which represent the charging curve without any delay and with maximum charging delay, respectively. Note that

[10]Or energy constraint graph, as defined in [76].

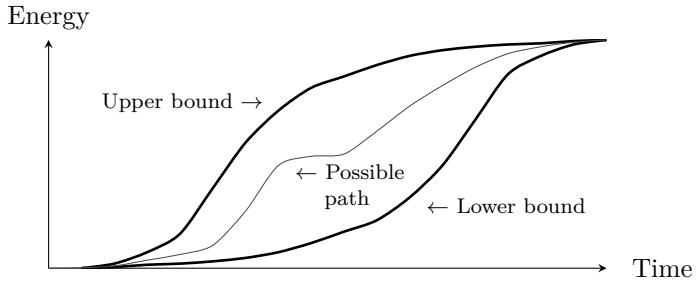


Figure 2.7: A flexibility curve for a fleet of EVs.

the possible charging paths at a certain time step depend on the charging profile of previous time steps.

This approach is also valid for other technologies, such as heat pumps and combined heat and power units, which provide a certain flexibility to shift the generation of heat and the consumption and production of electricity [19, 21, 84]. In future work, these technologies could be combined with the EV charging integration in buildings. This may result in improved solutions for the integration of these technologies in buildings.

## 2.5 Distribution grid impact

From the grid point of view, EVs have a twofold impact. First, the electricity consumption will increase [85]. Second, the EV charging power demand has an increased grid impact, both on the distribution and transmission grid level [86,87]. Also the electricity generation park is impacted [88]. Besides, the intermittent production character of RES and its potential nonsimultaneity with the power consumption has a grid impact [89]. To minimize the grid impact, a proper synchronization of consumption and production of both electricity and heat is needed through demand side management, electrical and thermal energy storage, and minimizing the power consumption [22].

EVs increase the power consumption in residential buildings. For full electric vehicles, charging the vehicle only at home nearly doubles the average household power consumption [90]. Given the Flemish mobility behavior, the specific power consumption of existing vehicles and a typical charging efficiency of 90 %, this results in an additional power consumption of about 2350 up to 3750 kWh per household using an EV [85]. Charging at home might be complemented

with charging at other locations (e.g., at the work place and public parking spots). This might decrease the residential grid impact (see Chapter 5).

### 2.5.1 Classification

An increased grid loading is observed, which may result in different grid regulation violations.

#### Power profile and grid congestion

Grid congestion might occur. Grid congestion means the available power capacity (of the transformer and cables) is exceeded. Besides, the extra loading of the grid results in increased grid losses, and an increased aging of the grid infrastructure assets, e.g., transformers and cables [91–94].

#### Voltage profile and unbalance

Power quality issues regarding the voltage profile and unbalance may occur due to loading of cables and the unbalanced exploitation of distribution grids. The European EN 50160 standard subjects the voltage magnitude $|u_{p,n,k}|$ (pu) and the voltage unbalance factor (VUF) (%) to:

$$0.9\,\text{pu} \leq |u_{p,n,k}| \leq 1.1\,\text{pu}, \text{ and} \tag{2.3}$$

$$VUF_{n,k} \leq 2\,\%, \tag{2.4}$$

for $> 95\,\%$ of all 10 min intervals for any week. $|u_{p,n,k}|$ should never drop below 0.85 pu. $|u_{p,n,k}|$ and $VUF_{n,k}$ are the voltage magnitude and VUF at phase $p$, grid node $n$ and time step $k$.

### 2.5.2 Grid impact mitigation

Different solutions can be used to mitigate the grid impact. One of these are grid reinforcements or an optimal sizing/design of the in-building grid. The following mitigation options have been discussed in this dissertation:

- Local EV charging strategies (see Section 2.6);
- DC grids in buildings (see Section 2.7).

## 2.6 Coordinated EV charging

Mobility behavior offers flexibility towards the EV charging process, both in time and charging power, as defined in Section 2.4, while still respecting the mobility requirements. This flexibility can be used to coordinate the EV charging. In general, it is widely accepted that EV charging coordination may reduce the power system impact [18, 95], as the available capacity is used more efficiently. Typical coordination objectives are peak shaving [86, 96, 97], minimum charging cost [98–102], voltage or grid loss reduction [17], frequency regulation [103, 104], portfolio imbalance [105], maximum integration of RES [100, 106–110], etc. Several coordination scales of the EV integration have been investigated in the literature, as summarized in the literature study, performed in the scope of the Linear project [111]: the vehicle, building, residential LV distribution and transmission grid scale. Vehicle-to-building (V2B) and vehicle-to-grid (V2G) service opportunities are envisioned [87, 112, 113]. However, V2B nor V2G are within the scope of this dissertation.

Coordination systems are effective when the results approach the benchmark results, i.e. optimal results, related to the coordination objective. Different types of objectives can be taken into account: technical, economical and techno-economical objectives. Coordination systems use a certain method to meet these objectives, as shown in Fig. 2.8 [76]:

- **Centralized methods:** A central scheduler, collecting all the required information, optimizes and schedules the EV charging profile. Communication is required between each vehicle and the central scheduler, which typically involves a large complexity. However, a highly optimal solution is achieved for the objective.
- **Distributed methods:** The scheduling is performed throughout the system, not centrally. The optimization problem is split into smaller optimization problems at different layers, and typically solved iteratively by communication between the different systems. The communication requirements are limited, compared to centralized methods.
- **Hierarchical methods:** Hierarchical coordination methods lie between centralized and distributed methods. A hierarchical structure is used to perform the optimizations, in which only adjacent levels communicate with each other. Higher levels receive aggregated information, optimize and dispatch the solution to a lower level.

On the building scale, EV charging coordination in residential and office buildings is discussed in the literature, for which the literature mainly focusses on the optimization for technical and/or economical objectives. As a technical objective,

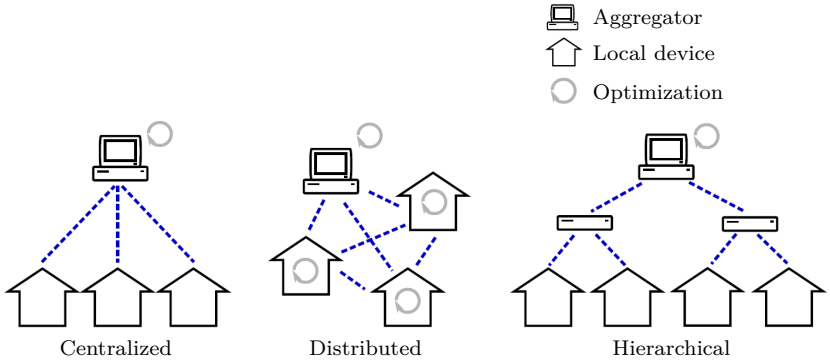


Figure 2.8: Illustration of coordination methods (source: [76]).

the literature mainly focuses on the peak shaving objective which uses the information from the building and/or district level to coordinate the EV charging [114–116], which may also be complemented by discharging the EVs for V2B [117]. As an economical objective, the minimization of charging cost or total cost is often used, on the one hand for an optimal building EV integration [118, 119], or on the other hand for EV integration in buildings with several distributed energy resources (DER) [120–123].

However, these aforementioned coordination methods (with a technical objective[11]) in buildings, require (one or more):

- communication between the EVs and the building and/or grid;
- future knowledge on the EV state and usage, building power profile, and/or electricity cost;
- prediction or knowledge on the local generation power profile;
- knowledge on local information, such as the grid topology.

In case of malicious or absent communication, these strategies are ineffective regarding the grid impact minimization. In case of local optimization at, e.g., an EV, the knowledge on the complete grid lay-out and/or the grid impact sensitivity of the EV may be required.

Despite the fact that the rollout of EVs has already started, uncoordinated EV charging will remain the most common charging method for the near future as wide-spread coordination mechanisms, for so-called *smart charging*, have not yet been implemented. These large-scale coordination mechanisms require a

[11] Or when the electricity cost (in the charging cost minimization strategies) reflects the grid impact.

relative high penetration rate of EVs on a regional/national level in order to be beneficial [124]. However, for the initial EV rollout and before a widespread coordination is expected, the cost of charging infrastructure should be low [125]. Also, a substantial EV penetration rate is not expected on large-scale in the near future. However, a local clustering of EVs is expected to happen sooner, e.g., in LV distribution grids or buildings. This may severely impact the local distribution grids and may require infrastructure investments, requiring local solutions to coordinate and charge the EVs.

However, these local EV charging strategies, or grid stabilizing strategies have not been widely discussed in the literature for EV charging in buildings or LV distribution grids. Therefore, this dissertation focuses on rule-based local EV charging strategies, which require limited prior knowledge of the EV behavior (only the next departure time and current battery SoC), no future knowledge of electricity demand or production, no local information (e.g., grid topology), and limited or no communication. The charging strategies under consideration, are developed from a technical objective (DSO and grid point of view), taking into account the flexibility offered by the EV owners. These strategies do not rule out other coordination mechanisms which optimize the EV charging process, but in that case, these local strategies can be used as emergency strategies or as strategies to deviate from the charging power set-point in case grid constraints are violated. Only local information within the building is used to control the EV charging process:

- Based on the required charging energy and next departure time, the EV charging power can be reduced to maximally use the available charging time (EV based peak shaving) [28, 126, 127], or the EV charging can be delayed (delayed charging) [126].
- Correction of local grid constraints through grid stabilizing EV charging, i.e. voltage dependent EV charging [28, 128, 129].
- Renewable self-consumption, by measuring the local electricity demand and production (no future knowledge or prediction required) [126, 127].
- Building peak shaving by reducing the EV charging power, by measuring the local electricity demand and production (no future knowledge or prediction required).

These local EV charging strategies can be implemented, e.g., on the on-board battery management system or in mode 3 charging infrastructure (see Section 2.3). A building energy management system may be required to communicate the charging power set-point deviation in case of a RES surplus or to perform building peak shaving. These EV charging strategies will be discussed in Section 6.3.

## 2.7 DC electricity distribution

Nowadays, AC electricity grids are well established at all levels of the power system. Although, in the high voltage grids, DC grids are becoming standard practise for some applications, e.g., to transport high power over long distances [23]. On the other hand, a high interest is present for the use of DC grids for data centers or ICT purposes [24, 130, 131]. The literature also focuses more and more on DC electricity grid in LV distribution grids and DC distribution inside buildings [132–147]. In recent years, multiple initiatives have been set up for DC distribution standardization and opportunities:

- EMerge Alliance [24]: an open industry association developing standards for DC distribution in buildings and data/telecom centers.
- The *DC in the Home* initiative of the IEEE Standards Association [25], which investigates the possible business cases, the possible required research and the standards to be considered.
- IET code of practice for DC distribution in buildings [26].

The interest for DC distribution in buildings is growing due to the increasing number of DC loads, such as computers and lighting, and inverter driven AC loads [132,134]. Also most DER, such as PV systems, require a DC interface [148]. The same applies to new application in buildings, such as battery storage or EVs. The main interest for DC grids is the possible increase in energy efficiency, since AC-DC conversions can be omitted. However, this dissertation will discuss the distribution grid impact of DC grids in combination with EV charging in an apartment building.

### 2.7.1 DC grid topology

In the literature [143–145, 148, 149], two common DC grid topologies are found, i.e. unipolar and bipolar DC grids. Fig. 2.9 gives a representation of both grid topologies, including the load connection possibilities [150]. The unipolar topology has a positive and negative phase conductor, while the bipolar topology has three conductors, including a neutral conductor at an intermediate voltage level. The loads can be connected between the positive or negative and neutral conductor, or between the positive and negative conductor. The bipolar topology has an increased reliability and power transfer capability, but may result in unbalance within the DC grid [144, 145]. In this dissertation, the focus does not lie on the grid topology. Therefore, a unipolar DC grid topology is chosen. Existing AC grids could be rearranged in a unipolar or bipolar configuration [145].

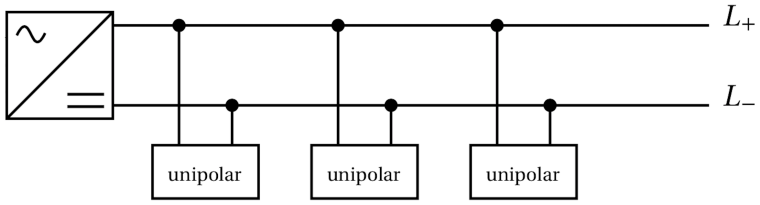


(a) Unipolar DC grid.

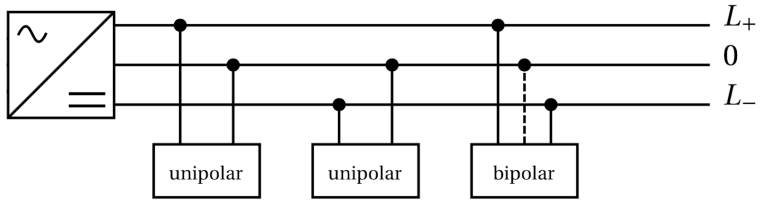


(b) Bipolar DC grid.

Figure 2.9: Unipolar and bipolar DC grid topologies (figure based on [150]).

As shown in Fig. 2.9, an AC-DC interface inverter is required between the DC and AC grid. In case DER are present in the DC grid, a bidirectional AC-DC converter is required. No standardized voltage level is available yet. Different voltage levels have been proposed in the literature [24, 133, 141, 148, 149]. A DC voltage of 380 V is chosen.

### 2.7.2 Opportunities and challenges

The use of DC grids offer many different opportunities and challenges [148, 151]. One of the main advantages of DC grids, is the possible increase in efficiency, resulting in lower cable and converter losses [137–147,149,151]. Other advantages are an increased power transfer capability [145, 152] and an increased power quality. For instance, there is a significant reduction in harmonic distortion, which saves energy and improves the equipment lifetime [131]. Also less AC voltage fluctuations propagate to the DC grid, and it is possible to regulate the reactive power drawn or injected in the AC grid [153]. To conclude, DC grids offer an easier integration of DER since no frequency synchronization is required, which simplifies the converter control.

The main challenges for DC grids are the fact that standardization is not yet fully in place, and protection of DC grids is more difficult compared to AC grids

due to the absence of a voltage zero cross point [147, 154]. Another research topic focuses on the stability in DC grids [150, 154, 155].

Research regarding DC grids for LV distribution currently mainly focuses on the possible efficiency gains, DC grid stability and control. In this dissertation, the impact of DC grids, in combination with EV charging, on the AC grid is assessed in Chapter 8. In this way, it can be assessed whether the use of DC grids allows a higher EV penetration rate.

## 2.8 Grid and fleet impact indicators

The different EV charging strategies have been compared using different grid and fleet impact indicators, which will be discussed in the following sections.

### 2.8.1 Grid impact indicators

To evaluate the single building impact on the LV distribution grid, several grid impact and load matching indicators have been defined in [156]. These indicators do not need any information from the LV distribution grid itself and are therefore particularly suitable to assess the grid impact of different EV charging strategies within a single building:

- power profile: peak power and one percent peak powers (demand and injection);
- voltage magnitude profiles;
- voltage unbalance factor;
- cover factors: self-consumption and self-generation;
- energy exchange.

#### Active power exchange

The LV distribution grid impact of a building is determined by the local demand and generation. The active power exchange with the LV distribution grid, $P^{\text{exch}}$, at each time step $k$, is equal to:

$$P_k^{\text{exch}} = P_k^{\text{HL}} + P_k^{\text{HP}} + \sum_{i=1}^{n^{\text{EV}}} P_{i,k}^{\text{EV}} - |P_k^{\text{PV}}| + P_k^{J,\text{grid}}, \tag{2.5}$$

with $P^{\mathrm{HL}}$, $P^{\mathrm{HP}}$, $P^{\mathrm{EV}}$ and $P^{\mathrm{PV}}$, the household, the heat pump and the EV charging power demand, and the PV power production, respectively. Only $P^{\mathrm{EV}}$ is considered as controllable. $P^{J,\mathrm{grid}}$ consists of the cable losses:

$$P_k^{J,\,\mathrm{grid}} = \sum_{p=1}^{4} \sum_{c} R_{p,c} |i_{p,c,k}|^2 \tag{2.6}$$

with $p$ the number of conductors, $c$ the number of cables connecting the different nodes, $R_{p,c}$ the resistance of the cables and $i_{p,c,k}$ the current in a cable at time step $k$. $p = 4$ or 2 for three-phase and single-phase grids, respectively.

These power profiles have been presented as load duration curves[12]. Modified box plots[13] (see Fig. 2.10) have been defined in [153] to emphasize the occuring peak values. In this dissertation, the 1st and 99th percentile have been added and replaced by the injection and demand one percent peak power (OPP), respectively, when power profiles are shown.

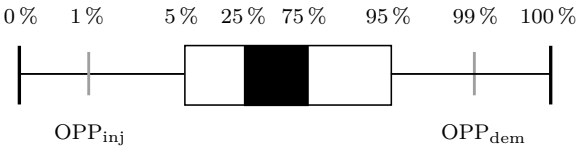


Figure 2.10: Modified box plot to represent the distribution of time profiles. The inner box (black) spans the 25th to 75th percentiles. The outer box (white) spans the 5th to 95th percentiles. The outer whiskers extend to the minimum and maximum values. The 1st and 99th percentiles (or OPPs for power profiles) have been included.

### Energy exchange

The total energy exchange $E^{\mathrm{exch}}$ at a node includes both the electricity consumption and production exchanged $|P^{\mathrm{exch}}|$ at this node, as defined in [156]:

$$E_k^{\mathrm{exch}} = \int_{t=0}^{\mathrm{period}} |P_k^{\mathrm{exch}}| dt, \tag{2.7}$$

[12] A load duration curve shows how long the power demand/injection is larger than a given power.

[13] The modified box plots, as used in this dissertation, are not to be confused with regular box plots to represent statistical data points.

### Peak power

The demand $P^{\text{dem}}_{\text{peak}}$ and injection peak power $P^{\text{inj}}_{\text{peak}}$ have been defined as the maximum demand (positive) and injection (negative) power exchange with the LV distribution grid during the simulation period:

$$P^{\text{dem}}_{\text{peak}} = \max(P^{\text{exch}}), \tag{2.8}$$

$$P^{\text{inj}}_{\text{peak}} = |\min(P^{\text{exch}})|. \tag{2.9}$$

### One percent peak power

The one percent peak power (OPP) is the mean power of the one percent highest power peaks [156]:

$$OPP = \frac{E_{1\%\text{peak}}}{\Delta t/100}, \tag{2.10}$$

with $E_{1\%\text{peak}}$ the energy in the one percent highest peak powers, and $\Delta t$ the total time corresponding to the 1 % peak. In this work, the OPP is calculated for both the positive (demand OPP) and negative power exchange (injection OPP), as discussed in Fig. 2.10.

### Voltage magnitude and voltage unbalance factor

The power profile impacts both the voltage magnitude profile and the voltage unbalance factor. Voltage unbalance occurs due to the uneven distribution of single-phase loads and asymmetric conductor configurations. Both the voltage magnitude and VUF are subject to the European EN 50160 standard in LV distribution grids [157][14], as defined in Section 2.5.

The voltage unbalance factor is defined as the magnitude of the ratio of the negative $U^{\text{inv}}$ over the positive sequence voltage $U^{\text{dir}}$:

$$VUF = |U^{\text{inv}}/U^{\text{dir}}|. \tag{2.11}$$

[14]The DSO is responsible for the voltage magnitude and VUF till the point where the electricity meter is installed.

#### Self-consumption and self-generation

The energy match between local demand and generation is represented by cover factors:

$$\gamma_x = \frac{\int_{t_1}^{t_2} \min\{P_k^S, P_k^D\} dt}{\int_{t_1}^{t_2} P_k^x dt}, \tag{2.12}$$

with $x \in [S, D]$. $P^S$ and $P^D$ the local electricity supply and demand, respectively, at each time step $k \in [t_1, t_2]$. $\gamma_S$ and $\gamma_D$ are the electric supply (self-consumption) and demand cover factors (self-generation), respectively. The self-consumption defines how much of the locally generated electricity is instantaneously consumed ($\min\{P^S, P^D\}$) between time steps $t_1$ and $t_2$. Vice versa, the self-generation defines how much of the local demand is instantaneously covered by the local generation units.

### 2.8.2 Fleet impact indicators

The fleet impact of the different EV charging strategies on the EV use and charging behavior will be assessed on the following fleet impact factors:

- the utility function (UF) or the fraction of electrically driven kilometers;
- the EV charging simultaneity, i.e. the number of EVs charging simultaneously;
- the average charging duration, i.e. the total time that an EV is grid-connected and charging[15];
- the average charging power;
- the total electricity consumption;
- the battery utilization factor (BUF).

#### Utility function

The utility function (UF) for an individual PHEV is defined by the Electric Power Research Institute (EPRI) in [32]. The UF for a vehicle $e$ is calculated as follows:

$$UF_e = \frac{d_e^{\text{elec}}}{d_e^{\text{tot}}}, \tag{2.13}$$

[15]I.e. the time between the start and end (fully charged battery or leaving for next trip) of the charging process.

with $d_e^{\text{elec}}$ the annual electric kilometers and $d_e^{\text{tot}}$ the annual vehicle kilometers driven by EV $e$. The UF varies for each EV and depends on the available charging opportunities, charging rate, charging strategy, the total driven distances and the all-electric range (AER) of the EV, which is related to the specific electricity consumption while driving.

### Battery utilization factor

In the scope of this work, the battery utilization factor (BUF) is defined to have a better indication of the utilization of the battery capacity of an EV [42]:

$$BUF_e = \frac{E_e^{\text{ch}}}{E_{\text{nom,e}}}, \tag{2.14}$$

with $E_e^{\text{ch}}$ the total yearly electricity charged by vehicle $e$, and $E_{\text{nom,e}}$ the nominal battery capacity of vehicle $e$.

An increased BUF results in a more optimal use of the available battery capacity, i.e. a higher return on investment.

## 2.9 Conclusions

This chapter discussed the background of electric vehicle charging, including the standardization of the EV charging infrastructure. According to IEC 61851-1, mode 3 charging infrastructure allows to adapt the charging current, which allows to coordinate the EV charging process locally. Several local EV charging strategies will be discussed in Chapter 6 that can be implemented locally in the vehicle or in the charging infrastructure, and which rely on mimimum communication and minimum local or (future) EV internal knowledge .

Chapter 7 and Chapter 9 assess the different EV charging strategies in an apartment and office building, respectively, for different grid and fleet impact indicators, as defined in Section 2.8. In Chapter 8, it is investigated how DC grids can further increase the EV penetration rate without violating the grid constraints.

# Chapter 3

# EV mobility behavior modeling

This chapter discusses the EV behavior modeling. Section 3.1 discusses a simulation tool to create a unique driving behavior profile for individual vehicles in a fleet, including the segmentation of the fleet in different vehicle segments. Section 3.2 and 3.3 give a short overview of the specific electricity use while driving and the battery model, respectively. The content of this chapter is based on the following conference paper:

> J. Van Roy, N. Leemput, S. De Breucker, F. Geth, P. Tant, and J. Driesen, "An availability analysis and energy consumption model for a Flemish fleet of electric vehicles," in *European Electric Vehicle Congr.*, Brussels, Belgium, Oct. 2011.

Section 3.1 describes the development of a simulation tool that can be used to create and analyse the driving behavior of individual (electric) vehicles in a Flemish vehicle fleet. A first version of this simulation tool is developed in [158] and [159], based on Dutch mobility studies. In the scope of this dissertation and the Linear project [27], the simulation tool is further expanded to include Flemish statistical data on mobility behavior [160]. This mobility simulation tool is used to generate a unique mobility behavior profile for each vehicle (EVs in this context) in a fleet. This allows to assess the impact of charging EVs, and the impact of charging strategies on both the individual and aggregated level. Both work- and nonwork-related trips have been taken into account. The mobility behavior profile defines when a vehicle is driving or standing still and

the place (not geographically) where it is parked, e.g., at home, at work or at another location.

Section 3.1 also describes the segmentation of a fleet of vehicles in different vehicle segments, i.e. small, medium-class and large vehicles. Section 3.2 describes the calculation of the specific electricity use of EVs during electric driving (kWh/km). The vehicle segmentation and electricity use calculations are based on real vehicle data and statistical driving cycles. A combined driving cycle is used to calculate the average electricity use for each vehicle segment.

## 3.1 Mobility behavior simulation tool

In traffic research, spatial and temporal mobility behavior modeling is a common practice with many different applications. The dynamics of human mobility are important for applications [161–165], such as:

- traffic demand forecast;
- traffic demand management: impact of policy measures on traffic volumes or the travel behavior;
- urban, transportation and infrastructure planning and management;
- psychological impact on human driver behavior.

Detailed mobility data, such as recorded data, can be used to investigate the flexibility of EV charging and their grid impact. However, recorded mobility data is not always available, especially not for EVs because of their low share in the Flemish vehicle fleet anno 2015. To take the stochastic variations of individual users into account, a mobility behavior simulation tool is implemented to create vehicle driving patterns based on available statistical data of present mobility behavior[1]. Combined with a proper EV charging strategy, the results of this simulation tool can be used to calculate the battery charge and grid impact in time.

First, a literature review is given on different mobility behavior modeling techniques in Section 3.1.1. In Section 3.1.2, the different use cases of this simulation tool will be given, including a literature overview in which the results of this tool have been used. The mobility behavior simulation tool is discussed in Sections 3.1.3 – 3.1.6.

[1]No data is available on the mobility behavior sensitivity to the switch to electric mobility. The mobility behavior depends on various factors, including the fuel price, net household income, home location, available vehicle types and other transport means, policy, etc. It may also be expected that people might adapt their type of vehicle to their behavior in order to attain the same comfort.

### 3.1.1 Literature overview

In the literature, many different approaches exist to model the mobility behavior for assessments of a fleet of plug-in (hybrid) EVs. Almost all of the research discussed in this section, makes use of measured or tracked travel behavior data for a specific country. Examples of mobility studies, which have been commonly used in the literature, are:

**Onderzoek Verplaatsingsgedrag Vlaanderen (OVG)** (Flemish Mobility study) commissioned by the Flemish Department of Mobility and Public Works (see also Section 3.1.6) [160].

**Mobiliteitsonderzoek Nederland (MON)** (Dutch Mobility study) from the Dutch Ministry of Infrastructure and Environment [166].

**The National Household Travel Survey (NHTS)** from the US Department of Transportation [167].

**Transportation Secure Data Center (TSDC)** from the National Renewable Energy Laboratory (NREL), combining transportation data from various surveys and studies across the US [168].

**Mobilität in Deutschland (MiD)** (Mobility in Germany) from the Federal Ministry of Transport, Building and Urban Development [169].

**The United Kingdom Time of Use Survey (UKTUS)** from the UK Office for National Statistics [170].

Some research studies, such as [171], use the driving patterns as recorded by the participants in survey diaries. Others generate driving profiles using data sets available from GPS or mobile phone network tracking [161]. However, most research obtains the statistical data from surveys to create activity schedules. From these statistical data, probability distribution functions have been extracted for the departure and return times at home and/or for the duration or distance of trips [113, 172–183].

In some works, only the start and end time of respectively the first and last trip for each day have been defined [113, 179, 181, 183]. Others use a probability distribution function for the EV charging start time, which depends on the chosen charging strategy [173]. Therefore, any presence during the day at home (or other locations) is neglected in the literature, resulting in only one opportunity per day for charging, typically during the evening/night. This is an unrealistic approach since, e.g., from the results in Chapter 5, it is shown that at least 24.2 % of a fleet of vehicles is standing still at home during the day.

Other simplified models define random arrival times, e.g., at home [184, 185] or at the work place [117, 180].

As a consequence of modeling only the departure and/or arrival of respectively the first and last trip of each day, these models need to calculate the initial battery SoC at the start of the charging period. In these models, there is only one charging period each day. To calculate the initial battery SoC, different approaches have been used in the literature:

- calculate energy use from a probability distribution function of the daily distances driven [173, 179, 183];
- randomized initial battery SoC [117, 180, 181];
- fixed initial battery SoC [184];
- fixed distance driven each day [185];
- fixed charging time [180, 186].

In this work, it is opted for to simulate all occurring trips during each day. Hence, the complete driving and activity schedule for each vehicle in the fleet is known. Multiple trips per day are possible, each with varying distances driven. In the simulation tool in this work, it is known for each vehicle at which location the vehicle is parked. However, this is not a geographical location, since it only defines if the vehicle is driving or parked at home, at the work place or at another location. Thus, a spatial component, as modeled in [175, 176], is omitted. Other models use a dynamic traffic model [187] or traffic volume data [180] to define the arrival rate of vehicles at a certain location.

### 3.1.2 Use cases

The simulation tool, as developed in this work, is extensively used for different use cases, such as grid impact assessments (DSO and TSO level) [188], EV charging coordination (slow and fast charging) and grid services.

In [88], the initial version of this tool [158] is used to assess the distribution grid impact of EV charging, to optimize the EV charging for different objectives, V2G applications and the impact on the central electricity generation. This initial version is also used in [105, 159, 189–191]. Recent EV coordination research focuses on different coordination layers, objectives, methods and scales [111].

On the TSO scale, the tool is used to integrate the EV demand response in the unit commitment of the electricity generation [192], and to optimize the portfolio, which includes large-scale RES, of a balance responsible party [100, 107]. Also

the grid impact and the V2G availability is assessed [42, 188]. However, the tool is mainly used on smaller scales: the DSO and building level.

On the DSO scale, coordination is applied on different coordination layers. The EV charging can be coordinated for different objectives, mainly based on a market-based multi-agent system (hierarchical method). Often, they have been benchmarked with the optimal solution. Different objectives have been identified:

- minimizing the charging cost [99–101];
- grid peak-shaving, e.g., to prevent transformer or cable overloading [86, 96, 105, 191];
- respecting the grid voltage limits [96];
- balancing of RES production [193];
- grid services: primary and secondary frequency support [103], imbalance cost reductions [191], and primary reserve capacity [105].

Steps have been taken to adapt this market-based multi-agent system to an event-driven multi-agent system to also include the randomized arrival and departure times of EVs at the charging location [194] or to combine both [98]. Also, local grid constraints have been integrated in this multi-agent control system: a discrete voltage dependent charging behavior in [195–197] and a voltage droop mechanism in the event-driven multi-agent system in [198]. The voltage droop mechanism is introduced for EVs in [128].

Different local EV charging strategies, which require a minimum amount of knowledge and communication, have been introduced in [28, 126, 127].

So far, the literature in this section mainly focuses on EV charging at home and at the work place. In [199], charging at public spaces is investigated, whereas [200] and [201] focus on the EV charging in fast charging stations.

### 3.1.3 Mobility behavior simulation tool

The flow diagram of the mobility behavior simulation tool is shown in Fig. 3.1, which is described in this section. Section 3.1.4 and 3.1.6 describe the data and model assumptions more in detail. This tool is developed in Matlab® .

Mobility behavior is inherently related to the population (who), space (where) and time (when) parameters [202]. The following inputs are required to create the vehicle mobility behavior:

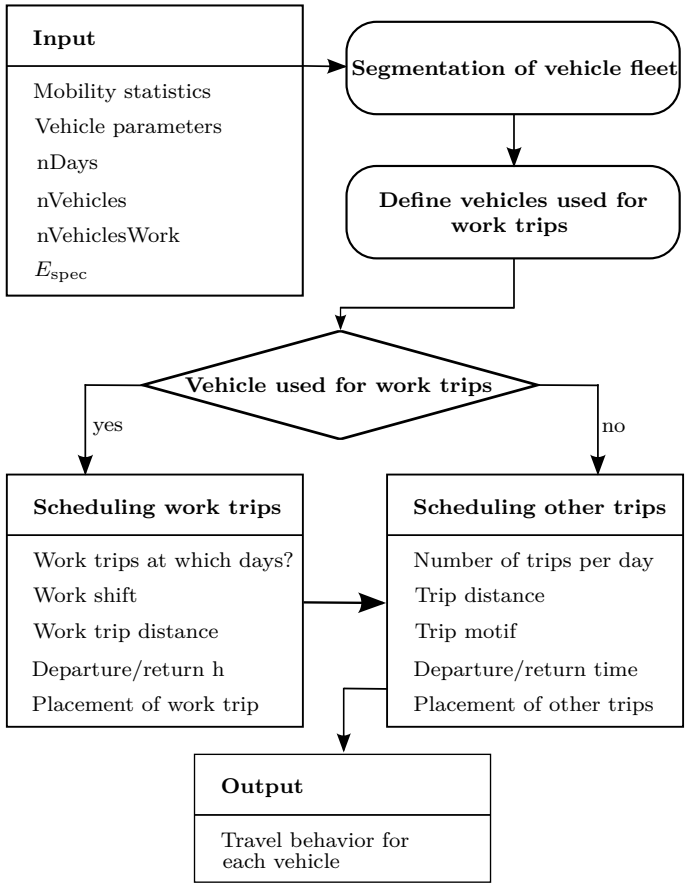


Figure 3.1: Flow diagram of mobility behavior simulation tool.

- the mobility statistics;
  - trip duration distribution function;
  - motif distance scale factors;
  - average number of trips per day;
  - departure/arrival time distribution functions.
- vehicle parameters and fleet segmentation;
  - average speed, which is assumed to be constant (km/h);
  - average yearly distance driven (km);
  - specific electricity consumption $E_{\text{spec}}$ during electric driving (kWh/km).

- number of days (nDays) to simulate ($\leq 365$);
- number of vehicles (nVehicles) to simulate;
- share (%) of vehicles used for work trips (nVehiclesWork).

Using randomization, the mobility profiles are generated using the statistical data on travel behavior. First, the vehicles have been divided in their specific vehicle mobility segment with their respective characteristics, such as the average total yearly distance driven and the specific energy use $E_{\text{spec}}$ while driving electrically. Next, it is defined which vehicles of the fleet are used for work trips.

Trips to and from work are very predictable and can in general be scheduled in time well in advance. Therefore, trips to and from the work place are defined and scheduled first. For the vehicles which are used for work trips, first the days have been defined on which they are used to drive to work. Also the work shift, the trip distance and the departure and return time have been set. To conclude, all work trips and the attendance at work for the whole simulation period have been scheduled.

In the next step, the other trips have been scheduled. For each vehicle in the fleet, the number of other trips for each day have been defined. For each trip, the trip distance and motif are set. In function of the motif, the distance can be scaled, and the departure and return times can be defined. Afterwards, the trips can be scheduled, while keeping in mind that no other trips (except for business trips) may overlap with work trips. Compared to other work in the literature [174], trips or activities may cover parts of two days.

The mobility behavior simulation tool gives the following outputs (at a 1 min time resolution), related to the mobility behavior for each individual vehicle in the fleet:

- vehicle characteristics, such as the vehicle segment, yearly driven distance, which days used for work trips, etc.;
- unique mobility behavior profile;
- electricity consumption, which is used for the SoC calculations when driving fully electrically[2].

Fig. 3.2 shows an example of a mobility behavior profile that is generated with this mobility behavior simulation tool. In this example, a random vehicle, which is used for trips to work (part-time), is shown for three consecutive days. Besides the work-related trips in this example, also four other trips have been planned with different motifs, i.e. recreation, visit and other trips.

[2]Note that this model does not make a distinction in the type of electric vehicle (ICE, HEV, PHEV or BEV).

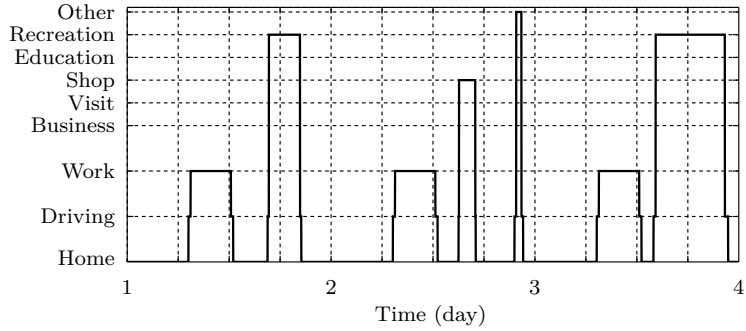


Figure 3.2: Sample mobility behavior profile (three consecutive days).

### 3.1.4 Data sources

The 3rd Flemish Mobility Study (OVG3) is used as main data source (a 1 h time resolution) for the statistical data on mobility behavior (see Section 3.1.6) [160]. Other data have been taken from the Belgian automotive and cycle federation (Febiac[3]) [203], the Belgian Statistics from the Federal Public Service Economy (FPS Economy – Statbel[4]) [31] and the Federal Public Service Mobility and Transport (FPS Mobility and Transportation[5]) [204].

### 3.1.5 Segmentation of vehicles

In the present vehicle fleet, there is a large difference in mobility behavior regarding distances driven each year. A segmentation is assumed for fuel type and the present distribution in engine displacements for these fuel types. Thus, the vehicles have been divided in segments, based on the present vehicle characteristics. It is assumed that mobility behavior will not change when switching to EVs, as defined in Section 3.1.

In Flanders, the share of diesel vehicles is relatively high, i.e. 60 %. The small fraction of LPG (less than 1 %) is neglected [203]. Presently, gasoline cars drive on average 8545 km per year, versus 19 340 km for diesel cars [31, 203, 205][6]. This results in a yearly average of about 15 000 km per vehicle in the fleet, which is consistent with [160] and [205].

[3]De Belgische federatie van de auto- en tweewielerindustrie.
[4]FOD Economie – Statbel.
[5]FOD Mobiliteit en Vervoer.
[6]No information available to define a distribution of the yearly distance drivens driven as a function of the fuel type.

Three vehicle types $s$ have been used to differentiate the EVs in a fleet into different vehicle segments, with:

$$s \in \mathcal{S} = \{\text{small}, \text{middle-class}, \text{large}\} \text{ vehicles}. \tag{3.1}$$

It is assumed that these vehicle types $s$ coincide with the present engine displacements, i.e. $< 1.4\,\text{l}$, $1.4 - 2.0\,\text{l}$ and $> 2.0\,\text{l}$ [205][7]. These vehicle segments are equivalent to the present fleet segments, which is similar to [206]. For each vehicle type $s$, two representative vehicles have been taken. These representative vehicles and their physical characteristics are listed in Appendix A.1.

Table 3.1 shows the distribution of the vehicles according to the fuel type and engine displacement [205]. Small engine displacements are typically found in gasoline cars. The table also includes the average yearly distance traveled by each vehicle segment. Section 3.2 discusses the specific electricity use of these different vehicle segments.

Table 3.1: Vehicle segmentation according to the fuel and engine displacement [31, 203, 205].

| | **Share (%)** | | **Average distance** (km) | |
|---|---|---|---|---|
| **Engine** | **Gasoline** | **Diesel** | **Gasoline** | **Diesel** |
| $< 1.4$ l | 22.64 | 4.86 | 7960 | 18 045 |
| $1.4 - 2.0$ l | 14.36 | 44.40 | 9095 | 19 565 |
| $> 2.0$ l | 3.00 | 10.74 | 10 335 | 18 955 |
| | 40.00 | 60.00 | 8545 | 19 340 |

### 3.1.6 Flemish statistical data on travel behavior

The 3rd Flemish Mobility Study (OVG3) is conducted between September 2007 and 2008 among 8800 people ($\geq$ 6 years old) [160][8]. This research is commissioned by the Flemish government (Department of Mobility and Public Works). The people surveyed, were asked to keep track of all their trips and the respective transport means, including information such as the number of trips per day, the distance (and duration) of trips, the motif of each trip and the departure and return times for each trip, etc. This approach is similar to keeping track of activity schemes to model the electricity demand of households [207].

[7] Currently, there is a trend towards smaller engine displacements. Therefore, these distributions might change in the future.

[8] Since September 2008, OVG4 is conducted, each year among about 1600 people.

The available statistical data in OVG3 compromise the average daily behavior of the Flemish population. No geographical data is available in the report.

In the context of this dissertation, only the vehicle trips have been considered. A distinction has been made between weekdays and weekend days in order to consider the difference in travel behavior. Other differences, such as holiday or seasonal differences, have not been taken into account, due to the lack of data. This section discusses the statistics to set up the mobility behavior simulation tool. Compared to the literature (see Section 3.1.1), the simulation tools accounts for many uncertainties for mobility behavior, by making use of the available probability density functions, e.g., for the departure and arrival times, the trip distance, etc.

### Number of vehicles per household

On August 1, 2014, the Belgian vehicle fleet consisted of 5 555 499 passenger vehicles (+1.1 % compared to 2013), of which 1792 have an electric motor[9] (+95 % compared to 2013) [31]. Table 3.2 gives the number of vehicles per household [160]. The average number of vehicles per household is about 1.1. Therefore, one vehicle per household is assumed in this dissertation.

According to [208], about 20 % of the employees in Belgium have a company car. Another report states that between 6 and 10 % of all registered cars in Belgium are company cars [209]. In this dissertation, no distinction in mobility behavior has been made between personal and company cars.

Table 3.2: Number of vehicles per household [160].

| **Number of vehicles** | 0 | 1 | 2 | $\geq 3$ |
|---|---|---|---|---|
| **% of households** | 18.21 | 53.65 | 24.75 | 3.39 |

### Number of vehicle trips

On average, there are 3.14 trips per day per person by all transport means. 65 % of all trips are by means of a passenger vehicle (as driver or passenger). Other important transport means are by foot (13.4 %) and by bike (14.2 %). Of these vehicle trips, 1.47 trips are as a driver. Considering an average of 2.3 inhabitants per household [31] and assuming one vehicle per household, this results in 3.39 trips per day per vehicle. During the week, on average more trips per day are driven (3.60) compared to 2.85 during the weekend.

[9] Plug-in hybrid (PHEV) and battery electric vehicles (BEV).

A trip is defined as the trip from home to the activity and back home. This approach is justified, as about 73.4 % of all trips are limited to one activity [160]. However, a vehicle may start an activity chain in the simulation tool. Thus, different consecutive activities and trips can take place by starting another trip while being present at another activity or while driving home from a previous activity. During office hours, only other business trips can start.

### Trip duration

Fig. 3.3 shows the probability distribution function for the duration of vehicle trips [160]. The sum under the graph is equal to the average number of trips per day per vehicle, which is 3.39 trips per day. Therefore, this distribution function is scaled for week and weekend days. This figure already shows that the average duration of a trip is relatively short, which may indicate that a large part of the trips may be covered electrically with a modestly sized battery.

On average, vehicles are driven for about 41 km per day during just less than an hour [31, 160]. Therefore, a constant average speed $v$ of 42 km/h has been assumed for each modeled trip. Speed variations have been taken into account for the calculation of the specific electricity use during electric driving by using representative driving cycles (see Section 3.2).

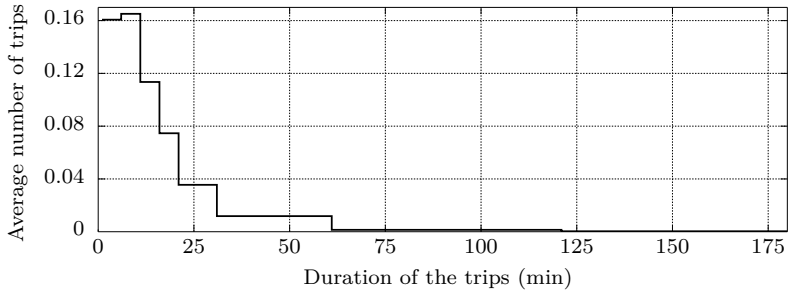


Figure 3.3: Distribution of the average number of trips as a function of the duration of a trip [160].

### Trip motifs

Vehicle trips have been categorized in different motifs $m$, being work-related and nonwork-related trips:

$$m \in \mathcal{M} = \{\overbrace{\text{work}, \text{business}}^{\text{work-related}}, \underbrace{\text{visit}, \text{shopping}, \text{education}, \text{recreative}, \text{other}}_{\text{nonwork-related}}\}. \quad (3.2)$$

Table 3.3 gives the probability of occurrence for the different motifs[10] during week and weekend days[11] (excluding trips to and from work). Fig. 3.3 shows the distribution of the average number of trips as a function of the duration of a trip. An extra scale factor for the trip duration is required, since the average distance differs for the different trip motifs. For instance, shopping trips are on average shorter than work or business trips. Table 3.4 shows the distance scale factors for each motif.

Table 3.3: Probability (%) for a motif for week and weekend days (excluding work trips) [160].

| Motif | Week | Weekend |
|---|---|---|
| Business | 8.54 | 2.07 |
| Visits | 12.50 | 19.38 |
| Shopping | 23.82 | 28.45 |
| Education | 10.52 | 0.82 |
| Recreation | 23.56 | 32.42 |
| Others | 21.06 | 16.86 |

Table 3.4: Distance scale factors for the different trip motifs [160].

| Motif | Factor | Motif | Factor |
|---|---|---|---|
| Work | 1.37 | Education | 1.13 |
| Business | 1.92 | Recreative | 1.00 |
| Visits | 0.99 | Others | 0.76 |
| Shopping | 0.51 | | |

[10]The motif *others* include motifs such as picking up someone, a doctor visit, etc.
[11]Saturdays and Sundays have been assumed to be identical.

### Trips to the work place

The trips to and from the work place are handled first. During presence at the work place or the trip to work, no other trips but business trips may overlap. Therefore, trips to and from the work place are handled separately from the business and nonwork-related trips. About 82 % of the people have fixed working hours [160]. Thus, trips to and from work are predictable and can be scheduled well in advance.

In 2010, about 67.1 % of all working people, traveled to work by car [204]. According to [31], about:

- 54 % of the Flemish population ($\geq$ 18 years old) were active on the labor market.
- 69.9 % of the Flemish population (18 – 64 years old) were active on the labor market.

This results in about 36.2 – 46.9 % of all vehicles being used for work-related trips, with the assumption that there is only one vehicle per household. Households with working people have in general a higher net income. According to [160], these households have a higher number of vehicles [160]. Therefore, it is expected that the actual number is closer to 46.9 % of all vehicles to be used for work-related trips[12].

The average commuter distance in Flanders is 18.82 km. 82 % of the people live at a distance of less than 30 km from their work [160]. For each vehicle in the fleet, used for work-related trips, the commuter distance of the work trips is defined using Fig. 3.3[13] and using the scale factor in Table 3.4. The commuter distance is fixed for each vehicle.

On weekdays, the probability of a work-related trip is 65.81 %, while in the weekends only 13.01 % of the working people go to work [160]. A fixed work shift $w$ is assigned to each vehicle (see Table 3.5):

$$w \in \mathcal{W} = \{\underbrace{\text{day}, \text{morning}, \text{afternoon}, \text{night}}_{\text{full-time}}, \text{part-time}\}. \tag{3.3}$$

Depending on the work shift, the departure and return hour have been defined according to the distribution functions given in Fig. 3.4 [158]. Similar to the

[12] For the residential case in Chapter 6, 46.9 % of all vehicles have been assumed to be used for work-related trips, whereas for the office building in Chapter 9, all vehicles in the fleet are used for work-related trips.

[13] Fig. 3.3 is normalized, since it is assumed that a vehicle is only used for a maximum of one trip to work a day.

Table 3.5: Probability (%) for a work shift [158].

| **Shift** | **Probability** | **Shift** | **Probability** |
|---|---|---|---|
| Day | 73.3 | Night | 6.8 |
| Morning | 3.7 | Part-time | 12.5 |
| Afternoon | 3.7 | | |

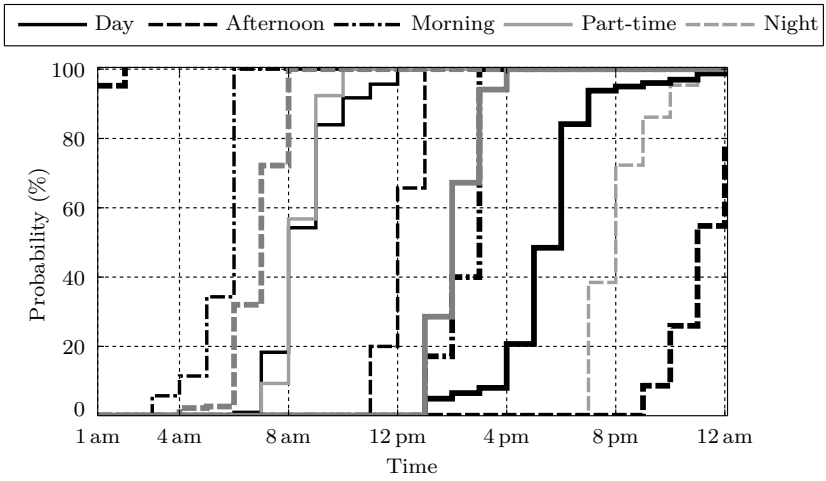


Figure 3.4: Cumulative probability density function for departure (thin line) and return (thick line) hour for work shifts [158].

commuter distance and the work shift, this departure and return hour (on an hourly resolution) are fixed for each vehicle. This is an acceptable assumption, since about 82 % of the population have fixed working hours [160]. To introduce some daily variation, the exact moment of departure and return (on a minute resolution) is variable. A uniform probability distribution function is used to determine the exact departure and return minute. It is assumed that the return trip is within 24 h. This means that trips, as is also the case for the other trips, are not limited to take place on just one day.

### Other trips

Different motifs are available for the nonwork-related trips (see Table 3.3)[14]. For each motif, OVG provides a probability distribution function for the departure and return times [160]. For each motif, two probability distribution functions have been defined, for trips during the week and weekend, respectively. However, the distribution function for the return times is not given as a function of the departure times, nor a distribution of the total activity duration (including the trip duration) is available. This could lead to less reliable results (e.g., picking up someone takes a whole day, even if the distance is limited). Therefore, the data from OVG is adapted and the following assumptions have been taken:

- **Variable activity duration:** Probability distribution functions for both the departure and return hours have been used. It is assumed that education trips end the same day.
  **Motifs**: Business, education, recreative
- **Fixed activity duration:** The total duration of the activity (trip and presence at the activity) is fixed. Only the probability distribution functions for the departure hour have been used.
  **Motifs**: Visits (180 min), shopping (120 min), others (60 min)

Work-related trips are scheduled first. To define the number of the other trips, Fig. 3.3 is scaled when a work trip is scheduled during a day. The scale factors in Table 3.4 have been used to define the distance for each scheduled trip.

As to the scheduling of the other trips in time, a distinction is made between business trips and the other motifs:

- **Business trips** may overlap with work trips. These can also take place on days without a work trip. Furthermore, it is not only possible to start a business trip at work, but also on the way to or from work.
- **Other trips** have more constraints. There is no overlap with trips to work and the time at work. These trips will be placed before or after work[15]. It is also important to take into account any work trip during the next day. These other trips may overlap with each other.

[14]Note that also business trips have been taken into account in this paragraph.
[15]The constraints are checked as the profiles are generated.

### 3.1.7 Results

The results of the mobility behavior regarding the driving behavior (number of vehicles on the road) and the analysis of the different EV charging location opportunities, will be discussed in Chapter 5.

### 3.1.8 Future work

The mobility behavior simulation tool is implemented based on a number of assumptions, due to the unavailability of actual data. Therefore, an overview is given of some future possible additions to improve the simulation tool.

The behavioral functions are an important determinant in the use of vehicles and their total energy demand. For instance, the ownership and the use of vehicles, including EVs, heavily depend on, e.g., the composition of household, the net income and the age of the inhabitants [160]. This is comparable to the impact of these factors on the electricity and heat demand in buildings [210–214]. The fleet of vehicles could be segmented according to behavior as a function of these parameters.

A distinction is made between week and weekend days in order to consider the difference in travel behavior. Seasonal variations, such as holiday periods, can also be taken into account to include possible trips with longer distances. Also, the available data in OVG allows to make a distinction between the different days during the week and weekend.

Other possible additions (non-exhaustive list) are:

- The duration of an activity absence and the return time do not yet depend on the departure time, since this data is not available.
- It is expected that there is a difference in mobility behavior between personal and company cars. However, in the present model the behavior is assumed to be identical.
- Now, every trip is driven at the same average speed (42 km/h), which can be made dependent on the trip distance. Related, real driving profiles, as for instance shown in Appendix A.2.4 and the literature [215], can be used to attain energy efficiency variations between trips, e.g., as a function of the trip length.

## 3.2 EV energy efficiency calculation

In Section 3.1.5, the EVs in a fleet have been divided into different vehicle segments, which are equivalent to present fleet segments. This section describes the calculation of the specific electricity use while driving electrically (kWh/km) of the different vehicle segments for representative driving cycles. The specific electricity use of EVs is an important parameter to calculate the battery SoC. In the literature, a large range of values is presented. Here, this parameter is calculated for different representative driving cycles. The calculations are based on the battery model used in [153] (see Section 3.3).

### Calculation of the specific electricity use

The specific electricity use is calculated with physical vehicle parameters (as defined in Table A.1 in Appendix A.1) and different drive cycles (urban, rural, highway or mixed). These parameters have a significant impact on the energy use.

The methodology and required parameters for the specific energy use calculations is shown in Appendix A.2.

### Representative driving cycles

A representative driving cycle is composed with American test cycles. The American cycles (see Fig. A.1 in Appendix A.2.4) have been preferred instead of artificial European cycles for emission testing. The US test cycles have been based on real traffic behavior [216].

More background on the use of these drive cycles and the calculation of a combined driving cycle has been given in Appendix A.2.4.

### Results

The specific electricity consumption for respectively the small, medium-class and large vehicles is 0.185, 0.220 and 0.293 kWh/km. Compared to [85], an extra correction factor of 15 % on the specific power consumption is used to take the impact of the ambient temperature, wind, altitude, road grade and surface into account [217].

In [85], a sensitivity analysis on different parameters is also performed. Since this sensitivity analysis is out of the scope, this is not included here.

## 3.3 Battery model

The battery model is implemented with dynamic SoC equations and battery parameter constraints [153]. The physical model description and Modelica implementation will be described in Section 4.5.

## 3.4 Conclusions

To investigate the electricity grid impact of EV charging and to assess the EV charging flexibility, the knowledge on the mobility behavior and specific energy use while driving is required. Detailed mobility data, e.g., recorded data, is not always available, especially not for EVs.

Therefore, a detailed mobility behavior simulation tool, which takes into account the stochastic variations of individual users, is set up to create vehicle driving patterns for a Flemish fleet of EVs. This chapter thoroughly discussed the different parts of the EV mobility behavior modeling, regarding:

- the mobility behavior modeling tool to create and analyse the driving behavior profiles of (electric) vehicles in a Flemish fleet of vehicles.
- the segmentation of the fleet in different vehicle segments with each segment their respective specific electricity use during electric driving.

The driving patterns describe when a vehicle is driving, and when and where (not geographically) the vehicles are parked. The simulation tool is extensively used at the KU Leuven and partner institutions for different use cases, such as grid impact assessments, EV charging coordination and grid services [28, 42, 86, 96, 98–101, 103, 105, 107, 126–128, 188, 191–198, 200, 201].

The simulation tool uses the statistical data from a Flemish mobility study. This data includes the departure and return times, the duration of trips, the motif of a trip, etc. Compared to a majority of the literature, multiple vehicle trips are possible per day. Hence, the complete driving and activity schedule for each vehicle in the fleet is known. This means that multiple EV charging opportunities at different places (e.g., at home and at the work place) during one day are possible. Also, a difference in mobility behavior between week and weekend days, and vehicle segments is taken into account.

Chapter 5 discusses the results of this mobility behavior simulation tool more in detail.

# Chapter 4

# Energy system integration: Electrical modeling in buildings and districts

The energy systems in buildings and building districts consist of several energy sources, e.g., renewables and fossil fuels, and carriers, e.g., electricity and heat. The integration and interaction of these sources and carriers have become more interwoven in recent years. This is shown schematically in Fig. 4.1 for the integration of different electrical systems and networks in buildings and districts. Multiple domains become more integrated with these electrical systems, such as heating by means of a heat pump or CHP, electrical and thermal energy storage, ICT services for control purposes, etc.

The IDEAS library provides a comprehensive Modelica library to model and simulate the integration of multidisciplinary energy systems in individual buildings and neighbourhoods/districts for energy and thermal comfort simulations. IDEAS is the acronym for *Integrated District Energy Assessment by Simulation*. IDEAS is jointly developed by the Applied Mechanics and Energy Conversion[1], Building Physics[2], and Electrical Energy[3] divisions at the University of Leuven (KU Leuven) [19, 218, 219].

This chapter first focuses on the advantages of energy system integration (ESI) regarding electrical modeling (Section 4.1). Section 4.2 discusses the IDEAS

[1] `http://www.mech.kuleuven.be/en/tme`
[2] `http://www.bwk.kuleuven.be/bwf`
[3] `http://www.esat.kuleuven.be/electa`

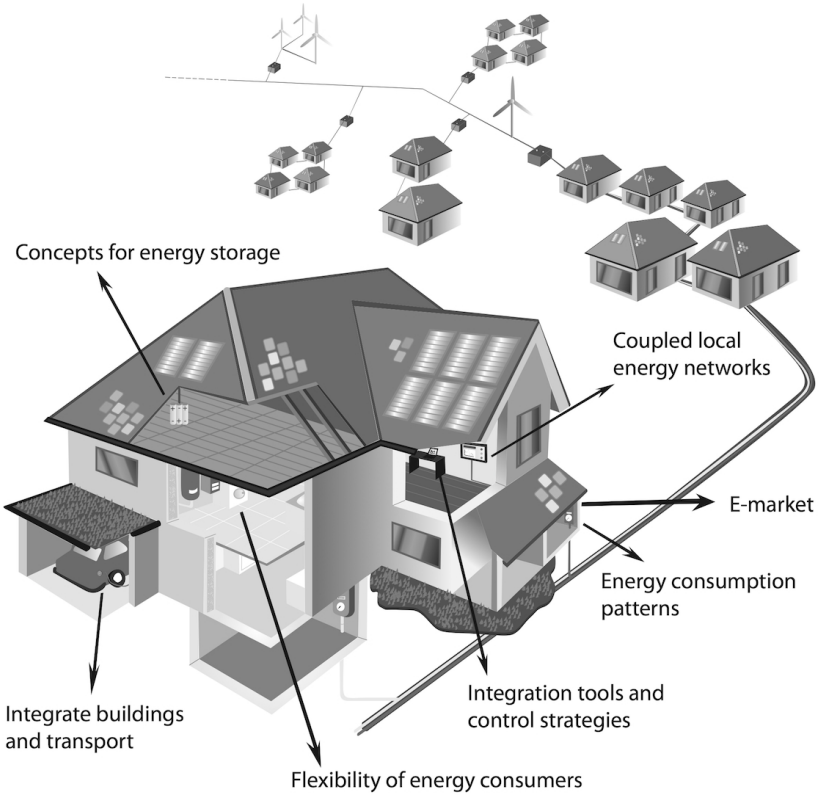


Figure 4.1: ESI in buildings and districts (Source: KU Leuven/Electa – Nathalie Belmans).

library, and more specifically the electrical modeling sublibrary. Sections 4.3 – 4.5 discuss the modeling background of the electricity distribution grids, loads and generation units, and battery storage and EVs, respectively.

The content of this chapter is based on the following peer-reviewed article and conference paper:

J. Van Roy, B. Verbruggen, and J. Driesen, "Ideas for tomorrow: New tools for integrated building and district modeling," *IEEE Power Energy Mag.*, vol. 11, no. 5, pp. 75–81, Sep. 2013.

J. Van Roy, R. Salenbien, and J. Driesen, "Modelica library for building and low-voltage electrical AC and DC grid modeling," in *Proc. of the 10th Modelica Conf.*, Lund, Sweden, Mar. 2014, pp. 301–309.

## 4.1 Energy system integration

As individual buildings and district energy systems have been evolving towards smart buildings and smart grids, the different energy sources, carriers and the connections between the different energy systems, become increasingly integrated. This poses new challenges for the simulation tools allowing the simultaneous modeling and simulation of multidisciplinary energy systems (ESI).

Traditionally, the simulation and assessment of buildings, thermal building systems, and electrical systems have been performed in their respective simulation tools. Different tools are available to simulate the various domains separately, but they are only of limited use for integrated modeling. Therefore, the impact on, or the (possible) interactions with the other domains have often not or simplified been taken into account.

As discussed earlier, the different climate and energy targets that have been adopted in Europe and globally at the level of buildings and the electricity system have been leading to an increased energy efficiency of buildings and energy systems, and the integration of renewable and distributed energy sources in buildings, such as PV systems, and CHPs. On the other hand, other technologies, such as EVs and heat pumps, have been increasing the energy efficiency of the whole energy system. As a result, this has some consequences regarding the electricity system, among them:

- an increase in the electricity use (e.g., heat pump and EV);
- an increasing non-simultaneity of local production and consumption of electricity due to the intermittent and non-controllable electricity generation profile of local generation;

This may lead to an increasing grid impact due to an increasing demand and injection of electricity into the grid (see Section 2.5). To maximize the integration of these systems, it is important to integrate all energy systems, including control systems, in simulations. For instance, ESI can be used for the following assessments:

- Easily assess the impact and interaction with other energy systems. For instance, the assessment of the distribution grid impact of a heat pump for a change in building design.

- Integrated control to control systems based on the operating point of another system. For instance, the curtailment of PV systems based on the grid voltage.
- Using the available technology operation flexibility to limit the grid impact without impacting the comfort requirements.
- ...

This indicates the importance of ESI in building and district simulations to obtain better system design, demand-side management, and storage solutions [220]. By making use of ESI, the unique benefits of each system can be utilized, while maintaining comfort and robustness levels and improving system efficiency levels.

This is also recognized by the recently started IEA EBC Annex 60 regarding the use of Modelica for *New generation computational tools for building and community energy systems*, in which the KU Leuven is involved [221]. The objectives of the IEA EBC Annex 60 are to develop and demonstrate next-generation computational tools that allow building and community energy systems to be designed and operated as integrated, robust, performance based systems. One activity is dedicated to the design and requirements of district energy system simulation tools.

## 4.2 The IDEAS library, including an electrical sublibrary

IDEAS, *Integrated District Energy Assessment by Simulation*, allows a simultaneous transient simulation of thermal and electrical systems at both building and feeder level (see Fig. 4.2). For neighbourhood/district modelling, the interactions between the buildings and the electricity distribution grid is taken into account.

### 4.2.1 Overview IDEAS library

IDEAS allows to describe the built environment, energy use and supply, network and control in one model, which allows to perform more effective analyses and better control of the energy system under consideration. Fig. 4.3 shows an overview of the different sublibraries in IDEAS: climate, building and occupant, thermal (HVAC) systems, electrical systems and the possibilities for integrated

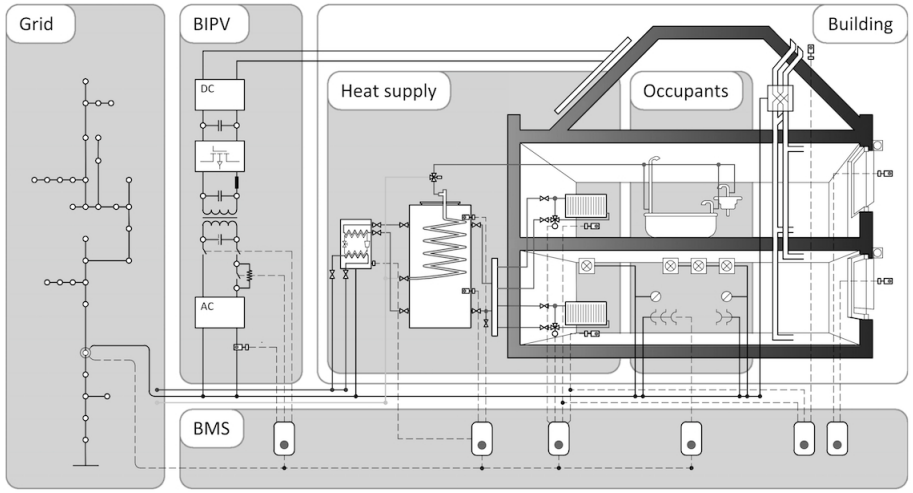


Figure 4.2: A schematic overview of the IDEAS tool [218].

control. These different components can be easily interconnected for ESI, as shown for instance in Fig. 4.2.

The boundary conditions (BC) library is required to calculate the heat gains and heat losses in the buildings, the solar shading and the PV power production. In this dissertation, the Meteonorm system [222], typically used in Europe, is taken as a source for weather data.

The building library consists of a dynamic multi-zone building model, which allows to simulate the heating and cooling energy demand of a building, the energy flows in a building and the interconnection with the thermal and electrical systems.

In the thermal system library, models for heating and cooling systems are available, such as heat pumps for space heating and domestic hot water buffers for storage, boilers, floor heating, ventilation, etc. These thermal systems are used to meet the comfort requirements in the building.

The overview of the sublibrary for electrical modeling is given in the following section.

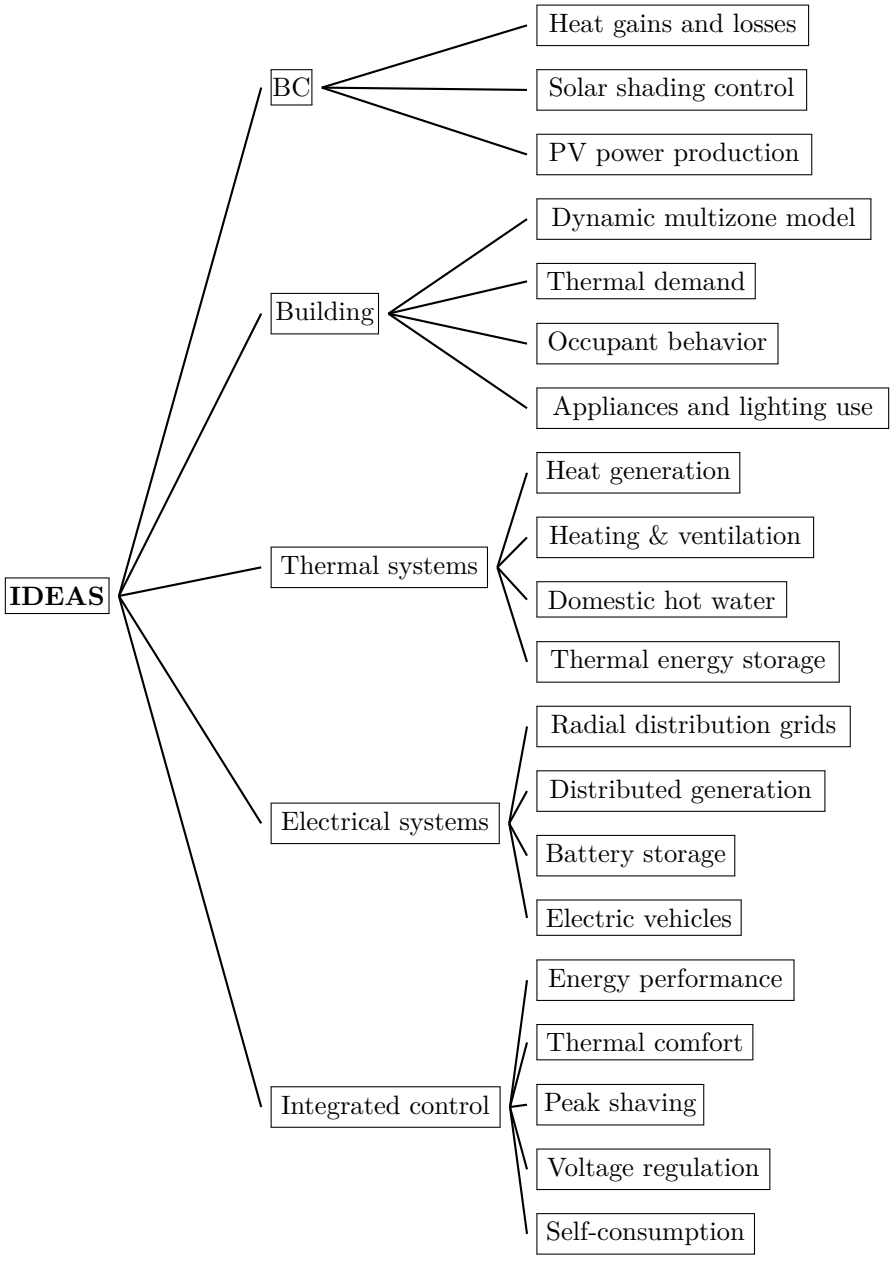


Figure 4.3: The IDEAS sublibraries, including a non-exhaustive list of possible assessments.

### 4.2.2 Electrical modeling in Modelica

The electrical component library, developed together with Bart Verbruggen [29], consists of models to simulate[4]:

- radial AC and DC electricity distribution grids, both in-building and LV distribution grids;
- photovoltaic systems;
- battery storage systems;
- electric vehicles;

The grid-modeling capabilities include:

- low-voltage and in-building AC distribution grids, both single- and three-phase unbalanced grids;
- in-building unipolar DC distribution grids.

LV distribution grids connect different buildings and energy systems within districts, while electricity grids in buildings connect the different electrical loads and generation units within the building. Both grid types are typically radial. Therefore, the models are similar. The electricity grid topologies are described using only the incidence (or connection) matrix and the cable impedance matrix. This makes for a very flexible and scalable approach to the modeling of electricity grids. Grid variables, such as nodal voltages and power exchanges, can serve as an input to control strategies of appliances (to shift or adapt their operation), e.g., to assure that grid constraints are not violated.

The PV system model simulates the electricity power production of one PV panel, as a function of the tilt angle and orientation, based on parameters from existing panels on the market and meteo data.

The battery storage model in IDEAS can be used to simulate both decentralized and centralized storage units in grids or buildings. Since most electric vehicles use batteries as storage units, the same battery model is reused in the EV model.

The electrical modeling sublibrary has been used for several purposes, such as assessing the LV distribution grid impact of residential net zero-energy buildings with heat pumps and building integrated PV systems, including a curtailment system for the PV systems as a function of the grid voltage [19, 218, 223], and assessing the LV distribution grid of electric vehicle charging in buildings [126].

[4] Part of this sublibrary is discussed more in detail in [29].

### 4.2.3 Models developed in the scope of this dissertation

The library, which is discussed in this chapter, is based on work in cooperation with Bart Verbruggen [29, 224]. A library is co-developed, which allows the simulation of:

- unbalanced three-phase AC grids;
- balanced three-phase AC grids, which can be represented as an equivalent single-phase grid.

In the scope of this dissertation, this work is further extended with:

- unipolar DC grids in buildings;
- single-phase AC grids in buildings;
- battery energy storage;
- electric vehicles.

### 4.2.4 The use of Modelica as a simulation tool

IDEAS is implemented in the Modelica® modeling language, using the Modelica Standard Library (MSL), which is available as an open source library [225]. The MSL contains a sublibrary with multiple base models for analog and quasi-stationary electrical modeling. Dymola is used as the Modelica simulation environment, which allows both textual and graphical modeling [226].

Modelica is an open-source, object-oriented, and equation-based (using differential and algebraic equations) modeling language [225, 227, 228]. It is well suited for physical modeling and offers an easier integration of different domains in a single model. The object-oriented approach in Modelica offers a flexible use of the different models, while introducing scalability and inheritance between models. For instance, the models can be simulated in their respective domains before interconnecting them. This is useful for the development, testing, and validation of models.

### 4.2.5 Availability of IDEAS

The IDEAS library is available as an open-source library under the Modelica Licence Version 2[5]. Open-IDEAS v0.2 (and other development versions) is

[5] `https://www.modelica.org/licenses/ModelicaLicense2`

available online at `https://github.com/open-ideas/IDEAS`. The IDEAS library is developed and tested in Dymola.

A large part of the library is already well-documented, and a manual is available describing the specifications, model descriptions, validation and verification results. Validation of the models is done through comparative testing, verification-only, and verification and validation based on manufacturer data or literature. Various scientific publications describe the different sublibraries and models [19, 218, 229]. The developers of IDEAS have also been co-leading the IEA EBC Annex 60 regarding *"new generation computational tools for building and community energy systems based on the Modelica and Functional Mockup Interface standards"* [221].

### 4.2.6 Advantages and unique selling points of IDEAS

It is possible to assess the integration, interaction, control and feedback of multidisciplinary energy systems (such as building physics aspects, thermal HVAC systems, electrical systems, etc.), buildings and district systems in one single simulation model. IDEAS provides a flexible use of the different models. Models can be separately simulated in their respective domains and they can be combined for energy system integration.

The added values of IDEAS are:

- **Multidisciplinary** assessments of energy systems in buildings and districts/neighbourhoods.
- **User friendly:** documented models, examples available, parameter studies.
- **Post processing and reporting** possible in simulation environment (e.g., Dymola) or other tools (e.g., Python and Matlab).
- **Data** available in the library based on scientific literature or data sheets. User can overwrite or add new data.
- **Detailed** models available: models of different degree of detail.
- **Granularity:** output time scale can be chosen; input data with different time scales can be handled.

## 4.3 AC and DC electricity grid modeling

As stated in Section 4.1, there is a need to include the electricity grids for ESI modeling and simulations for different reasons:

- Assessing the grid impact of different energy systems.
- Assessing the interaction of different energy systems and the electricity grid.
- Integrated control of the different energy systems (using their operation flexibility) based on the grid conditions.

In this library, quasi-stationary simulations are possible for the following grid types:

- low-voltage and in-building AC distribution grids, both single- and three-phase unbalanced;
- in-building unipolar DC distribution grids.

An alternative Modelica library regarding electricity grid modeling is for instance the SPOT library [230], which allows both steady-state and transient simulations in one framework by using a transformation to represent the multi-phase electric systems. Transient simulations are out of scope in the framework for which the IDEAS library has been developed, and according to [230], the alternative representation has a slower simulation speed for non-linear systems. Other Modelica libraries are available, which use the modeling techniques of the SPOT library: the Electric Power Library (commercially available) [231], the PowerSystems library [232], and the District library recently developed at the Lawrence Berkeley National Lab [233].

First, this section gives a brief background on electricity grids and power flow analysis (Section 4.3.1). The functional requirements of the grid simulation tool will be discussed in Section 4.3.2, before giving the physical model description (Section 4.3.3) and the basics of the Modelica implementation (Section 4.3.4).

### 4.3.1 Background electricity grids and power flow analysis

Two types of electricity grids exist in the power system, namely distribution and transmission grids [234]. Distribution grids (low to medium voltage level) often differ fundamentally from transmission grids (high voltage level):

- Transmission grids are typically meshed grids, whereas distribution grids are typically radially. Radial grids only have one point of common coupling (PCC). This reduces the reliability of the network. In case of a fault, all loads behind the fault are switched off.
- The R/X (resistance/reactance) ratio increases for lower voltage levels. Thus, LV residential distribution grids are highly resistive.

Electricity grids in buildings are similar to LV distribution grids. Both are radially exploited, meaning there is a single feeding point, e.g., a transformer in a LV distribution grid. Loads can be single or three-phase connected to the in-building grid, whereas buildings can be single or three-phase connected to the distribution grid. Electricity grids in buildings can be a combination of different single and three-phase cables which connect the loads, whereas LV distribution grids are typically three-phase grids (in Europe) with a single or three-phase connection to buildings.

To assess the grid impact, a power flow analysis tool is developed in Modelica. Therefore, a physical grid model is developed in IDEAS which allows to assess this grid impact, similarly to traditional power flow analysis tools. A power flow analysis is performed to obtain the voltage and current information in each node and line of the electrical grid, based on the Laws of Kirchhoff:

**Kirchhoff's current law: Conservation of electric charge**
The sum of currents $I_l$ flowing into a node is equal to the sum of currents flowing out of a node:

$$\sum I_l = 0. \tag{4.1}$$

**Kirchhoff's voltage law: Conservation of energy**
The sum of the voltage drops $v_l$ in any closed circuit is zero:

$$\sum v_l = 0. \tag{4.2}$$

The voltage drop in a line $l$, $\Delta v_l$, between nodes $n$ and $n+1$ is defined as:

$$\Delta v_l(t) = v^n(t) - v^{n+1}(t) = Z_l i_l(t), \tag{4.3}$$

with $Z_l$ the impedance of the line and $i_l$ the line current. When the nodal currents, line currents and nodal voltages are known, the apparent power $S$ in one phase $p$ can be calculated. $S$ consists of active power $P$ and reactive power $Q$:

$$S_p(t) = P_p(t) + jQ_p(t) = v_p i_p^*, \tag{4.4}$$

with a non-linear relation between $S_p$, $v_p$ the phase voltage and $i_p^*$ the complex conjugate of the total phase current $i_p$. The total apparent power is calculated as $S(t) = \sum_p S_p$. For DC grids: $Q = 0$.

The joule losses $P^{J,\text{grid}}$ in a grid are the sum of the losses in all phases and neutral (or negative) conductor. The joule losses in a line $l$ are calculated as follows:

$$P_l^{J,\text{grid}} = R_l |i_l|^2, \tag{4.5}$$

with $R_l$ the resistance of a line $l$. Note that also the reactive current is responsible for a part of the losses.

The non-linear system requires numerical methods to obtain a solution for the power flow analysis. Direct and iterative methods exists. Typically, the *backward-forward sweep* is used [229], which is well suited for radial grids. For instance, the model for three-phase unbalanced grids in [153] makes use of this iterative method. In Dymola, different solvers are available to solve the power flow analysis, e.g., the DASSL solver [235].

### 4.3.2 Functional requirements

In the scope of the IEA EBC Annex 60, functional requirements[6] have been defined for integrated building and district modeling tools during design and operation [221]. This section focuses on the functional requirements for the electricity grid models developed within IDEAS.

The library, which is discussed in this chapter, is based on work in cooperation with Bart Verbruggen [29, 224]. A library is co-developed, which allows the simulation of:

- unbalanced three-phase AC grids;
- balanced three-phase AC grids, which can be represented as an equivalent single-phase grid.

In the scope of this dissertation, this work is further extended with:

- unipolar DC grids in buildings;
- single-phase AC grids in buildings.

#### Quasi-stationary modeling

Different types of grid simulation tools exist: from static to dynamic transient modeling tools. The IDEAS library allows to perform quasi-stationary analyses of electricity grids. In electricity grids, nearly perfect sinusoidal voltages, with a fixed frequency, are generated by the generation units[7]. Therefore, quasi-stationary analyses are often used for electricity grid analyses. This kind of analyses assumes a fixed grid frequency (e.g., 50 Hz in Europe) to calculate the unknown voltages and currents waveforms (amplitude and their phase shift).

[6] Functional requirements include here the physics to be modeled.

[7] The impact of LV distribution feeders on the grid frequency can be neglected.

Dynamic transient simulation tools include the dynamic transient states in the system (e.g., frequency harmonics), as well as the steady-state solutions. In this way, the impact of events, such as lightning and short circuit conditions can be assessed. For planning and impact assessments in distribution grids, mostly the steady-state solutions are sufficient. Therefore, dynamic transient simulations are out of the scope.

#### Reactive power

The impedance $Z$ of grid elements, such as cables and transformers, consists of a resistive part $R$ and a reactive part $X$. Therefore, a reactive current will flow in the electricity grid. Typically, $R >> X$ for LV distribution grids, although the $R/X$ ratio of different low-voltage distribution grids can vary significantly as a result of different cable types and cable sections being used. Reactive power is limited in order to be compatible with the protection devices and because it is limited by the grid components [236, 237]. Therefore, a fixed power factor close to unity is often imposed by grid regulations [238].

However, reactive power should not be omitted in the LV distribution grid modeling, namely because of:

- the impact of reactive power on the grid losses;
- the impact on voltage deviations and possibilities for voltage regulation [153].

### 4.3.3 Physical model description

In this section, the physical description of the different elements in an electricity grid is given. The model implementation is given in Section 4.3.4.

#### Grid topology representation

Traditionally, radial grids have been represented by an incidence matrix (or connection matrix) $\mathbf{T}$. Eq. (4.6) gives an example of an incidence matrix of a

grid in which consecutive nodes are connected.

$$\mathbf{T} = \begin{bmatrix} -1 & 0 & 0 & \cdots & 0 & 0 \\ 1 & -1 & 0 & \cdots & 0 & 0 \\ 0 & 1 & -1 & \cdots & 0 & 0 \\ \vdots & \vdots & \vdots & \ddots & \vdots & \vdots \\ 0 & 0 & 0 & \cdots & -1 & 0 \\ 0 & 0 & 0 & \cdots & 1 & -1 \end{bmatrix}. \tag{4.6}$$

The columns of $\mathbf{T}$ correspond with the number of nodes (or connection points), whereas each row is a line or cable, between two nodes. The start and end node of each line are represented by respectively 1 and $-1$. Radial grids consist of $n$ nodes and $(n-1)$ line segments. Therefore, an additional (first) row is introduced to represent the imaginary line segment between the transformer and the first node (with a length of 0 m). In this way, a square matrix is attained. This imaginary line segment only has an end node.

This representation with an incidence matrix is valid for all types of radial grids, i.e. for:

- AC or DC grids;
- low-voltage distribution grids and in-building grids;
- single phase and three-phase grids.

In each node of a grid, the Laws of Kirchhoff (see Section 4.3.1) are valid.

Single-phase AC and unipolar DC grids contain two conductors, i.e. a phase/neutral conductor and a positive/negative (or positive/neutral) conductor, respectively. Three-phase grids have typically three phase conductors and one neutral conductor (total of four conductors).

### Cables

Cables, with a length $f_L$ (m), for the line segments are characterized by an impedance $Z = R + jX$, with $R$ the resistance and $X$ the reactance of the cable:

$$R = f_L r \quad \text{and} \quad X = f_L x, \tag{4.7}$$

with $r$ the characteristic resistance and $x$ the characteristic reactance ($\Omega$/m). An impedance matrix $\mathbf{Z} = \mathbf{R} + j\mathbf{X}$ represents the cable impedances.

#### Transformer

In an AC distribution grid, a transformer transforms a higher three-phase voltage level to a lower one. The transformer is modeled with a phase impedance $Z_{\text{tr}} = R_{\text{tr}} + jX_{\text{tr}}$, which is assumed identical for the three phases. This is the same approach as in [153].

The transformer losses $P_{\text{tr}}^{\text{loss}}$ are the sum of the no-load losses $P_0$ (assumed constant) and the joule losses $P_J$ in each phase $p$ of the transformer:

$$P_{\text{tr}}^{\text{loss}} = P_0 + P_J = P_0 + \sum_{p=1}^{3} R_{\text{tr}} |i_{p,k}|^2. \tag{4.8}$$

### 4.3.4 Modelica implementation

This section gives the basic ideas behind the model implementations in Modelica.

#### Connectors (grid nodes)

A connector is used as a port or node, for the connection of different objects. It allows no equations, but connections between two connectors (in two models) are realized as equations. For instance, for an electrical connector, the connector consists of two variables:

- a non-flow variable, i.e. the voltage;
- a flow variable, i.e. the current.

The IDEAS library uses the connectors available in the Standard Modelica Library:

- AC connectors: `Electrical.QuasiStationary.SinglePhase.Interfaces.Pin`
- DC connectors: `Electrical.Analog.Interfaces.Pin`

When connecting two connectors, the Laws of Kirchhoff are applied to both variables. This process is shown in Code 1.

Besides the voltage and current (flow), the AC positive and negative pin also include a reference angle, which is used to represent the phase shift.

```
/* Connect statement to connect two electrical pins. */
connect(pin1,pin2);

/* Laws of Kirchhoff are applied when compiling the model. */
pin1.v = pin2.v;
pin1.i + pin2.i = 0;
```

Code 1: Use of connectors in Modelica.

The grid contains both *internal* and *external* nodes. The internal nodes include the neutral or negative connector, while the external nodes are used to connect the loads and generation units. These external nodes do not include the neutral or negative connector.

- **External nodes:** The external connection nodes have been defined as `.Pin Nodes[numPha,nNodes]`, with `nNodes` the number of grid nodes and `numPha=1` for single-phase AC and unipolar DC nodes, and `numPha=3` for three-phase AC nodes.
- **Internal nodes:** The internal connection nodes have been defined as `.Pin gridNodes[numCon, nNodes]`, with `numCon` the number of conductors: two for single-phase AC and unipolar DC grids, and four for three-phase AC grids.

Adapters are available to connect the internal and external nodes (see Code 2). For single-phase and DC grids, the adapter connects the two wires to a single wire system. For three-phase grids these are respectively four and three wire systems.

Fig. 4.4 shows the use of an adapter in a three-phase grid. The three-phase grid is represented by a four-wire system (three phase conductors and one neutral conductor). The nodes of this grid are grouped in the internal node array (`internalNode`). The external node array (`externalNode`) groups the nodes which are used to connect loads, generation units or converters. The electricity grid (`grid`) connects the `gridNode` (e.g., voltage source or transformer) with the internal nodes.

### Grid topology

The grid topology is described by the incidence matrix and the cable impedances. This is shown in Code 6 in Appendix B.1.1. Code 3 shows the grid construction

by using the incidence matrix (scalable approach). This code is used to construct each phase (and neutral) of the grid by connecting the different line segments (conductor) and grid nodes.

```
/* Two wires to single wire */
  twoWire[1].v - twoWire[2].v = oneWire[1].v "Phase voltage";
  oneWire[1].i = -twoWire[1].i;
  twoWire[1].i = -twoWire[2].i;
  if AC then
    .Connections.branch(oneWire[1].reference,twoWire[1].reference);
    oneWire[1].reference.gamma = twoWire[1].reference.gamma;
  end if;

/*Four wires to three wires */
  for p in 1:3 loop
    fourWire[p].v - fourWire[4].v = threeWire[p].v "Phase voltage";
    threeWire[p].i = -fourWire[p].i;
    .Connections.branch(threeWire[p].reference,fourWire[p].reference);
    threeWire[p].reference.gamma = fourWire[p].reference.gamma;
  end for;
  fourWire[1].i + fourWire[2].i + fourWire[3].i = -fourWire[4].i;
```

Code 2: Adapters for internal and external nodes.

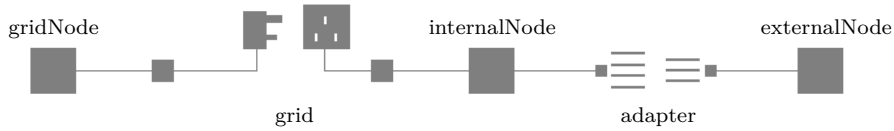


Figure 4.4: Use of adapter for three-phase grids.

```
/* For each conductor i: phase + neutral/negative */
connect(internalNode[i],conductor[i].pin_p);
for x in 1:nNodes loop
  for y in 1:nNodes loop
    if nodeMatrix[x,y] == 1 then
      connect(conductor[x].pin_p,node[2,y]);
    elseif nodeMatrix[x,y] == -1 then
      connect(conductor[x].pin_n,node[2,y]);
    end if;
  end for;
end for;
```

Code 3: Connect statements for the grid construction.

#### Cables

A record `Cable` describes the cable, i.e. the cable type and characteristic impedance ($\Omega$/m). This is also shown in Code 6 in Appendix B.1.1.

#### Transformer

The transformer model consists of an impedance for each of the three phases, similar to [153]. The record interface to define the transformer data is shown in Code 7 in Appendix B.1.2.

#### Comparative model validation

In [229], a comparative model validation is performed to validate the developed models for three-phase unbalanced grids against the power flow analysis tool developed in Matlab® [153]. For a simple case study, the results show that the absolute voltage difference (for the nominal voltage of 230 V) in both models is in the order of $10^{-2}$ V. The minimum difference is less than 1 mV.

This difference between both models is a function of the loads and the grid topology, since an error in one node will propagate through the grid as a result of the Laws of Kirchhoff in an electrical circuit. Therefore, the difference in results will also increase for nodes further from the feeding point. A second source of the difference in results is the stop criterion for the iteration in both simulations. The Matlab code uses a maximum allowed voltage error (1 mV) as a stop criterion. In Dymola, a tolerance of $10^{-4}$ is used[8]. A last aspect of the difference is that the shunt admittance and mutual impedance between cables in three-phase systems is neglected in this Modelica library. The differences between the results of both models are very limited. Since both stop criteria for the iterative solution method are different, the results show that the accuracy is sufficient to apply this Modelica library.

### 4.3.5 Out of the scope functionalities for grid models

Currently, out of the scope are modeling of the following phenomena:

- meshed grids;

[8]For the grid simulations, no impact on the results has been observed for the different available solvers, and tolerances.

- transient simulations;
- temperature dependent losses of cables and transformer, including possible overloading;
- shunt admittance and mutual impedance between three-phase cables (and in transformer).

For three-phase AC grids, only four-wire systems (three phase conductors and one neutral conductor) are possible. For DC grids, only unipolar DC grids have been modeled.

### 4.3.6 Simulation of multiple (type of) grids

The Modelica implementation allows to simulate multiple grid types in one simulation. Therefore, there is no need to iterate between different grid simulations to solve the different AC and DC grids seperately.

Fig. 4.5 shows an example with different grids types, i.e. a single-phase and three-phase AC grid and one DC grid. For the DC grid, a converter is required as well as a separate DC grounding to fix the DC voltage.

## 4.4 Load and generation models

### 4.4.1 Physical model description

In this section, the physical description of the different load models and the photovoltaic system is given. Loads and generation units can be connected single or three-phase (balanced) to an electricity grid. The model implementation is discussed in Section 4.4.2.

#### Loads and generation units

Loads and generation units can be modeled as resistive, capacitive and inductive loads. This means both active and reactive power can be consumed and/or produced. For loads and generation units with a power electronic interface to the electricity grid, the power factor can be set. The power factor $pf$ is defined as: $pf = P/|S|$. It can be leading (drawing reactive current) or lagging (injecting reactive current). Typically, a unity power factor is assumed.

This Modelica library allows to model loads and generation units as:

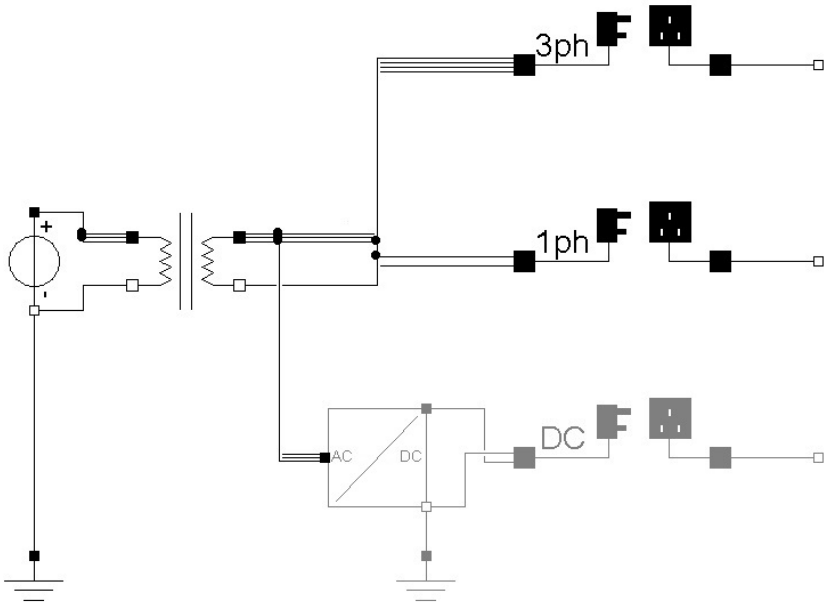


Figure 4.5: Simulation of multiple grid types in one simulation.

- constant power loads;
- voltage dependent power loads.

For a constant power load, the power is not depending on the solution of the power flow analysis. The non-linear relation in Eq. (4.4), defines the voltage and current. However, this means that for a constant power, the load current increases when the grid voltage drops, which may further increase the voltage drop, and vice versa. Constant power loads are typically assumed for loads equipped with power electronics in simulations.

Another load type used in this dissertation are voltage dependent power loads. With a voltage droop mechanism, the power $P^{\mathrm{vd}}$ that is drawn from or injected in the grid, is a function of the grid voltage $u$:

$$P^{\mathrm{vd}} = f(|u|). \tag{4.9}$$

For instance, in Germany, PV installations are required to have a frequency droop mechanism and reactive support mechanism according to VDE-AR-N 4105 [238, 239]. Similarly, these mechanisms have been investigated for EV chargers [128].

### Photovoltaic PV system

A PV system is implemented based on the five-parameter model to calculate the power output of a PV panel under operational conditions. The five-parameter model, which is temperature dependent, is based on the single diode equivalent circuit of a PV panel [240]. The five parameters have been indicated in Appendix B.2. These parameters can generally be calculated from data gathered from the manufacturer's specifications of solar panels. The required specifications are:

- the current $I_{\mathrm{MPP}}$ and voltage $V_{\mathrm{MPP}}$ at maximum power point (MPP) under standard testing conditions (STC);
- the short circuit current $I_{\mathrm{sc}}$ and open circuit voltage $V_{\mathrm{oc}}$ under STC;
- the temperature coefficients $k_i$ and $k_v$ of the short circuit current and open circuit voltage, respectively.

The PV parameters are adjusted, as illustrated in Appendix B.2, to take into account:

- the position of the sun;
- the direct and indirect radiation;
- the ambient temperature.

The PV cell temperature is adjusted to the ambient temperature increased with the panel losses. The tilt angle and orientation of the PV system are parameters of the model. The ambient temperature and the direct and diffuse radiation are read from a meteorological data file, as discussed in Appendix C.1.

Based on these specifications, Sera et al. [241] give the calculation method for the five parameters. Appendix B.2 gives a general overview of these calculations.

### Power electronic converters

While transformers are used to transform voltages in AC systems, converters are used to convert voltages between different AC and DC systems. Here, the following converter types have been used:

- rectifiers: AC to DC;
- inverters: DC to AC;
- bidirectional converters.

The ratio between the DC and AC power is defined by the efficiency of the converter. Converters can also regulate the reactive power consumption or injection [153]. The power factor can be leading or lagging. The power electronics level of converters is not modeled.

### 4.4.2 Modelica implementation

This section gives the basic ideas behind the model implementations in Modelica.

#### Constant power loads

Code 4 shows the non-linear relation between the apparent power, voltage and current shown in Eq. (4.4). The apparent power $S$ of a load or generation unit is constant during a time step.

```
model AC
  parameter Integer numPha;
  Modelica.Blocks.Interfaces.RealInput P;
  Modelica.Blocks.Interfaces.RealInput Q;
  Modelica.Electrical.QuasiStationary.SinglePhase.Interfaces.Negative
    Pin[numPha] vi
equation
  for f in 1:numPha loop
    P/numPha = Modelica.ComplexMath.real(vi[f].v*
      Modelica.ComplexMath.conj(vi[f].i));
    Q/numPha = Modelica.ComplexMath.imag(vi[f].v*
      Modelica.ComplexMath.conj(vi[f].i));
  end for;
end AC;

model DC
  Modelica.Blocks.Interfaces.RealInput P;
  Modelica.Electrical.Analog.Interfaces.PositivePin vi
equation
  P = vi.v * vi.i;
end DC;
```

Code 4: Relation apparent power, voltage and current for both AC (single/three-phase) and DC systems.

### Voltage dependent load models

The power demand or generation is implemented as a function of the grid voltage. Any function is possible. The solver executes an iteration until convergence is reached to calculate the power demand or generation.

### Photovoltaic system

The PV system notes have been discussed in detail in [29].

### Power electronic converters

Converters use both the AC and DC connectors. The AC connector can be single or three-phase. For three-phase converters, it is assumed that the apparent power is equally divided over the three phases: $S_p(t) = S(t)/3$. Code 5 shows the bidirectional converter implementation which extends the partial model `Converter`. A boolean `inverter` defines the operation: rectifier or inverter. For the `Rectifier` and `Inverter` model, this boolean is a parameter.

```
model BidirectionalConverter
  extends .BaseClasses.Converters.Partials.Converter;
  Boolean inverter "Inverter: true / Rectifier: false";
equation
  inverter = if pDC >= 0 then true else false
    "Define converter mode";
  pAC = if inverter then -pDC*eff else -pDC/eff
    "DC/AC power ratio";
end BidirectionalConverter;
```

Code 5: Converter mode and DC/AC power ratio.

## 4.5 Battery storage and EVs

A battery model is implemented in Modelica which can be used for both:

- battery storage in buildings and electricity grids;
- battery storage in electric vehicles.

The battery model is implemented with dynamic SoC equations and battery parameter constraints [153], meaning that the power electronics level is neglected. No temperature-dependency is included.

### 4.5.1 Physical model description

The SoC is calculated for each time step $k$ by:

$$SoC_k = SoC_{k-1} - \delta_k^{\text{sd}} + (\eta^c P_k^c T_s - 1/\eta^d P_k^d T_s)/E_{\text{nom}}, \tag{4.10}$$

with $\delta_k^{\text{sd}}$ the self-discharge of the battery during a time step $k$, and $T_s$ the time step resolution. $\eta^c$ and $\eta^d$ are the charging and discharging efficiency of the power electronics and the battery, respectively. The charging and discharging power have been denoted by $P^c$ and $P^d$, with $P^c P^d = 0$ at each time step $k$. The SoC at time step $k$ is defined as:

$$SoC_k = E_k^{\text{bat}}/E_{\text{nom}}, \tag{4.11}$$

with $E_k^{\text{bat}}$ the battery capacity at time step $k$ and $E_{\text{nom}}$ the nominal battery capacity. The usable battery capacity $E_{\text{eff}}$ is limited to extend the battery cycle life[9] [60]: $0 \leq E_k^{\text{bat}} \leq E_{\text{eff}} \leq E_{\text{nom}}$.

The maximum charging and discharging power depend on $\gamma^c$ and $\gamma^d$, the charging and discharging power-to-energy ratios, which are specific for each battery technology:

$$P_k^c \leq \gamma^c E_{\text{nom}}, \qquad P_k^d \leq \gamma^d E_{\text{nom}}. \tag{4.12}$$

### 4.5.2 Modelica implementation

Different battery chemistries, including their parameters, can be defined. The different parameters have been listed in Code 8 in Appendix B.3.

#### Battery SoC calculations

The dynamic SoC equation, as defined in Eq. (4.10), has been implemented as shown in Code 9 in Appendix B.3.1.

[9] The cycle life of a battery is defined as the number of cycles until the remaining usable battery capacity drops below 80 %.

#### Battery control: charging and discharging power limit

The power flow to and from the battery is controlled based on following aspects:

- limiting the power when the battery is almost fully charged or discharged, i.e. when the remaining capacity to charge or discharge is smaller than the amount of energy that can be charged or discharged at maximum power[10];
- taking into account the maximum charging or discharging power of the battery;
- taking into account the maximum charging power of the grid connection.

### 4.5.3 Electric vehicles

It is assumed in this text that EVs use battery units to store electricity, which is used to propel the vehicle. Therefore, the EV model extends the battery model, which is discussed earlier.

The extended EV model also includes the EV charging strategy model, which calculates the charging power drawn from the electricity grid at each time step $k$. The charging strategy model takes the following inputs and one or more constraints at each time step $k$ into account:

- Vehicle mobility behavior input:
  - grid connection availability;
  - next departure time.
- Constraints:
  - battery SoC[11];
  - grid voltage;
  - start and/or end charging time (e.g., for night charging);
  - local electricity generation;
  - maximum power capacity of building and/or grid.

[10] This also includes stopping the charging and discharging when the battery is fully charged or discharged.

[11] To limit the charging and discharging power when the battery is almost fully charged or discharged.

## 4.6 Conclusions

This chapter discusses the electrical modeling for buildings and districts in Modelica. As electrical systems and other domains get more integrated with each other in buildings and districts, there is a need for modeling tools for easy energy system integration. Therefore, a Modelica library, i.e. IDEAS (Integrated District Energy Assessment by Simulation), is developed at the KU Leuven, which allows the simultaneous modeling and simulation of multidisciplinary energy systems at both building and district level in one simulation model.

Furthermore, this chapter elaborates on the structure and modeling background of the electrical sublibrary of IDEAS. The following models have been specifically developed for this dissertation:

- radial electricity distribution grids, both in-building and LV distribution grids;
  - AC single/three-phase grids;
  - DC unipolar grids.
- battery storage systems;
- electric vehicles (extending the battery storage system).

The radial electricity distribution grids (three-phase unbalanced) has been co-developed with Bart Verbruggen [29].

The Modelica implementation allows to simulate multiple grid types in one simulation, e.g., a DC grid connected to a three-phase AC grid.

# Chapter 5

# Residential EV charging requirements, flexibility and impact

This chapter focuses on the residential EV charging flexibility and the fleet and residential grid impact of different EV charging opportunities, i.e. at home, at the work place and at other locations. First, general results of the mobility behavior model (see Chapter 3) will be discussed, i.e. the number of vehicles on the road and the different EV charging location opportunities. The content of this chapter has been based on the following conference paper:

> J. Van Roy, N. Leemput, S. De Breucker, F. Geth, P. Tant, and J. Driesen, "An availability analysis and energy consumption model for a Flemish fleet of electric vehicles," in *European Electric Vehicle Congr.*, Brussels, Belgium, Oct. 2011.

Thereafter, the EV charging flexibility at home has been assessed in Section 5.2. Section 5.3 discusses the residential grid impact and fleet impact of different EV charging location opportunities. These results are based on the following book chapter:

> N. Leemput, J. Van Roy, F. Geth, J. Driesen, and S. De Breucker, *Data Science and Simulation in Transportation Research.* Hershey, PA: IGI Global, 2014, *ch. 17: Grid and fleet impact mapping of EV charge opportunities,* pp. 364–390.

To conclude, the residential charging power requirements will be assessed in Section 5.4, while Section 5.5 discusses additional fast charging requirements while driving.

## 5.1 Mobility behavior

This section discusses the results of the mobility behavior model (see Chapter 3) regarding the average number of vehicles on the road and their presence (and possible grid connectivity) at different locations. A distinction is made between week and weekend days. The results in the following subsections have been shown for a fleet of 10 000 vehicles during one week. As discussed in Section 3.1.6, 46.9 % of all vehicles are used for trips to and from work.

### 5.1.1 Driving behavior

Fig. 5.1 shows the average number of vehicles on the road during an average week and weekend day. The results are divided in vehicles on the road for work trips (Fig. 5.1 (a)) and vehicles on the road for nonwork-related trips (Fig. 5.1 (b)). The sum of both figures represents the average number of vehicles on the road.

Since there are on average more trips per day during the week, a first observation is that there are more vehicles on the road during week days. However, on average less than 9.2 % of the vehicle fleet is on the road simultaneously (less than 7.2 % during weekend days), which is in line with the results in [172].

A significant distinction can be observed in the timing and magnitude of work- and nonwork-related trips [173]. For the trips to and from work, there is a clear morning and evening peak during the week. This is due to the fact that most people work in normal day shifts and part-time shifts. During the night, almost no vehicles are on the road for work-related trips.

On the other hand, nonwork-related trips account for a larger load of vehicles on the road. There is no clear morning peak, but during the first part of the evening, it is observed that more vehicles are on the road for nonwork-related trips. On the one hand, this can be explained by the higher number of work-related trips during daytime. On the other hand, nonwork-related trips are spread over the day, but are postponed for working people. Also, in the weekend, nonwork-related trips are shifted in time, as can be observed in Fig. 5.1 (b) as a shift between the graphs for week and weekend days, respectively.

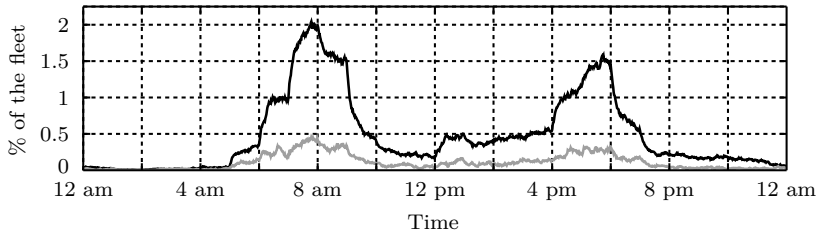


(a) Work-related trips.

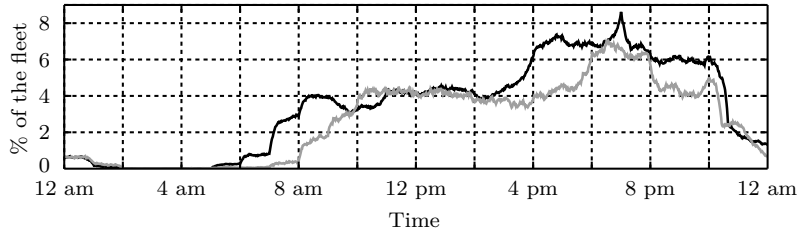


(b) Nonwork-related trips.

Figure 5.1: Average number of vehicles (% of the fleet) on the road for (a) work-related trips and (b) nonwork-related trips during week (black line) and weekend days (grey line).

### 5.1.2 EV charging location opportunities

Compared to traditional vehicles with a combustion engine, each location with a socket available can be considered as an EV charging location. Different EV charging locations can be considered:

- home;
- the workplace;
- other (public) locations;
- fast charge stations.

In Fig. 5.2, the average presence for the simulated fleet of 10 000 vehicles at (a) home, (b) work and (c) other locations[1] is shown, which is discussed below. This dissertation focuses on home charging and charging at the workplace.

[1] Other locations include the other activities and driving.

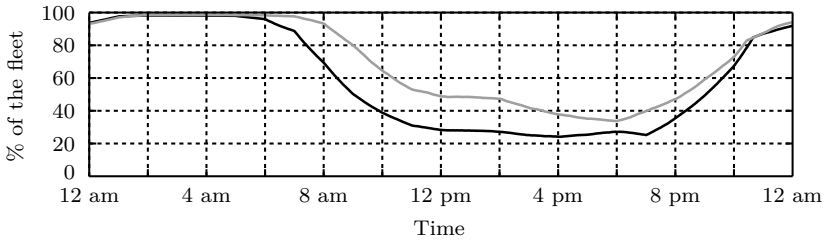


(a) At home.

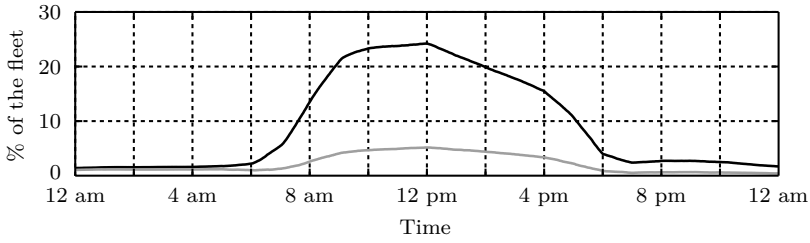


(b) At work.

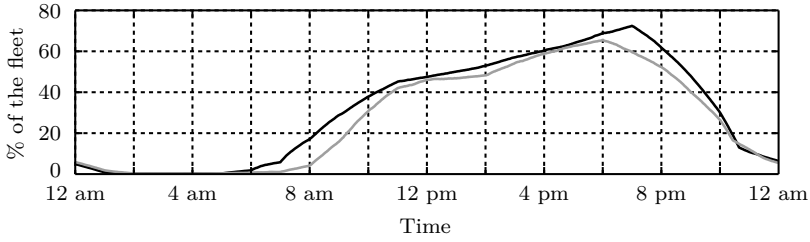


(c) At another location (including driving).

Figure 5.2: Average number of vehicles (% of the fleet) at (a) home, (b) at work or (c) at another location (another activity or driving) during week (black line) and weekend days (grey line).

## Home charging

From the results in Fig. 5.2 (a), it follows that on average, a minimum of about 24.2 % and 33.8 % of the vehicle fleet is standing still at home during a weekday and weekend day, respectively. The amount of vehicles at home is at its maximum during the night, with more than 90 % parked at home.

In Fig. 5.2 (a), a distributed arrival at home in the evening (starting around

8 pm) can be observed, which means that in an uncoordinated charging strategy, not all EVs will be plugged in at the same time. The latter results in a partial natural load spreading behavior. It is also shown that there are charging possibilities during the day at home. Therefore, EV charging strategies can take this into account in order to limit the simultaneity with the evening household power demand to limit the peak power demand and to enable the integration with local renewable energy sources, such as PV systems.

### Charging at the workplace

According to Fig. 5.2 (b), a maximum of about 24.2 % and 5.2 % of the fleet is at the work place during daytime on week and weekend days, respectively. On the other hand, during the evening and night, only a small fraction of vehicles is parked at the work place. During the week, at least 48 % of the fleet is standing still at home or at the work place during each moment of the day. Therefore, this shows that both places are obvious places for EVs to be grid-connected.

In general, people are at the work place mainly during daytime. Therefore, there is a large possibility to integrate the EV charging at the workplace with local renewable energy sources, such as PV systems, and other distributed energy resources, such as CHPs. However, Fig. 5.2 (b) shows that vehicles in general arrive early in the morning. Since the average commuter distance is rather small, as discussed in Section 3.1.6, the energy demand for charging the EVs at the work place will be low, if the EVs are fully recharged at home overnight. Thus, solutions to coordinate the EV charging are required to increase the integration with local electricity generation.

### Other charging locations

As discussed in Section 5.1.1, nonwork-related trips account for a large part of the vehicle trips. In Fig. 5.2 (c), it can be observed that during the day and early evening a lot of vehicles are parked at another location or are driving.

Without public charging and fast charging, it is already shown in [200, 242] that the average SoC of a vehicle fleet is at its highest in the morning (around 7 am) and at its lowest in the evening (around 7 pm). Therefore, it can be concluded that the energy demand for charging EVs at other and public locations, and fast charging stations, may increase towards the evening.

## 5.2 EV charging flexibility at home

In Section 5.1.2 and Fig. 5.2 (a), it is shown that at each moment a certain number of vehicles are standing still at home (at least 24.2 % of the vehicle fleet), while during the night at least 90 % of the vehicles is parked at home. In this section, it is shown that EVs have a certain flexibility to coordinate their charging process in time and power (see Section 2.4).

### Daily driven distance

The cumulative distribution function of the daily driven distances is illustrated in Fig. 5.3 (a) for a fleet of 10 000 EVs during one week. This figure shows that days with long driven distances are rare. For about 80 % and 90 % of the days, the total driven distance is less than 55 km and 80 km, respectively. The average daily driven distance is about 36.1 km, which is in line with the statistics on mobility behavior [160]. Note that the average daily driven distance is a little lower compared to the statistics on mobility behavior. This is due to the fact that mobility behavior simulation tool does not include holiday trips/periods, during which on average longer trips are driven.

As discussed in [188], vehicles, which are used for work trips, drive in general longer daily distances.

### Daily electricity consumption for a BEV

In Fig. 5.3 (b), the average daily driven distance is translated to an average daily electricity consumption if the EVs purely drive on electricity[2]. Note that this cumulative distribution function is not a scaled version of Fig. 5.3 (a) due to the vehicle segmentation, i.e. a different yearly driven distance and specific electricity consumption while driving for each vehicle segment.

Again, the cumulative distribution function shows that days with a high daily electricity consumption are rare. For about 50 % and 90 % of the days, the total electricity charged is less than 5.4 kWh and 18 kWh, respectively. The average daily electricity consumption is about 8 kWh, if the EVs purely drive on electricity. This results in a yearly average of about 3000 kWh per EV.

The results suggest that an increasing battery size will have a decreasing marginal impact on the UF.

[2] This is the required energy from the batteries for the vehicle propulsion.

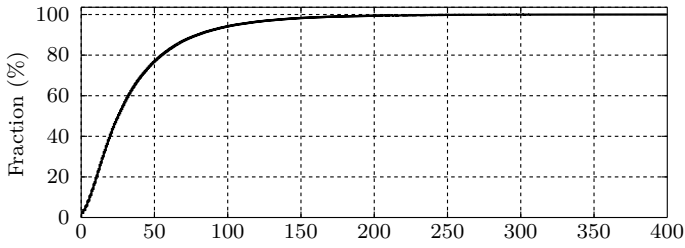


(a) Daily driven distance (km).

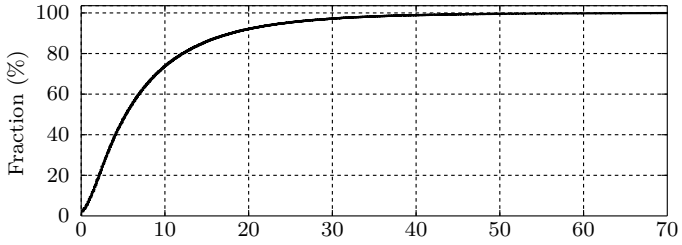


(b) Daily electricity consumption (kWh).

Figure 5.3: Cumulative distribution function of (a) the daily driven distances and (b) the daily electricity consumption for a BEV.

### Standstill time at home

As illustrated in Fig. 5.2 (a), it may be expected that vehicles are parked for a long time at home. On average, a vehicle is parked for nearly 15 hours at home. Although, there are a few occasions that vehicles are not parked at home for at least one day or that vehicles are parked at home during a whole day.

Table 5.1 summarizes the daily electricity consumption and standstill time of a fleet of EVs. On average, if EVs[3] are only charged at home, there is about 15 h to charge a daily average of 8 kWh[4]. If the full standstill time of an EV can be used for charging its batteries, the results in Table 5.1 show that:

- on average a low charging power is required if the full standstill time is used for charging the EVs;

[3]EVs which purely drive on electricity.
[4]Excluding the charging efficiency losses.

Table 5.1: Daily electricity use and standstill time during $x$ % of the days.

| % days | Electricity use | Standstill time |
|---|---|---|
| 10 % | > 18 kWh | > 21 h |
| 30 % | > 8.9 kWh | > 17.3 h |
| 50 % | > 5.4 kWh | > 14.4 h |
| 70 % | > 3.1 kWh | > 12.1 h |
| 90 % | > 1.2 kWh | > 9.7 h |

- there is a certain flexibility to shift and coordinate the EV charging in time.

However, it must be noted that these numbers do not reflect the durations of the individual charging opportunities, nor the charging availability. For instance:

- The time an EV is fully charged, limits the EV's available time to charge the required energy during that day.
- During short charging opportunities, it may be required to charge a high amount of electricity.

The possibilities for coordinating the EV charging is further discussed in Chapter 6 and Chapter 7 with a case study of EV charging in an apartment building. In Chapter 9, EV charging in an office building is assessed.

## 5.3 Grid and fleet impact mapping of EV charging opportunities

Considering Section 5.2, the majority of EV charging is expected to occur when the EV is parked at home, if a grid connection is available. Therefore, first the grid and fleet impact of only home charging is discussed. Besides the residential grid impact and fleet impact of additional charging opportunities, i.e. at the work place and public places, have been assessed. The scope of this section is to show the general impact of additional charging locations on the residential impact of EV charging.

To assess the general fleet and residential grid impact trends of different EV charging opportunities, the impact of different battery capacity scenarios and

charging rates, i.e. (a) 2.1 kW (mode 2) and (b) 6.6 kW (mode 3) for a fleet of 100 EVs is discussed in [188] and summarized below:

- **Battery scenario 1:** 5, 7.5 and 10 kWh for small, middle-class and large vehicles, respectively.
- **Battery scenario 2:** 10, 15 and 20 kWh for small, middle-class and large vehicles, respectively.
- **Battery scenario 3:** 20, 30 and 40 kWh for small, middle-class and large vehicles, respectively.

For uncoordinated charging, EV charging starts whenever arriving at the charging location. The different EV charging locations are:

- **Scenario 1:** home
- **Scenario 2:** home + work place
- **Scenario 3a:** home + work place + 25 % other locations
- **Scenario 3b:** home + work place + 50 % other locations

### 5.3.1 Residential LV grid impact

This section gives an overview on the the general EV grid impact on the residential LV grid.

#### Total electricity consumption

The average yearly electricity consumption at home for a charging rate of 6.6 kW is shown in Table 5.2. Depending on the battery size of the EVs, the yearly electricity consumption at home is between 2022 and 3212 kWh/vehicle. As the specific electricity use during electric driving is kept constant (see Section 3.2), the UF and yearly electricity consumption are directly proportionally related. The yearly electricity consumption is higher for larger battery packs, as more energy can be stored and used for electric driving, as the UF is lower than 100 % (see Section 5.3.2).

When additional work charging is possible, the residential electricity consumption drops by 9.3 to 13.6 %. However, it must be noted that, due to the increased number of charging locations, the total electricity consumption (home + work), to charge an EV, increases by 1.4 to 10.7 %. Therefore, the electric range of the vehicles increases (see Section 5.3.2). When the number of charging

Table 5.2: Impact on the average yearly residential EV power consumption (kWh/vehicle) for a charging rate of 6.6 kW (all EVs used for trips to/from work).

| | **Battery scen. 1** | **Battery scen. 2** | **Battery scen. 3** |
|---|---|---|---|
| **Scen. 1** | 2022 kWh | 2740 kWh | 3212 kWh |
| **Scen. 2** | -9.3 % | -11.8 % | -13.6 % |
| **Scen. 3a** | -23.2 % | -27.6 % | -30.1 % |
| **Scen. 3b** | -35.0 % | -40.9 % | -43.9 % |

opportunities increases (scenario 3b), the yearly residential power consumption per vehicle drops by 35 to 43.9 % compared to the case with only home charging.

### Peak power demand

The average EV charging peak demand power is summarized in Table 5.3. For mode 2 charging, the residential peak charging power is 1.24 kW/vehicle, for battery scenario 1, i.e. a total peak charging power of 124 kW. For an increasing battery size, the residential peak charging power increases to 1.37 kW/vehicle, due to a longer charging duration (an increased electricity consumption), resulting in an increased EV charging simultaneity. For mode 3 charging at 6.6 kW, the residential peak charging power only increases by 54–88 % compared to mode 2 charging. The increase is limited due to the reduced charging duration, which results in a decreased charging simultaneity of the different EVs.

At work, a relatively small amount of electricity is charged due to the, on average, short commuter distances (see Chapter 9). Thus, the charging duration and

Table 5.3: Impact on the peak charging power (kW/vehicle), for a fleet of 100 EVs (all EVs used for trips to/from work) for a charging rate $P^{\mathrm{ch}} \in \{2.1; 6.6\}$ kW.

| | **Battery scen. 1** | | **Battery scen. 2** | | **Battery scen. 3** | |
|---|---|---|---|---|---|---|
| | 2.1 kW | 6.6 kW | 2.1 kW | 6.6 kW | 2.1 kW | 6.6 kW |
| **Scen. 1** | 1.24 kW | 1.91 kW | 1.37 kW | 2.38 kW | 1.37 kW | 2.57 kW |
| **Scen. 2** | -3.3 % | -0.0 % | -4.5 % | -5.6 % | -4.5 % | -7.7 % |
| **Scen. 3a** | -11.9 % | -6.9 % | -10.6 % | -19.4 % | -10.6 % | -20.5 % |
| **Scen. 3b** | -25.0 % | -22.4 % | -27.2 % | -27.8 % | -25.8 % | -28.4 % |

charging simultaneity at home (after work) is only slightly impacted. Therefore, when charging at the work place is possible (scenario 2), the residential peak charging power only slightly decreases. The residential peak charging power is further reduced when charging at other locations is possible. A relatively larger reduction in the residential peak charging power can be attained when charging at other locations is possible (scenario 3a and 3b), compared to the impact of charging at the work place.

Thus, the results indicate that the residential grid impact, regarding the peak charging power, of EV charging is reduced with an increasing amount of EV charging opportunities at work and other locations.

### 5.3.2 Fleet impact

#### Utility function

The utility function strongly varies for the different battery scenarios and the availability of charging locations. For instance, when only home charging is available, the average UF is around 65, 85 and 95 % for the three battery scenarios, respectively. Note that the UF is lower than 100 %. This means that the EVs (EREVs in this context, see Section 2.1) do not purely drive on electricity.

The UF increases when charging locations are added, as also shown by the increasing total electricity consumption (see Section 5.3.1). For instance, for battery scenario 1, the average UF increases up to 70 % when work charging (scenario 2) is possible and up to 80 % for scenario 3b. The marginal impact decreases for increasing battery sizes [188].

As will be shown in Chapter 6, the sensitivity of the UF towards the charging rate is small. This is the case, especially for scenario 1 and 2, due to the relatively long standstill times at home and at the work place. Thus, the small benefit in user comfort should be outweighed with the increase in charging infrastructure cost.

#### Battery utilization function

The EV battery utilization function is summarized in Table 5.4. Significant differences in BUF are visible for the different battery scenarios. The battery utilization function decreases for increasing battery sizes, since the battery capacity is relatively large compared to the average daily electricity consumption.

Table 5.4: Impact on the average EV battery utilization function (all EVs used for trips to/from work) for a charging rate $P^{\text{ch}} \in \{2.1; 6.6\}$ kW.

| | **Battery scen. 1** | | **Battery scen. 2** | | **Battery scen. 3** | |
|---|---|---|---|---|---|---|
| | 2.1 kW | 6.6 kW | 2.1 kW | 6.6 kW | 2.1 kW | 6.6 kW |
| **Scen. 1** | 288 | 300 | 198 | 203 | 98 | 117 |
| **Scen. 2** | +12.2 % | +10.7 % | +6.1 % | +4.9 % | +2.6 % | +1.7 % |
| **Scen. 3a** | +20.8 % | +20.3 % | +9.6 % | +9.4 % | +3.4 % | +2.5 % |
| **Scen. 3b** | +28.8 % | +29.0 % | +12.6 % | +12.3 % | +4.3 % | +3.4 % |

The BUF increases for an increasing number of charging locations. Thus, batteries are more intensively used.

## 5.4 Residential charging power requirements

There is a trend towards higher EV charging rates, because it may help to overcome range-anxiety. It might be required to meet the mobility behavior requirements, and it increases the flexibility for EV charging. In earlier work [126], the need for higher charging rates at home has been investigated:

> J. Van Roy, N. Leemput, F. Geth, R. Salenbien, J. Büscher, and J. Driesen, "Apartment building electricity system impact of operational electric vehicle charging strategies," *IEEE Trans. Sustain. Energy*, vol. 5, no. 1, pp. 320–327, Jan. 2014.

In the case study in Chapter 6, EV charging at home is limited to single-phase charging, limiting the charging rate to 6.6 kW. However, there is an increasing interest for three-phase charging (charging rates up to 19.8 kW). In this section, the charging power requirements have been investigated in order to discuss the charging rate requirements for home charging. The results have been given for the following EV charging coordination strategies:

- **Scenario A:** Uncoordinated charging limited to the off-peak period.
- **Scenario B:** Uncoordinated charging during both the peak and off-peak periods.

Table 5.5: The number of charging opportunities (%) at home that the required charging power, to fully charge the EVs by the next departure moment, is higher than a certain power.

| | > 2.1 kW | > 3.3 kW | > 6.6 kW | > 9.9 kW | > 19.8 kW |
|---|---|---|---|---|---|
| **Scenario A** | 18.6 % | 4.8 % | 1.6 % | 1.2 % | 0.7 % |
| **Scenario B** | 22.2 % | 14.5 % | 8.4 % | 5.6 % | 2.3 % |

For the case study in [126], the EVs are charged at a charging rate of 2.1 kW. Table 5.5 presents the number of charging opportunities[5] (> 15 min), for which a charging power is required which is higher than 2.1, 3.3, 6.6, 9.9 and 19.8 kW, respectively, to fully charge the battery by the next departure time. During each charging opportunity, the charging power $P^{\text{ch,req}}$, which is required to fully charge the battery before leaving for a next trip, is calculated as follows:

$$P^{\text{ch,req}} = \frac{E_{\text{req}}}{\Delta T_k}, \tag{5.1}$$

with $E_{\text{req}}$ the required energy to fully charge the EV, and $\Delta T_k$ the time until the next departure time.

When EVs are only charged during the off-peak period (scenario A), there are on average 1.02 charging opportunities per day for each vehicle. Thus, some vehicles may leave from home and may arrive later at home during the off-peak period. As the standstill times are generally longer during the off-peak period, the EVs require on average low charging powers. Only about 1.6 % of the off-peak charging opportunities require a charging power above 6.6 kW.

In case EVs can be charged during the whole day (scenario B), this number increases up to 8.4 %. This number is higher since there are more charging opportunities (1.54 per day per vehicle), and the time at home between two trips is generally shorter during daytime, resulting in higher $P^{\text{ch,req}}$ during those charging opportunities.

Nevertheless, it should be noted that Table 5.5 represents the worst-case numbers, as it is assumed that fully charged batteries are expected when leaving for the next trip. This can be explained as follows:

- Charging at a higher power during a charging opportunity may reduce the required charging power during future charging opportunities.

[5] A charging opportunity is defined as each period when a vehicle arrives at home until it leaves again for a trip.

- The numbers do not take into account whether the mobility behavior requires a fully charged battery each time the EV owner is leaving at home.
- The numbers do not include other charging locations. Charging at other locations, such as the work place or public locations, may decrease the charging requirements at home.
- These numbers do not contain information on the length of each charging opportunity, which may result in high $P^{\mathrm{ch,req}}$ for charging opportunities with a short duration.

Thus, it can be observed that for the majority of charging opportunities, a low charging power ($< 6.6\,\mathrm{kW}$) is sufficient. Therefore, when multiple EVs are charged at one location, i.e. at an apartment building (with a common EV charging infrastructure), one can opt for a combination of EV charging infrastructures with different charging rates. In this way, EV owners can choose a charging rate which suits the requirements for that specific charging opportunity. Besides, in Chapter 6, it will be shown that the EV charging rate has a very low impact on the average UF, due to the, on average, long standstill times at home. Thus, the EV user will have to outweigh the user comfort benefits against the cost of the charging infrastructure.

## 5.5 Additional fast charging requirements

Despite the long standstill times at home and work, additional fast charging opportunities to avoid range anxiety and to cover occasional long trips may be required, such as fast charging infrastructure, i.e. at fast charge stations (usually at 50 kW or more [243]). In [200, 242], the technical design criteria for fast charging infrastructure to cover the mobility requirements and to complement slow charging opportunities[6], have been investigated. Some results regarding the use of fast charging infrastructure have been summarized here. Fig. 5.4 shows the lowest SoC each EV in the fleet attains during a week, including a sensitivity to:

- Maximum DOD: 65 % and 95 % vs. 80 %;
- Battery capacity: −23 % and +23 %;
- Charging probability at other locations of 0 % and 80 % vs. 40 %.

[6]The slow charging opportunities contain home charging and charging, with a 40 % probability, at other locations (work and public locations).

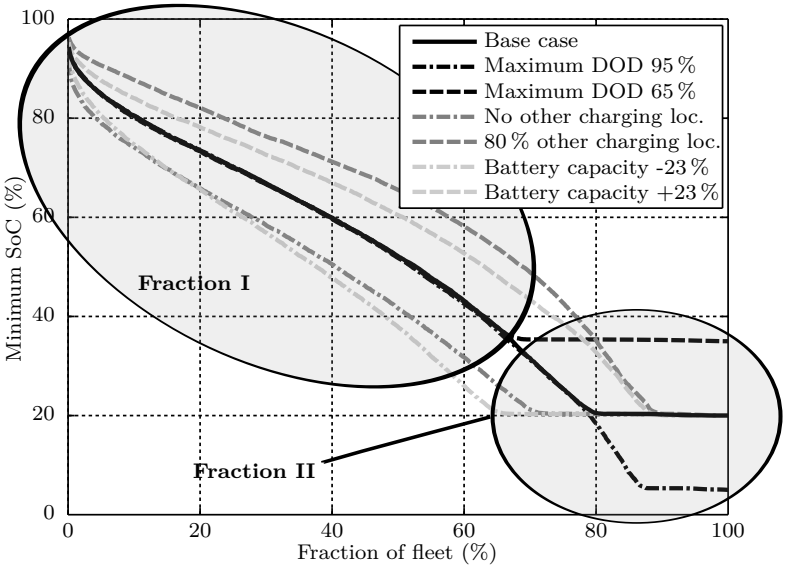


Figure 5.4: Sensitivity analysis: Minimum occurring SoC in the fleet.

It can be observed that both the battery capacity and the number of other charging locations have a large impact on the SoC profile of an EV. For the base case, only about 20 % of the EVs reach an empty battery, i.e. a maximum DOD of 80 %, at least once a week. The different curves show a certain trend, as shown in Fig. 5.4:

- **Fraction I:** Fraction of the fleet that never reaches maximum DOD;
- **Fraction II:** Fraction of the fleet that requires fast charging opportunities.

For the assumption that people will stop at a fast charge station when their battery SoC reaches 20 %[7], it is observed in [200] that only about 20 % of the EVs in the fleet use a fast charge station during a one-week period. Fig. 5.5 illustrates the fast charging frequency of the EVs that use a fast charge station. More than 75 % of the EVs which use the fast charge station, only use it once a week. More than 90 % only use it once a day. Not a single EV in the investigated fleet of 1000 vehicles, visited the fast charge station more than 4 and 8 times a day and week, respectively. A maximum of 9 EVs charge simultaneously if charging has to start immediately after arrival at the station.

[7]Note that a perfect spatial allocation of the fast charge stations is assumed, i.e. the EVs stop at a fast charging station at the moment their battery SoC reaches 20 %.

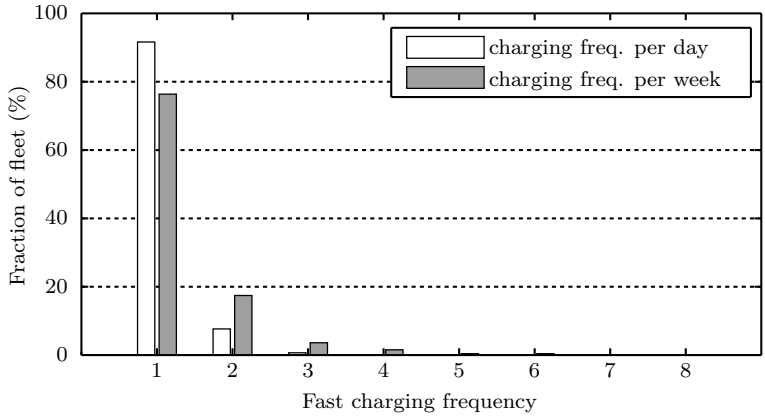


Figure 5.5: Fast charging frequency per day and per week of the EVs that use the fast charge station at least once.

The technical design criteria of the fast charge station configuration is further detailed in [200, 242].

## 5.6 Conclusions

This chapter focuses on the residential EV charging requirements, flexibility and grid impact of different EV charging opportunities. On average, the daily driven distance is about 40 km, and for 80 % of the days it is less than 55 km. This results in an average daily electricity use of about 8 kWh. This means that already a large part of our daily mobility needs can be covered by P(H)EVs currently on the market, moreover when there are sufficient charging locations.

Based on the mobility behavior, the majority of EV charging is expected to occur when the EV is parked at home and at the work place, if a grid connection is available. At both these locations, the EVs are standing still for a large part of the day. It is shown that the average standstill time at home is around 15 h a day. This means there is a certain flexibility in time and charging power to shift and coordinate the EV charging at home.

However, compared to traditional vehicles with dedicated fuel stations, each parking spot with the availability of a socket can be considered as a possible EV charging location. This results in the principle of *charging when the car is parked instead of stopping for refuelling, as for conventional vehicles* [73].

Although the latter, e.g., by stopping at fast charge stations, may be inevitable due to a limited electric range for occasional long trips. According to [200, 242], about 20 % of the EVs in a fleet require fast charging at least once a week.

EV charging at work, public locations, and fast charging infrastructure, may complement home charging, including following advantages for home charging:

- a decreased electricity consumption at home;
- an increased total electricity consumption, resulting in a higher UF, i.e. electrical range, and an improved battery utilization;
- a decreased peak power demand at home, i.e. a decreased grid impact.

For a majority of the residential charging opportunities, a low charging rate ($< 6.6\,\mathrm{kW}$) is sufficient. Higher power ratings require extra investments in charging infrastructure and have an increasing grid impact. On the other hand, higher charging rates increase the charging flexibility and might be needed in some occasions. One can opt for a combination of EV charging infrastructure with different charging rates in a building/location where multiple EVs are charged. In that way, a suitable charging rate can be chosen upon arrival.

# Chapter 6

# Residential EV charging: scenario description

This chapter discusses the scenario for residential EV charging. In Chapter 7, the grid and fleet impact of the different EV charging strategies will be discussed. A larger residential building has been chosen to discuss the impact of multiple EVs charging in the building. Therefore, a representative apartment building (20 apartment units) has been chosen. The apartment building has a large PV system, and a heat pump is used for space heating and DHW. The scenario has been based on the following peer-reviewed paper:

> J. Van Roy, N. Leemput, F. Geth, R. Salenbien, J. Büscher, and J. Driesen, "Apartment building electricity system impact of operational electric vehicle charging strategies," *IEEE Trans. Sustain. Energy*, vol. 5, no. 1, pp. 320–327, Jan. 2014.

The apartment building is connected to a LV distribution grid. Section 6.1 describes the investigated scenario. The following parts are different or have been added to the scenario used in the paper mentioned above [126]:

- addition of a transient building response model to define the heating demand of the building;
- addition of the in-building grid topology, including a three-phase unbalanced power flow analysis, which is connected to a (simplified) LV distribution grid;
- addition of the heat pump demand profile;

- the use of a load profile generator [210] instead of using SLPs.

The grid impact is discussed for the reference scenario in Section 6.2. In this scenario, no EVs are charged in the apartment building. In Section 6.3, the different EV charging strategies will be discussed. The focus lies on simple, local EV charging strategies, as discussed in Section 2.6. The strategies have been slightly adapted compared to [126]. The impact of these EV charging strategies in an apartment building will be assessed in Chapter 7 and Chapter 8.

## 6.1 Scenario description

This section describes the scenario and the used models, which have been defined in Chapter 3 and Chapter 4.

### 6.1.1 Apartment building

As a representative case, an apartment building is chosen, which is originally representative for the Brussels-Capital Region [244].

#### Transient building response model

The transient building response model of IDEAS has been used, which allows to simulate the energy demand for heating (and cooling) of a multi-zone building, the energy flows in the building and the interconnection with thermal and electrical building systems [245]. The transient zone model consists of both the convective and radiative heat transfers, influencing the thermal zone comfort.

A short description of the transient building response model has been given in Appendix C.3. Appendix C.2 describes the solar shading for the building. The complete model description is available in [246].

#### Building topology description

The building consists of a ground floor with garage space and five floors with four individual apartment units each [244]. One garage (or parking spot) per apartment unit is assumed, including a grid connection possibility (including an electricity meter).

Each flat has a floor surface of 89 $m^2$ and thet have been all assumed to be identical. Therefore, it is assumed that the roof and ground slab have a total area of 356 $m^2$. Due to shading effects (e.g., tilted PV panels and other obstacles) the roof can only be partially covered with a perfectly oriented PV installation. This available surface is set to 65 % of the roof surface, i.e. 231 $m^2$ [247].

A one zone model has been developed for the transient building response model, in order to obtain a heating demand profile for the apartment building under consideration. The total zone air volume $V_{\text{zone}}$ is 5054 $m^3$, the air tightness of the building, i.e. the $n_{50}$ value, is 0.3. The total transmission heat loss area is equal to 2164 $m^2$.

For new buildings in Flanders, a maximum K value[1] of 40 is required since 2014 [249]. The insulation of the walls, the roof and ground slab have been chosen according to the values given in [244], resulting in a (more strict) K value of 24.2 [244].

**Wall characteristics** According to [244], the width of the building is at least 20 m. Therefore, the (interior) dimensions of the building have been set to 20 × 17.8 × 14.2 m. The wall characteristics (surface and orientation) are listed in Table 6.1. The walls are insulated with 0.1 m rockwool [245][2].

Table 6.1: Wall surfaces and orientations.

| Wall | Surface ($m^2$) | Orientation |
|---|---|---|
| Front | 284.00 | North |
| Left | 252.76 | East |
| Back | 284.00 | South |
| Right | 252.76 | West |

**Window characteristics** The total glass surface has been divided over the four different walls, proportional to the surface of the wall. Table 6.2 lists the window characteristics. The window area includes the window frame (area fraction of 0.15). The following glazing type has been chosen: Saint Gobain Climaplus Futur AR 1.1 4/15/4 ($U_{\text{ht}} = 1.10\,\text{W/m}^2\text{K}$, $g_s = 0.589$) [245][3].

The windows have exterior solar screens. The shortwave solar transmittance $f_s$ is equal to 0.24. The exterior solar screens are automated. The screens are

[1] Measure of the insulation quality [248].

[2] The thermal properties have been taken from the standard insulation materials available in the IDEAS library [245].

[3] Heat transfer coefficient $U_{\text{ht}}$, and $g_s$ a measure for the solar energy transmittance.

Table 6.2: Window surfaces and orientations.

| Window | Surface ($m^2$) | Orientation |
|---|---|---|
| Front | 39.87 | North |
| Left | 35.49 | East |
| Back | 39.87 | South |
| Right | 35.49 | West |

lowered when the horizontal solar irradiation is higher than $250\,W/m^2$ and raised when it drops below $150\,W/m^2$.

**Roof characteristics** The total roof surface is $356\,m^2$ and is insulated with extruded polystyrene, XPS (0.20 m).

**Ground slab characteristics** The total ground slab surface is $356\,m^2$ and is insulated with polyurethane foam, PUR (0.10 m). The total wall perimeter is 75.6 m.

### 6.1.2 Low-voltage and in-building electricity grid topology

Fig. 6.1 gives a representation of the considered grid topology. The apartment building, including the in-building electricity grid, is connected to a low-voltage distribution grid at the point of common coupling.

The scope of this work is to assess the impact trends of EV charging in the considered apartment building. Therefore, the LV distribution grid, to which the apartment building is connected, have been simplified as an aggregated load. This aggregated load has been included to obtain a more realistic voltage profile at the apartment building PCC. For EV charging integration in residential districts, the considered local solutions (see Chapter 7 and Chapter 8) can also be applied for EV charging integration in residential single dwellings. As equal impact trends may be expected [28], the assessment of the complete low-voltage distribution grid is out of the scope in this dissertation.

#### Low-voltage distribution grid

A residential LV distribution grid ($U^{\mathrm{nom}} = 230\,V$) with TT grounding has been used to observe a realistic unbalanced voltage profile at the apartment building

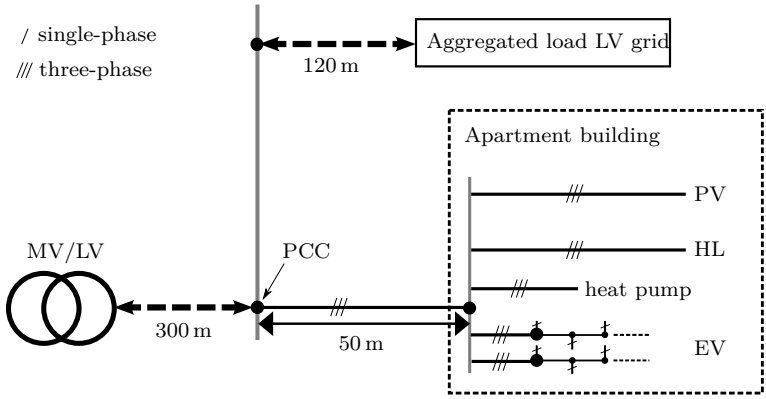


Figure 6.1: Schematic overview of the low-voltage and in-building electricity grid topology.

PCC. Note that a scenario has been created which will result in (under)voltage problems when EVs charge in the apartment building.

The LV grid is shown in Fig. 6.2. This feeder has been based upon a real urban feeder located in Flanders, Belgium [28, 250]. This feeder consists of 39 residential loads, connected to the grid through 29 nodes $n$ at a distance between 310 and 550 m from the 160 kVA MV/LV transformer (impedance of $0.0204 + 0.0675\,j\Omega$). Cable parameters have been taken from the design specifications of the standard for underground distribution cables, i.e. NBN C33-322 [251]. For the main feeder, the specifications of cable type EIAJB 1 kV $3 \times 70 + 1 \times 50\,\text{mm}^2$ have been used. To connect the different houses to the main feeder, the following cable specifications ($5.3 - 14.8$ m in length) have been used:

- EXVB 1 kV $4 \times 16\,\text{mm}^2$;
- EXVB 1 kV $4 \times 35\,\text{mm}^2$ at node 28 (houses 33 – 37).

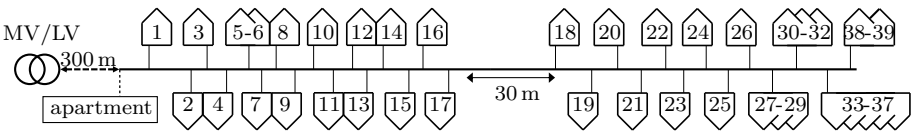


Figure 6.2: Schematic overview of the residential LV distribution grid topology with the connection to the apartment building and 29 connection nodes serving 39 households.

Since the analysis of the LV grid is out of the scope, and because of computational reasons, i.e. simulation time, the LV distribution grid feeder is represented as an unbalanced aggregated load as shown in Fig. 6.1. The aggregated load, including the losses in the grid, is located 420 m from the MV/LV transformer. The apartment building is connected 300 m from the MV/LV transformer.

This unbalanced aggregated load consists of the residential household load profiles, EV charging load profiles and PV production profiles. It is assumed that 50 % of the households in the LV distribution grid have a PV system and/or EV. These PV systems and EVs have been randomly placed. All households, EVs and PV systems have been assumed to have a single-phase grid connection between one of the three phases and the neutral conductor.

The residential load profiles, PV production profiles and EV charging load profiles have been generated using the models explained in Sections 6.1.3, 6.1.4 and 6.1.6, respectively. It is assumed that the EVs in these houses charge uncoordinatedly and that no heat pumps have been installed in these houses. The PV systems of the houses (limited <5 kVA) in this LV distribution grid have been sized to meet the yearly electricity demand of the respective households (without EVs).

### In-building distribution grid (apartment building)

At the PCC, the in-building grid of the apartment building is connected to the LV distribution grid through a separate feeder. The radial topology of the in-building network is shown in Fig. 6.1. The following cable specifications have been used [251]:

- EIAJB 1 kV $3 \times 70 + 1 \times 50\,\mathrm{mm}^2$;
- EAXVB 1 kV $4 \times 35\,\mathrm{mm}^2$.[4]

Due to their size, the PV system and heat pump of the apartment building are three-phase connected to the grid. On the other hand, the households and EVs are single-phase connected. The households have been aggregated at one node. The aggregated household profile for each phase is connected to the respective phase at this common node resulting in an unbalanced aggregated load. For the EVs, two three-phase feeders have been assumed at the garage floor. The number of EVs $n^{\mathrm{EV}}$ charged in the building is varied to assess the impact:

$$n^{\mathrm{EV}} \in \{10; 15; 20\}\ . \tag{6.1}$$

[4] Used to connect the aggregated households, the PV system, the heat pump and EVs.

### 6.1.3 Residential power consumption

Typically, synthetic load profiles (SLPs), which represent the average power consumption profile of residential electricity consumers, are used. However, a typical household power consumption profile has faster varying temporal load profiles [210].

Therefore, a stochastically representative set of single-phase grid-connected Flemish household active power demand profiles, with a 15 min time resolution, is generated. A load profile generator, as defined in [252], has been used. There is no information available on the reactive power consumption, nor on the voltage dependency. A constant power load, with a unity power factor, has been assumed in this dissertation. The week with the highest weekly residential energy use has been chosen to compare the different EV charging strategies.

### 6.1.4 Photovoltaic system

The PV production profile has been generated using the five-parameter model of [240], which is temperature-dependent. The description of the model has been given in Section 4.4. The five parameters are calculated based on characteristics provided by the solar panel manufacturer[5] [253]. The required specifications are:

- the current $I_{\mathrm{MPP}}$ and voltage $V_{\mathrm{MPP}}$ at maximum power point (MPP) under standard testing conditions (STC)[6];
- the short circuit current $I_{\mathrm{sc}}$ and open circuit voltage $V_{\mathrm{oc}}$ under STC;
- the temperature coefficients $k_i$ and $k_v$ of the short circuit current and open circuit voltage, respectively.

These parameter values (including the solar panel surface) are listed in Table 6.3. It is assumed that the panels are perfectly oriented southwards with an optimal inclination of 34°. This fixed orientation results in the maximum annual electricity production for the considered location[7]. This perfect orientation is a valid assumption for flat roofs.

Typically, the so-called European efficiency is used to compare grid-connected PV inverters [254]. This efficiency takes into account the different operating regimes, i.e. part load operation of the converters, over the entire production period. In

[5] Sanyo HIP-230HDE1 [253].

[6] STC: air mass of 1.5, an irradiance of 1000 $\mathrm{W/m^2}$ and a cell temperature of 25°C.

[7] A different orientation might yield an increased simultaneity of PV power production and local electricity consumption, but the total electricity production will decrease.

Table 6.3: PV panel ratings and parameters [253].

| | | | | | |
|---|---|---|---|---|---|
| $I_{\mathrm{MPP}}$ | (A) | 6.71 | $V_{\mathrm{oc}}$ | (V) | 42.3 |
| $V_{\mathrm{MPP}}$ | (V) | 34.3 | $k_i$ | (mA/°C) | 2.17 |
| $I_{\mathrm{sc}}$ | (A) | 7.22 | $k_v$ | (V/°C) | -0.106 |
| $A_{\mathrm{panel}}$ | ($\mathrm{m}^2$) | 1.386 | | | |

accordance, a constant converter efficiency is assumed for the PV system, i.e. 99 % and 98 % for the DC-DC and DC-AC converter, respectively [253, 255].

The total yearly electricity consumption of the households in the apartment building is 59.1 MWh, which would require 273 PV panels to cover the yearly electricity consumption. Based on the manufacturers data and the available roof area of the apartment building (see Section 6.1.1), the PV system has a peak power of about 38.4 kW. Due to the limited roof surface, the PV system is undersized relative to the yearly power consumption.

PV power production can vary significantly from day to day. To take the variable output into account and to limit the number of simulations or simulation duration, a week with a variable PV power output has been chosen [200]. This profile contains days with a high and low energy output, as well as fast varying outputs.

### 6.1.5 Heating system

It is assumed that the heating system consists of an air-to-water heat pump, including a thermal energy storage system (assuming one water storage tank, $3\,\mathrm{m}^3$) for the domestic hot water demand (DHW). The heating system has been based upon models available in IDEAS. A heating system, based upon the work in [19], is available for a single dwelling. It is assumed that this system is applicable for the apartment building under consideration. Appendix C.4 briefly discusses the modeling background of the heating system.

A new apartment building has been considered, for which it is assumed that heat is emitted to the building interiors through a floor heating system. Since a night setback is difficult to implement and has a limited impact for new buildings [19, 256, 257] and due to the stochastic user presence, a fixed zone temperature set-point of 21°C is taken. The nominal power $Q_{\mathrm{nom}}$ (35 kW) of the heat production unit and emission system components are based on the design[8] heat demand of the dwelling.

[8]Design parameters: outdoor temperature of -8°C and no solar irradiation.

The heat pump is grid-connected through power electronic converters. The converter efficiencies have been assumed identical to the converters used for the PV system (see Section 6.1.4).

### 6.1.6 Electric vehicles

The EV model consists of three submodels: a battery model, the mobility behavior and the charging behavior. The local EV charging strategies will be discussed in Section 6.3.

#### Battery model

The implementation of the battery model has been based on the model used in [153], which has been discussed in Section 4.5.

Li-ion type batteries have been chosen. The charging $\eta^c_{\text{bat}}$ and discharging efficiencies $\eta^d_{\text{bat}}$ of the battery are 88.2 % and 98 %, respectively[9]. The self-discharge $\delta^{\text{sd}}$ is 3.0 %/month [153]. The inverter efficiency[10] is 96 % [258, 259]. It is assumed that the efficiency of the DC-DC converter is 98 % [260].

The EVs have been modeled as extended range electric vehicles in order to meet all mobility requirements, even if the battery is depleted, as defined in Section 2.1. EREVs drive fully electrically until the battery is depleted. At that moment, the internal combustion engine is engaged.

As discussed in Section 3.1.5, the vehicle fleet is divided into three vehicle segments, i.e. small, middle-class and large vehicles. Each vehicle segment is given a different battery capacity, namely a nominal battery capacity of 10, 15 and 20 kWh. These are battery capacities which can be found in different PHEVs and BEVs on the market (see Section 2.2.1). As mentioned before, the usable battery capacity $E_{\text{eff}}$ is limited to 80 % of the nominal battery capacity to extend the battery cycle life [60].

#### Mobility Behavior

A mobility simulation tool has been used to generate the mobility behavior profiles for a fleet of EVs [85], which has been discussed in Chapter 3. The specific electricity consumption of the EVs are 0.185, 0.220 and 0.293 kWh/km for small, middle-class and large vehicles, respectively.

[9] $\eta^c_{\text{bat}}$ includes the Coulomb efficiency, $\eta^d_{\text{bat}}$ only includes the DC-link efficiency [153].
[10] During both charging and discharging.

#### Charging rates

Different charging rates $P^{\text{ch}}$ have been examined, which are typical for mode 2 and mode 3 charging, as defined in IEC 61851-1 [73]. Single-phase charging (230 V) is assumed with the following charging rates available: 2.1 kW (10 A), 3.3 kW (16 A) and 6.6 kW (32 A). These include a 10 % margin to take into account the maximum allowed voltage deviations (EN 50160). The minimum charging power, to avoid low converter efficiencies at partial load, is set to $P_{\text{min}} = 1/16 P^{\text{ch}}$.

### 6.1.7 Simulation specifications

A three-phase unbalanced load flow is performed using the IDEAS library. Unbalanced loads have been taken into account, as well as the resulting zero-point shift due to currents running through the neutral conductor.

For computational reasons, i.e. calculation time, the simulations have been performed for a one week period (Monday till Sunday) with a 1 min time resolution ($\Delta t$). The one week period, i.e. the week with the highest electricity demand, has been taken from yearly demand and production profiles for the households, heat pump demand and PV generation. The household power profiles are available on a 15 min time resolution, which are interpolated on a 1 min time resolution (within Dymola). The heat pump and EV demand profiles, and PV production profiles are available on a 1 min time resolution.

## 6.2 Results: reference scenario (no EVs)

This section discusses the grid impact results for the reference scenario, i.e. the scenario without EVs charging in the apartment building. Fig. 6.3 shows the load duration curve of the apartment building in the reference scenario without EVs. The demand and injection peak power are 33.9 kW and 23.6 kW, respectively. The demand OPP is 27.5 kW, which is about 19 % lower than the peak demand. The injection OPP is 22.3 kW. For about 15 % of the time, there is a net-injection of PV power in the LV distribution grid.

Due to the non-coincidence of the household and heat pump demand, and the local PV production, the self-consumption of the local PV production is 56.2 %. This means 43.8 % of the surplus electricity is injected into the LV distribution grid. Only 19.2 % of the local demand is instantaneously covered by PV power.

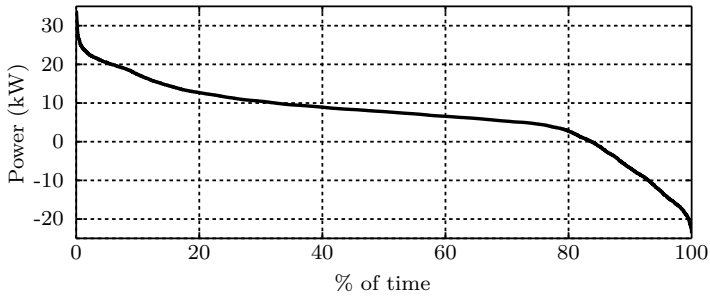


Figure 6.3: Load duration curve for the reference scenario without EVs.

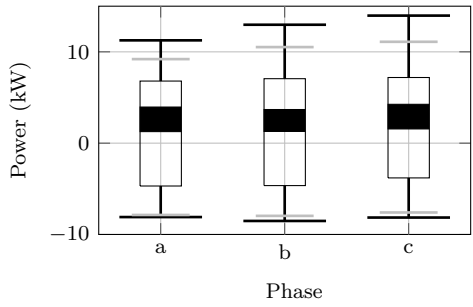


Figure 6.4: Distribution profiles for each phase of the apartment building net power profiles.

Fig. 6.4 shows the unbalanced power profiles in the three phases of the grid. This unbalance translates to voltage unbalances in the electricity grid. Fig. 6.5 (a) shows the distribution of the voltage profile at the apartment building PCC. No overvoltages occur, but the minimum voltage is 0.87 pu. In both the first and third phase, the voltage drops below 0.90 pu. The VUF distribution is given in Fig. 6.5 (b). The maximum VUF is 2.5 %. Since the voltage only drops for 0.1 % of the time below 0.90 pu, and the VUF is only 0.1 % of the time beyond 2 %, the PCC is compliant with the EN 50160 regulations (see Table 6.4).

Table 6.4: Apartment building PCC: voltage magnitude and VUF.

| | | | **Weekly duration** | |
|---|---|---|---|---|
| $\boldsymbol{u}_{\min}$ | $\boldsymbol{u}_{\max}$ | $\boldsymbol{VUF}_{\max}$ | $\boldsymbol{u < 0.9\,\text{pu}}$ | $\boldsymbol{VUF > 2\,\%}$ |
| 0.87 pu | 1.05 pu | 2.5 % | 0.1 % | 0.1 % |

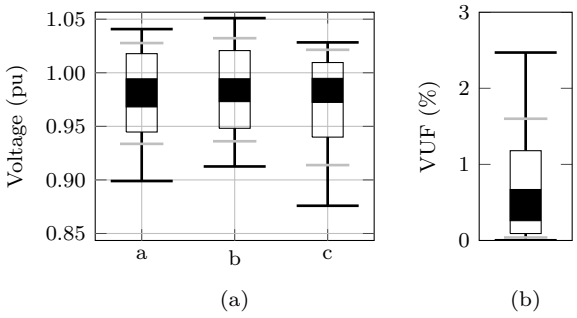


Figure 6.5: (a) Phase voltage magnitude and (b) VUF at the apartment building PCC.

## 6.3 EV charging strategies

Different rule-based EV charging strategies have been assessed for a certain charging rate $P^{\text{ch}}$ (Section 6.1.6), which is the maximum charging power. The charging strategies under consideration, are developed from the DSO and grid point of view, taking into account the flexibility offered by the EV owners.

For the residential case, only charging at home is considered. This can be considered as the worst-case from the residential building point of view. Two periods of charging have been considered: charging during the peak (7 am – 10 pm) and off-peak period (10 pm – 7 am). These periods coincide with the typical double day-night tariff periods in Belgium [90][11].

As discussed in Section 2.6, the focus lies on simple, local EV charging strategies. No optimization to coordinate the EV charging is performed. The analyzed charging strategies require limited future knowledge on the mobility behavior, and require no local information, such as the grid topology. They can be easily implemented on-board or in mode 3 charging infrastructure. To charge EVs with a DER surplus, only local communication within the building is needed, e.g., with a building energy management system. No prediction is required regarding the local generation production profile. The discussed strategies can still be complemented by a charging optimization strategy, which sets a charging power set-point that can be deviated from.

[11] Other off-peak periods exist, e.g., 9 pm – 6 am.

### 6.3.1 Uncoordinated charging, EV based peak shaving and delayed charging

First, three different EV charging strategies will be discussed which set a certain charging power set-point.

#### Uncoordinated charging

In the uncoordinated charging strategy, EV charging at maximum power $P^{\mathrm{ch}}$ starts as soon as the vehicle arrives at the charging spot. The charging power set-point $P^{\mathrm{set}}$ at each time step $k$ is:

$$P_k^{\mathrm{set}} = P^{\mathrm{ch}}. \tag{6.2}$$

#### EV based peak shaving

The EVs charge at a reduced charging power in order to maximize the charging duration during each charging opportunity, i.e. between the time of arrival at home and leaving for the next trip, while maintaining the mobility requirements. The objective is to reduce the local grid impact, i.e. minimizing the charging power[12], without interaction between the end user and the grid. The simultaneity of the EV charging with local generation may increase. Besides, the EV owner in turn might benefit from an increased battery lifetime due to lower charging currents [59, 60, 62].

Therefore, the charging power set-point $P^{\mathrm{set}}$ at each time step $k$ is reduced as much as possible to allow to fully charge the battery during each charging opportunity. Moreover, this strategy still allows to further shift the charging load if required (e.g., by increasing or decreasing the charging power). For this strategy, only the knowledge of the next departure time $T_{\mathrm{dep}}$ and the battery SoC are required. The reduced charging power set-point $P^{\mathrm{set}}$ is calculated at each time step $k$:

$$P_k^{\mathrm{set}} = \max\left[\min\left(\frac{E_{\mathrm{req}}}{\Delta T_k}, P^{\mathrm{ch}}\right), P_{\mathrm{min}}\right], \tag{6.3}$$

with $\Delta T_k$ $(= T_{\mathrm{dep}} - k\Delta t)$ the time until the next departure time and $E_{\mathrm{req}}$ the required energy to fully charge the EV[13].

[12] A reduced charging power also reduces the grid losses.
[13] The required energy $E_{\mathrm{req}}$ includes the losses during charging.

This strategy can be easily implemented on-board or in mode 3 charging infrastructure (using the PWM duty cycle to set the charging power). In the latter case, the battery SoC has to be communicated with the charging infrastructure. In both cases, the next departure time is required. Here, the exact knowledge of the next departure time $T_{\text{dep}}$ is assumed. In reality, people may leave earlier or later than the predetermined time. This spread may be in the order of minutes to hours. The charging power set-point is reduced or increased whether the EV is leaving later or earlier, respectively. When the change in $T_{\text{dep}}$ is known well in time[14], no impact on the UF is observed. In case the charging power set-point is limited by the EV charging rate, the UF is impacted.

### Delayed charging

In order to lower the simultaneity of the EV charging load with the building load in the evening, and in order to anticipate on possible local electricity production during the daytime period, e.g., PV power production, the EV charging can be postponed during each charging opportunity. The EV charging is postponed until the EV has to start charging to have a fully charged battery when leaving for the next trip, i.e. when no charging flexibility (in time) is left to maintain the mobility requirements. Besides, it is expected that a lower average SoC may increase the battery lifetime [59].

For this strategy, only the knowledge of the next departure time $T_{\text{dep}}$ and the battery SoC are required, as implemented in for instance the Nissan Leaf [52]. At each time step $k$, the required time $t_{\text{req}}$ to fully charge the battery is calculated:

$$t_{\text{req},k} = \frac{(E_{\text{eff}} - E_k^{\text{bat}})}{\eta^c P^{\text{ch}}}. \tag{6.4}$$

The charging power set-point $P^{\text{set}}$ at each time step $k$ is:

$$P_k^{\text{set}} = \begin{cases} 0 & \text{if } t_{\text{req},k} < \Delta T_k, \\ P^{\text{ch}} & \text{if } t_{\text{req},k} \geq \Delta T_k. \end{cases} \tag{6.5}$$

Here, the exact knowledge of the next departure time $T_{\text{dep}}$ is assumed. In reality, people may leave earlier or later than the predetermined time. This spread may be in the order of minutes to hours. The impact on the UF depends on the time the change in $T_{\text{dep}}$ is made. As a result of the spread on $T_{\text{dep}}$, the UF might decrease.

[14] This time is function of the total standstill time, EV charging rate and the battery SoC, i.e. amount of electricity to be charged.

### 6.3.2 Off-peak charging and local generation surplus charging

The EV charging process can deviate from the charging power set-point in function of the time of the day (off-peak charging) or a local generation surplus.

#### Off-peak charging

In order to lower the simultaneity of the EV charging load with the building load in the evening, the EVs only charge during the off-peak period, i.e. between 10 pm and 7 am [90]. Off-peak charging also reduces the charging cost of the EV owner as the electricity price is reduced during the off-peak period.

$$P_k^{\text{set,night}} = \begin{cases} 0 & \text{if } 7\,\text{am} \leq k\,[\text{h}] < 10\,\text{pm}, \\ P_k^{\text{set}} & \text{if } 10\,\text{pm} \leq k\,[\text{h}] < 7\,\text{am}. \end{cases} \tag{6.6}$$

In this dissertation, off-peak charging has only been investigated in combination with uncoordinated charging.

#### Charging local generation surplus

To increase the self-consumption of locally generated PV power, i.e. reducing the PV surplus injection into the distribution grid, the surplus of PV power $P^{\text{surplus}}$ at time step $k$ is divided over the nonfully charged EVs $n^{\text{gEV}}$, which are connected to the grid at time step $k$. The PV power surplus is defined as the power that is injected into the LV distribution grid:

$$P_k^{\text{surplus}} = |P_k^{\text{PV}}| - P_k^{\text{HL}} - P_k^{\text{HP}} \tag{6.7}$$

The PV power surplus is divided equally in order not to give preference to one or more EVs.

$$P_k^{\text{set,PV}} = \begin{cases} P_k^{\text{set}} & \text{if } \frac{P_k^{\text{surplus}}}{n_k^{\text{gEV}}} \leq P_k^{\text{set}}, \\ \frac{P_k^{\text{surplus}}}{n_k^{\text{gEV}}} & \text{if } P_k^{\text{set}} < \frac{P_k^{\text{surplus}}}{n_k^{\text{gEV}}} < P^{\text{ch}}, \\ P^{\text{ch}} & \text{if } \frac{P_k^{\text{surplus}}}{n_k^{\text{gEV}}} > P^{\text{ch}}. \end{cases} \tag{6.8}$$

Note that this EV charging strategy assumes that the building load, including the heat pump, is covered by the available PV power. The PV power surplus is charged by the EVs, i.e. the controllable loads.

This strategy requires a detection of the number of grid-connected EVs, which still need to be charged. This detection can be achieved by a building energy management system, through interfacing with the EV supply equipment. The energy management system communicates the extra power that can be drawn by the EVs by changing the PWM duty cycle of the control pilot as defined in IEC 309-2 [78]. It is assumed that the building power demand (excluding the EV demand) and DER power production are measured and communicated with the building energy management system.

### 6.3.3 Voltage droop mechanism and building peak shaving

The EV charging process can also deviate from the charging power set-point as a function of grid conditions, i.e. the grid voltage (voltage droop mechanism) or power demand (building peak shaving).

#### Voltage droop mechanism

In the EV voltage droop mechanism, comparable to a PV voltage droop mechanism [238, 239, 261], the charging power set-point $P^{\text{set,dr}}$ depends on the grid voltage magnitude at the respective phase $p$ and node $n$ to which the EV is connected:

$$P_k^{\text{set,dr}} = f(|u_{p,n,k}|), \tag{6.9}$$

with $u_{p,n,k} = U_{p,n,k}/U^{\text{nom}}$ (pu) and $U^{\text{nom}}$ the nominal voltage (230 V). $f(|u_{p,n,k}|)$ is a linear function between 0 and 1 between the deterministic ($|u_l| = 0.85\,\text{pu}$) and probabilistic ($|u_h| = 0.9\,\text{pu}$) voltage limits in the EN 50160 standard measurement procedure [157], which is shown in Fig. 6.6. The objective is to reduce the voltage deviations in the grid.

$$P_k^{\text{set,dr}} = \begin{cases} 0 & \text{if } |u_{p,n,k}| < |u_l|, \\ \frac{|u_{p,n,k}|-|u_l|}{|u_h|-|u_l|} P^{\text{ch}} & \text{if } |u_l| \leq |u_{p,n,k}| \leq |u_h|, \\ P^{\text{ch}} & \text{if } |u_{p,n,k}| > |u_h|. \end{cases} \tag{6.10}$$

A voltage droop mechanism can be easily built in on-board as a voltage measurement is present in EVs. On the other hand, a voltage measurement can be added to mode 3 charging infrastructure to implement a voltage droop mechanism off-board. However, in the latter case, EVs only have to adapt their charging power within 5 s (PWM duty cycle).

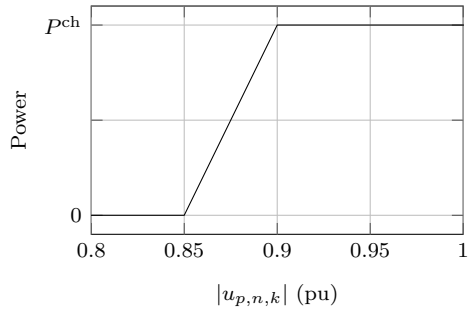


Figure 6.6: Voltage droop charging behavior profile in function of the grid voltage ($f(|u_{p,n,k}|)$).

### Building peak shaving (BPS) mechanism

The charging power set-point $P^{\text{set}}$ of the EVs is equally lowered if the total power demand from the households $P^{\text{HL}}$, heat pump $P^{\text{HP}}$ and EVs charging exceed the available capacity $P^{\text{cap}}$. The available (total) EV charging power $P^{\text{set,av}}$ at time step $k$ is:

$$P_k^{\text{set,av}} = P^{\text{cap}} - P_k^{\text{HL}} - P_k^{\text{HP}} + |P_k^{\text{PV}}|. \tag{6.11}$$

At each time step $k$, $P^{\text{set,av}}$ is divided equally over all nonfully charged EVs connected to the grid ($n^{\text{gEV}}$):

$$P_{\text{EV},k}^{\text{set,av,}} = P_k^{\text{set,av}} / n_k^{\text{gEV}}. \tag{6.12}$$

The charging power set-point $P_k^{\text{set,peak}}$ for each EV is:

$$P_k^{\text{set,peak}} = \max\left[\min(P^{\text{ch}}, P_k^{\text{set}}, P_{\text{EV},k}^{\text{set,av,}}), P_{\min}\right]. \tag{6.13}$$

A building energy management system can be used to detect the number of grid-connected EVs, which still need to be charged, and to measure the building power demand and production. This system interfaces with the EVSE to communicate to lower the power drawn from the grid, and requires no user interaction. A similar commercial implementation is found in [262].

The total load, including the EV charging, can still exceed the maximum capacity, since the grid losses have not been included to calculate $P^{\text{set,av}}$. A margin may be foreseen.

## 6.4 Conclusions

This chapter describes the residential scenario, for which the impact of different EV charging strategies will be assessed in Chapter 7. A representative apartment building has been chosen. Therefore, the impact of multiple EVs charging in the building can be assessed. The following parts have been described:

- a transient building response model of the considered building to define the heating demand;
- an in-building electricity network, which is connected to a residential LV distribution grid;
- a large PV system on the roof of the building;
- a heat pump used for space heating and domestic hot water;
- EVs which are charged inside the apartment building.

Due to the single-phase connection of the household loads, unbalance is present in the in-building three-phase network, which results in an unbalanced three-phase voltage profile. The reference scenario is compliant with the EN 50160 regulations regarding the voltage magnitude profile and voltage unbalance. When no EVs charge in the apartment building, around 56 % of the local PV production is consumed inside the building. There is a net-injection of PV power in the LV distribution grid for about 15 % of the time.

To conclude, different local EV charging strategies have been defined, for which the grid and fleet impact is assessed in Chapter 7. Table 6.5 gives an overview of the different EV charging strategies, including their DSO POV objective. The table also mentions if a charging strategy sets a charging power set-point or if it deviates from a given charging power set-point.

First, Section 6.3.1 discusses three strategies, which set a charging power set-point. For uncoordinated and delayed charging, the EVs charge at maximum power, but the EV charging process is shifted in time. If EV based peak shaving is applied, EVs charge at a reduced charging power in order to maximize the charging duration and to minimize the charging power during each EV charging opportunity. Furthermore, different EV charging strategies have been defined which can deviate the EV charging power from the given set-point (of one of the three strategies above). The charging power can deviate from the power set-point depending on:

- the timing of the charging process, i.e. off-peak charging (Section 6.3.2);
- the availability of local generation surplus (Section 6.3.2);

Table 6.5: Overview of local EV charging strategies.

| **Strategy** | **Objective** | **Set-point?** |
|---|---|---|
| Uncoordinated | No coordination mechanism present | Set-point |
| EV based peak shaving | Minimizing EV charging power<br>Increasing simultaneity with local electricity generation | Set-point |
| Delayed | Minimizing simultaneity with other building loads<br>Increasing simultaneity with local electricity generation | Set-point |
| Off-peak | Minimizing simultaneity with other building loads | Deviation set-point |
| Local generation surplus | Maximizing self-consumption | Deviation set-point |
| Voltage droop mechanism | Reducing voltage deviations | Deviation set-point |
| Building peak shaving | Reducing building peak power | Deviation set-point |

- the grid conditions (Section 6.3.3), i.e. the grid voltage (voltage droop mechanism) or the total building power demand (building peak shaving).

The following chapter discusses the grid and fleet impact trends of the different EV charging strategies.

# Chapter 7

# Impact EV charging in an apartment building

As indicated in Chapter 2, EV charging is likely to have an impact on the in-building electricity grid and LV distribution grid when EVs are charged uncoordinatedly. Therefore, this chapter focuses on the impact assessment of different local rule-based EV charging strategies for the case study defined in Chapter 6. These charging strategies use the available EV charging flexibility, both in time and in charging power. The objective of this chapter is to perform a comparison to investigate the impact trends of different local EV charging strategies, which use minimal local or EV internal knowledge, and which do not require any optimization process. Both the grid and fleet impact have been assessed. The objective is to examine how these strategies can already limit the grid impact (as short-term solutions). This reduced grid impact allows more EVs or other systems, such as PV systems or heat pumps, to be integrated within the system.

First, the EVs are charged uncoordinatedly as a reference case in Section 7.1. In Section 7.2, the impact trends of delayed charging and EV based peak shaving are investigated, including charging a local surplus of PV power. Section 7.3 describes the impact of the voltage droop mechanism, while the building peak shaving mechanism is described in Section 7.4. To conclude, Section 7.5 compares uncoordinated charging, including a combination of the voltage droop and building peak shaving mechanism, to the *optimal capacity charging* algorithm, which is developed at the Electricity Research Centre in University College Dublin [263, 264].

## 7.1 Uncoordinated EV charging

First, EVs are uncoordinatedly charged at maximum charging rate $P^{\text{ch}}$. In this section, results are discussed for a number of grid and fleet impact indicators, as discussed in Section 2.8. Two scenarios have been investigated:

- **Scenario 1:** Uncoordinated EV charging whenever EVs arrive at home.
- **Scenario 2:** Uncoordinated EV charging limited to the off-peak period.

### 7.1.1 Fleet impact

Not all EVs arrive/leave at home at the same time, and a different amount of electricity is required to be charged. Therefore, an inherent EV charging load spreading is present. Fig. 7.1 represents the EV charging simultaneity. The maximum number of EVs charging simultaneously in the apartment building is equal or less than the number of EVs charged in the building. For instance, in scenario 1 and a charging rate of 2.1 kW, a maximum of 12 EVs is charging simultaneously, for a fleet of 20 EVs in the building, while the average number of EVs charging simultaneously at each time step is only 2.9. For an increasing charging rate, the charging simultaneity decreases. The simultaneity decreases due to a decreasing charging duration, as shown in Fig. 7.2. Fig. 7.2 shows the minimum, mean and maximum charging duration in the EV fleet of 20 vehicles.

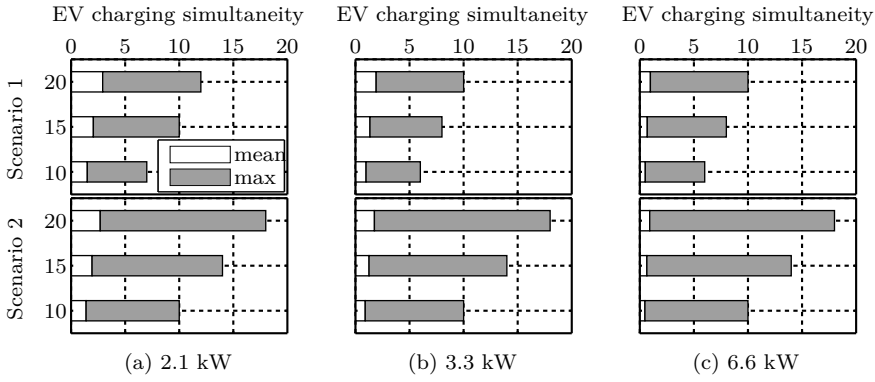


(a) 2.1 kW (b) 3.3 kW (c) 6.6 kW

Figure 7.1: EV charging simultaneity as a function of the charging rate ($P^{\text{ch}} \in \{2.1; 3.3; 6.6\}$ kW) and number of EVs ($n^{\text{EV}} \in \{10; 15; 20\}$) charged in the apartment building.

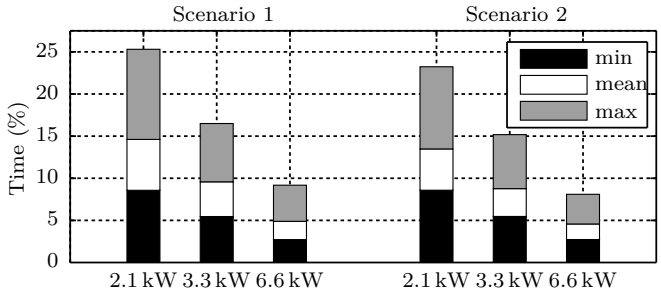


Figure 7.2: EV charging duration (% of the week) as a function of the charging rate ($P^{\text{ch}} \in \{2.1; 3.3; 6.6\}$ kW) for a building fleet of 20 EVs.

In the second scenario, EV charging is limited to the off-peak period. Due to the synchronization of EV charging at the start of the off-peak period, the EV charging simultaneity increases compared to scenario 1. The maximum number of EVs charging simultaneously is independent of the charging rate since the EV charging start time remains identical. However, for an increasing charging rate, the mean EV charging simultaneity decreases, since the EV charging duration decreases due to the limited time window in which charging is allowed.

Fig. 7.3 shows the average UF of the building fleet. It can be observed that with a limited battery size a relatively high UF can already be obtained. Increasing the charging rate may result in a higher UF in case the battery was not fully charged at some occasions for a lower charging rate. This means that more electricity is charged for an increasing charging rate. Therefore, an increasing amount of kilometres can be driven fully electrically. Scenario 2 results in a reduced UF, since the charging time window is limited to the off-peak period.

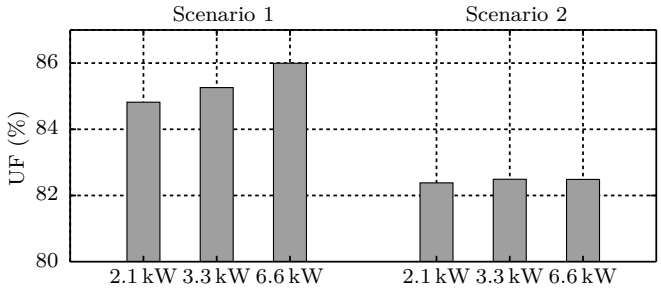


Figure 7.3: Average EV utility factor as a function of the charging rate ($P^{\text{ch}} \in \{2.1; 3.3; 6.6\}$ kW) for a building fleet of 20 EVs.

### 7.1.2 Grid impact

#### Peak power demand and injection

Fig. 7.4 shows the modified box plots, as defined in Fig. 2.10, of the apartment building load duration curves for the different scenarios, EV penetration rates and EV charging rates.

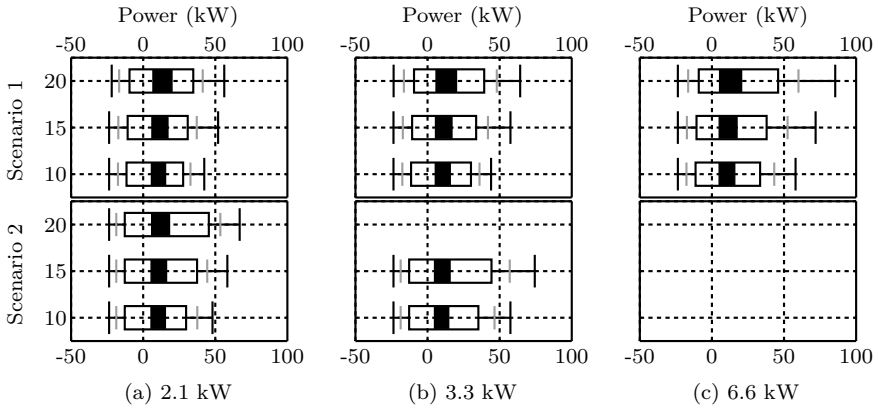


Figure 7.4: Modified box plots for load duration curves as a function of the charging rate ($P^{\mathrm{ch}} \in \{2.1; 3.3; 6.6\}$ kW) and number of EVs ($n^{\mathrm{EV}} \in \{10; 15; 20\}$) charged in the apartment building.

In scenario 1, the peak power demand increases for an increasing number of EVs and charging rate. For instance, the peak power demand for a charging rate of 6.6 kW is 19.2 – 52.1 % higher compared to a charging rate of 2.1 kW. The injection peak is only lower for 20 EVs charging at a rate of 2.1 kW. In this case, the injection peak is about 7.7 % lower compared to the reference scenario. This indicates a very low simultaneity of EV charging for uncoordinated charging and the peak injection due to PV power production. Only in the given case, the EV charging takes long enough to coincide with the PV power production peak. Nevertheless, the increasing percentile values ($OPP_{\mathrm{inj}}$ and 5th percentile) show that the EVs consume a small part of the locally generated PV power.

In the second scenario, only off-peak charging is possible. Therefore, there is no impact on the injection peak, nor self-consumption. As a result of the higher synchronization of the EV charging load, the demand peak powers increase compared to scenario 1. Note that the power flow analysis of some cases in scenario 2 is infeasible. This is due to the synchronization of the EV charging

loads, which leads to too high loads for the given network and too high voltage drops. Therefore, these results are not included[1].

A rule of thumb[2] has been used to define the building connection capacity of an apartment building, namely 2.5 kVA per apartment unit, i.e. 50 kVA for the given apartment building. For the lowest EV charging rates, there are virtually no cases with any overload, assuming a power factor of one, i.e. no reactive power. For increasing charging rates, overloading occurs more frequently, however for less than 5 % of the time.

### Minimum voltage magnitude

As discussed in Section 6.2, only undervoltage problems will occur in this case study. The minimum occuring grid voltages (PCC of the apartment building and in-building grid) are displayed in Fig. 7.5 (a). Fig. 7.5 (b) shows the % of the time that the grid voltage is lower than 0.90 pu.

In all cases, the minimum voltage drops below 0.90 pu. However, only in scenario 1 with 20 EVs and a charging rate of 6.6 kW, the voltage drops for more than 5 % of the time below 0.90 pu. Therefore, the latter case is not compliant with the EN 50160 regulations. In a few more cases, the voltage also drops below 0.85 pu, which means that these cases are also not compliant with the grid regulations. It can be observed, that the minimum voltage decreases for an increasing number of EVs and an increasing charging rate due to the increasing demand peaks. These are the result of an increased EV charging simultaneity. However, this dependency is much lower (to non-existent) for the feasible cases in scenario 2 ($P^{\text{ch}} = 2\,\text{kW}$). The latter means that in scenario 2, the minimum voltages are the result of the other building loads (residential power consumption and heat pump), which occur during the evening outside the off-peak period.

### Voltage unbalance

Fig. 7.6 (a) shows the maximum VUF, while Fig. 7.6 (b) shows the % of the time that the VUF exceeds 2 %. There is no clear relation between the increase in VUF and the number of EVs and charging rate. This is due to the fact that the VUF is a function of the load unbalance. For all cases but one, the VUF is higher than 2 % for less than 5 % of the time. For the lowest charging rates, the maximum VUF is almost independent of the number of EVs charging.

[1] Note that the results are given in Section 7.1.1 (fleet impact) and Fig. 7.7 (cover factors). These results (infeasible cases) are only valid in case the power flow is feasible.

[2] Internal communication with Eandis [265], a Flemish distribution system operator.

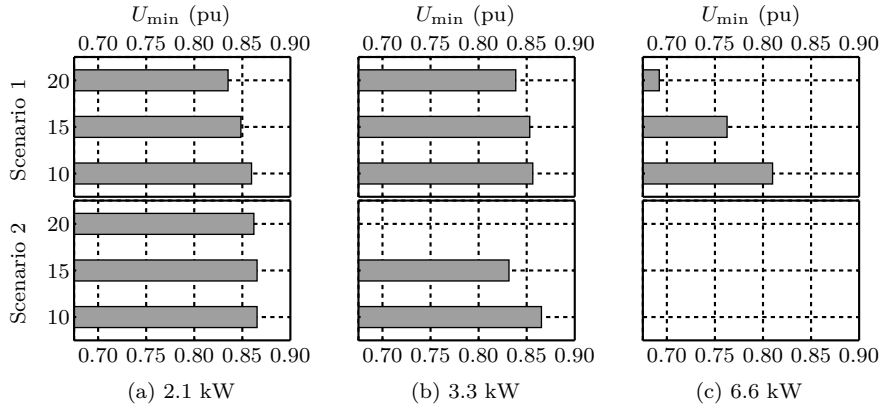


(a) 2.1 kW (b) 3.3 kW (c) 6.6 kW

(a) Minimum voltage magnitude.

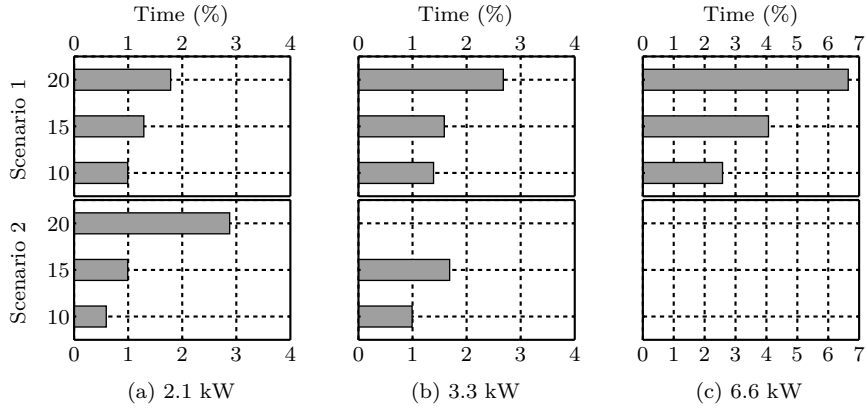


(a) 2.1 kW (b) 3.3 kW (c) 6.6 kW

(b) % of the time that the grid voltage is lower than 0.90 pu.

Figure 7.5: (a) Minimum voltage magnitude in the apartment building, and (b) % of the time that the grid voltage is lower than 0.90 pu, as a function of the charging rate ($P^{\text{ch}} \in \{2.1; 3.3; 6.6\}$ kW) and number of EVs ($n^{\text{EV}} \in \{10; 15; 20\}$) charged in the apartment building.

## Self-consumption and self-generation

The self-consumption, $\gamma_S$, and self-generation, $\gamma_D$, are shown in Fig. 7.7. In the reference scenario, the self-consumption and self-generation are 56.2 % and 19.0 %, respectively. For the second scenario, there is no simultaneity with the PV power production. The self-consumption is identical to the reference scenario. Therefore, it is not shown.

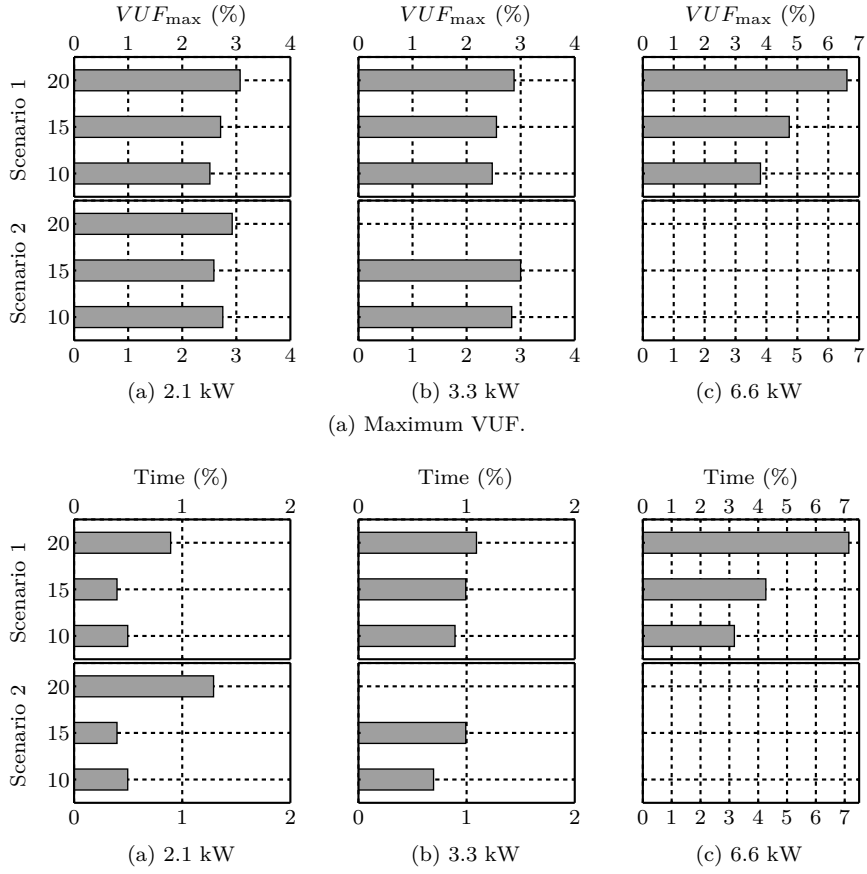


(a) Maximum VUF.

(b) % of the time that the VUF goes beyond 2 %.

Figure 7.6: (a) Maximum VUF in the apartment building, and (b) % of the time that the VUF goes beyond 2 %, as a function of the charging rate ($P^{\text{ch}} \in \{2.1; 3.3; 6.6\}$ kW) and number of EVs ($n^{\text{EV}} \in \{10; 15; 20\}$) charged in the apartment building.

In scenario 1, the self-consumption increases for an increasing number of EVs due to an increase in simultaneity of EV charging and PV power production. On the other hand, the self-generation decreases since the total electricity consumption increases. There is a very low (to non-existent) sensitivity to the EV charging rate.

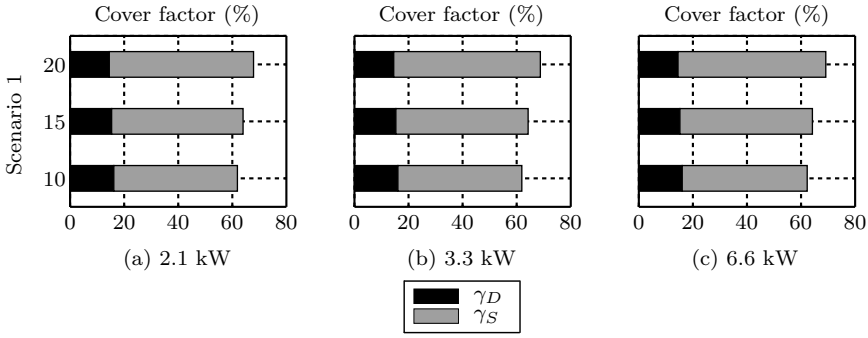


Figure 7.7: Cover factors $\gamma_S$ and $\gamma_D$ as a function of the charging rate ($P^{\text{ch}} \in \{2.1; 3.3; 6.6\}$ kW) and number of EVs ($n^{\text{EV}} \in \{10; 15; 20\}$) charged in the apartment building.

### 7.1.3 Conclusions

When EVs are uncoordinatedly charged, charging at maximum power starts whenever EVs arrive at home. Off-peak charging can be preferred to decrease the charging cost. In the latter case, EVs start charging at the start of the off-peak period or whenever arriving at home during the off-peak period. Due to the stochastic mobility behavior, not all EVs will charge at the same time. An inherent low EV charging simultaneity is present. For instance, for 20 EVs in the building, a maximum of 12 EVs will charge simultaneously. On average, only 2.9 of the EVs charge at the same time. When only off-peak charging is allowed, the charging simultaneity increases to a maximum of 18 EVs.

EV charging will have an impact on the LV distribution grid, depending on the EV penetration rate, the charging power, and thus the EV charging simultaneity:

- an increase in the demand peak power;
- a possible reduction in the injection peak power;
- a decrease in the minimum occurring grid voltage.

In Fig. 5.2 (a), it is shown that even during the day at least 24.2 % of the vehicles are parked at home. As a result of the long standstill times and the high grid connection probability during daytime at home, additional daytime charging (scenario 1) results in different benefits for different actors, such as a decreased grid impact and an increased user comfort:

- an increased electric driving range (increased UF, up to 3–4 % in this case study) for the **EV user**;

- a decreased EV charging simultaneity with the residential power peak during the evening, and a decreased synchronization of EVs charging at the start of the off-peak period;
  - the power demand peaks in the LV distribution grid (**DSO**) decrease, up to a maximum of 23 % in this case study.
  - flattening out of EV demand profile for both the **DSO** and **TSO**.
- increased renewable integration;
  - local consumption of locally produced electricity (**building owner/residents**), i.e. an increase in self-consumption of up to 23 % in this case study;
  - decreased injection of locally produced electricity (**DSO**), i.e. a decrease in injection peaks of up to 7.7 % in this case study.

Therefore, the simplest solution to decrease the local grid impact and to increase the EV user comfort (electric range), is to encourage additional daytime EV charging at home (and other possible charging locations).

## 7.2 Delayed charging and EV based peak shaving

In this section, two local coordination strategies have been investigated, namely delayed charging and EV based peak shaving (Section 6.3.1), and compared with the uncoordinated charging scenarios (Section 7.1). Results are discussed for a number of grid and fleet impact indicators, as discussed in Section 2.8. The following scenarios have been assessed[3]:

- **Scenario 3:** Delayed EV charging at maximum power $P^{\text{ch}}$.
- **Scenario 4:** Delayed EV charging at maximum power $P^{\text{ch}}$, including charging the local PV generation surplus (Section 6.3.2).
- **Scenario 5:** EV based peak shaving; EV charging starts whenever EV arrives at home at reduced power.
- **Scenario 6:** EV based peak shaving, including charging the local PV generation surplus (Section 6.3.2); EV charging starts whenever EV arrives at home at reduced power.

Fig. 7.8 shows the impact of the different EV charging strategies on the EV charging profile for a sample EV in the fleet ($P^{\text{ch}} = 3.3\,\text{kW}$). Uncoordinated

[3]Scenario 1 and scenario 2 are identical to the uncoordinated scenarios in Section 7.1.

charging is represented in Fig. 7.8 (a). The EV charging starts, at maximum power $P^{\text{ch}}$, when the EV arrives at home around noon.

Delayed EV charging is shown in Fig. 7.8 (b)–(c). If the strategy does not anticipate on PV power surplus, the charging process starts around 5:15 pm at maximum power (3.3 kW) and ends when leaving for the next trip, as illustrated in Fig. 7.8 (b). The final part of the charging process starts around 6 pm when PV power surplus is charged during the day (Fig. 7.8 (c)). During the day, the PV surplus is divided over the grid-connected EVs, which have to be charged. In the latter scenario, the average charging power for this EVs decreases.

When EV based peak shaving is applied, the EV uses its total standstill time at home to charge at a reduced power, which is about 630 W in Fig. 7.8 (d). When the local surplus of PV generation is charged by the grid-connected EVs, which are charging, Fig. 7.8 (e) shows that the EV first starts to charge at the same power as in Fig. 7.8 (d) until there is a surplus of PV power, which is higher than the reduced power. At the end of the charging period, the reduced charging power is about 225 W. Thus, the reduced charging power is adapted when a surplus of PV power is stored in the EV battery, in order to keep maximizing the charging duration and minimizing the charging power.

### 7.2.1 Fleet impact

The same amount of electricity is charged by the EVs compared to uncoordinated charging (scenario 1). Thus, the electric driving range (or UF) remains equal.

#### Delayed charging

The EV charging simultaneity is nearly identical to scenario 1. Since the same amount of energy is charged, the time required to charge the EVs for delayed charging (scenario 3) is identical to uncoordinated charging (scenario 1), as shown in Fig. 7.9. However, when a surplus of locally generated PV power is charged (scenario 4), the charging duration increases, due to the reduction in average charging power. The latter is also illustrated in Fig. 7.8 (c). This conclusion is valid for this case study, since the PV power surplus is not sufficient for all EVs to charge at maximum power.

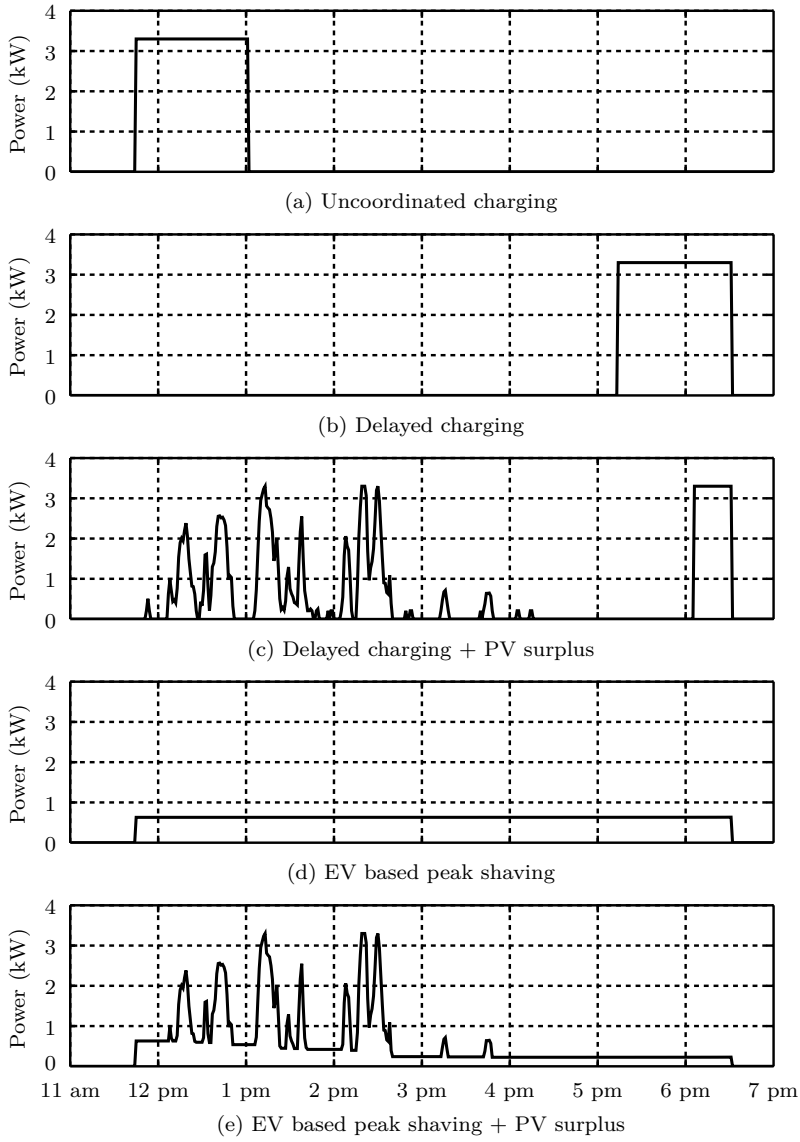


Figure 7.8: Sample EV charging profile (random EV) for different EV charging strategies for a charging rate of 3.3 kW.

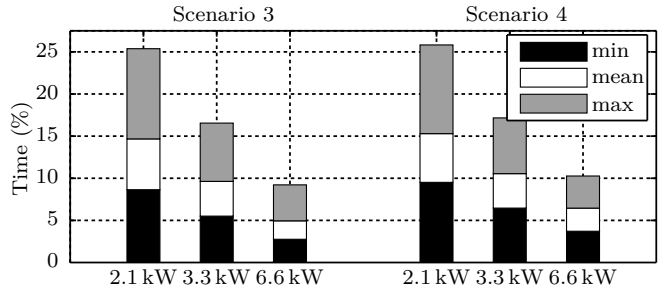


Figure 7.9: Delayed charging – EV charging duration (% of the week) as a function of the charging rate ($P^{\mathrm{ch}} \in \{2.1; 3.3; 6.6\}$ kW) for a building fleet of 20 EVs.

## EV based peak shaving

For EV based peak shaving, each EV maximally uses the available time (when parked at home) to charge its battery. The average EV charging power is drastically decreased, as shown in Fig. 7.10. In scenario 5, the average charging power is about 3.6–7.8 times lower compared to $P^{\mathrm{ch}}$. Therefore, the total charging duration also increases, as shown in Fig. 7.11. In theory, it is expected that the average charging power (and time) is identical for all three charging rates. However, the average charging power increases for an increasing charging rate due to $P_{\mathrm{min}}$, which depends on the charging rate (see Section 6.1.6).

In scenario 6, EV based peak shaving is combined with charging the PV power surplus. The average charging power may increase compared to scenario 5. Therefore, the charging duration may decrease. The average charging power

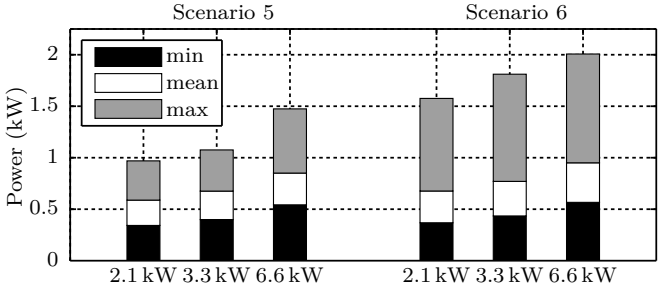


Figure 7.10: EV based peak shaving – Average EV charging power as a function of the charging rate ($P^{\mathrm{ch}} \in \{2.1; 3.3; 6.6\}$ kW) for a building fleet of 20 EVs.

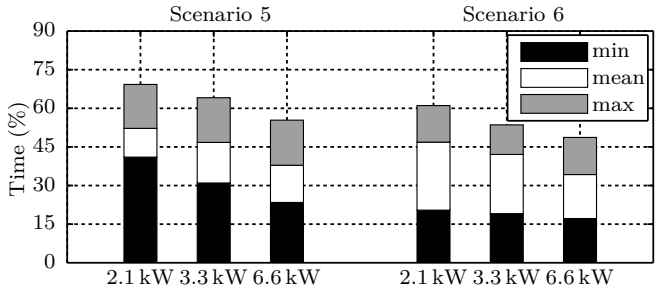


Figure 7.11: EV based peak shaving – EV charging duration (% of the week) as a function of the charging rate ($P^{\mathrm{ch}} \in \{2.1; 3.3; 6.6\}$ kW) for a building fleet of 20 EVs.

only increases when the PV power surplus is high enough, i.e. larger than the reduced charging power. In that case, also the average EV charging simultaneity decreases.

As a result of the increased charging duration for EV based peak shaving, the EV charging simultaneity (Fig. 7.12) increases remarkably. For some cases of scenario 5, all vehicles are charging simultaneously during at least one time step. In two cases ($n^{\mathrm{EV}} = 20$), at least one EV is charging during each time step. For an increased charging rate, the simultaneity might slightly decrease, due to the change in $P_{\mathrm{min}}$. A similar trend is observed when it is possible to charge the surplus of locally generated PV power (scenario 6).

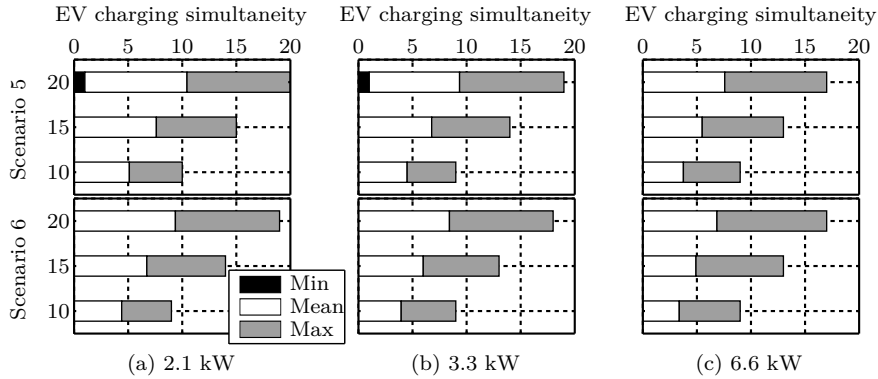


Figure 7.12: EV based peak shaving – EV charging simultaneity as a function of the charging rate ($P^{\mathrm{ch}} \in \{2.1; 3.3; 6.6\}$ kW) and number of EVs ($n^{\mathrm{EV}} \in \{10; 15; 20\}$) charged in the apartment building.

### 7.2.2 Grid impact

#### Delayed charging

**Power profile and cover factors** During each charging opportunity, i.e. the time between arrival at home and leaving for a next trip, the EV charging process to fully charge the batteries, is delayed as long as possible, while still meeting the mobility requirements. Compared to uncoordinated charging (scenario 1), the power demand peaks are lower for delayed charging, up to 30 % in this case study (see Fig. 7.13), which can be explained as follows:

- In general, EVs are standing still for a long time during the off-peak period, i.e. during the night. When EV charging is delayed, this results in a decreased simultaneity with the residential evening power demand peak.
- Due to the stochastic nature of the trip departure and arrival times, as illustrated in Chapter 3, there is a spreading of the departure times at home. Therefore, there is a spreading of the EV charging compared to e.g. scenario 2, in which the charging is synchronized in the off-peak period.

Second, it can be observed that more local generation is locally consumed (moving percentiles: injection peak, $OPP_{\text{inj}}$ and 5th percentile) compared to uncoordinated charging. However, since the EVs start charging from the moment there is a small PV power surplus in scenario 4, there is no guarantee that the injection peak decreases in this scenario, as is the case for a charging rate of

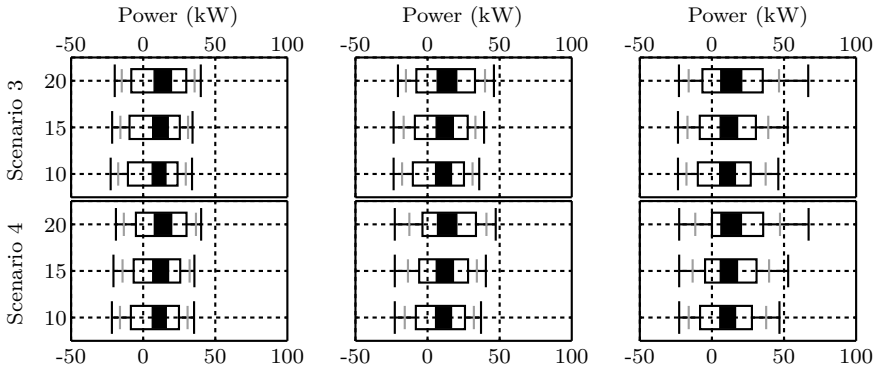


Figure 7.13: Delayed charging – Modified box plots for load duration curves as a function of the charging rate ($P^{\text{ch}} \in \{2.1; 3.3; 6.6\}$ kW) and number of EVs ($n^{\text{EV}} \in \{10; 15; 20\}$) charged in the apartment building.

3.3 and 6.6 kW in this case study. It might happen that an EV is already fully charged before the PV power production peaks occur. On the other hand, in scenario 3 the charging is delayed as long as possible. In this case study, it results in a higher coincidence with the PV power production peaks, resulting in a decreased injection peak power.

The increased self-consumption for delayed charging, compared to uncoordinated charging (Fig. 7.7), is shown in Fig. 7.14. When anticipating on the local PV production (scenario 4), the self-consumption further increases compared to scenario 3.

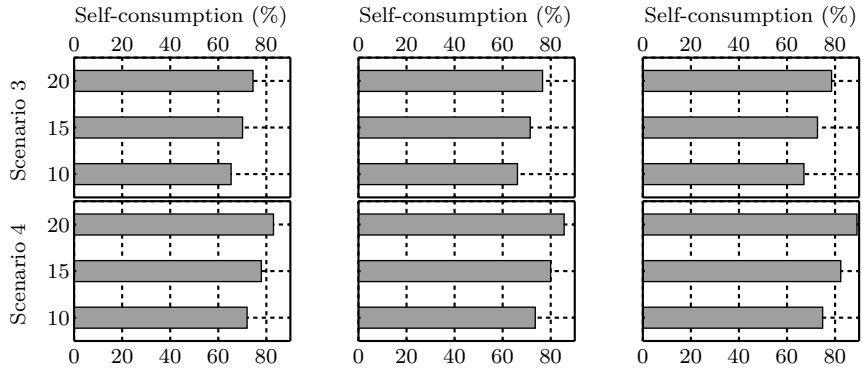


Figure 7.14: Delayed charging – Self-consumption as a function of the charging rate ($P^{\mathrm{ch}} \in \{2.1; 3.3; 6.6\}$ kW) and number of EVs ($n^{\mathrm{EV}} \in \{10; 15; 20\}$) charged in the apartment building.

**Minimum voltage magnitude** In Fig. 7.15, the minimum occurring voltage magnitude is shown. In all cases, the minimum voltage is still below 0.9 pu. However, for a charging rate of 2.1 and 3.3 kW, $U_{\mathrm{min}}$ is (nearly) independent from the number of EVs and not dependent on the charging rate, indicating $U_{\mathrm{min}}$ is the result from the residential power demand peak (including the heat pump demand). However, compared to scenario 1, the minimum voltages increase by almost 0.10 pu ($P^{\mathrm{ch}} = 6.6$ kW). In scenario 4, the minimum voltages are equal. Therefore they are not shown here, due to identical power demand peaks causing the minimum voltages.

For a charging rate of 6.6 kW, the voltage profile still does not meet the EN 50160 regulations. In Section 7.3, it is investigated whether these voltage problems can be solved by a voltage droop mechanism. However, since charging is already

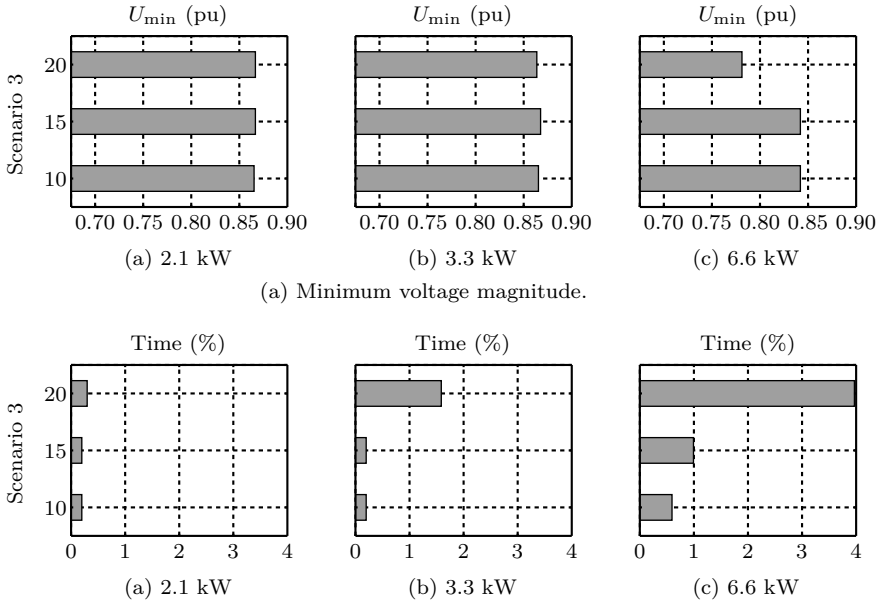


(a) Minimum voltage magnitude.

(b) % of the time that the grid voltage is lower than 0.90 pu.

Figure 7.15: Delayed charging – (a) Minimum voltage magnitude in the apartment building, and (b) % of the time that the grid voltage is lower than 0.90 pu, as a function of the charging rate ($P^{\text{ch}} \in \{2.1; 3.3; 6.6\}$ kW) and number of EVs ($n^{\text{EV}} \in \{10; 15; 20\}$) charged in the apartment building.

delayed as long as possible, this might have an impact on the total energy charged and thus may have a negative impact on the UF.

### EV based peak shaving

**Power profile and cover factors** Compared to uncoordinated charging, the demand power peaks (including the OPP and 95th percentile) decrease for EV based peak shaving, as shown in Fig. 7.16. The demand power peaks are up to almost 40 % reduced compared to uncoordinated charging. Only for a charging rate of 2.1 kW, the demand peaks are slightly higher for EV based peak shaving for this case study, which is due to an overlap of the EV charging with a high residential peak demand at a certain time step. This is due to longer charging durations for a charging rate of 2.1 kW. Nevertheless, the OPP and 95th percentile decrease, showing the decreased grid impact of EV based peak shaving compared to delayed charging.

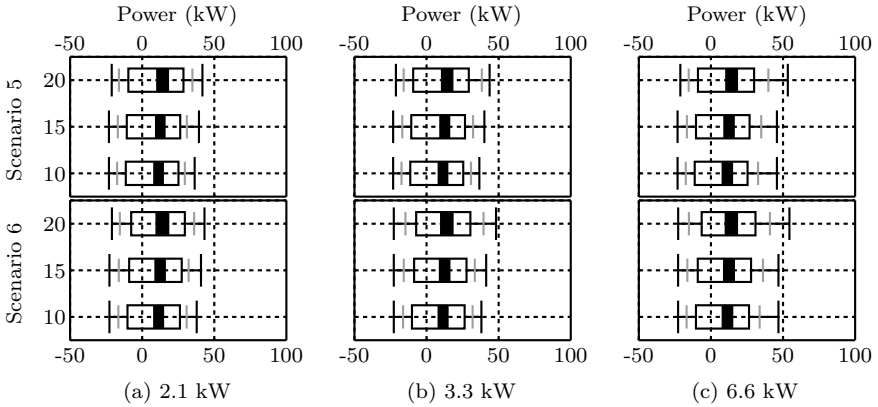


Figure 7.16: EV based peak shaving – Modified box plots for load duration curves as a function of the charging rate ($P^{\mathrm{ch}} \in \{2.1; 3.3; 6.6\}$ kW) and number of EVs ($n^{\mathrm{EV}} \in \{10; 15; 20\}$) charged in the apartment building.

However, as discussed before, as the EV charging is spread over the total standstill times of the vehicles, the EV charging simultaneity increases. Therefore, the EV charging load and the total building load is spread, as indicated by the decreased 95th percentile, compared to uncoordinated charging and delayed charging.

Since the EV charging is spread, there is an increased simultaneity with PV power production. Therefore, the injection peaks are lower in scenario 5 compared to uncoordinated charging, while the self-consumption is higher, as shown in Fig. 7.17. Nevertheless, when EV charging anticipates on the PV power surplus (scenario 6), the injection peaks are higher than in scenario 5, despite the increased self-consumption. This is due to the shorter charging time in scenario 6, which might lower the probability of simultaneity with the PV power production peaks.

**Minimum voltage magnitude** As discussed for delayed charging, the minimum occurring voltage is independent of the number of EVs in this case study for a charging rate of 2.1 and 3.3 kW. Only for a charging rate of 6.6 kW and 20 EVs in the building, $U_{\mathrm{min}}$ drops slightly below 0.85 pu (see Fig. 7.18). Nevertheless, the minimum voltages increase by up to almost 0.14 pu compared to uncoordinated charging. The results for scenario 6 are equal and therefore not shown.

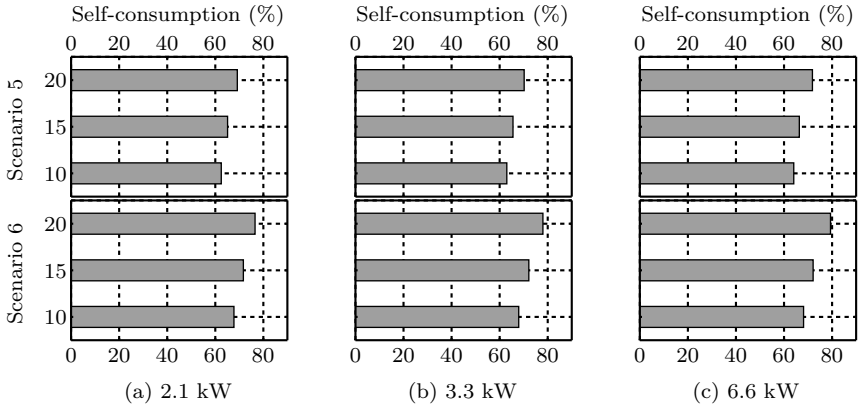


(a) 2.1 kW (b) 3.3 kW (c) 6.6 kW

Figure 7.17: EV based peak shaving – Self-consumption as a function of the charging rate ($P^{\text{ch}} \in \{2.1; 3.3; 6.6\}$ kW) and number of EVs ($n^{\text{EV}} \in \{10; 15; 20\}$) charged in the apartment building.

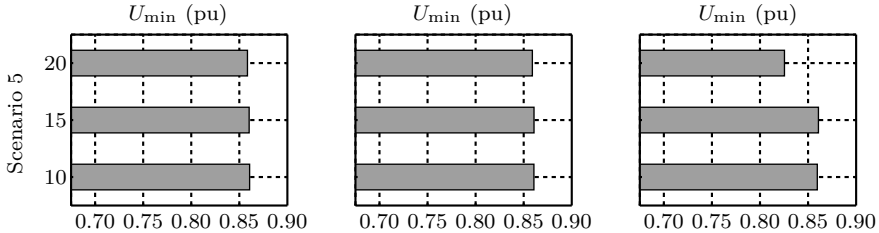


(a) 2.1 kW (b) 3.3 kW (c) 6.6 kW

Figure 7.18: EV based peak shaving – Minimum voltage magnitude in the apartment building as a function of the charging rate ($P^{\text{ch}} \in \{2.1; 3.3; 6.6\}$ kW) and number of EVs ($n^{\text{EV}} \in \{10; 15; 20\}$) charged in the apartment building.

**Voltage unbalance** Fig. 7.19 shows the maximum voltage unbalance for both delayed charging (scenario 3) and EV based peak shaving (scenario 5). Due to the load spreading in both charging strategies, the VUF decreases compared to uncoordinated charging. The VUF now complies with the EN 50160 regulations. Moreover, for EV based peak shaving the maximum occurring VUF is even lower compared to delayed charging. This is due to the fact that the average EV charging load is lower compared to delayed charging. Due to the longer charging durations and the higher EV charging simultaneity, the phase unbalance decreases.

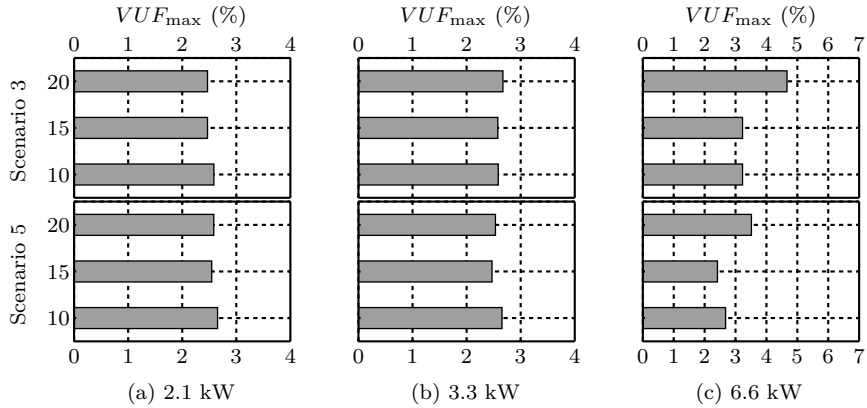


(a) 2.1 kW (b) 3.3 kW (c) 6.6 kW

Figure 7.19: Maximum VUF in the apartment building as a function of the charging rate ($P^{\mathrm{ch}} \in \{2.1; 3.3; 6.6\}$ kW) and number of EVs ($n^{\mathrm{EV}} \in \{5; 10; 15; 20\}$) charged in the apartment building.

### 7.2.3 Conclusions

This section discusses the impact trends of two local EV charging strategies, namely (i) delayed charging, and (ii) EV based peak shaving. These strategies only require the knowledge on the next departure time and the battery SoC. For both strategies, the whole EV flexibility in time is used, while for EV based peak shaving also the charging power flexibility is utilized. Both delayed EV charging and EV based peak shaving can be implemented to anticipate on possible local electricity production, e.g., a PV power production surplus.

For delayed EV charging (scenario 3), the charging process within a charging opportunity is delayed as long as possible. Therefore, it has no impact on the charging duration. When EVs anticipate on the PV power surplus, the average charging power may drop. Nevertheless, delayed charging may impact the user comfort. A user might adapt the departure time when an extra trip is planned, but depending on the moment the extra trip is planned, the EV user might have to give in on the electrical range (a reduced UF) if it is impossible to charge the required amount of electricity. On the other hand, the EV charging duration (and simultaneity) is drastically increased for EV based peak shaving. On average, EVs are charging about 50–70 % of the time (depending on the charging rate), compared to only 5–15 % for uncoordinated or delayed charging. However, by reducing the average EV charging power, a certain flexibility in charging power is present in case trips are added or rescheduled.

The demand peak powers are reduced compared to uncoordinated EV charging,

up to almost 30 and 40 % for delayed charging and EV based peak shaving, respectively. For delayed charging, this is mainly due to a reduced simultaneity with the evening peak demand in the building. On the other hand, the EV charging load is spread in the case of EV based peak shaving. The impact on the grid losses has not been discussed in this chapter. However, in [28], it has been shown that the grid losses decrease when EV based peak shaving is applied.

Anticipating and charging the local PV power surplus is relatively easy for both strategies. It results in an increased self-consumption of PV power. However, charging the PV power surplus does not guarantee that the injection peaks will decrease, since the charging starts whenever there is a small PV power surplus. Therefore, to decrease the injection powers, other solutions, such as a prediction of the PV production, might be required.

The two discussed strategies are also beneficial regarding the minimum occurring voltage. However, some cases are still not compliant with EN 50160. Therefore, Section 7.3 and Section 7.4 discuss additional mechanisms to adapt the EV charging profile to take grid constraints, i.e. grid voltages (voltage droop mechanism) and power capacity (building peak shaving) into account. However, these measures may lead to a reduced UF, especially for delayed EV charging since charging may be postponed to subsequent charging opportunities.

## 7.3 Voltage droop mechanism

This section discusses the impact of the voltage droop mechanism. The results regarding the fleet and grid impact are compared with the scenarios without a voltage droop mechanism (see Sections 7.1 and 7.2). The EV charging powers will deviate from the power set-point as a function of the nodal grid voltage at the EV, for the following three scenarios:

- **Scenario 1:** Uncoordinated EV charging.
- **Scenario 3:** Delayed EV charging.
- **Scenario 5:** EV based peak shaving.

Fig. 7.20 shows the impact of a voltage droop mechanism on the EV charging profile for a sample EV in the fleet ($P^{\mathrm{ch}} = 3.3\,\mathrm{kW}$). In the case without a voltage droop mechanism, the EV is uncoordinatedly charged at maximum power, i.e. $P^{\mathrm{ch}}$, as shown in Fig. 7.20 (a). The voltage magnitude profile at the EV is shown in Fig. 7.20 (b). When a voltage droop mechanism is applied, as discussed in Section 6.3, the charging power is reduced when the grid voltage

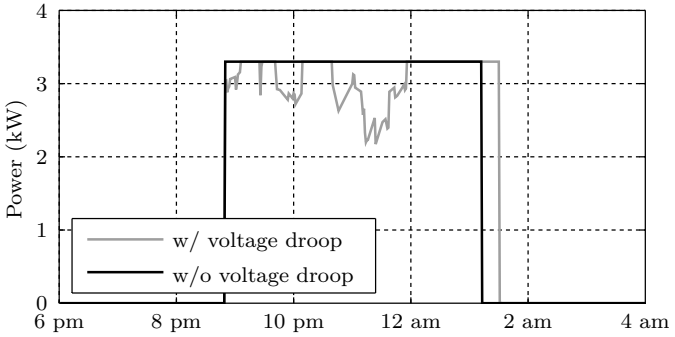


(a) EV charging profile.

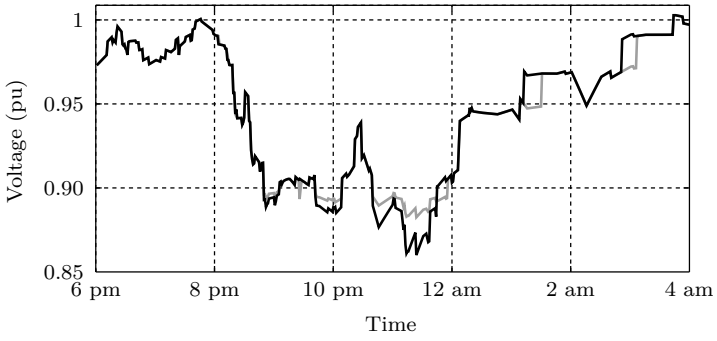


(b) Voltage magnitude profile at EV.

Figure 7.20: Impact of a voltage droop mechanism on a sample EV charging profile (uncoordinatedly charged) for a charging rate of 3.3 kW.

drops below 0.90 pu. For the example in this figure, the average charging power decreases about 7.2 %. This results in an increased charging duration of this EV, which is shown in Fig. 7.20 (a).

Fig. 7.20 (b) represents the impact of the voltage droop mechanism on the grid voltage at the node the EV is connected to. Note that also the other EVs charging (also in other phases) have an impact on the grid voltage at the node to which the sample EV is connected. This can be observed in Fig. 7.20 (b):

- the grid voltage changes outside the charging period of the sample EV (around 3 am);

- the charging power reduction is different to what the voltage (without a voltage droop mechanism) suggests.

### 7.3.1 Fleet impact

#### Charging duration

An activation of the voltage droop mechanism leads to an increase in the charging duration, as shown in the example in Fig. 7.20. It may lead to a decreased electric range when the duration of the charging opportunity, in which the voltage droop mechanism is active, is too short to compensate for the loss in electricity charged.

Fig. 7.21 shows the increase in charging duration, due to the voltage droop mechanism, for the different scenarios. For all scenarios, the charging duration increases, up to 10 % for uncoordinated charging. The increase in charging duration is larger for higher charging rates, since the voltage droop mechanism is activated more due to the higher voltage drops in these cases. For delayed EV charging, a charging duration increase is also observed. The EV batteries are less charged when the voltage droop mechanism is activated. Therefore, the charging duration of subsequent charging opportunities increases.

For EV based peak shaving, the increase in charging duration is negligible since the charging duration is maximized for this strategy. There is only a charging duration increase during the charging opportunities for which the reduced power is equal to the charging rate, or when the voltage droop mechanism kicks in at the end of the charging opportunity. In the latter case, the average charging power or the charging duration of subsequent charging opportunities may increase.

#### Utility function

The voltage droop mechanism could lead to a UF reduction in case the standstill time is not long enough to charge enough electricity for the upcoming trips until the next charging opportunity. For uncoordinated charging and EV based peak shaving, the voltage droop mechanism does not result in a decreased UF for this case study, despite the increase in charging duration. However, for delayed charging, the voltage droop mechanism has a negative impact on the UF, reducing the all-electric range of the EVs. The change in UF for delayed charging is shown in Fig. 7.22. Although, the reductions are limited in this case study, due to the relatively large battery packs in the considered case study.

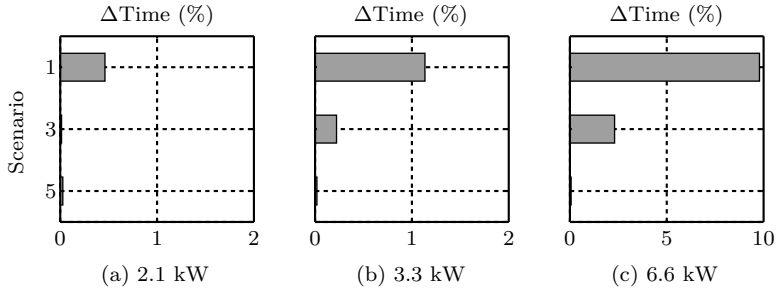


(a) 2.1 kW (b) 3.3 kW (c) 6.6 kW

Figure 7.21: Charging duration increase (%) due to the voltage droop mechanism, as a function of the charging rate ($P^{\text{ch}} \in \{2.1; 3.3; 6.6\}$ kW) for a building fleet of 20 EVs.

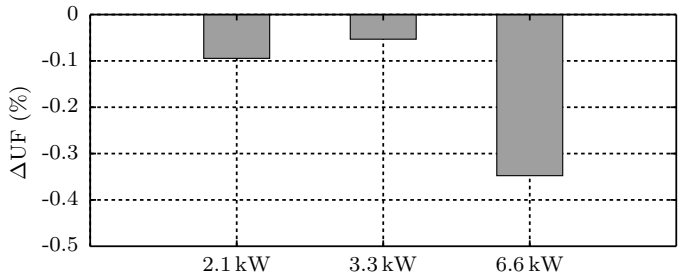


Figure 7.22: Change (%) in UF (ΔUF) due to the voltage droop mechanism (for delayed charging), as a function of the charging rate ($P^{\text{ch}} \in \{2.1; 3.3; 6.6\}$ kW) for a building fleet of 20 EVs.

## 7.3.2 Grid impact

### Average charging power

As shown in Fig. 7.21, the charging duration increases due to the voltage droop mechanism. This increase is the result of a decreasing charging power when the grid voltage (at the EV connection point) drops below 0.9 pu. This change in charging power is illustrated in Fig. 7.23. This figure shows the decrease in average charging power of the EV fleet for uncoordinated (scenario 1) and delayed charging (scenario 3). For EV based peak shaving, the impact on the charging power is negligible, as shown in Section 7.3.1. For uncoordinated charging, the average charging power decreases up to 10 % compared to the scenario without a voltage droop mechanism. Since the voltage drops for delayed charging are lower, compared to uncoordinated charging, the decrease in average charging power is lower.

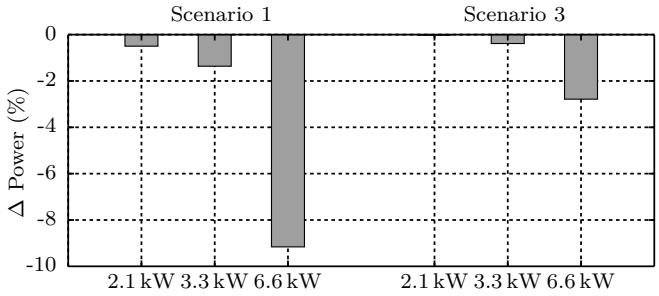


Figure 7.23: Change (%) in average charging power due to the voltage droop mechanism, as a function of the charging rate ($P^{\text{ch}} \in \{2.1; 3.3; 6.6\}$ kW) for a building fleet of 20 EVs.

### Minimum voltage magnitude

The objective of the voltage droop mechanism is to decrease the voltage magnitude deviations when the grid voltage drops below 0.9 pu. Whereas in some cases without a voltage droop mechanism, $U_{\min}$ drops below 0.85 pu, the voltage droop mechanism is able, as required by EN 50160, to keep the voltage magnitude above 0.85 pu for all cases, as shown in Fig. 7.24 (a). Thus, the droop mechanism succeeds in limiting the voltage deviations caused by EV charging. The minimum voltage is nearly independent of the EV charging rate and number of EVs charged in the apartment building. Therefore, the minimum voltage occurring is mainly defined by the other building loads. However, depending on the scenario and the EV penetration rate, the minimum voltage varies a little, depending on the simultaneity of the EVs charging and the other building loads.

Besides, all cases in scenario 2 are now feasible, meaning that a higher amount of EVs or higher charging rates are allowed for off-peak uncoordinated charging. For all cases, $U_{\min}$ is above 0.85 pu. However, these results have not been shown.

All cases but one, i.e. scenario 1 with 20 EVs and a charging rate of 6.6 kW, meet the EN 50160 regulations regarding the time the voltage drops below 0.9 pu. Since there is an increase in charging duration, the time that the minimum grid voltage drops below 0.9 pu is not always positively affected by the voltage droop mechanism (see Fig. 7.24 (b)). Thus, other solutions might be needed to comply with the grid regulations, such as grid reinforcements to reduce the voltage drops or other voltage droop parameters[4], i.e. $|u_l|$ and/or $|u_h|$.

[4]However, increasing $|u_h|$ may result in increased minimum voltage magnitudes. Nevertheless, it will further decrease the average charging power [128], which may negatively affect the UF.

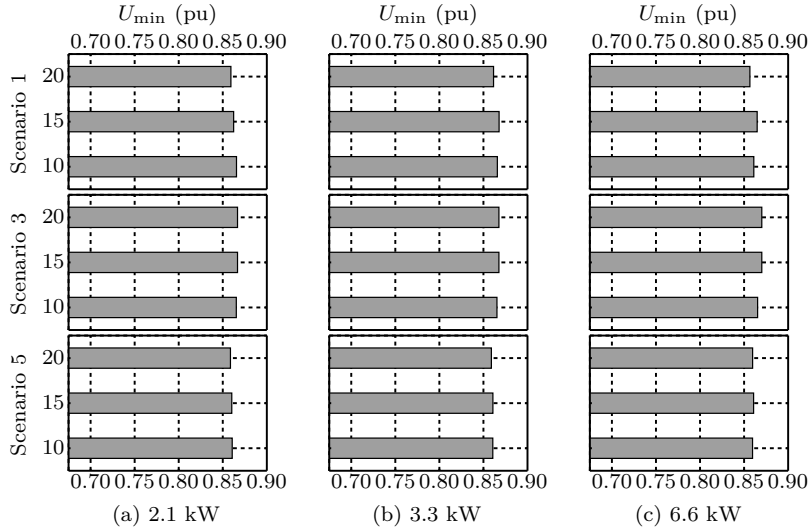


(a) Minimum voltage magnitude.

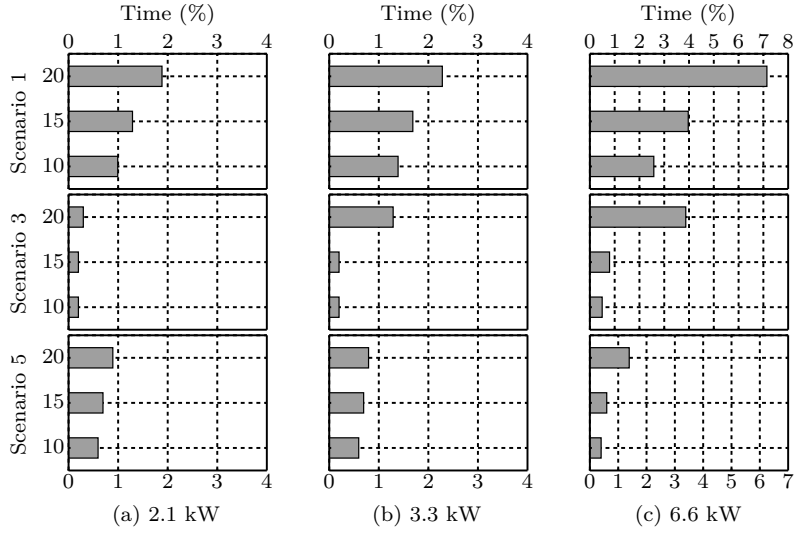


(b) % of the time that the grid voltage is lower than 0.90 pu.

Figure 7.24: Voltage droop mechanism – (a) Minimum voltage magnitude in the apartment building, and (b) % of the time that the grid voltage is lower than 0.90 pu, as a function of the charging rate ($P^{\text{ch}} \in \{2.1; 3.3; 6.6\}$ kW) and number of EVs ($n^{\text{EV}} \in \{10; 15; 20\}$) charged in the apartment building.

#### Voltage unbalance

For scenario 1 and scenario 3, the voltage droop mechanism also substantially reduces the voltage unbalance (see Fig. 7.25). Since the reduction in average charging power is higher, the reduction in VUF is larger for uncoordinated charging and higher charging rates. All scenarios are now compliant with EN 50160.

#### Peak power demand

Fig. 7.26 shows the change in peak power demand due to the voltage droop mechanism. For a grid voltage between 0.85 and 0.9 pu, the EV charging power is decreased, which could result in both an increase and decrease of peak power demand compared to the scenario without a voltage droop mechanism, depending on the average EV charging simultaneity, grid load and the moment of the voltage droop activation.

For instance, when uncoordinated or delayed EV charging is applied, the peak power demand decreases. In the uncoordinated charging case (scenario 1), the peak power reduction is rather limited. For delayed charging (scenario 3), the reduction is larger due to:

- the load spreading to subsequent charging opportunities, which may result in a lower coincidence with other loads;
- less electricity being charged, as shown by a decreasing UF (see Fig. 7.22).

For EV based peak shaving (scenario 5), the reduced charging power is calculated at each time step. When the voltage droop is activated, the charging power at later moments during that charging opportunity increases, which may result in a peak power demand increase.

### 7.3.3 Conclusions

The objective of the voltage droop mechanism is to decrease the voltage deviations. The EV charging power is reduced when the grid voltage drops below 0.9 pu; charging stops below 0.85 pu. The voltage droop mechanism succeeds in eliminating the grid voltages below 0.85 pu. But it does not yet guarantee an EN 50160 compliant operation of the grid regarding the voltages due to too much voltage deviations below 0.9 pu for some cases. Other solutions, such as a voltage droop mechanism with adapted settings for the upper-limit

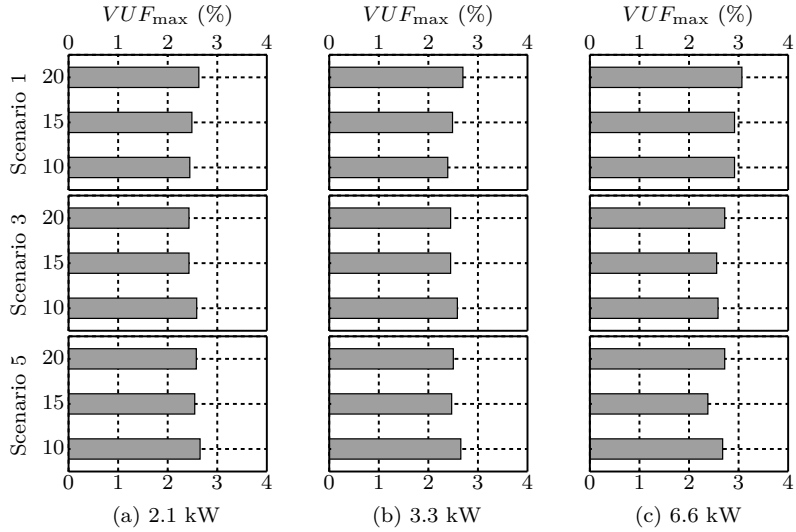


(a) Maximum VUF.

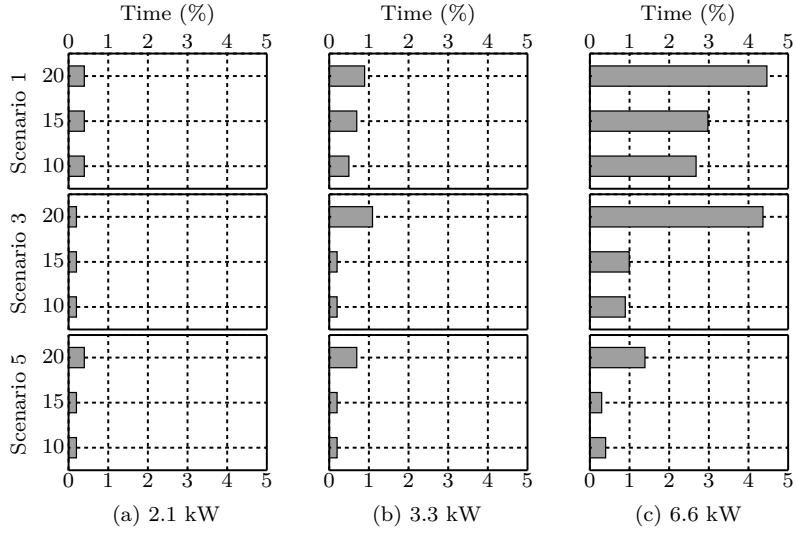


(b) % of the time that the VUF goes beyond 2 %.

Figure 7.25: Voltage droop mechanism – (a) Maximum VUF in the apartment building, and (b) % of the time that the VUF goes beyond 2 %, as a function of the charging rate ($P^{\text{ch}} \in \{2.1; 3.3; 6.6\}$ kW) and number of EVs ($n^{\text{EV}} \in \{10; 15; 20\}$) charged in the apartment building.

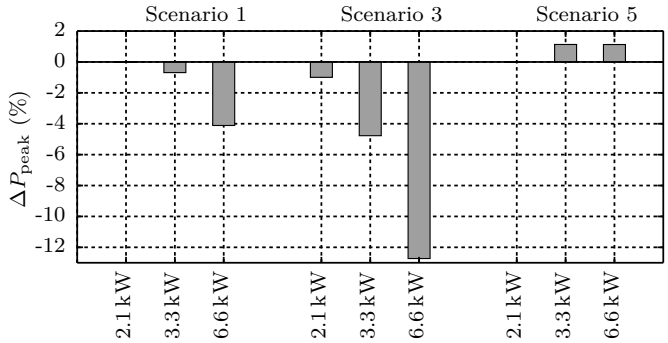


Figure 7.26: Change (%) in peak power demand ($\Delta P_{\text{peak}}$) due to the voltage droop mechanism, as a function of the charging rate ($P^{\text{ch}} \in \{2.1; 3.3; 6.6\}$ kW) for a building fleet of 20 EVs.

voltage, might be required. The grid is compliant with EN 50160 regarding the voltage unbalance factor. Besides the reduced voltage deviations, also the peak power demand may be reduced, up to 13 % in this case study, due to:

- the EV charging load spreading;
- a possible lower amount of electricity being charged (delayed charging).

An activation of the voltage droop mechanism results in an increase in charging duration and decrease in average charging power. This increase in charging duration may lead to a reduced UF. This is especially a threat for delayed charging, since EV charging is already delayed as long as possible.

## 7.4 Building peak shaving mechanism

This section discusses the impact of the building peak shaving mechanism. The EV charging power is reduced as a function of the total building load and the capacity of the connection to the LV distribution grid. Since some fleet and grid impact trends are similar to the impact of the voltage droop mechanism (Section 7.3), the working principle has been explained for the uncoordinated EV charging scenario only (scenario 1). The results have been compared with the scenario without a BPS mechanism.

As mentioned in Section 7.1.2, DSOs take in general a capacity of 2.5 kVA for each apartment unit in an apartment building. For the considered apartment

building, this results in a capacity of 50 kVA. Overloading of cables can result in an accelerated aging of the insulation material [92].

Fig. 7.27 shows the impact of a BPS mechanism on the EV charging profile for a sample EV in the fleet ($P^{\text{ch}} = 6.6\,\text{kW}$). The EV charging power is reduced when the total demand power in the building, including EV charging at $P^{\text{ch}}$, exceeds the available capacity $P^{\text{cap}} = 50\,\text{kW}$[5]. In the case without a BPS mechanism, the EV is uncoordinatedly charged at maximum power, i.e. $P^{\text{ch}}$, as shown in Fig. 7.27 (a). As illustrated, the EV charging power is reduced when the BPS mechanism is applied, depending on the building loads and PV power production in the building. This reduction in charging power results in a charging duration increase.

Fig. 7.27 (b) illustrates that the BPS mechanism is capable of reducing the demand power profile at the building PCC. However, the power profile lies a little above $P^{\text{cap}}$. This is due to the fact that the total grid losses, which depend on the magnitude and location of the different loads, have not been taken into account in the calculation of the reduced EV charging power.

### 7.4.1 Fleet impact

As a result of the activation of the BPS mechanism, the charging duration will increase. Therefore, the fleet impact trends for the charging duration and UF are similar to the trends observed for the voltage droop mechanism in Section 7.3. Therefore, these results have not been repeated in this section.

### 7.4.2 Grid impact

#### Power profile

Fig. 7.28 illustrates the impact of the building peak shaving mechanism on the building power profile. The BPS mechanism is able to reduce the demand peak power to 50 kW, excluding the occurring grid losses, for all cases. Besides, a reduction in the demand OPP can be observed. On the other hand, due to a reduction in average EV charging power, the EV charging load is spread. This can be observed by increasing 75th and 95th percentiles. For the cases in which the demand peak power did not exceed $P^{\text{cap}}$, the building power profile is not influenced by the BPS mechanism.

[5]Since all loads and generation units have a unity power factor, a capacity limit is put on the active power.

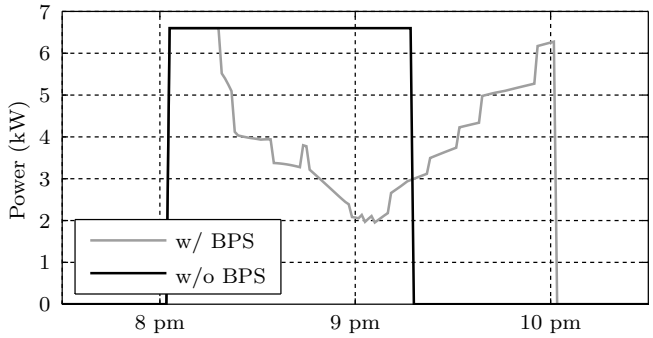


(a) EV charging profile.

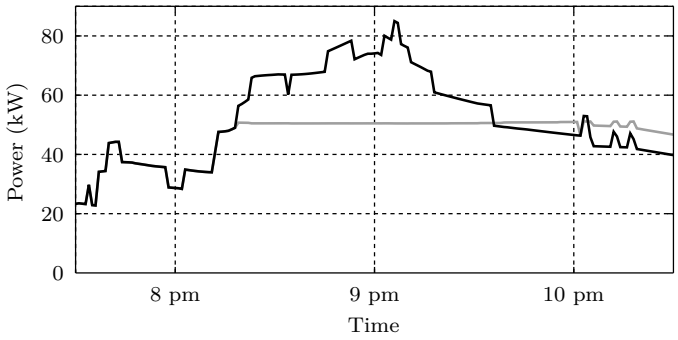


(b) Power profile at building PCC.

Figure 7.27: Impact of the building peak shaving (BPS) mechanism on a sample EV charging profile (uncoordinatedly charged) for a charging rate of 6.6 kW.

The BPS mechanism, as introduced in this work, proves to be a reliable measure to limit the demand peak power, despite it is only required to:

- measure the aggregated household power consumptions and individual loads, i.e. the heat pump, and generation units, i.e. the PV system;
- keep track of the number of EVs to be charged.

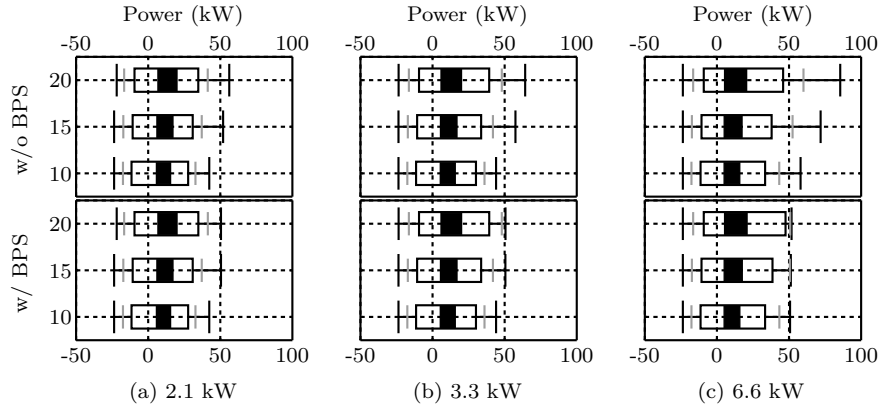


Figure 7.28: Impact of a BPS mechanism on the building power profiles (uncoordinated EV charging) – Modified box plots for load duration curves as a function of the charging rate ($P^{\mathrm{ch}} \in \{2.1; 3.3; 6.6\}$ kW) and number of EVs ($n^{\mathrm{EV}} \in \{10; 15; 20\}$) charged in the apartment building.

#### Minimum voltage magnitude

As shown in Fig. 7.29, $U_{\min}$ is positively impacted for some cases, especially for the 6.6 kW case. For other cases, $U_{\min}$ remains unchanged. Despite the voltage magnitudes may be positively influenced, the BPS mechanism does not assure that the grid will comply with the voltage magnitude requirements of the EN 50160 regulations.

Since the impact on the voltage unbalance factor is very limited, these results have not been shown. The cases which are not compliant with the EN 50160 regulations in Fig. 7.6, still do not meet these regulations.

### 7.4.3 Conclusions

The objective of the building peak shaving mechanism is to decrease the power demand profile at the PCC with the LV distribution grid in order to decrease the grid impact. The results show that the mechanism succeeds in spreading the EV charging load, resulting in a reduced peak demand power of about 50 kW in this case study. Besides, the BPS mechanism can positively impact the voltage deviations. However, it does not assure the grid complies with the EN 50160 regulations. Voltages still drop below 0.85pu.

Both the voltage droop and building peak shaving mechanism have a positive

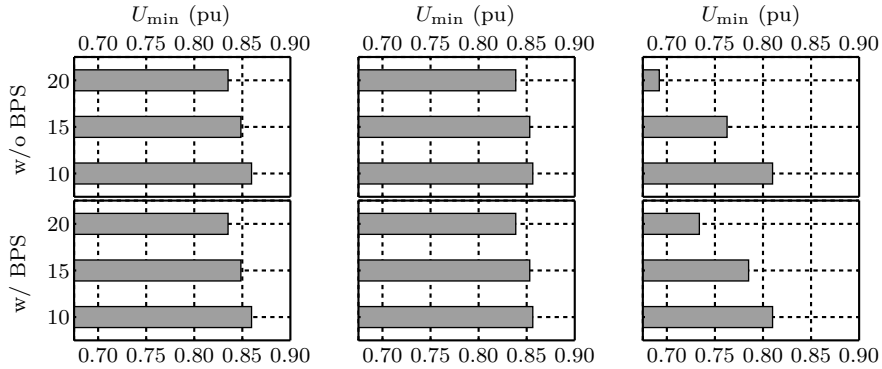


Figure 7.29: Impact of a building peak shaving mechanism on the minimum voltage magnitude in the apartment building as a function of the charging rate ($P^{\text{ch}} \in \{2.1; 3.3; 6.6\}$ kW) and number of EVs ($n^{\text{EV}} \in \{10; 15; 20\}$) charged in the apartment building.

impact on both the voltage deviations and peak demand power. Therefore, these two strategies have been combined in Section 7.5.

## 7.5 Comparison with the *optimal capacity charging* algorithm

This section focuses on the comparison of uncoordinated charging, including a combination of a voltage droop and building peak shaving mechanism, with a centralized optimization EV charging strategy. In the *optimal capacity strategy*[6], the EV charging power is optimized to maximize the total delivered power to each EV, without violating the grid limitations, i.e. cable power capacity and voltage deviations. The performance of the different strategies have been compared. This section has been based on the following submitted manuscript:

> J. Van Roy, P. Richardson, N. Leemput, A. Keane, and J. Driesen, "Local rule-based versus centralized optimal capacity charging coordination for EVs," *IEEE Trans. Smart Grid*, Mar. 2015, submitted for review.

[6]The *Optimal capacity charging* strategy is developed during the PhD research of Dr. Peter Richardson at the Electricity Research Centre in University College Dublin [263, 264].

The effectiveness and robustness of these EV charging strategies have already been separately discussed:

- Voltage droop mechanism in Section 7.3.
- Building peak shaving mechanism in Section 7.4[7].
- Optimal capacity charging in [263, 264].

### 7.5.1 Optimal capacity charging

The *Optimal capacity charging* strategy sets the charging power of each vehicle in order to maximize the total amount of power delivered to all of the EVs on the feeder at regular intervals, thereby making best use of the available network capacity. The strategy is based on the centralized control of EV charging within a network whereby certain points of the network are continuously monitored and data is sent back to the central control unit. The data, which includes voltage and load measurements, is then processed, together with pre-calculated network sensitivity values, using a linear-programming based algorithm in order to determine the optimal charging power for each individual EV in the network.

The objective function, $F$, of the *Optimal capacity charging* strategy is given as:

$$F = \sum_{i=1}^{n^{\mathrm{EV}}} P_i^{\mathrm{EV}} x_i, \tag{7.1}$$

with $n^{\mathrm{EV}}$ the number of EV charging points served by the network, i.e. the number of EVs in the building fleet, and $P_i^{\mathrm{EV}}$ the power delivered to the EV connected at the $i$th charging point. It is assumed that $P_i^{\mathrm{EV}}$ is a continuous control variable that can vary between 0 kW and the maximum power output of the charger, $P^{\mathrm{ch}}$, at node $i$. $x_i$ is zero when an EV is not connected at the $n$th charging point or when the EV battery is fully charged, while $x_i$ equals one when the EV is connected at the $i$th charging point and the EV battery SoC is less than 100 %.

The objective function is subject to the following constraints:

- minimum/maximum voltage deviations at the EV nodes $i$;
- maximum building power capacity $P^{\mathrm{cap}}$ per phase.

A more detailed description of the *Optimal capacity charging* strategy can be found in [263, 264].

[7] The BPS mechanism has been adapted here to a capacity of $\frac{50}{3}$ kW per phase.

### 7.5.2 Scenario description

The case study is similar to the scenario defined in Section 6.1. Since the scope of this part is to compare the local EV charging strategies with a centralized optimization strategy, the scenario differs on the following points:

- No PV system and heat pump are taken into account.
- The battery capacity is 20, 30 and 40 kWh for small, middle-class and large vehicles, respectively. Besides, no minimum EV charging power is set. A fleet of 18 EVs is taken[8].

#### EV charging strategies

The following EV charging strategies have been compared in this section:

- **Scenario A:** Uncoordinated charging (see Section 6.3.1).
- **Scenario B:** Combination of the voltage droop and building peak shaving mechanism (see Section 6.3.3).
- **Scenario C:** Optimal capacity charging (see Section 7.5.1).

### 7.5.3 Results: reference scenario (no EVs)

This section discusses the grid impact results for the reference scenario, i.e. the scenario without EVs charging in the apartment building. Fig. 7.30 shows the load duration curve of the apartment building in the reference scenario without EVs. The peak demand power and OPP are 24.8 kW and 17.7 kW, respectively.

No overvoltages occur, but the minimum voltage is 0.86 pu. In both the second and third phase, the voltage drops below 0.90 pu. The maximum VUF is 2.9 %. Since the voltage only drops for 0.5 % of the time below 0.90 pu, and the VUF is only 0.5 % of the time beyond 2 %, the in-building grid is compliant with the EN 50160 regulations (see Table 7.1). Table 7.1 shows the results for all nodes in the building, including the PCC, and the results for only the EV nodes, to which no load is connected.

[8]Taken from the same 20-vehicle fleet discussed before.

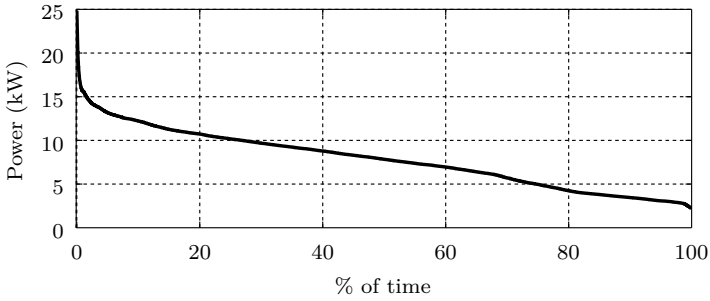


Figure 7.30: Load duration curve for the reference scenario without EVs.

Table 7.1: Apartment building: voltage magnitude and VUF.

| | | | | **Weekly duration** | |
|---|---|---|---|---|---|
| | $\boldsymbol{u}_{\min}$ | $\boldsymbol{u}_{\max}$ | $\boldsymbol{VUF}_{\max}$ | $\boldsymbol{u < 0.9\,\text{pu}}$ | $\boldsymbol{VUF > 2\,\%}$ |
| All nodes | 0.86 pu | 1.02 pu | 2.9 % | 0.5 % | 0.5 % |
| EV nodes | 0.87 pu | 1.02 pu | 2.7 % | 0.5 % | 0.5 % |

### 7.5.4 Results: grid and fleet impact

#### Average charging power, charging duration and SoC

Fig. 7.31 shows the average charging power for the EV fleet for all EV charging strategies. When the EVs are uncoordinatedly charged, the average charging powers are nearly equal to the EV charging rate, i.e. 2.1, 3.3 and 6.6 kW[9]. For the other EV charging strategies, the charging power may deviate from these EV charging rates in case the voltage deviations or total building load are too high. Thus, the average charging power may be reduced, as is the case in this case study. For increasing EV charging rates, the voltage deviations and the total building load increase, resulting in an increased charging power reduction, up to about 15 % for an EV charging rate of 6.6 kW in scenario B and C.

It can be observed that the average charging power is nearly equal between scenario B and C, i.e. a maximum deviation of about 1 percentage point. As the average charging power decreases for scenarios B and C, the EV charging duration increases accordingly, as shown in Fig. 7.32. However, despite the nearly equal average charging power, the relative EV charging duration increase

[9]Including the power limitations in each last time step when the SoC reaches 100 %.

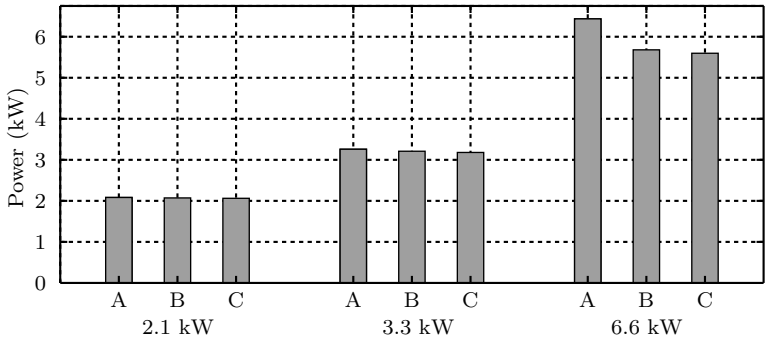


Figure 7.31: Impact on the average EV charging power as a function of the charging rate ($P^{\mathrm{ch}} \in \{2.1; 3.3; 6.6\}$ kW) for a building fleet of 18 EVs.

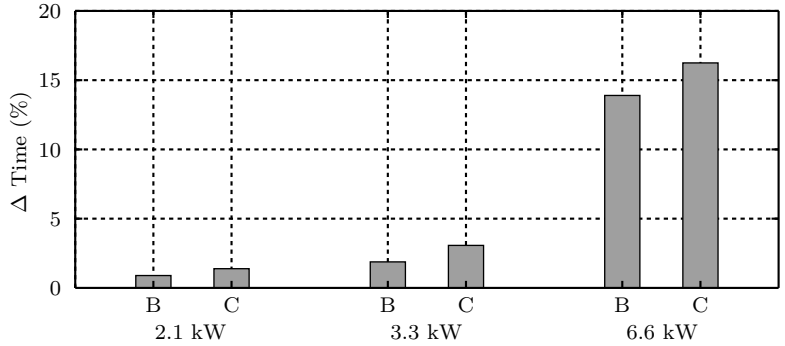


Figure 7.32: Impact on the average EV charging duration as a function of the charging rate ($P^{\mathrm{ch}} \in \{2.1; 3.3; 6.6\}$ kW) for a building fleet of 18 EVs.

is higher for scenario C. This is due to the fact that the SoC is not always 100 % at the end of each charging period. Therefore, subsequent charging periods may be further extended.

Due to the mobility behavior, some EV charging opportunities might not be long enough to fully recharge the battery, as shown in Fig. 7.33. This figure shows the average SoC values measured at the end of each charging period, which increase for higher EV charging rates. As these short charging periods may have a small impact on the average charging power (see Fig. 7.31), the impact is much larger, i.e. a reduction of the average SoC for scenario C up to 4 percentage points compared to scenario A, as shown in Fig. 7.33. In order

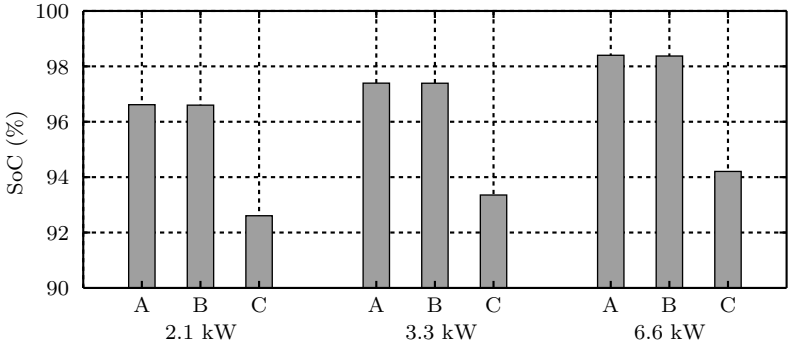


Figure 7.33: Impact on the average SoC at the end of each charging opportunity as a function of the charging rate ($P^{\text{ch}} \in \{2.1; 3.3; 6.6\}$ kW) for a building fleet of 18 EVs.

to alleviate this effect, a weighted objective function could be included in the optimization, as suggested in [263, 264], so as to prioritize batteries with a low SoC to be charged initially, as some EVs might be negatively impacted due to the radial grid, i.e. EVs at the end of a feeder see larger voltage deviations.

Since the batteries are sized relatively large in this case study, the UF (or electric range) is not affected. However, for other case studies, the user comfort might be impacted.

### EV charging profile impact

Fig. 7.34 (a) shows the impact of the different EV charging strategies, which have been discussed in this section, for a sample EV charging profile. The voltage magnitude profile, which corresponds to this EV node, is shown in Fig. 7.34 (b). It can be observed that in the uncoordinated charging case (scenario A), the voltage drops for nearly 45 min below 0.85 pu. As a result of the voltage droop mechanism (scenario B), the voltage profile stays above 0.85 pu. However, as already discussed in Section 7.3, the mechanism does not guarantee that the % of time below 0.9 pu decreases, as proven in this sample.

The optimal capacity charging algorithm (scenario C) does not result in an equal EV charging profile as for scenario B, as can be observed in Fig. 7.34 (a), since it does not take into account the actual voltage profile. Nevertheless, the average charging power/duration is nearly equal. It can be observed that the charging power reduction is higher in scenario C (compared to scenario B) when the voltage profile shows larger voltage deviations in the uncoordinated case,

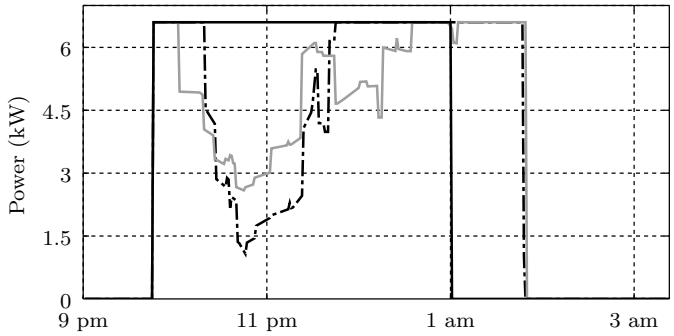


(a) EV charging profile.

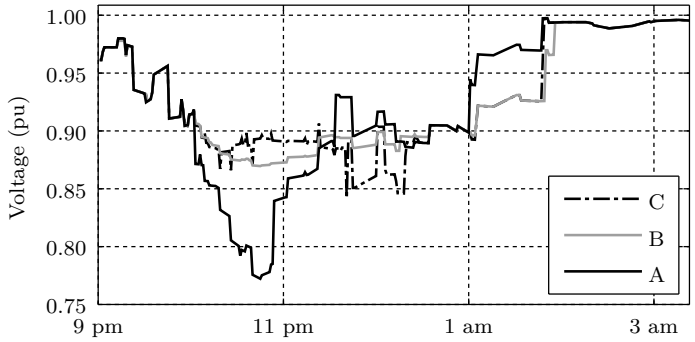


(b) Voltage magnitude profile at EV.

Figure 7.34: Impact of the different EV charging strategies on a sample EV charging profile for a charging rate of 6.6 kW.

and vice versa[10]. This is not a general trend, but this trend has been observed in many other EV charging periods.

The latter is also noticeable in the load duration curves of the total EV charging power, which are shown in Fig. 7.35. This figure shows that in scenario C, in general, the charging power profile lies below the total charging power profile of scenario B when the total EV charging power is high (left part in the graph). A higher total charging power is in general related to higher voltage drops. The opposite is valid when the total charging power is lower. In that case, the EV charging power is reduced less compared to scenario B.

[10]Except when there is a high simultaneity of few EVs charging with a high power demand of the households in the building (see further).

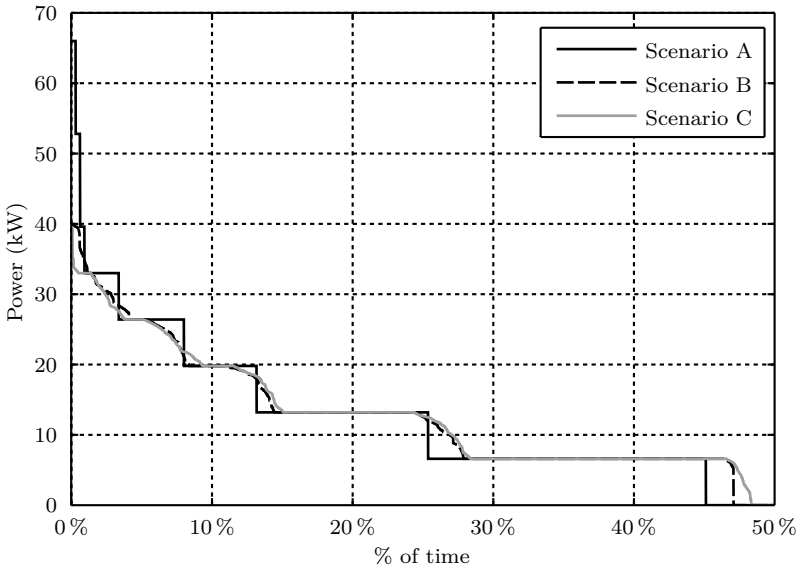


Figure 7.35: EV charging power load duration curve for the different strategies for a building fleet of 18 EVs ($P^{\text{ch}} = 6.6\,\text{kW}$).

### Apartment building load duration curve

Fig. 7.36 shows the impact of the different EV charging strategies on the apartment building load duration curve at the PCC with the LV distribution grid. For an EV charging rate of 2.1 and 3.3 kW, the demand peak power is well below 50 kW. However, since a capacity is set per phase ($\frac{50}{3}$ kW), the building peak shaving mechanism is active at a few moments (decreasing 95th percentile, OPP and peak power). For the 6.6 kW case, a clear reduction in peak demand power is visible due to the building peak shaving mechanism in scenarios B and C.

Also the voltage droop mechanism impacts the power profiles. For all scenarios, a load spreading can be observed: reducing OPP and 95th percentile, and an increasing 5-25th percentile. The optimal capacity charging algorithm reduces the peak demand power more compared to scenario B. This is due to the fact that the charging power is reduced more when the power demand is higher, as proven in Fig. 7.34 and Fig. 7.35.

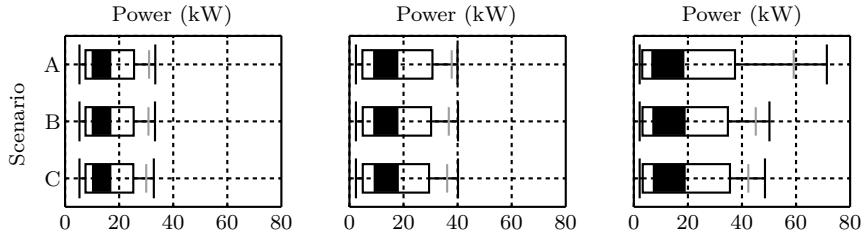


(a) 2.1 kW (b) 3.3 kW (c) 6.6 kW

Figure 7.36: Impact on the building power profiles – Modified box plots for load duration curves as a function of the charging rate ($P^{\mathrm{ch}} \in \{2.1; 3.3; 6.6\}$ kW) for a building fleet of 18 EVs.

### Minimum voltage magnitude at EV nodes

Fig. 7.37 (a) shows the impact on the minimum voltage magnitude at the EV nodes in the apartment building. For all EV charging rates, the minimum voltage magnitude drops below 0.85 pu for uncoordinated EV charging. Due to the voltage droop mechanism in scenarios B and C, the minimum voltage magnitude increases in both scenarios. However, scenario B performs better and keeps the voltages above 0.85 pu. For scenario C, the voltage magnitude still drops below 0.85 pu during three small time periods ($P^{\mathrm{ch}} = 6.6$ kW). This is due to the simultaneity of a few EVs charging with a very high apartment building household peak demand. As discussed in Fig. 7.35, scenario C reduces the charging power less for a few EVs charging.

As mentioned before, the objective of the voltage droop mechanism is only to avoid voltage deviations below 0.85 pu. Therefore, scenario B does not guarantee less voltage deviations below 0.9 pu, as shown in Fig. 7.37 (b). However, in that perspective, scenario C performs better. The number of voltage drops below 0.9 pu reduces in scenario C. Note that both scenarios reduce the voltage magnitude deviations, but for this case study (weak grid and high loading), they do not guarantee that the grid complies with EN 50160.

### Maximum VUF at EV nodes

Fig. 7.38 shows the positive impact of the different EV charging strategies (scenarios B and C) on the maximum occurring VUF at the EV nodes. Also, the time that the VUF exceeds 2 % is reduced. Despite it is not the objective of these strategies to reduce the voltage unbalance, the EV charging power reductions have a positive impact on the VUF, as mentioned before in this

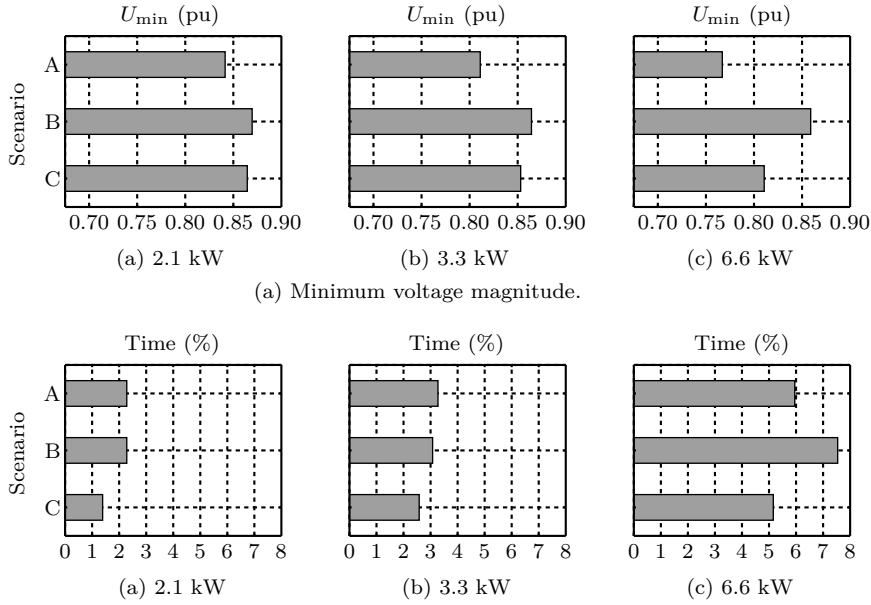


Figure 7.37: Impact on (a) the minimum voltage magnitude at the EV nodes, and (b) % of the time that the grid voltage is lower than 0.90 pu, as a function of the charging rate ($P^{\text{ch}} \in \{2.1; 3.3; 6.6\}$ kW) for a building fleet of 18 EVs.

chapter. However, it is not guaranteed that the grid is compliant regarding the VUF.

### 7.5.5 Conclusions

This section compares two EV charging strategies which reduce the EV charging power as a function of the grid voltage (voltage droop mechanism) and the building power demand (building peak shaving). The combination of two local EV charging strategies from Section 7.3 and 7.4 have been compared with a central optimization algorithm, the *optimal capacity charging*. Both EV charging strategies do succeed in their objectives, namely:

- reducing the voltage deviations;
- reducing the peak demand power to the available capacity.

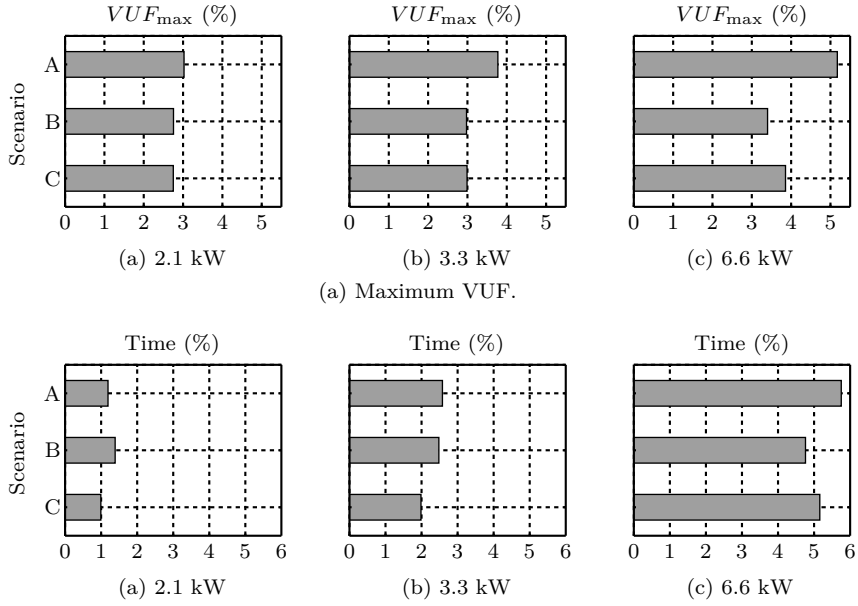


(a) Maximum VUF.

(b) % of the time that the VUF exceeds 2%.

Figure 7.38: Impact on (a) the maximum VUF at the EV nodes, and (b) % of the time that the VUF exceeds 2 %, as a function of the charging rate ($P^{\text{ch}} \in \{2.1; 3.3; 6.6\}$ kW) for a building fleet of 18 EVs.

The results show that the average EV charging power is nearly equal between both strategies. Besides, a positive impact on the voltage unbalance has been observed.

However, it has been observed that both EV charging strategies result in different EV charging profiles, and this results in some disadvantages for the optimal capacity charging algorithm: it is not guaranteed that the minimum voltage is above 0.85 pu. If the total EV charging load is high, the optimal capacity charging algorithm tends to be too responsive, and vice versa. In general, this strategy leads to a lower average SoC at the end of short charging periods, which results in an increased EV charging duration. In this case study, this does not have a negative impact on the user comfort, i.e. electric range.

It can be concluded that both strategies perform well regarding the objectives of the strategies, but additional measures are required for short charging opportunities for the optimal capacity charging algorithm to perform better [263, 264]. These short charging opportunities tend to occur in the early evening, resulting in a high simultaneity with the evening demand of the households in

the building.

## 7.6 Discussion and conclusions

This chapter discusses the impact of different local EV charging strategies, as defined in Table 6.5, regarding their grid and fleet impact, compared to uncoordinated charging. When EVs are uncoordinatedly charged, charging at maximum power starts whenever EVs arrive at home. The different EV charging strategies have been compared to this reference scenario with uncoordinated EV charging. Detailed conclusions of the charging strategies have been given in Sections 7.1.3, 7.2.3, 7.3.3, 7.4.3 and 7.5.5, respectively. As discussed in Chapter 6, all strategies can be implemented locally in the EV and/or mode 3 charging infrastructure. A building energy management system may be required.

All EV charging strategies succeed in reducing the grid impact, compared to uncoordinated charging: reductions of peak powers (demand and/or injection), voltage deviations and/or voltage unbalance. However, compared to uncoordinated charging, i.e. charging as soon as possible, the EV user comfort is impacted for all EV charging strategies since the charging process is extended, postponed or shortly interrupted. This has been illustrated in Table 7.2, which gives a summary of the grid and fleet impact[11]. While EV based peak shaving has a negative impact on the charging duration (minimizing the charging power), the charging process is delayed for both delayed charging and off-peak charging[12]. The electric range is not impacted for these two strategies. The additional strategies, which deviate the charging power from the charging power set-point, extend and/or postpone the charging duration whether or when these strategies are activated. On the other hand, for delayed charging, the charging process may start early in case of local electricity generation surplus. To conclude, off-peak charging limits the electric range.

To compensate for the loss in comfort and for EV owners to adopt these strategies, incentives are required for the different charging strategies. Besides, the strategies in this dissertation assume a perfect knowledge of the next departure time. In reality, the strategies should take into account a spread around this departure time, and trips might be cancelled or added. Therefore, the strategies should allow to alter the EV owners schedule. Depending on the moment an extra trip is scheduled, the electric range might be impacted,

[11] For some strategies, the impact depends whether or when the strategy is activated.

[12] For off-peak charging, the charging process is postponed when the EV arrives at home during the peak period.

Table 7.2: Overview of local EV charging strategies: grid and fleet impact indicators from the EV user and DSO point of view (POV).

| | | **EV owner POV** | | | | **DSO POV** | | | | | | |
|---|---|---|---|---|---|---|---|---|---|---|---|---|
| | | UF / Electric driving range | Charging duration | Average charging power | Charging start time | Average charging power | Charging load spreading | Peak power demand | Peak power injection | Minimum voltage magnitude | Maximum VUF | Self-consumption |
| **Set-point** | Uncoordinated charging | *Uncoordinated charging whenever arriving at home used as a reference* | | | | | | | | | | |
| | EV based peak shaving | o | - | - | o | + | + | + | + | + | + | + |
| | Delayed charging | o | o | o | - | o | o | + | + | + | + | + |
| **Deviation set-point** | Off-peak | - | + | o | - | o | - | - | - | - | o | - |
| | Local generation surplus | o | o/- | o/- | o/+ | o/+ | + | + | o/+ | o | o | + |
| | Voltage droop mechanism | o/- | - | - | o/- | + | + | +/- | o | + | + | o |
| | Building peak shaving | o/- | - | - | o/- | + | + | + | o | + | o | o |

*Legend* – o: no impact; +: positive impact; −: negative impact

which is especially a threat for delayed charging as no flexibility might be left to reschedule the charging process.

Table 7.2 also shows a comparison of the grid impact indicators, shown from the DSO point of view. First, two charging strategies have been assessed, which make use of the available EV charging flexibility in time and power. EV based peak shaving lowers the charging power as much as possible by maximally using the available flexibility in time and power, while delayed charging postpones the charging process as long as possible by using the maximum available flexibility in time. Both strategies have a positive grid impact regarding peak power[13], voltage deviations and unbalance reductions. For EV based peak shaving, the EV charging load is spread in time, while for delayed charging the simultaneity with the evening peak demand power is reduced. Therefore, these strategies allow a higher amount of EVs to be charged before grid reinforcements are required. Also, the self-consumption is positively impacted.

Limiting the EV charging to the off-peak period minimizes the charging cost in the present dual tariff scheme, but results in an increased grid impact (peak power increase) from the DSO point of view, due to an increase in EV charging simultaneity in the evening. Therefore, encouraging additional daytime charging (and charging at other locations) is preferred.

Furthermore, additional strategies have been discussed which deviate the charging power from the set-point set by uncoordinated charging, delayed charging or EV based peak shaving. All strategies succeed in their objective, i.e. increasing the self-consumption of locally generated electricity, reducing the voltage deviations (voltage droop mechanism) and reducing the peak power demand to the available capacity (building peak shaving), respectively. This allows more EVs to be charged in the building, and/or EVs can be charged at a higher charging power before violating the grid regulations. In addition, also other grid impact indicators may be positively impacted, as indicated in Table 7.2.

To conclude, this chapter discusses in Section 7.5 a combination of a voltage droop and building peak shaving mechanism, compared to the *optimal capacity charging* strategy. In this central optimization strategy, the charging power of each vehicle is optimized in order to maximize the total amount of power delivered to all of the EVs, taking into account the maximum allowed voltage deviations and power capacity.

[13]However, this impact is very small regarding the peak injection power.

# Chapter 8

# Hybrid in-building AC-DC electricity distribution

This chapter focuses on the impact assessments of the combination of DC in-building grids and EV charging, for the case study defined in Chapter 6. The in-building grid topology of this case study has been adapted to a hybrid AC-DC grid, in which the PV system, heat pump and EVs are connected to the DC grid (see Section 8.1). The objective of this chapter is to assess the advantages of the use of DC grids regarding the grid impact of the apartment building, including EV charging. The scope of this chapter is not to look at the efficiency impact, nor at the optimal grid design.

First, Section 8.2 discusses the results of the reference scenario, which does not include any EV charging. Section 8.3 discusses shortly the impact of DC grids on the fleet impact indicators. To conclude, the grid impact has been assessed in Section 8.4.

## 8.1 Scenario description

This section describes the models and the scenarios for this case study of a hybrid AC-DC electricity distribution in an apartment building. The case is based on the scenario description in Chapter 6.

### 8.1.1 Apartment building

The following models and (demand/production) profiles, as used in Chapter 6, remain unchanged:

- the transient building response model and building topology description (Section 6.1.1);
- the residential power consumption (Section 6.1.3);
- the PV system and power production profile (Section 6.1.4);
- the heating system and heat pump power demand profile (Section 6.1.5);
- the electric vehicles (Section 6.1.6).

The converter efficiencies for the PV system, heat pump and EVs have been given in the respective sections in Chapter 6. This means that, due to the higher converter efficiency[1], the PV system has a higher power production output and the heat pump has a decreased power demand. The EV charging rate remains unchanged, resulting in a faster charging process of the vehicles.

### 8.1.2 Low-voltage and in-building electricity grid topology

Section 6.1.2 describes the residential LV distribution grid. The aggregated load of the LV distribution grid remains unchanged.

Fig. 8.1 gives a representation of the considered in-building hybrid AC-DC grid topology of the apartment building, which is connected to the LV distribution grid at the PCC. The DC grid is used to interconnect the PV system, heat pump and EVs. These are connected to the DC grid through a DC-DC converter, omitting the inverter. The cable sizing is based on the *American Wire Gauge Conductor Size Table*, in order to comply with the cable current ratings [266,267], which results in lower impedances compared to the AC cables in the previous analyses.

A central AC-DC bidirectional converter is added to the grid to connect the DC grid (380 V and unipolar) to the three-phase AC grid. At the AC side, the demand or injection power is balanced over the three phases. For the base case, it is assumed that the bidirectional AC-DC converter has an efficiency of 97 % [258]. As discussed in [268], the bidirectional converter is responsible for the largest share in the total losses in the AC-DC grid topology. Therefore, a sensitivity analysis has been performed (efficiency ± 2 percent points) to assess the impact of the converter efficiency.

[1] The AC-DC conversion is omitted in a DC grid.

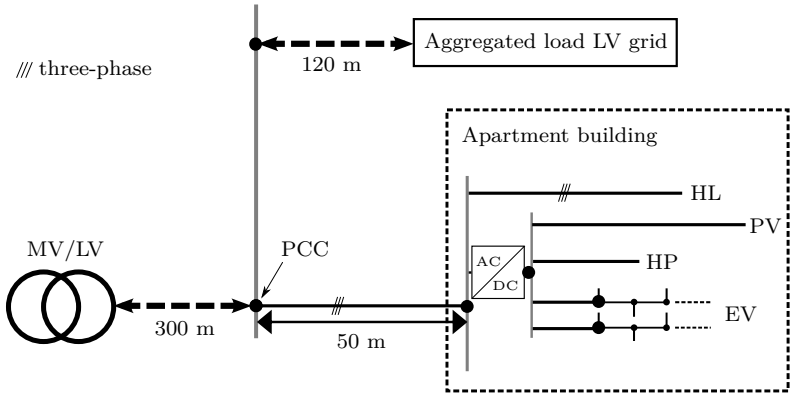


Figure 8.1: Topology of the low-voltage and hybrid AC-DC in-building electricity grid.

### 8.1.3 Simulation specifications

As indicated in Section 4.3.6, the Modelica implementation allows to simulate multiple grid types in one simulation. Here, a hybrid AC-DC grid topology, using the IDEAS library, is simulated consisting of:

- a three-phase unbalanced load flow;
- a load flow of a unipolar DC grid;
- a bidirectional AC-DC converter connecting both grids.

For the three-phase unbalanced load flow, unbalanced loads have been taken into account, as well as the resulting zero-point shift due to currents running through the neutral conductor.

For computational reasons, i.e. calculation time, the simulations have been performed for a one week period (Monday till Sunday) with a 1 min time resolution ($\Delta t$). This is the identical week as used in Chapter 6. The household power profiles are available on a 15 min time resolution, which are interpolated on a 1 min time resolution (within Dymola). The heat pump and EV demand profiles, and PV production profiles are available on a 1 min time resolution.

## 8.2 Results: reference scenario (no EVs)

As indicated in [268], the total losses in the system, for both AC and DC grids, consist of:

- the cable (Joule) losses;
- the losses in the AC-DC and DC-DC converters of the appliances;
- the bidirectional AC-DC converter losses in case a DC grid is connected to an AC grid.

As shown earlier in [268], the cable losses and converter losses reduce in DC grids. However, extra losses are induced in the bidirectional converter when a DC grid is connected to an AC grid, which are not to be neglected if the self-consumption of local generation within the DC grid is low. Therefore, to minimize the losses in the bidirectional AC-DC converter, the following solutions can be applied:

- DSM for the appliances connected to the DC grid, in order to improve the simultaneity of demand and production within the DC grid;
- local storage within the DC grid[2];
- optimal DC grid design, i.e. cable design and grid topology.

This dissertation does not focus on local storage connected to the DC bus, nor the optimal DC grid design. Since the total losses largely depend on the DC grid design and the converter parameters, i.e. efficiency curve, the impact of DC grids on the total losses has not been further discussed in this chapter. Therefore, this work focuses on the grid impact of the EV charging (see Chapters 6 and 7) in combination with a DC grid.

In Fig. 8.2, the load duration curves are shown for both the reference AC and hybrid AC-DC grid topology. No EVs are present in the building. For the hybrid AC-DC grid topology, a sensitivity analysis has been performed regarding the efficiency of the bidirectional converter, i.e. an efficiency $\eta^{\text{AC-DC}} \in \{95; 97; 99\}$ %.

Depending on the efficiency of the bidirectional converter, the peak demand and injection increase or decrease compared to the AC case. In other words, the change in efficiency of the bidirectional converter, compared to the efficiency gains in the appliance converters, has an impact on the peak powers. Although, this impact on the peak powers is limited. For instance, for an increasing

[2] Although storage losses have been induced.

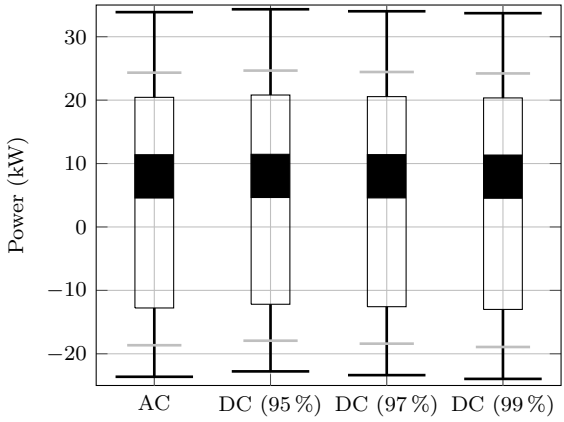


Figure 8.2: Load duration curves for the reference scenario without EVs, for both the AC and hybrid AC-DC case, including the sensitivity to the bidirectional converter efficiency $\eta^{\text{AC-DC}} \in \{95; 97; 99\}$ %.

efficiency of the bidirectional converter, the peak power demand reduces, while the peak power injection increases. Since the impact on the peaks largely depends on the chosen parameters of the different converters, no general conclusions can be taken regarding the increase or decrease of the demand and injection peaks. Although, it allows to discuss the impact trends of EV DC charging in the building.

Nevertheless, it can be observed in Fig. 8.2 that the change in the load duration diagrams is limited due to the limited share of losses in the grids compared to the total load. Therefore, also the impact on the voltage profile, which is related to the load profile, at the building PCC is very limited. This is due to the fact that both the PV system and heat pump are three-phase connected to the AC grid in Chapter 6. In Section 8.4.4, the impact of the EV charging in combination with a DC grid on the voltage profile is shown.

## 8.3 Fleet impact

The same EV charging rates, as defined before in Chapter 6, have been used, i.e. $P^{\text{ch}} \in \{2.1; 3.3; 6.6\}$ kW. Thus, the same amount of power is drawn from the grid while charging an EV. Therefore, the total charging duration decreases a little due to the efficiency gains in the EV converters[3]. Nevertheless, due to

[3]The AC-DC conversion is omitted, as discussed in Section 8.1.1.

the limited efficiency gains, the impact of DC grids on the fleet indicators is limited. Therefore, the fleet impact is not discussed in detail. The main trends have been described, since the impact trends are similar to those discussed for the AC cases in Chapter 7.

### Uncoordinated charging

The fleet impact trends are similar to charging at a higher charging rate, discussed in Section 7.1.1. The EV charging duration decreases due to the efficiency gains in the EV converters. Therefore:

- the EV charging simultaneity decreases;
- the UF increases.

### Delayed charging

For delayed charging, the EV charging process will start later due to the decreased EV charging duration. This is the result of the converter efficiency gains. Therefore:

- the EV charging simultaneity decreases;
- the simultaneity with PV power production might decrease.

### EV based peak shaving

Due to the efficiency gains in the EV converters, the reduced EV charging power $P^{\text{set}}$, as calculated in Section 6.3.1, decreases, in order to maximize the EV charging duration. However, depending on the reduced EV charging power, the EV charging duration may decrease:

- the EV charging duration remains unchanged for $P^{\text{set}} > P_{\text{min}}$;
- the EV charging duration decreases when $P^{\text{set}} = P_{\text{min}}$, due to the higher conversion efficiency.

In case of an EV charging duration decrease:

- the EV charging simultaneity decreases;
- the simultaneity with PV power production might decrease.

## 8.4 Grid impact of EV charging and DC grids

In this section, the impact trends of DC grids, in combination with the local EV charging strategies, have been discussed. The results have been compared with the uncoordinated EV charging strategy in the AC grid case (scenario 1 in Section 7.1). The following EV charging strategies have been examined:

- **Scenario 1:** Uncoordinated EV charging whenever EVs arrive at home.
- **Scenario 3:** Delayed EV charging.
- **Scenario 4:** Delayed EV charging, including charging the local PV generation surplus.
- **Scenario 5:** EV based peak shaving.
- **Scenario 6:** EV based peak shaving, including charging the local PV generation surplus.

### 8.4.1 Energy exchange at the building PCC

The total energy exchange at a node of the grid is defined in Section 2.8. In Fig. 8.3, the impact on the total energy exchange, compared to scenario 1 (uncoordinated EV charging) in an AC grid, at the building PCC is shown for:

- the impact of the different EV charging strategies in the AC case;
- the impact of the use of DC grids, including a sensitivity analysis for the bidirectional converter efficiency $\eta^{\text{AC-DC}} \in \{95; 97; 99\}$ %.

#### AC grid

In case of an AC grid, all EV charging strategies (scenario 3–6) result in decreased energy exchanges at the building PCC, due to:

- an increased simultaneity of the EV charging and the local PV power production, which results in an increased self-consumption, as discussed in Section 7.2;
- decreased grid losses as a result of the EV charging load spreading, i.e. reducing the peak power demand.

It can also be noted that less energy is exchanged at the building PCC when the EV charging strategies anticipate on the local PV power production surplus,

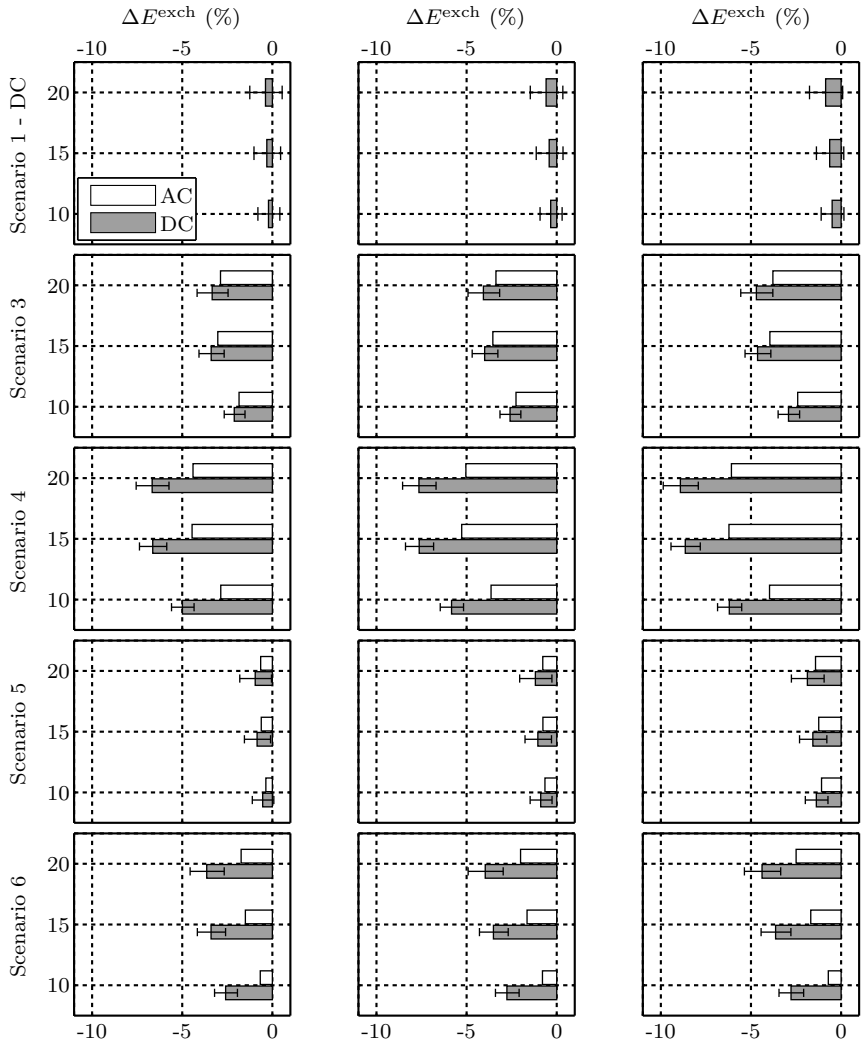


(a) 2.1 kW (b) 3.3 kW (c) 6.6 kW

Figure 8.3: Change (%) in energy exchange ($\Delta E^{\text{exch}}$) at the building PCC, compared to uncoordinated EV charging (scenario 1 in an AC grid), for the different EV charging strategies, as a function of the charging rate ($P^{\text{ch}} \in \{2.1; 3.3; 6.6\}$ kW) and number of EVs ($n^{\text{EV}} \in \{10; 15; 20\}$) charged in the apartment building, including the sensitivity to the bidirectional converter efficiency $\eta^{\text{AC-DC}} \in \{95; 97; 99\}$ %, indicated by the error bars.

up to about 4.2 percentage points. In that case, the self-consumption increases, as discussed in Section 7.2, resulting in less energy exchanged with the LV distribution grid.

#### Hybrid AC-DC grid

Fig. 8.3 also shows the impact, for all EV charging strategies, when using a hybrid AC-DC grid to interconnect the EVs on a common DC bus with the PV system and heat pump. The results are shown for the base case with an efficiency of 97 % for the bidirectional AC-DC converter. Markers have been included to show the sensitivity for the efficiency of this converter, i.e. a converter efficiency $\eta^{\text{AC-DC}} \in \{95; 97; 99\}$ %. The lower the efficiency, the more energy is exchanged with the LV distribution grid.

As observed in the reference scenario (Section 8.2), the impact of the use of DC grids on the energy exchange is relatively limited, although it heavily depends on the simultaneity of the EV charging and the local PV power production. It can be observed that the energy exchange decreases more when a strategy anticipates on the local PV power production (scenario 4 and 6). This is the result of the increased self-consumption, which limits the extra losses induced in the bidirectional converter.

On the other hand, it is also important to note the importance of the converter efficiency gains on the energy exchange impact, as shown by the markers, i.e. a bidirectional converter efficiency of 95 % and 99 %, in Fig. 8.3. It is important to note that the use of a DC grid does not always guarantee a reduction in energy exchanged, especially when the EV charging strategies do not anticipate on charging the PV power surplus.

### 8.4.2 Peak power demand

Fig. 8.4 shows the change in peak power demand of the building, compared to scenario 1 (uncoordinated EV charging) in an AC grid, for:

- the impact of the different EV charging strategies in the AC case;
- the impact of the use of DC grids, including a sensitivity analysis for the bidirectional converter efficiency $\eta^{\text{AC-DC}} \in \{95; 97; 99\}$ %.

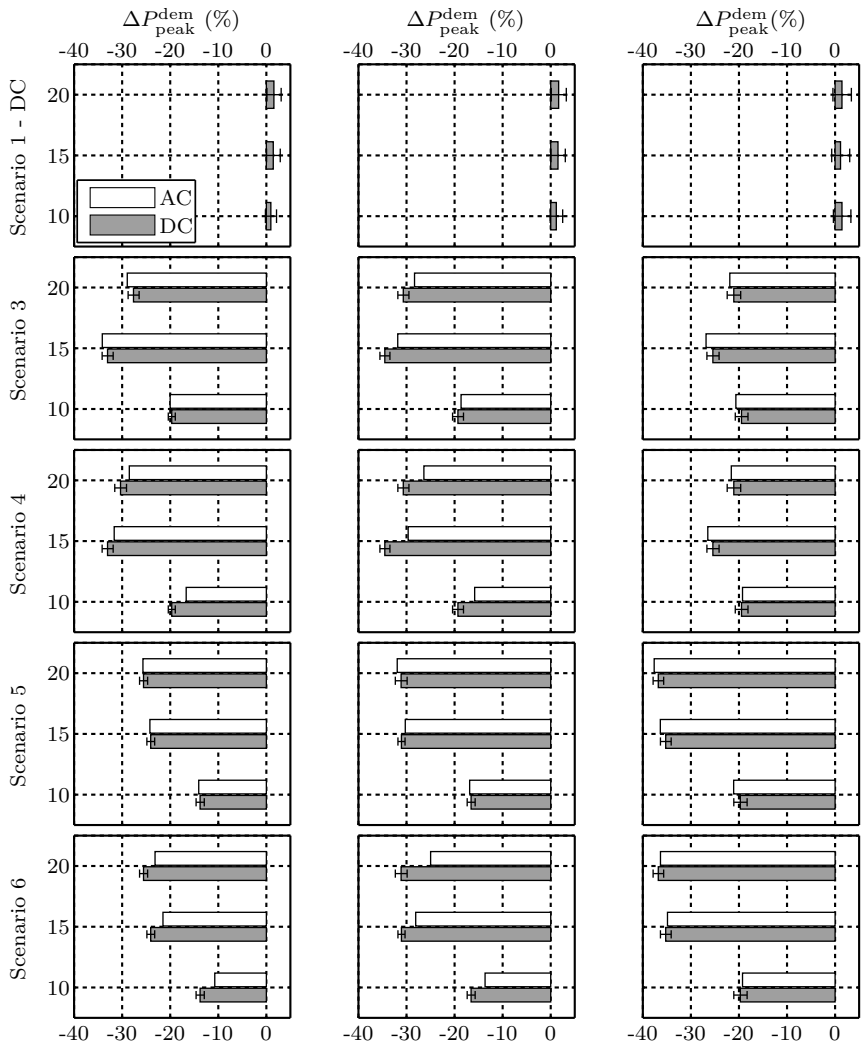


(a) 2.1 kW (b) 3.3 kW (c) 6.6 kW

Figure 8.4: Change (%) in the building peak power demand ($\Delta P^{\text{dem}}_{\text{peak}}$), compared to uncoordinated EV charging (scenario 1 in an AC grid), for the different EV charging strategies, as a function of the charging rate ($P^{\text{ch}} \in \{2.1; 3.3; 6.6\}$ kW) and number of EVs ($n^{\text{EV}} \in \{10; 15; 20\}$) charged in the apartment building, including the sensitivity to the bidirectional converter efficiency $\eta^{\text{AC-DC}} \in \{95; 97; 99\}$ %, indicated by the error bars.

### AC grid

In Chapter 7, the impact of the EV charging strategies on the peak demand powers is already discussed. For both delayed charging and EV based peak shaving, the peak demand powers reduce compared to uncoordinated EV charging, as shown in Fig. 8.4. Anticipating on the local PV power production does not guarantee a reduction of the building peak demand power due to the decreased simultaneity with the local PV production at later moments during the charging opportunity, as discussed earlier.

### Hybrid AC-DC grid

Fig. 8.4 includes the results of the peak power demand impact, for all EV charging strategies, when using a hybrid AC-DC grid. The results have been shown for the base case with an efficiency of 97 % for the bidirectional AC-DC converter. Markers have been included to show the sensitivity for the efficiency of this converter, i.e. a converter efficiency $\eta^{\text{AC-DC}} \in \{95; 97; 99\}$ %. A lower efficiency results in an increased peak power demand.

As already observed in the reference scenario without EVs (Section 8.2), the impact of using a DC grid on the peak power demand is small for all scenarios. However, due to the small impact, it is difficult to draw general conclusions for the change (positive or negative) in peak power demand due to the use of DC grids, since the change in peak power demand depends on:

- the grid losses[4];
- the efficiency gain/loss in the appliance converters and bidirectional AC-DC converter;
- the power demand of the EVs and its simultaneity with the local PV production, which is related to the EV charging rate, EV charging simultaneity and charging duration (see Section 8.3).

It can be concluded that the peak power demand impact of DC grids is much smaller than the impact of the different EV charging strategies, as discussed in Chapter 7. For instance, the impact of DC grids is in the order of up to about ±5 percentage points, while the peak power demand is reduced by almost 40 % when implementing EV based peak shaving.

[4]The grid losses are also impacted by the change in voltage unbalance (see Section 8.4.3).

### 8.4.3 Voltage unbalance at building PCC

In the AC case, EVs are single-phase connected to the AC grid. Therefore, the use of the hybrid AC-DC grid, including the central bidirectional AC-DC converter, will impact the voltage unbalance and the occurring voltage magnitudes in the AC grid of the building. In the hybrid AC-DC grid, the EV charging load is balanced through the bidirectional AC-DC converter.

As can be observed in Fig. 8.5 (a), and as shown in Fig. 7.6 (Section 7.1.2) for the AC grid case, the maximum occurring VUF largely increases for an EV charging rate of 6.6 kW. For an EV charging rate of 2.1 and 3.3 kW, the maximum VUF mainly depends on the other single-phase loads in the grid. When making use of a DC grid, the maximum VUF at the building PCC reduces for an EV charging rate of 6.6 kW. On the other hand, Fig. 8.5 (b) shows that for all EV charging rates, the unbalance at the building PCC is largely reduced when a DC grid is

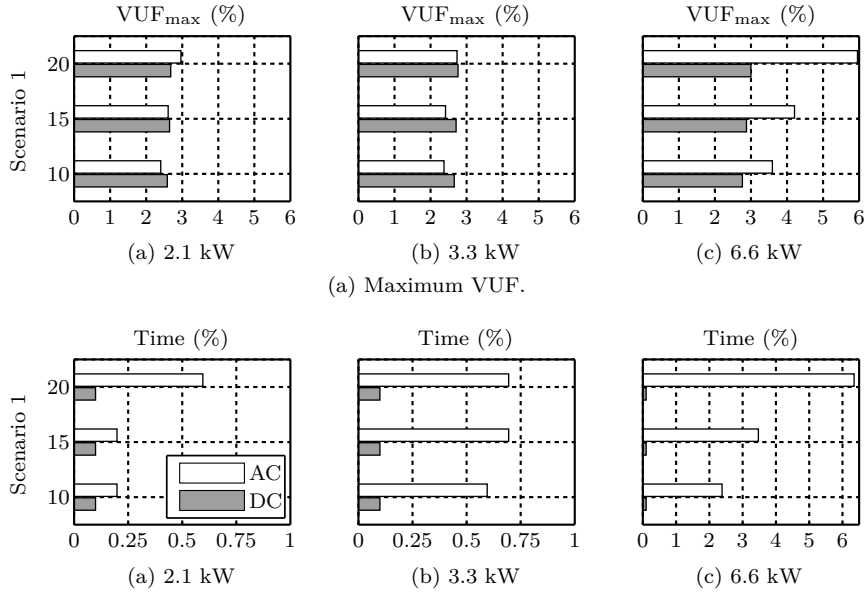


(a) Maximum VUF.

(b) % of time that the VUF goes beyond 2 %.

Figure 8.5: Impact of DC grids on (a) the building PCC VUF for uncoordinated EV charging, and (b) the % of time that the building PCC VUF goes beyond 2 %, as a function of the charging rate ($P^{\mathrm{ch}} \in \{2.1; 3.3; 6.6\}$ kW) and number of EVs ($n^{\mathrm{EV}} \in \{10; 15; 20\}$) charged in the apartment building, with a bidirectional AC-DC converter efficiency of 97 %.

implemented. It can be observed in this figure that the VUF exceeds 2 % less frequently, and it is independent of the EV charging. Identical conclusions can be drawn for the other EV charging strategies.

### 8.4.4 Minimum voltage at building PCC

The impact of DC grids on the minimum voltage at the building PCC for uncoordinated EV charging (scenario 1) is shown in Fig. 8.6. The results for the other EV charging strategies follow the same impact trends.

The changes in the voltage drop at the building PCC in the hybrid AC-DC grid, compared to the AC grid, are a function of:

- the power demand profile in the three phases of the AC grid;

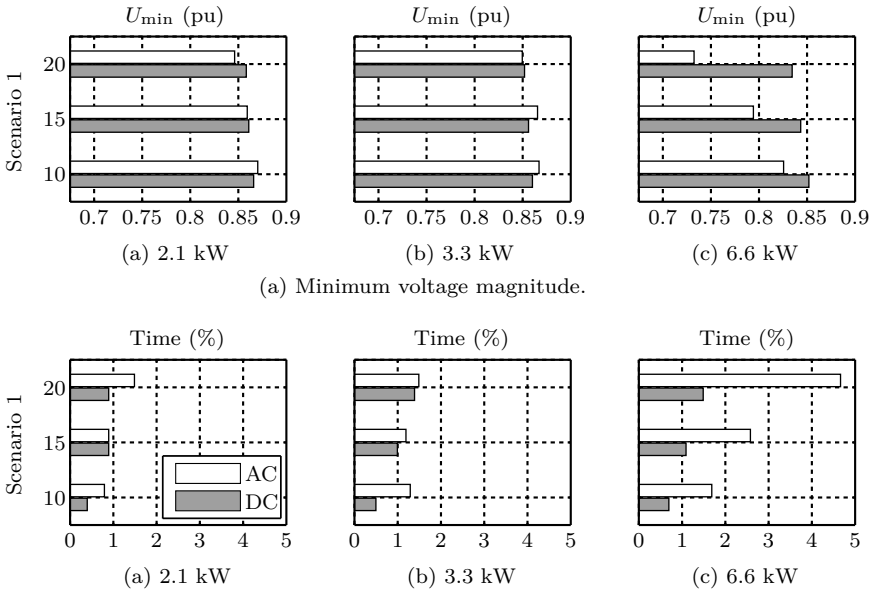


(a) 2.1 kW (b) 3.3 kW (c) 6.6 kW

(a) Minimum voltage magnitude.

(a) 2.1 kW (b) 3.3 kW (c) 6.6 kW

(b) % of time that the grid voltage is lower than 0.90 pu.

Figure 8.6: Impact of DC grids on (a) the building PCC minimum voltage for uncoordinated EV charging, and (b) the % of time that the grid voltage is lower than 0.90 pu at the building PCC, as a function of the charging rate ($P^{\text{ch}} \in \{2.1; 3.3; 6.6\}$ kW) and number of EVs ($n^{\text{EV}} \in \{10; 15; 20\}$) charged in the apartment building, with a bidirectional AC-DC converter efficiency of 97 %.

- the balancing of the EV charge load through the bidirectional AC-DC converter.

In Fig. 8.6 (a), the minimum voltages at the PCC, in the hybrid AC-DC case, increase up to 0.10 pu for an EV charging rate of 6.6 kW, as a result of the reduced unbalance (see Section 8.4.3). The minimum voltage mainly depends on the other single-phase loads in the grid for an EV charging rate of 2.1 and 3.3 kW. In the hybrid AC-DC case, the minimum voltage changes only slightly when EVs are charged at a rate of 2.1 and 3.3 kW. Due to the change in unbalance, no general conclusions can be drawn in these charging rate cases. However, in Fig. 8.6 (b), it can be concluded that in general the occurring voltages increase since the voltages drop less frequently below 0.90 pu for all three EV charging rates.

## 8.5 Conclusions

This chapter discusses the grid impact of the combination of different local EV charging strategies, as defined in Table 6.5, and the use of in-building DC grids. This chapter allows to discuss the advantages of the use of DC grids regarding the grid impact of the apartment building.

The main advantage of the DC grid is the balancing of the AC in-building grid through the central AC-DC bidirectional converter, as the EV charging load is balanced over the three phases. The results show that the unbalance is largely reduced, which allows more EVs to be charged in the building. Related to the voltage unbalance reduction, also the minimum occurring voltages are positively impacted. The voltages drop less frequently below 0.90 pu.

This chapter also discusses the grid impact regarding the energy exchange of the building with the LV distribution grid, and the peak power demand of the building. It is shown that the impact of the use of DC grids is minimal, compared to the impact of the different local EV charging strategies, and heavily depend on the efficiency of the converters. When the EV charging strategies anticipate on the PV power surplus, the use of DC grids is largely beneficial regarding the energy exchanged with the LV distribution grid.

# Chapter 9

# Impact EV charging in an office building

This chapter discusses the EV charging in an existing office building microgrid equipped with a PV system and a CHP unit. EV charging at the work place is seen as an important additional charging location. Moreover, a high simultaneity between EV charging and the local electricity production may be expected due to the high share of vehicles parked at the work place during daytime.

Due to the short commuter distances and the long standstill times at the work place, different local EV charging strategies have been assessed in this chapter, in order to maximize the amount of EVs that can be charged. A second option to minimize the grid impact is to limit the number of EVs charging simultaneously. Therefore, this chapter also discusses the case of a limited number of EVSEs.

This chapter has been based on the following peer-reviewed article[1]:

> J. Van Roy, N. Leemput, F. Geth, J. Büscher, R. Salenbien, and J. Driesen, "Electric vehicle charging in an office building microgrid with distributed energy resources," *IEEE Trans. Sustain. Energy (Special Section on "Microgrids for Sustainable Energy Systems")*, vol. 5, no. 4, pp. 1389–1396, Oct. 2014.

First, Section 9.1 describes the scenario of the investigated office building. Section 9.2 discusses the EV charging flexibility at the work place, while the results will be discussed in Section 9.3 and 9.4.

[1] The results in Section 9.2 have been added.

## 9.1 Scenario description

This section describes the models and the scenario for this chapter. The on-site and in-building electricity grid have not been taken into account in this case study. Measured load and generation profiles are available.

### 9.1.1 Volt-Air living lab

The case study has been based on the Siemens microgrid in Huizingen, Belgium. The building is part of the Volt-Air project, one of the five living labs for EVs in Flanders, Belgium [269]. This living lab focuses on the EV adoption in business fleets and their integration in company building microgrids.

### 9.1.2 Office building

The considered office building[2], the Siemens microgrid in Huizingen (Belgium), has a large PV park installed at the building site. A small CHP covers a small part of the heat demand.

Measurement data[3] is available for:

- the building power profile;
- the PV power production profile;
- the CHP power production profile.

Measurements have been performed on a 5 min time resolution. The measurements have been adapted to a 1 min time resolution. A constant power profile is used on the 1 min time resolution within the time resolution of the original data. The simulations in this chapter cover the first five months of 2013 (January – May). However, only the power demand profile of the considered building and the power production profile of the PV system have been used. The CHP measurements show different operating regimes in the considered period. Therefore, these measurements have not been used (see Section 9.1.3). Missing measurement points (about 7 %) have been replaced by measurements from similar weeks with a comparable consumption or production profile.

[2]Electricity consumption of 395.1 MWh during the considered period.

[3]Accuracy of 1 % for the current transformer and respectively 0.5 % and 0.2 % for the PV and building power measurement devices at nominal current.

### 9.1.3 Distributed energy resources

Local electricity production is achieved through both a large PV system and a small CHP.

#### Photovoltaic system

A large PV installation (500 $kW_p$) produces electricity for the building and the EVs. The installation covers an area of about 10 000 $m^2$. The PV power surplus is injected into the grid. During the considered simulation period, 164.5 MWh is produced.

#### Combined heat and power system

A small CHP is installed at the Siemens microgrid with an installed electric power of 9 kW. This CHP is used to generate heat and hot water to the cafeteria. As mentioned in Section 9.1.2, the measurements of the CHP power production have not been used.

To generate a production profile for the heat and electricity in the office building, it is assumed for this case study that the CHP, which is heat driven with no thermal energy storage, follows the production profile for a reference office building. The COGENscan 2008 simulation tool is used to generate the production profiles [270][4]. This tool allows to calculate a CHP production profile with a 1 h time resolution[5]. The CHP is sized for the heat base load. During the considered period, 18.7 MWh of electricity is produced. It is assumed that the remaining heat demand is covered by other heat generation units.

#### Complementarity of PV and CHP power production

Fig. 9.1 shows the seasonal complementary between PV and CHP systems for the considered simulation period. This figure shows the monthly electricity production of both systems scaled to their respective month with maximum production. Since the CHP is heat driven, it is expected that the electricity production in winter will be higher than in spring, while the PV system produces more electricity in spring/summer.

[4] COGENscan is a tool to define the technical and economical feasibility for a CHP installation [270].

[5] A constant power profile has been used on the 1 min time resolution, within the time resolution of the original data.

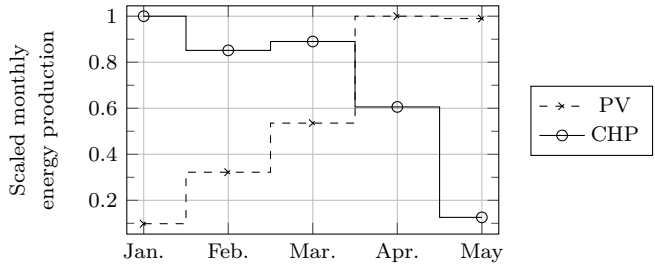


Figure 9.1: Monthly electricity production of the PV system and CHP, scaled to their respective month with maximum production.

In this case study, the electrical power of the CHP is limited compared to the PV system (9 $kW_p$ vs. 500 $kW_p$). Future work may focus on a more optimal sizing of both systems, including the coordination of the CHP system, in order to improve the simultaneity between electricity production and consumption.

### 9.1.4 Electric vehicles

As discussed in Section 6.1.6, the EV model consists of three submodels: a battery model, the mobility behavior and the charging behavior. The local EV charging strategies will be discussed in Section 9.1.5. They have been based on the charging strategies discussed in Section 6.3.

#### Battery Model

The implementation of the battery model has been based on the model used in [153], which has been discussed in Section 4.5. Li-ion type batteries have been chosen, with identical parameters and efficiencies as given in Section 6.1.6. As before, the EVs have been modeled as EREVs, with a battery size of 10, 15 and 20 kWh for small, middle-class and large vehicles, respectively.

#### Mobility Behavior

A mobility simulation tool has been used to generate the mobility behavior profiles for a fleet of EVs [85], which has been discussed in Chapter 3. All vehicles in the fleet are used for work trips. Each respective vehicle has a fixed commuter distance based on the mobility behavior statistics. Also the work shift, departure and return hours of each respective vehicle are fixed, as discussed

in Section 3.1.6. The time of departure and return (on a 1 min resolution) is variable with a uniform probability function in the fixed departure and return hours. Weekend and night shifts have been considered. Thus, a number of vehicles is parked at the work place during the night and weekend.

The specific power consumption of the EVs are 0.185, 0.220 and 0.293 kWh/km for small, middle-class and large vehicles, respectively.

### Charging rates

Different charging rates $P^{\mathrm{ch}}$ have been examined, which are typical for mode 3 charging as defined in IEC 61851-1 [73]. The EV charging rates are listed in Table 9.1. At home, single-phase charging (230 V) is assumed with a power rating of 3.3 kW (16 A), including a 10 % margin, to take into account the maximum allowed voltage deviations (EN 50160). At the work place, three different mode 3 charging rates have been assessed for both single-phase, i.e. 3.3 kW (16 A) and 6.6 kW (32 A), and three-phase connections, i.e. 19.8 kW (32 A), as indicated in Table 9.1. The minimum charging power, to avoid low converter efficiencies at partial load, is set to $P_{\mathrm{min}} = 1/10 P^{\mathrm{ch}}$

Table 9.1: EV charging rates for charging at home and the work place.

| Location | Connection | Maximum current | EV charging rate |
|---|---|---|---|
| Home | Single-phase | 16 A | 3.3 kW |
| Work | Single-phase | 16 A | 3.3 kW |
| | Single-phase | 32 A | 6.6 kW |
| | Three-phase | 32 A | 19.8 kW |

### EV supply equipment

The results in Section 9.4 discuss two different cases regarding the availability of the required EVSE:

- **Case 1:** The impact of a fixed number of EVs ($n^{\mathrm{EV}} \in \{25; 50; 75; 100\}$) is assessed.
- **Case 2:** The impact of a fixed number of EVSE ($n^{\mathrm{EVSE}} \in \{1; 2; 4; 6; 8; 10\}$) is assessed.

For **case 1**, it is assumed that enough charging spots are available at the work place at any time for all EVs to be charged when arriving at the work place (see Section 9.4.2).

In **case 2** (see Section 9.4.3), a fixed number ($n^{\text{EVSE}}$) of dedicated charging infrastructures (EVSE) is available. The EVs are charged (at maximum power $P^{\text{ch}}$) in order of arrival[6]. It is assumed that each vehicle can be plugged in at arrival. The sockets can be controlled by, e.g., the use of relays, in order to switch the charging between EVs. Thus, a maximum of $n^{\text{EVSE}}$ sockets[7] are delivering power simultaneously.

Other solutions are available in the literature, such as dividing the available power of an EVSE over different parking spots [271].

### 9.1.5 EV charging strategies

Different local EV charging strategies, both at home and at the work place, have been examined, based on the EV charging strategies discussed in Section 6.3.

#### EV charging strategies at home

Home charging is not the scope of this chapter. However, the amount of charging at home impacts the EV charging at the work place. Therefore, two home charging strategies have been considered:

- **Fully charging at home (H.1):** The EVs are fully charged at home.
- **Partly charging at home (H.2):** The EVs are sufficiently charged at home in order to arrive at the work place with a depleted battery. Depending on the commuter distance, EVs may not be fully charged at home.

For both EV charging strategies, the EVs start charging when arriving at home at maximum power ($P^{\text{ch}} = 3.3\,\text{kW}$), i.e. uncoordinated charging.

The second EV charging strategy (H.2) considers the benefits of the combination of the, in general, short commuter distances (see Section 9.2), the long standstill times at the work place and the decreased residential grid impact due to partly

[6] A *first come, first served* principle is used since the scope of this chapter is mainly to assess the grid impact. More sophisticated EV charging strategies may include the priority of EVs in the charging sequence.

[7] In other words, a maximum of $n^{\text{EVSE}}$ EVs charge simultaneously.

charging EVs at home. Besides, non-residential electricity consumers typically benefit from a reduced electricity cost tariff, which is relevant to the employer.

### EV charging strategies at the work place

In addition to home charging, EVs are charged at the work place. The following EV charging strategies at the work place have been assessed:

- **Uncoordinated charging (W.1):** EV charging starts after arrival at the work place at maximum charging power $P^{\text{ch}}$.
- **EV based peak shaving (W.2):** EV charging starts after arrival at the work place at a reduced charging power.
- **W.2 and local generation surplus charging (W.3):** EV charging starts after arrival at the work place at a reduced charging power. The surplus of locally produced electricity is equally divided over all grid-connected EVs in order not to give preference to one or more vehicles.

The combinations of charging strategies are depicted in Table 9.2. More details on the charging strategies can be found in Sections 6.3.1 and 6.3.2.

Table 9.2: EV charging strategies for charging at home and at the work place.

| **Charging** | **Work** | | | **Home** | |
|---|---|---|---|---|---|
| **strategy** | W.1 | W.2 | W.3 | H.1 | H.2 |
| 1a | x | | | x | |
| 2a | | x | | x | |
| 3a | | | x | x | |
| 1b | x | | | | x |
| 2b | | x | | | x |
| 3b | | | x | | x |

## 9.2 EV charging flexibility at the work place

If EVs are used for all trips, the majority of EV charging is expected at home[8]. However, charging at the work place is a second important charging location,

[8]The charging behavior at home will also depend on, e.g., if the electricity charged at home is paid by the employer or not, etc.

due to the long standstill times. Additional charging locations, such as charging at the work place, decrease the power consumption and peak power demand at home (see Chapter 5).

The results in this section are shown for the vehicle fleet used in this chapter. This vehicle fleet consists of 100 vehicles, which are all used for work trips besides the private trips.

### 9.2.1 Presence at the work place

As mentioned in Section 5.1.2, vehicles are parked at the work place mainly during daytime. The average vehicle presence at the work place is repeated in Fig. 9.2. As expected, there is a high correlation between the arrival and presence of EVs at the work place and the increase in the building power consumption[9] during daytime. It can also be observed that the EV presence at the work place is highly correlated with the period of possible PV power production. Therefore, there is a large possibility to integrate the EV charging at the work place with local renewable energy sources, such as PV systems.

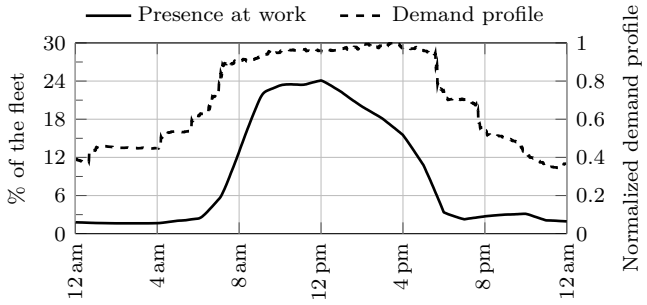


Figure 9.2: Average availability of a Flemish vehicle fleet at the work place, and the normalized average power consumption of the investigated office building during weekdays.

### 9.2.2 Commuter distance and electricity consumption

In Fig. 9.3 (a) the cumulative distribution function of the total commuter distance (to and from the work place) is shown for the fleet of 100 EVs used in this chapter. The average total commuter distance is 34.5 km. For the considered

[9]The building power consumption does not yet include the EV charging power demand.

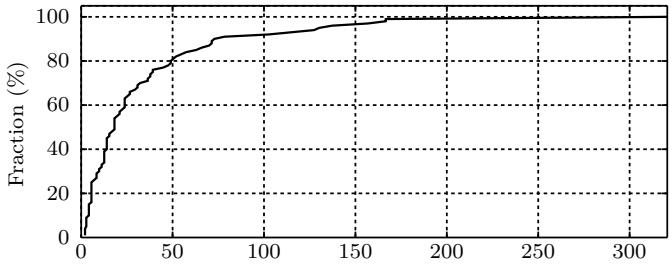


(a) Total commuter distance (km).

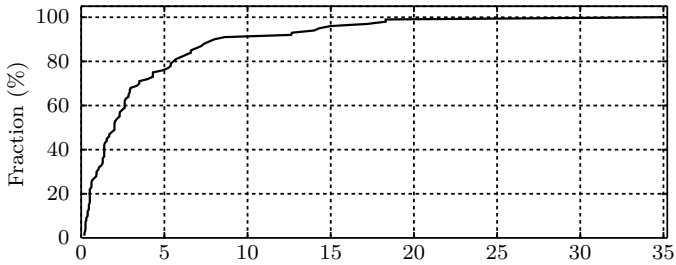


(b) Single way commuter charging energy (kWh).

Figure 9.3: Cumulative distribution function of (a) the total commuter distance and (b) the single way commuter charge energy.

fleet, about 80 % of the people live less than 25 km from work, which is a little lower than the statistics on mobility behavior [160].

Due to the low commuter distances, the EV charging energy demand is relatively low at the work place, if EVs are fully charged at home. Fig. 9.3 (b) shows the cumulative distribution function of the energy that has to be charged for the distance to the work place, which is around 3.7 kWh on average.

## 9.3 Results: reference scenario (no EVs)

This section first describes the results of the reference scenario without EVs. Thereafter, in Section 9.4, the results of the different local EV charging strategies will be discussed.

Fig. 9.4 shows the load duration curve of the aggregated building load profile, PV and CHP production profile without EVs. The demand and injection peak

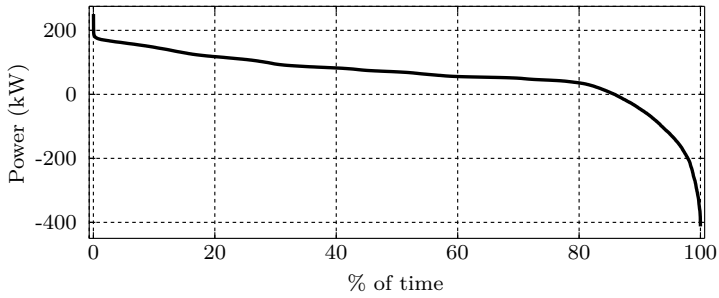


Figure 9.4: Load duration curve for the reference scenario without EVs.

power are 251 kW and 412.6 kW, respectively, while the demand and injection OPP are 179.6 kW and 371.2 kW, respectively.

There is a high simultaneity of the building load profile and the PV and CHP production during weekdays. As a result, the self-consumption of PV and CHP power is 70 %. However, the electricity consumption during the weekend is lower, which results in high grid injection peaks. During less than 15 % of the time (of the simulation period), there is a net-injection of a surplus of locally generated electricity.

## 9.4 Results

This section discusses the results of the different local EV charging strategies for different EV charging rates, EV penetration rates and number of charging spots for the considered period (January – May 2013).

### 9.4.1 EV electricity consumption at the work place

Table 9.3 shows the average EV energy use at the office building. When the charging rate increases, the relative energy use increases slightly.

When EVs are fully charged at home (strategy H.1), the electricity consumption at the work place amounts to about 21.5 % of the total electricity charged at home and the work place combined. If EVs are only partly charged at home (scenario H.2), the average electricity charged at the work place is more than doubled. This is advantageous regarding the grid impact at home, and the possible higher self-consumption at the work place.

Table 9.3: Average electricity demand of EVs at the office building as a function of the charging rate ($P^{\text{ch}} \in \{3.3; 6.6; 19.8\}$ kW) and the EV charging strategy at home.

| | **3.3** kW | **6.6** kW | **19.8** kW |
|---|---|---|---|
| **Strategy H.1** | 296.5 kWh | 308.1 kWh | 317.9 kWh |
| **Strategy H.2** | 725.9 kWh | 751.3 kWh | 767.1 kWh |

### 9.4.2 Case 1: Fixed number of EVs

In the first case, the different EV charging strategies have been assessed for different EV fleet sizes in terms of the grid impact, the self-consumption of locally generated electricity, and the UF of the fleet. It is assumed that enough charging spots are available at the work place for all EVs to be charged at any time.

#### EV charging simultaneity

Table 9.4 shows the EV charging simultaneity at the office building for a fleet of 100 EVs, namely:

- the maximum number of EVs charging simultaneously during the whole period;
- the average of the maximum number of EVs charging simultaneously during weekdays.

When EVs are uncoordinatedly charged at the work place (strategy W.1), a maximum of 25 % and 51 % of the EVs charge simultaneously when EVs are fully and partly charged at home, respectively. Partly charging the EVs at home (strategy H.2) increases the EV charging duration at the work place. Therefore, the EV charging simultaneity increases. For an increasing EV charging rate, the simultaneity decreases, due to a decreased EV charging duration.

In scenario W.2, EV based peak shaving is applied to charge the EVs at the work place. The EV charging duration increases, which also results in an increased EV charging simultaneity, up to 2.7 times. Note that the EV charging simultaneity is always less than 100 %. As discussed in Section 3.1.6, the probability for a vehicle to be used for a trip to work is only 65.8 % during weekdays.

Table 9.4: EV charging simultaneity (%), both the maximum for the whole period and the average of the maximum for weekdays, for the different EV charging strategies as a function of the charging rate ($P^{\text{ch}} \in \{3.3; 6.6; 19.8\}$ kW) for a fleet of 100 EVs.

| | Charging rate | Strategy H.1 max. | Strategy H.1 weekdays | Strategy H.2 max. | Strategy H.2 weekdays |
|---|---|---|---|---|---|
| **Strategy W.1** | 3.3 kW | 25 | 17.6 | 51 | 38.2 |
| | 6.6 kW | 20 | 12.3 | 38 | 26.0 |
| | 19.8 kW | 13 | 5.7 | 21 | 11.6 |
| **Strategy W.2** | 3.3 kW | 51 | 41.3 | 70 | 54.1 |
| | 6.6 kW | 46 | 35.8 | 70 | 52.2 |
| | 19.8 kW | 31 | 21.9 | 57 | 44.2 |
| **Strategy W.3** | 3.3 kW | 51 | 40.6 | 70 | 52.7 |
| | 6.6 kW | 46 | 35.5 | 70 | 50.9 |
| | 19.8 kW | 31 | 21.7 | 57 | 44.2 |

Charging the surplus of locally generated electricity has a small impact on the EV charging simultaneity. This simultaneity slightly decreases as a result of the charging duration reduction, as also discussed in Section 7.2.

### Grid impact

Fig. 9.5 shows the load duration curves for the different EV charging strategies, as listed in Table 9.2. A straightforward observation is the increasing grid impact for an increasing EV charging rate and number of EVs. On the other hand, the impact on the injection peak power and injection OPP is very limited. This is the result of the low building power consumption and the low presence of EVs at the work place during the weekend. Nevertheless, for an increasing number of EVs, the self-consumption will rise, which is shown by the increasing 5th percentiles. As more vehicles are charged at the work place, the simultaneity of the EV charging and the local electricity production will increase.

In the first scenario, the EVs are charged at maximum power, i.e. $P^{\text{ch}}$, when arriving at the work place. The peak demand power increases between 0 % to 42.5 % for scenario 1a depending on the EV charging rate and number of EVs. The increase of the OPP is between 1.5 % to 58.4 %. When the EVs are not fully charged at home (scenario 1b), the peak power demand and OPPs increase compared to scenario 1a due to the EV charging simultaneity increase,

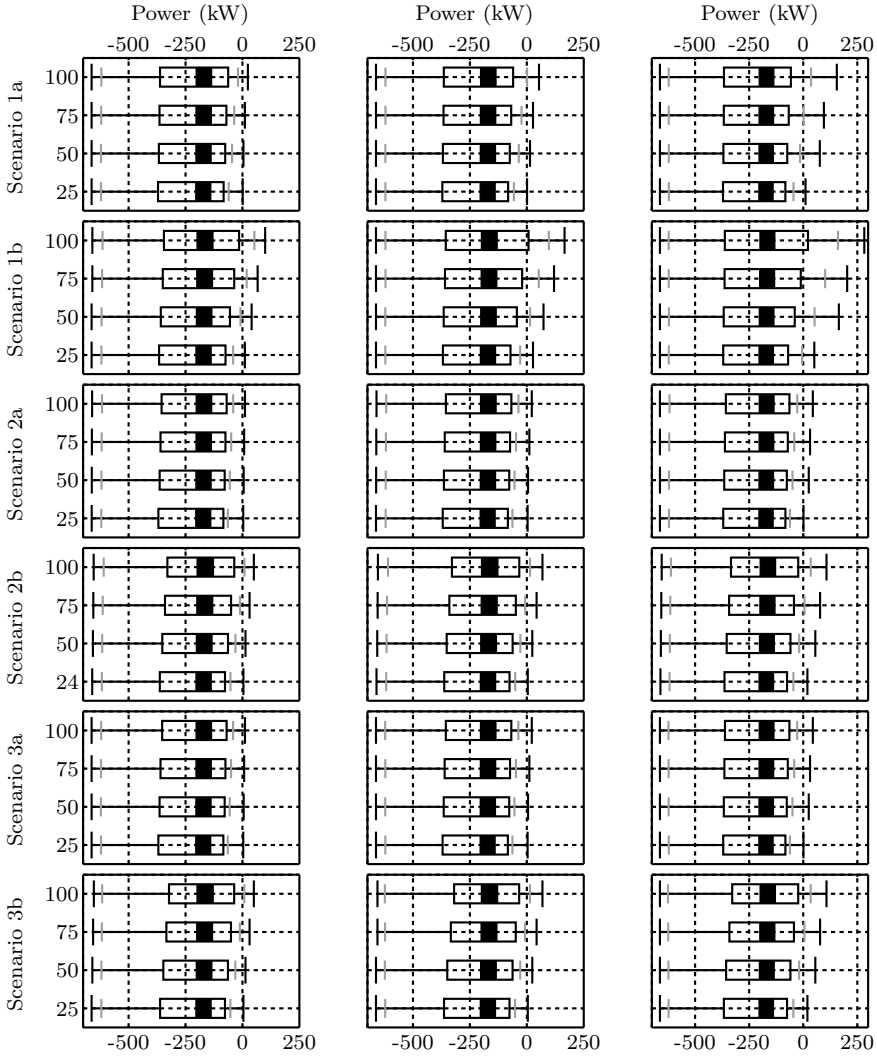


(a) 3.3 kW (b) 6.6 kW (c) 19.8 kW

Figure 9.5: Load duration curves (modified box plots) for the different EV charging strategies as a function of the charging rate ($P^{\mathrm{ch}} \in \{3.3; 6.6; 19.8\}$ kW) and number of EVs ($n^{\mathrm{EV}} \in \{25; 50; 75; 100\}$) in the fleet.

as shown in Table 9.4. The peak power demand increases up to two times the peak power demand in the reference scenario.

When EV based peak shaving is applied (scenario 2), the EVs will charge at a reduced power to maximally use the available standstill time at the work place. Due to the long standstill times at the work place and the low commuter distances, the average charging power is remarkably lower than $P^{\text{ch}}$ in scenario 1, as shown in Fig. 9.6. Since the DER surplus is charged in scenario 3, the average EV charging power increases compared to scenario 2. The maximum occurring EV charging power is remarkably higher compared to the average power, despite the on average long standstill times at the work place. The latter is due to EVs that are only standing still for a short time before leaving for a business trip. As a result of the decreased average charging power, the peak power demand and OPPs in scenario 2 are lower compared to the first scenario, up to 33 %. Besides, the simultaneity of the EV charging with the local electricity production increases due to the charging duration increase. Therefore, the injection peak powers decrease up to 2.1 % compared to the reference scenario.

In scenario 3, the EV based peak shaving can be overruled to charge the DER surplus by increasing the EV charging power at moments of DER surplus. As a result, the self-consumption increases, shown by the increasing 5th percentile. Besides, the increased average EV charging power results in a decreased EV charging duration. This may lower the simultaneity of the EV charging process with any high production peaks at future time steps, compared to scenario 2. In this case study, the injection peak powers are higher compared to the second scenario.

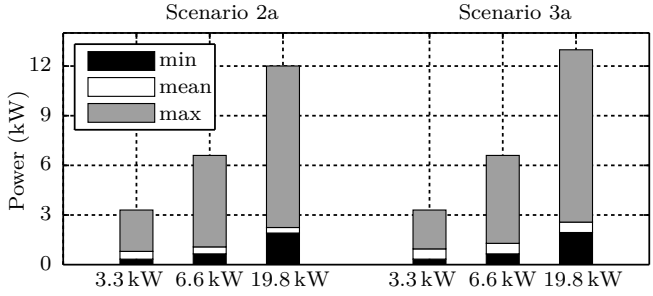


Figure 9.6: Average EV charging power as a function of the charging rate ($P^{\text{ch}} \in \{3.3; 6.6; 19.8\}$ kW) for a fleet of 100 EVs.

### Self-consumption

The self-consumption of the local PV and CHP electricity production is 70 % in the reference scenario (without any EVs). Fig. 9.7 shows the self-consumption for the different EV charging strategies, as listed in Table 9.2.

EV charging at an office building has a higher simultaneity with the local DER electricity production, compared to home charging. Therefore, the impact on the self-consumption at an office building will be higher. When the EVs are partly charged at home (EV charging strategy H.2), the self-consumption increases even more due to the longer charging time at the work place. For a fixed EV penetration rate, the self-consumption decreases for higher EV charging rates. A shorter EV charging time results in a lower simultaneity with DER production.

When the EVs are charged at a lower power (EV based peak shaving), the self-consumption increases compared to the first scenario. Spreading the charging during the day at the work place increases the simultaneity between the EV

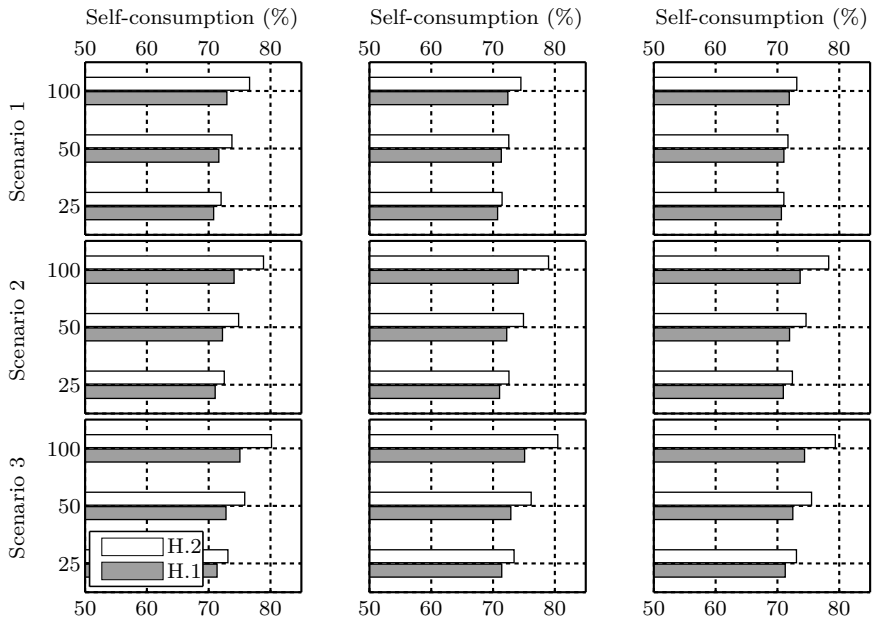


(a) 2.1 kW (b) 3.3 kW (c) 6.6 kW

Figure 9.7: Self-consumption (%) for the different EV charging strategies as a function of the charging rate ($P^{\mathrm{ch}} \in \{3.3; 6.6; 19.8\}$ kW) and number of EVs ($n^{\mathrm{EV}} \in \{25; 50; 100\}$).

charging and the local electricity production. Due to the long standstill times, the differences between the different EV charging rates is limited. However, charging at a higher charging rate increases the minimum charging power. Therefore, the self-consumption might decrease because of a lower simultaneity with the local generation.

In the third scenario, individual peak shaving is applied, but it can be overruled to charge the surplus of local electricity production. Therefore, this results in the highest self-consumptions, up to almost 7 percentage point (pp) compared to scenario 1 and up to about 10 pp compared to the reference scenario. Although, the difference with scenario 2 is limited.

### 9.4.3 Case 2: Fixed number of EVSEs

In the second case, a fixed number of EVSEs is assumed for a fleet of 100 EVs. It is assumed that EVs can plug in at arrival and charge at maximum power $P^{\text{ch}}$ in order of arrival (see Section 9.1.4). Each vehicle can be plugged in at arrival. Therefore, there are, for instance, a number $n^{\text{EVSE}}$ of dedicated charging infrastructures, which can control the different sockets by, e.g., the use of relays, in order that a maximum of $n^{\text{EVSE}}$ sockets are delivering power to the EVs. Note that it is assumed that the EVSE can switch charging between EVs, thus it is not required for EV drivers to move their EV after a full charge or before starting the charging process.

#### Amount of EVs charged

The average number of EVs used for work trips on weekdays is 65.8 %, as discussed earlier in Section 3.1.6. Therefore, not all EVs in the fleet are parked and charged at the office each day. Thus, each day, a different set of EVs is parked and charged at the office building. From these EVs, Table 9.5 (A) shows the average amount of EVs, that is charged at least for one minute a day at the work place. Moreover, not all EVs will be fully charged due to the limited number of EVSEs available, as indicated in Table 9.5 (B). The incomplete charging of EVs may be due to:

- an insufficient EV charging rate;
- EVs leaving from the work place before they are fully charged;
- EVs arriving late, which start charging too late as a result of the charging order.

Table 9.5: (A) Average amount of EVs (%) charged at the office building, and (B) fraction (%) fully charged EVs of EVs being charged, as a function of the charging rate ($P^{\text{ch}} \in \{3.3; 6.6; 19.8\}$ kW) and number of EVSEs ($n^{\text{EVSE}} \in \{1; 6; 10\}$).

| | **Charging rate** | **Strategy H.1** 1 | 6 | 10 | **Strategy H.2** 1 | 6 | 10 |
|---|---|---|---|---|---|---|---|
| | 3.3 kW | 34.0 | 87.7 | 93.8 | 13.8 | 58.2 | 77.9 |
| **(A)** | 6.6 kW | 51.4 | 94.2 | 95.3 | 19.9 | 77.9 | 90.6 |
| | 19.8 kW | 82.7 | 95.4 | 95.4 | 43.9 | 94.5 | 95.3 |
| | 3.3 kW | 84.2 | 85.5 | 92.7 | 50.7 | 50.2 | 51.5 |
| **(B)** | 6.6 kW | 86.2 | 96.3 | 96.3 | 69.1 | 72.1 | 89.3 |
| | 19.8 kW | 95.6 | 98.8 | 98.8 | 83.9 | 97.6 | 98.0 |

For instance, for an EV charging rate of 3.3 kW and one EVSE, on average only 34 % of the vehicles parked at the office building is charged at least for one minute a day. Only 84.2 % of these EVs is fully charged.

An increasing EV charging rate allows to (fully) charge more EVs for a fixed number of EVSEs, due to the shorter EV charging duration. However, this impact becomes less for a higher number of EVSEs. Besides, an increase in number of EVSEs results in more EVs being charged. The results in Table 9.5 show that a limited number of EVSEs already allow to fully charge a high number of EVs. Charging an EV partly at home limits the number of EVs that can be (fully) charged at the work place. To attain similar results as when EVs are fully charged at home, more EVSEs and a higher EV charging rate are required. Therefore, it is required to outweigh the extra infrastructure costs at the work place compared to the extra charging cost at home.

### Grid impact

Fig. 9.8 shows the load duration curves at the office building for fully (scenario A) and partly charging at home (scenario B). Since the number of EVSEs is lower than the number of EVs to be charged, the charging of the different EVs is spread over time. Therefore, the impact on the load profiles is lower compared to case 1, up to 28 % for 10 EVSEs. However, similar conclusions on the impact trends can be taken for the grid impact as in case 1 in Section 9.4.2.

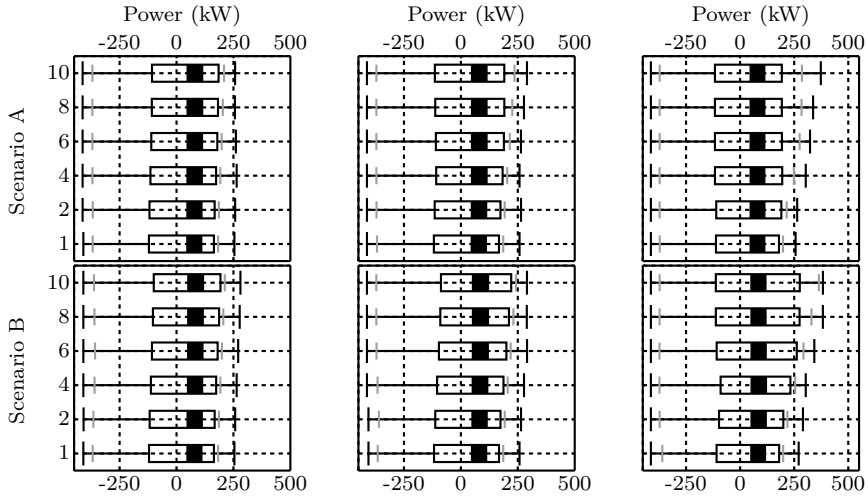


(a) 3.3 kW (b) 6.6 kW (c) 19.8 kW

Figure 9.8: Load duration curves (modified box plots) for (A) fully and (B) partly home charging as a function of the charging rate ($P^{\mathrm{ch}} \in \{3.3; 6.6; 19.8\}$ kW) and number of EVSEs ($n^{\mathrm{EVSE}} \in \{1; 2; 4; 6; 8; 10\}$).

## Self-consumption

Fig. 9.9 shows the impact on the self-consumptions. Due to a limited number of EVSE, the EV charging load is spread over the day. Therefore, the simultaneity with local electricity production increases. An increase in self-consumption of up to 7.5 percentage points compared to the reference scenario is possible. Similarly, the self-consumption increases when the EVs are partly charged at home (scenario H.2), due to the charging duration increase at the work place. However, increasing the EV charging rate does not always lead to a higher self-consumption since the charging duration will shorten. This results in a lower simultaneity with any local generation afterwards.

In Section 9.4.2 (case 1), the self-consumption increases for an increasing number of EVs charged at the office building. However, for a fixed number of EVs and EV charging rate, there is an optimal number of EVSEs to maximize the self-consumption, as shown in Fig. 9.9. Increasing the number of EVSEs lead to a higher self-consumption since more EVs are charged throughout the day. For a certain number of EVSEs, all EVs are charged (or partly charged before leaving the work place) and further increasing this number will decrease the self-consumption since the simultaneity with the DER production decreases.


(a) 2.1 kW (b) 3.3 kW (c) 6.6 kW

Figure 9.9: Self-consumption (%) for the different EV charging strategies at home as a function of the charge rate ($P^{\mathrm{ch}} \in \{3.3; 6.6; 19.8\}$ kW) and number of EVSEs ($n^{\mathrm{EVSE}} \in \{1; 6; 10\}$).

## 9.5 Conclusions

This chapter discusses the EV charging in an existing office building, equipped with a PV system and a CHP unit. Complementing the home with charging at the work place increases the electric range. Additionally, it decreases the electricity consumption and grid impact at home, which can benefit both the EV owner and grid operator. If EVs are fully charged at home, 20 % of the total electricity charged is charged at the work place. If they are only partly charged at home, this is nearly 50 %. Although, to overcome range-anxiety, people might be tended to foresee an extra margin at home.

The grid impact can be significantly reduced by using local charging strategies that rely on limited future knowledge of the EV mobility behavior and limited or no communication infrastructure within the building. These strategies allow a high number of EVs to be charged at an office building with a lower grid impact and an increased DER self-consumption.

EV based peak shaving reduces the average charging power significantly, due to the, on average, long standstill times at the work place. It can be implemented on the EV on-board battery management system or in a mode 3 EVSE and requires no communication within the building. However, the knowledge of the next departure time at work is required. An incentive for the EV driver, to indicate his/her departure time, is required when it is done on-board. For a mode 3 EVSE, the typical working hours can be estimated, or EV drivers need an incentive to specify the time of departure. In general, it can be expected that the departure moment at work is well-known in advance, which makes this a realistic EV charging strategy.

Due to the low power consumption and low EV availability at the work place in

the weekend, the impact on the grid injection peak is limited, requiring other solutions. On the other hand, the self-consumption increases when the charging strategy also charges a DER surplus, but the impact is limited. Therefore, the cost-benefits of this implementation have to be considered. Besides, the DER surplus charging strategy in this dissertation may decrease the simultaneity of EV charging with the injection peaks. Thus, there is no guarantee that it decreases the injection peaks. Furthermore, local storage may be considered for microgrids to further increase the self-consumption and further decrease the grid impact, but this is not considered here. However, the impact of local storage depends on the charging and discharging strategy and the storage sizing.

For a limited number of EVSEs ($n^{\mathrm{EVSE}}$) at the office building, a high number of EVs can be fully charged if they are charged at maximum power in order of arrival at work. It is assumed that all EVs can plug in at arrival and the EVSEs (or a central system) can control the different sockets such that a maximum of $n^{\mathrm{EVSE}}$ sockets can deliver power simultaneously. A limited number of EVs charging, spreads the EV charging. This limits the grid impact and increases the DER simultaneity. Thus, the cost difference for the infrastructure should be assessed regarding the needs to fully charge all vehicles at work. Here, the EVs charge in an uncoordinated manner in order of arrival until they are fully charged or until they have to leave. Future work may focus on a more optimal charging strategy for this case in order to take into account:

- the user comfort and user requirements to define how much electricity has to be charged and in which sequence;
- the objective of a minimal infrastructure cost, e.g., a minimum number of EVSEs;

# Chapter 10

# Conclusions and future work

This chapter summarizes the main conclusions and contributions of this research work. Suggestions for future work have also been discussed.

## 10.1 Summary and conclusions

This dissertation focuses on the integration of EV charging in large buildings, i.e. residential apartment and office buildings, with different energy systems, such as PV systems, and a heat pump and CHP in the apartment and office building, respectively. The dissertation has been split into two parts:

- Modeling
  - Mobility behavior simulation tool;
  - Electrical sublibrary for IDEAS[1], regarding energy system integration.
- EV charging case studies
  - Apartment building, including DC grids;
  - Office building.

The grid impact of EV charging in buildings or in low-voltage distribution grids is non-negligible: grid congestion (peak power demand/injection), voltage deviations and voltage unbalance. For weak electricity grids or high EV

[1] Integrated District Energy Assessment by Simulation.

penetration rates, grid cables may be overloaded or the EN 50160 regulations might be violated regarding the allowed voltage deviations or voltage unbalance. In order to reduce this grid impact and to allow more EVs to be charged through the power system, it has been widely accepted that EV charging coordination can be beneficial. Mobility behavior requirements, as they are today, allow to coordinate the charging process, as a certain flexibility in time and power is available. As local clustering of EVs in buildings and LV distribution grids will occur before a wide-spread roll-out of EVs, first local EV charging solutions are required to reduce the grid impact locally.

This dissertation assesses two local solutions to allow a higher penetration rate of EVs charging in buildings:

- Local EV charging strategies, which require minimal prior knowledge of the EV mobility behavior, no local information (grid topology), no prediction on the local load and generation power profiles, and minimal or no communication within the building. These strategies can also be easily scaled up to the district level [28, 128, 201].
- Using DC grids to interconnect large loads in buildings, i.e. the PV system, EVs and heat pump in an apartment building.

The following tools have been developed for this dissertation:

- An EV driving mobility simulation tool to create unique driving mobility profiles in order to assess the charging requirements and impact.
- An electrical Modelica sublibrary for IDEAS, which allows multi-disciplinary energy system integration, i.e. the modeling of electricity grids, electrical storage and electric vehicles.

Chapter 3 describes a detailed mobility behavior simulation tool taking the stochastic variations of individual users into account. This simulation tool creates unique driving patterns for a Flemish EV fleet. It describes when an EV is driving and where it is parked. Hence, the complete driving and activity schedule for each vehicle in the fleet is known. These results have been used in this dissertation to assess the EV charging flexibility, the mobility behavior and the specific electricity use (kWh/km) while driving. The simulation tool uses the statistical data from a Flemish mobility study. The simulation tool has been extensively used at the KU Leuven and partner institutions for different use cases.

In Chapter 4, a description has been given on the electrical modelling for buildings and districts in Modelica. This electrical sublibrary is (or will be) part

of the IDEAS library, developed at the KU Leuven. IDEAS is originated from the requirements for energy system integration simulations. The library allows the simultaneous modeling and simulation of multidisciplinary energy systems at both building and district level in one simulation model. The following models have been described: radial AC and DC electricity distribution grids, both in-buildings and LV distribution grids, battery storage systems and electric vehicles.

### 10.1.1 EV charging coordination

The EV charging process can be coordinated in time and power as a result of the present mobility behavior. The EV charging flexibility is limited by the mobility objective, the available charging power rates, battery state of charge and battery limitations. Coordination mechanisms can use this flexibility for different objective functions.

Chapter 5 and Section 9.2 discuss the EV charging requirements and flexibility at home and at the work place, respectively. On average, the daily distance driven is about 40 km. The average total commuter distance (by car) is around 34.5 km. Therefore, the average electricity consumption per vehicle per day is low compared to the standstill time at both locations. For instance, on average, vehicles are standing still for about 15 h a day at home. Therefore, for most EV charging opportunities, i.e. between arrival and the next departure, there is a high flexibility to shift the charging in time or to lower the charging power.

The vast majority of the EV charging will occur at home. Nevertheless, Chapter 5 concludes that additional charging, e.g., at the work place, may be beneficial for the residential EV charging grid impact. For instance, charging at work will decrease the electricity consumption at home and the peak power demand may be reduced. Besides, the electric range may increase if the battery size is small compared to the driven distances. However, it is important to note that EVs should also be charged in a grid-friendly manner at these other locations, as shown for work charging in Chapter 9.

To conclude, Chapter 5 defines the residential EV charging power requirements. Only during a few charging opportunities, a charging power higher than 6.6 kW (single-phase, 32 A) is required. Therefore, to minimize the grid impact, it is advisable to foresee a combination of EV charging infrastructure with different charging rates at a location where multiple EVs are charged. This allows the driver to choose a suitable charging rate upon arrival. For instance, a capacity payment (€/kW) can be chosen to incentivize the user to choose an optimal charging rate as a function of his mobility requirements.

The literature mainly focuses on optimization strategies for EV charging in buildings and LV distribution grids. However, these coordination mechanism in general require the future knowledge of the mobility behavior, a prediction of the future building load and power generation, local information on the grid topology, and/or communication between the vehicle, building, distribution grid and/or higher level scheduler. Therefore, this dissertation focuses on EV charging strategies, which require minimal future knowledge of the mobility behavior (only the next departure time, current battery SoC and/or commuter distance), no knowledge on local information (e.g., grid toplogy), no future knowledge of the building load profile or power generation, and minimal or no communication within the building. No communication outside the building is required. These local strategies can still be used as emergency strategies (robust fallback mechanisms) or as strategies to deviate from the charging power set-point (from a higher level scheduler) in case grid constraints are violated.

Chapter 2 gives an overview of the standardization efforts for EV charging infrastructure and the possibilities for (local) EV charging coordination. A control pilot signal is used for mode 2 and mode 3 charging to set the maximum charging current. It allows to adapt the charging current by making use of a PWM control pilot signal. Vehicles have to react in less than 5 s to a change in charging power. In this dissertation, an instantaneous (ideal) change is assumed, as a simulation time step of 1 min is in place. The charger within the vehicle limits the current as a function of the charging limitations of the EV.

Local EV charging strategies, as discussed in this dissertation, have not been widely discussed yet in the literature for EV charging in buildings or LV distribution grids. Only local information within the building is used to control the EV charging:

- Mobility requirements, i.e. next departure time and commuter distance. In general, a good estimation is possible, except for unplanned/emergency trips. An alternative to the next departure time is setting a time by which the EV has to be charged up to a certain level. Interaction with the EV user is required.
- Battery SoC is known within the vehicle.
- The voltage measurement at the EV connection point is measured within the charging infrastructure or vehicle.
- Mode 3 charging also checks if an EV is ready to charge.
- The building load profile and local generation surplus can be easily measured in the building.

Chapter 6 describes the following local EV charging strategies:

- Based on the required charging energy and next departure time, the EV charging power can be reduced to maximally use the available charging time (**EV based peak shaving**), or the EV charging can be delayed (**delayed charging**).
- Correction of local grid constraints through grid stabilizing EV charging, i.e. voltage dependent EV charging (**voltage droop mechanism**).
- **Renewable self-consumption**, by measuring the local electricity demand and production.
- **Building peak shaving** by reducing the EV charging power, by measuring the local electricity demand and production.

Uncoordinated charging, EV based peak shaving and delayed charging set a charging power set-point. In case of grid code violations (voltage droop and building peak shaving mechanism) or local generation surplus, these strategies can deviate from the charging power set-point. However, this might be a threat for the user comfort, as less electricity may be charged.

Chapter 7 discusses the impact of different local EV charging strategies for a residential apartment building by means of a case study. Besides, a comparison with the *optimal capacity charging* is performed, which optimizes the charging profile as a function of the total building load and expected voltage deviations. All EV charging strategies succeed in reducing the grid impact, compared to uncoordinated charging: reductions of peak powers (demand and/or injection), voltage deviations and/or voltage unbalance. Despite, every adaptation to the charging profile (uncoordinated charging) may prolong or postpone the charging process, which may negatively impact the user comfort. Nevertheless, the results show that these local EV charging strategies, which do not require any optimizations and any communication outside the building, already allow to increase the EV penetration rate largely in buildings.

EV based peak shaving and delayed charging require a change in user behavior, as these charging strategies require the knowledge of the departure time for the following trip. An alternative is to set a time (e.g., including a safety time margin) by which the EV has to be charged up to a certain percentage. As these strategies require interaction with the EV user, certain incentives are required to move people to lower the charging power or to postpone the charging process. It may be expected that EV based peak shaving is the more favourable strategy of both, as it still offers some flexibility to adapt the charging power in case an unplanned trip pops up without impacting the electric range, depending on the available charging power rating of the EV charging infrastructure.

Furthermore, other strategies have been discussed which alter, i.e. reduce, the charging power as a function of grid variables, i.e. the voltage magnitude,

grid or cable capacities, and local generation surplus. All strategies succeed in their objective, i.e. increasing the self-consumption of locally generated electricity, reducing the voltage deviations (voltage droop mechanism) and reducing the peak power demand to the available capacity (building peak shaving), respectively. As is the case for PV systems in, e.g., Germany (frequency droop mechanism and reactive power support [239]), grid regulations may require a voltage droop mechanism for EVs (or other loads). The results show that maximizing the local self-consumption does not always result in reducing the injection peaks. Therefore, other predictive controllers might still be required. Similar solutions to the building peak shaving mechanism were recently introduced to the market, which may be needed if the building capacity is limited. However, the latter two mechanism require some in-building communication.

Chapter 9 assesses the integration of EV charging in an existing office building. As commuter distances are in general relatively short, only a small amount of electricity is charged at the work place, i.e. around 20 % if the EVs are fully charged at home. Therefore EV based peak shaving is an effective charging strategy to reduce the grid impact of EV charging at an office building, especially since the departure time at work is in general well-known. Besides, charging at the work place assures a higher simultaneity of EV charging with local generation by, e.g., a PV system.

With a limited number of EVSEs ($n^{\mathrm{EVSE}}$) at the office building, a high number of EVs can already be fully charged if they are charged at maximum power in order of arrival at work. It is assumed that a central system, e.g., by means of relays, is present to control different sockets, such that a maximum of $n^{\mathrm{EVSE}}$ sockets can deliver power simultaneously. This results in a EV charging load spreading, limiting the grid impact and increasing the local generation simultaneity. A more sophisticated system to define the charging order may be required taking into account the individual charging needs, or the available charging capacity may be divided over all EVs which need to be charged.

### 10.1.2 DC grids

Chapter 8 introduces a hybrid AC-DC grid topology in the case study of the apartment building. The DC grid is used to interconnect the PV system, the heat pump and the EVs. This chapter investigates whether the use of DC grids, to interconnect these large loads, is beneficial regarding the grid impact of EV charging.

As EVs are mainly charged through a single-phase connection to the grid in residential buildings, the main advantage of using DC grids is the balancing

of the AC in-building grid. Both the voltage unbalance and the minimum occurring voltages are positively impacted. Therefore, DC grids allow more EVs to be charged in the building before the EN 50160 regulations regarding the voltage unbalance and deviations are violated.

The impact of using DC grids regarding the peak power demand and energy exchange with the LV distribution grid is small compared to the impact of the different EV charging strategies. This is due to the low share of grid losses in the total electricity demand. These losses also depend on the grid design and the converter efficiencies, which is however not in the scope of this dissertation. However, the use of DC grids (compared to AC grids) looks promising when the simultaneity of EV charging (or other loads) with the local generation increases, especially regarding the energy exchanged with the LV distribution grid.

To conclude, the results show that DC grids are primarily an interesting solution when the voltage unbalance or voltage deviations are too large. To decrease the energy exchange of the building with the distribution grid, the coordination strategies which anticipate on the local generation surplus are beneficial compared to using equal coordination strategies in AC grids. To decrease demand and/or injection peaks, other EV charging strategies or storage solutions might be required in combination with the DC grids.

## 10.2 Future work

Suggestions for further extensions or improvements to the mobility behavior simulation tool have already been given in Section 3.1.8. Regarding the charging profile, a constant power profile is assumed. Real charging profiles and end-of-charge profiles can be used, which depend on the chosen vehicle and may vary for slow and fast charging [64].

In this dissertation, only the EV charging has been coordinated to reduce the LV distribution grid impact of buildings. However, the operation of more energy systems can be coordinated, such as heat pumps [19], CHP units [21] or household appliances [210]. In order to obtain a better system design and to take the multidisciplinary interactions into account, the coordination of different technologies should be combined in future work, in combination with any storage solutions (electrical and/or thermal). Moreover, if multiple local generation options are available (e.g., a PV system and a CHP unit), one can optimize the sizing of these different generation units, e.g., as a function of the complementarity (intra-day or seasonal). This dissertation focuses on the EV integration in buildings, but the same strategies can also be investigated at, and in combination with the LV distribution grid level for EV charging, or for

other appliances which offer flexibility. Also, this dissertation only focuses on home and work charging. Future work should also include the combination with additional fast charging opportunities and charging at other locations.

Regarding the local EV charging strategies discussed in this dissertation, future work should focus on the implementation of these strategies inside the vehicle, charging infrastructure, and building energy management systems. Whereas a 1 min simulation time step is used in this dissertation, EVs will not react instantaneous, due to a delay between measurements and the adaptation of the charging power, and due to the fact that EVs are only required to react within 5 s to a current change for mode 3 charging infrastructure. The proposed strategies do not guarantee an improved simultaneity yet with local electricity production. To reduce injection power peaks, it may be required to have some kind of predictive controller, e.g., model predictive control (MPC). Besides, in particular, EVs are very complementary to fast varying production profiles, e.g., charging power variations as a function of fast varying PV production profiles.

Variations to the proposed EV charging strategies are possible in order to make them more user-acceptable, such as:

- Varying start time of the night-tariff period for EV charging load spreading;
- Build in a margin for EV based peak shaving and delayed charging, in case of unplanned trips (e.g., fully charge an EV by a specific time);
- A voltage droop mechanism inherently discriminates the EV users at the end of a feeder, as voltage deviations are larger;
- Reactive power grid support, e.g., for voltage support;
- A more sophisticated charging system to define the charging order if a limited number of EVSE is available (taking into account the individual charging needs), or the available charging capacity may be divided over all EVs which need to be charged.

In this dissertation, the impact of the different EV charging strategies has been discussed for two case studies. For the residential apartment building case, the in-building distribution grid has been considered. However, this work does not focus on the optimal grid design for the in-building network, nor for the AC and DC cases. The combination with a detailed study on the converter efficiencies allows to discuss the possible efficiency gains in more detail. As the results for the DC case show clear benefits regarding the voltage deviations and voltage unbalance in the AC LV distribution and in-building grid, future research should also focus on possible reactive power grid support by the central bidirectional AC-DC converter, and inter-phase active power exchange for an increased power balancing. As the interest in (DC) microgrids increases in the literature, the possibilities for storage solutions should be included.

# Appendices

# Appendix A

# EV mobility behavior modeling

## A.1 Choice of representative vehicles

Three vehicle types $s$ have been used to differentiate the fleet vehicles in segments. It is assumed that the three vehicle types coincide with the engine displacement categories, with:

$$s \in \mathcal{S} = \{\text{small}, \text{middle-class}, \text{large}\} \text{ vehicles.} \tag{A.1}$$

For each type, two representative vehicles have been taken:

- **Small vehicle:** Mitsubishi i-MiEV [51] and Smart Electric Drive [272];
- **Middle-class vehicle:** Nissan Leaf [52] and Chevrolet Volt [43];
- **Large vehicle:** Toyota RAV4 EV [273] and eRUF Cayenne [274].

The characteristics (mass $m$, frontal surface $S$ and drag coefficient $C_x$) of these vehicles have been listed in Table A.1 and come from specification sheets.

Table A.1: Characteristics of the considered vehicles.

| | $m$ (kg) | $S$ (m$^2$) | $C_x$ $(-)$ |
|---|---|---|---|
| Mitsubishi i-MiEV | 1100 | 2.37 | 0.33 |
| Smart Electric Drive | 975 | 2.40 | 0.35 |
| Nissan Leaf | 1521 | 2.70 | 0.28 |
| Chevrolet Volt | 1800 | 2.55 | 0.28 |
| Toyota RAV4 EV | 2000 | 3.10 | 0.33 |
| eRUF Cayenne | 2670 | 3.30 | 0.36 |

## A.2 Specific electricity consumption calculation

### A.2.1 Vehicle propulsion power

The required propulsion power $P_{\text{pr}}$ at each 1 s time step is calculated from the resulting forces acting on the vehicle, namely the air $F_a$, rolling $F_r$, inertia $F_i$ and slope resistance $F_s$ (N). The calculation of these forces at time step $k$ is shown in Eqns. (A.2) – (A.6).

$$F_{a,k} = \frac{SC_x\rho v_k^2}{2}, \tag{A.2}$$

$$F_{r,k} = mgf_r\cos(\alpha_{\text{road},k}), \tag{A.3}$$

$$F_{i,k} = ma_k, \tag{A.4}$$

$$F_{s,k} = mg\sin(\alpha_{\text{road},k}), \tag{A.5}$$

$$P_{\text{pr},k} = (F_{a,k} + F_{r,k} + F_{i,k} + F_{s,k})v_k, \tag{A.6}$$

with $\rho$ the volumetric density of the air (kg/m$^3$), $f_r$ the rolling resistance coefficient $(-)$, $v$ and $a$ respectively the vehicle speed (m/s) and acceleration (m/s$^2$), $g$ the gravity constant (9.81 m/s$^2$) and $\alpha_{\text{road}}$ the angle of the road (*rad*).

$P_{\text{pr}}$ can be either positive or negative, whether the batteries are discharged to propel the vehicle ($P^d$) or charged ($P^c$). A battery has a maximum charging power ($P^c_{\text{max}}$). The fraction of regenerative braking ($e_{\text{rec}}$) is limited, since a part of braking occurs mechanically (see Section A.2.5).

### A.2.2 State of charge calculation

The charging ($\eta^c$) and discharging efficiency ($\eta^d$) have been split in (i) the charging ($\eta^c_{\text{pe}}$) and discharging ($\eta^d_{\text{pe}}$) efficiencies of the power electronics and (ii) the energy storage charging ($\eta^c_{\text{bat}}$) and discharging ($\eta^d_{\text{bat}}$) efficiencies. $\eta_{\text{em}}$ is the electric motor efficiency. The electric motor acts as a generator (GEN) during regenerative braking.

Using these parameters, the charging and discharging power flow of the battery at time step $k$ can be calculated:

$$P^d_k = \frac{P_{\text{pr},k}}{\eta_{\text{em}}}, \tag{A.7}$$

$$P^c_k = \min(e_{\text{rec}}|P_{\text{pr},k}|\eta_{\text{em}}, P^c_{max}), \qquad \text{if} \qquad P_{\text{pr},k} < 0. \tag{A.8}$$

The state of charge (SoC) at time step $k$ is calculated as follows:

$$SoC_k = SoC_{k-1} - \delta^{\text{sd}}_k + (\eta^c P^c_k T_s - 1/\eta^d P^d_k T_s)/E_{\text{nom}}, \tag{A.9}$$

with $\delta^{\text{sd}}$ the battery self-discharge, $T_s$ the time step, and $E_{\text{nom}}$ the nominal battery capacity.

### A.2.3 Specific electricity consumption

The specific energy use $E_{\text{spec}}$ (kWh/km) is calculated as follows:

$$E_{\text{spec}} = \frac{\Delta E_{\text{cycle}}}{d_{\text{cycle}}\eta^c}, \tag{A.10}$$

with $\Delta E_{\text{cycle}}$ the consumed energy (kWh) during the driven cycle (see Appendix A.2.4) and the cycle distance $d_{\text{cycle}}$ (km). The electrical driving range of the vehicle $d_{\text{range}}$ is equal to $E_{\text{eff}}/E_{\text{spec}}$.

### A.2.4 Representative driving cycles

A representative drive cycle is composed of the following American test cycles. The American cycles (see Fig. A.1) are preferred instead of the artificial European cycles for emission testing, since the American cycles have been based on real traffic behavior [216]:

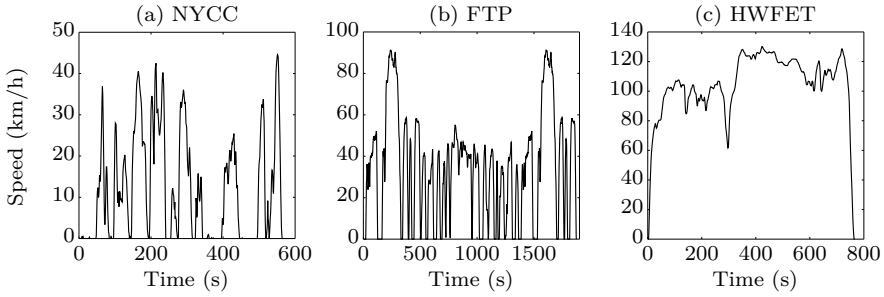


Figure A.1: The US driving cycles: (a) urban cycle, (b) rural cycle and (c) highway cycle.

- **Urban:** New York City Cycle (NYCC) represents a dense urban area with low average speed (11.42 km/h) and lots of stop-and-go traffic.
- **Rural:** Federal Test Procedure (FTP) represents extra-urban traffic with a significant share of high-speed driving (average speed of 34.11 km/h).
- **Highway:** Highway Fuel Economy Driving Schedule (HWFET)[1] represents highway driving with no stops (average speed of 104.94 km/h).

Two options are available to create a combined cycle from these three separate drive cycles. A first option is to make a composition, in which the three cycles occupy the same amount of time. This choice is similar to the approach used to set up the European Transient Cycle (ETC) [275]. However, this distribution is not representative for Flanders.

A more representative combination of the three cycles, is to make use of transport measurements in Flanders. The distribution of driven kilometers for each cycle type is known: urban (23.72 %), rural (39.82 %) and highway (36.46 %) traffic [204]. The ETC drive cycle composition has a 15 % higher specific energy use compared to the Flemish combined cycle [85].

### A.2.5 Results

For the calculation of the specific energy use, fixed parameters have been used for the auxiliary power consumption in vehicles ($P_{\text{aux}}$), the slope of the road, $e_{\text{rec}}$, $\eta_{\text{em}}$ and $f_r$. The parameters are shown in Table A.2 and discussed in the next paragraphs.

The vehicle rolling resistance depends on the rolling resistance factor $f_r$. This coefficient is not readily available in vehicle specification sheets, since it depends

[1] A scale factor of 1.35 has been taken into account to adjust for European highway speeds.

Table A.2: Parameters for the specific electricity consumption calculations.

| | | | | | |
|---|---|---|---|---|---|
| $P_{\text{aux}}$ | 500 W | $e_{\text{rec}}$ | 90 % | $f_r$ | 0.01 |
| $\alpha_{\text{road}}$ | no slope | $\eta_{\text{em}}$ | 90 % | | |

on the tire choice. In [276], measurement results on the rolling resistance have been shown. Here, an $f_r$ of 0.01 for modern tires with low resistance is considered.

$e_{\text{rec}}$ defines the amount of kinetic energy that can be recuperated during regenerative braking. Efficiencies of the generator, batteries and power electronics have not been included. No specific data on $e_{\text{rec}}$ is available in the literature. According to [277], the overall recovery rate is 50 – 60 %. With a value of 90 % for $e_{\text{rec}}$ an average overall recovery rate is found in this range due to the other losses in the system.

The efficiency of the electric motor ($\eta_{\text{em}}$) is set to 90 %. It is assumed that the efficiencies in motor and generator mode are identical.

The auxiliary loads in a vehicle, such as lights, entertainment and air conditioning, have a significant impact on the specific energy use of EV. In line with [278], $P_{\text{aux}}$ is set to 500 W.

The efficiencies of the power electronics ($\eta^c_{\text{pe}}$ and $\eta^d_{\text{pe}}$) and the energy storage system ($\eta^c_{\text{bat}}$ and $\eta^d_{\text{bat}}$) have been fixed for the calculations in this appendix and are listed in Table A.3.

Table A.3: Efficiencies of the power electronics and Li-ion battery [279].

| | | |
|---|---|---|
| Power electronics: | $\eta^c_{\text{pe}}$ | 95 % |
| | $\eta^d_{\text{pe}}$ | 98 % |
| Battery (Li-ion): | $\eta^c_{\text{bat}}$ | 95 % |
| | $\eta^d_{\text{bat}}$ | 95 % |

As mentioned in Section 3.2, an extra correction factor of 15 % on the specific electricity consumption has been used compared to [85] [217]. For the small, medium-class and large vehicles, $E_{\text{spec}}$ is equal to 0.185, 0.220 and 0.293 kWh/km. A sensitivity analysis on the vehicle mass, the auxiliary load, the slope of the road, the rolling resistance and the fraction of regenerative braking can be found in [85].

# Appendix B

# Electrical modeling in Modelica

## B.1 AC and DC electricity grid modeling: Modelica implementation

### B.1.1 Grid topology

The grid topology is described by the incidence matrix and the cable impedances. This is shown in Code 6. `GridType` extends `GridImp` and describes the grid topology.

### B.1.2 Transformer

The transformer model consists of an impedance for each of the three phases, similar to [153]. The record interface to define the transformer data is shown in Code 7.

## B.2 PV system: Five-parameter panel model

The five-parameter model, which is temperature dependent, is based on the single diode equivalent circuit of a PV panel [240]. The five parameters, which

```
record GridType
  extends GridImp(R=CabTyp.RCha.*LenVec, X=CabTyp.XCha.*LenVec);
  parameter Modelica.SIunits.Length LenVec[nNodes]
    "Length for each line";
  parameter Cable CabTyp[nNodes];
end GridType;

record GridImp
  parameter Integer nNodes;
  parameter Integer nodeMatrix "Incidence matrix";
  parameter Modelica.SIunits.Resistance R[size(nodeMatrix,1)];
  parameter Modelica.SIunits.Reactance X[size(nodeMatrix,1)];
  parameter Modelica.SIunits.ComplexImpedance
    Z[size(nodeMatrix,1)](re=R,im=X);
end GridImp;

record Cable
  parameter CharacteristicResistance RCha
    "Characteristic resistance";
  parameter CharacteristicReactance XCha
    "Characteristic reactance";
  parameter ComplexCharacteristicImpedance ZCha(re=RCha,im=XCha);
end Cable;
```

Code 6: Description of grid topology (interfaces).

```
record Transformer
  parameter Modelica.SIunits.ApparentPower Sn "Apparent power
    of the transformer";
  parameter Modelica.SIunits.ActivePower P0 "No-load losses";
  parameter Modelica.SIunits.Complex Impedance Z1 "Phase 1";
  parameter Modelica.SIunits.Complex Impedance Z2=Z1 "Phase 2";
  parameter Modelica.SIunits.Complex Impedance Z3=Z1 "Phase 3";
end Transformer;
```

Code 7: Transformer description (interface).

have been indicated in the equivalent circuit in Figure B.1, are:

- the light current $I_{\mathrm{ph}}$;
- the diode reverse saturation current $I_o$;
- a shunt resistance $R_{\mathrm{sh}}$;
- a series resistance $R_s$;
- the thermal voltage $V_t$.

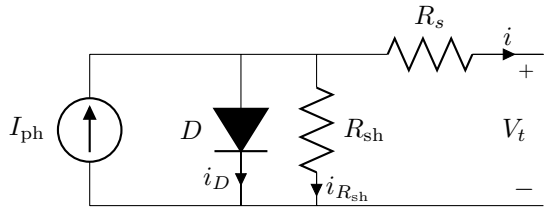


Figure B.1: Five parameter model of a PV panel [240].

The five parameters have been calculated based on characteristics provided by the solar panel manufacturer. The required specifications are:

- the current $I_{\text{MPP}}$ and voltage $V_{\text{MPP}}$ at maximum power point (MPP) under standard testing conditions (STC);
- the short circuit current $I_{\text{sc}}$ and open circuit voltage $V_{\text{oc}}$ under STC;
- the temperature coefficients $k_i$ and $k_v$ of the short circuit current and open circuit voltage, respectively.

The general current-voltage $(i - v)$ equation for the single diode equivalent circuit is calculated as follows:

$$i = I_{\text{ph}} - I_0\left(e^{\frac{v+iR_s}{n_s V_t}} - 1\right) - \frac{v + iR_s}{R_{\text{sh}}}, \tag{B.1}$$

with $V_t$ the junction thermal voltage and $n_s$ the number of cells in the panel connected in series.

The voltage $V_{\text{MPP}}$ and current $I_{\text{MPP}}$ at maximum power point should satisfy this equation. Therefore, the derivative of the power with respect to the voltage should be zero at this point, and the derivative of the current with respect to the voltage at short circuit current should be the negative of the shunt conductance $(1/R_{\text{sh}})$:

$$\left.\frac{dP}{dV}\right|_{\substack{V=V_{\text{MPP}} \\ I=I_{\text{MPP}}}} = 0, \tag{B.2}$$

$$\left.\frac{dI}{dV}\right|_{I=I_{\text{sc}}} = -\frac{1}{R_{\text{sh}}}. \tag{B.3}$$

The reverse saturation current $I_o$ and light current $I_{\text{ph}}$ at STC are the result of:

$$I_{\text{sc}} = I_{\text{ph}} - I_0 e^{\frac{I_{\text{sc}}R_s}{n_s V_t}} - \frac{I_{\text{sc}}R_s}{R_{\text{sh}}}, \tag{B.4}$$

$$I_{\text{oc}} = 0 = I_{\text{ph}} - I_0 e^{\frac{V_{\text{oc}}}{n_s V_t}} - \frac{V_{\text{oc}}}{R_{\text{sh}}}. \tag{B.5}$$

The PV parameters have been adjusted to take into account:

- the position of the sun;
- the direct and indirect radiation;
- the ambient temperature.

The PV cell temperature is adjusted to the ambient temperature increased with the panel losses. The tilt angle and orientation of the PV system are parameters of the model.

The ambient temperature and the direct and diffuse radiation have been read from a meteorological data file, as discussed in Appendix C.1.

The incidence angle of the direct beam radiation on a PV panel can be calculated. This allows to obtain the amount of radiation that reflects and passes through the PV panel. Incidence angle modifiers have been used, which have been derived from [240]. The incidence angle ($\theta$) modifier $K_{\tau\alpha}(\theta)$ can be found from the transmittance $\tau$ of the cover system with:

$$K_{\tau\alpha}(\theta) = \frac{\tau(\theta)}{\tau(0)}, \tag{B.6}$$

which is approximated by:

$$\tau(\theta) = e^{-\frac{KL}{\cos\theta_r}}\left[1 - \frac{1}{2}\left(\frac{\sin^2(\theta_r - \theta)}{\sin^2(\theta_r + \theta)} + \frac{\tan^2(\theta_r - \theta)}{\tan^2(\theta_r + \theta)}\right)\right], \tag{B.7}$$

with $K$ the glazing extinction coefficient and $L$ the glazing thickness. $K$ and $L$ can be adjusted. By default, $K$ is assumed to be $4\,\mathrm{m}^{-1}$ and $L$ is assumed to be $2\,\mathrm{mm}$.

The angle of refraction, $\theta_r$, is determined by Snell's law:

$$\theta_r = \arcsin(n \sin\theta), \tag{B.8}$$

with $\theta$ the incidence angle and $n$ the effective refraction index of the cell cover.

The absorbed solar radiation $S$ is calculated as follows:

$$\frac{S}{S_{\mathrm{ref}}} = \frac{G_b}{G_{\mathrm{ref}}} K_{\tau\alpha,b} + \frac{G_d}{G_{\mathrm{ref}}} K_{\tau\alpha,d} \frac{1 + \cos\beta}{2} + \frac{G}{G_{\mathrm{ref}}} \rho K_{\tau\alpha,g} \frac{1 - \cos\beta}{2} \tag{B.9}$$

with $G_b$ the direct, $G_d$ the diffuse and $G$ the total radiation. The slope of the PV panel is characterized by $\beta$.

To conclude, the parameters at non-reference conditions have been calculated. The open circuit voltage, as a function of $S$ and the temperature $T$, $V_{\mathrm{oc}}(S, T)$

is calculated with:

$$e^{\frac{V_{\text{oc}}(S)}{n_s V_t}} = \frac{I_{\text{ph}}(S)R_{\text{sh}} - V_{\text{oc}}(S)}{I_0 R_{\text{sh}}} \text{ and} \tag{B.10}$$

$$V_{\text{oc}}(T) = V_{\text{oc}} + k_v(T - T_{\text{stc}}). \tag{B.11}$$

The short circuit current $I_{\text{sc}}$ can be found using:

$$I_{\text{sc}}(S,T) = I_{\text{sc}}\left(\frac{S}{S_{\text{ref}}}\right)\left(1 + \frac{k_i}{100}(T - T_{\text{ref}})\right). \tag{B.12}$$

The reverse saturation current $I_0$ light current $I_{\text{ph}}$ have been calculated as follows:

$$I_0 = \left(I_{\text{sc}} - \frac{V_{\text{oc}} - I_{\text{sc}}R_s}{R_{\text{sh}}}\right)e^{-\frac{V_{\text{oc}}}{n_s V_t}} \text{ and} \tag{B.13}$$

$$I_{\text{ph}} = I_0 e^{\frac{V_{\text{oc}}}{n_s V_t}} + \frac{V_{\text{oc}}}{R_{\text{sh}}}. \tag{B.14}$$

## B.3 Battery storage: Modelica implementation

Different battery types can be defined. Battery types are described by different parameters as listed in Code 8.

```
record BatteryType "Battery type"
  parameter Modelica.SIunits.Efficiency eta_in, eta_out
    "Charging and discharging efficiency converter";
  parameter Modelica.SIunits.Efficiency eta_c, eta_d
    "Charging and discharging efficiency of battery";
  parameter Modelica.SIunits.Efficiency alpha_sd
    "Self-discharge (\%/100) per month";
  parameter Real e_c, e_d
    "Ratio: Maximum charging and discharging power to
    battery capacity";
end BatteryType;
```

Code 8: Battery type record.

### B.3.1 Battery SoC calculations

The dynamic SoC equation, as defined in Eq. (4.10), is implemented as shown in Code 9, with `dSoC` the SoC change between two time steps, and `P` the

power drawn from the grid (when charging) or drawn from the battery (when discharging).

```
model Battery
  parameter Modelica.SIunits.Efficiency eta_in, eta_c
    "Charging efficiency of converter and battery";
  parameter Modelica.SIunits.Efficiency eta_out, eta_d
    "Discharging efficiency of converter and battery";
  parameter Modelica.SIunits.Efficiency delta_sd "Self-discharge";

  parameter Modelica.SIunits.Conversions.NonSIunits.Energy_kWh
    EBat "Total battery capacity";
  Modelica.SIunits.Efficiency SoC(start=SoCinit)
    "State of Charge of battery capacity in [%/100]";
  Modelica.SIunits.Efficiency dSoC "SoC change";

equation
  if P <= 0 then // Discharging
    dSoC = (P*(2 - eta_out*eta_d)) / EBat;
  else           // Charging
    dSoC = (P*(eta_in*eta_c)) / EBat;
  end if;

  der(SoC) = dSoC - delta_sd;
end Battery;
```

Code 9: Battery model for SoC calculations.

# Appendix C

# Apartment building: building and thermal system design

This appendix describes the design of the apartment building model and the thermal system design, including a heat pump for space heating and DHW, and a thermal storage system for the DHW (Appendix C.4). This chapter also includes a brief overview on the modeling details of the climate model (Appendix C.1), the transient building response model (Appendix C.3) and the thermal system (Appendix C.4). This overview is based on the specification of the IDEAS library [246]. A more detailed description of these models is available online in the IDEAS specifications [246] and in the literature [19, 280].

## C.1 Climate model

To calculate the transient heat losses by conduction and radiation, and solar gains by solar irradiation, the following external parameters are required:

- external temperature $T_e$;
- ground temperature $T_{\text{gr}}$;
- sky temperature $T_{\text{sky}}$;
- solar irradiation $E$.

The Meteonorm system [222] has been used as a source of (European) weather data. The following required weather data is available:

- ambient dry-bulb temperature $T_{\mathrm{db}}(t)$;
- outdoor relative humidity $\varphi_e(t)$;
- wind speed $v_{10}(t)$;
- diffuse horizontal solar radiation $E_{d,h}(t)$;
- direct normal solar radiation $E_{D,\perp}(t)$.

The direct and diffuse solar irradiation on a tilted surface is determined by means of the position of the sun. The position of the sun relative to the tilted surface is uniquely defined by, the zenith angle $\xi(t,x)$ of the surface with inclination $i(x)$ and azimuth $a(x)$. The zenith angle is the angle between the normal of the surface and the beam of the sun.

The total solar irradiation $E(t,x)$ on a surface is the sum of the direct $E_D(t,x)$, diffuse $E_d(t,x)$ and reflected $E_r(t,x)$ radiation on the surface. Meteonorm contains the direct solar irradiation $E_{D,\perp}(t,x)$ perpendicular on the beam radiation. The direct, diffuse and reflected radiation on the surface have been calculated as described in [246].

The (black body) sky temperature $T_{\mathrm{sky}}$ is calculated as described in [246].

## C.2 Solar shading: Exterior solar screen

Solar shading can be used to reduce the short-wave radiation on a surface, i.e. to reduce the solar gains.

An exterior solar screen has a position $f_p \in [0,1]$. $f_p$ is zero when the solar screen is fully closed and one when fully opened. The transmitted direct solar irradiation is $E_D(t,x)\,(1-f_p(t))$. The transmitted diffuse and reflected solar irradiation is equal to $E_d(x,t)\,(1-f_p) + f_p(t) f_s E(x,t)$, with $f_s$ the shortwave transmittance of the exterior screen.

## C.3 Transient building response model

The transient building response model allows to simulate the energy demand for heating and cooling of a multi-zone building, the energy flows in the building and the interconnection with thermal and electrical building energy systems.

### C.3.1 Transient model for walls

A wall has been described as a structure of parallel opaque layers [246]. Three heat processes take place:

- the heat balance of the exterior wall surface;
- the heat conduction between the interior and exterior wall surface;
- the heat balance of the interior wall surface.

The heat balance of the interior and exterior wall surfaces are defined by:

- the conductive heat flow into the wall;
- the heat transfer by convection;
- the short-wave absorption of direct and diffuse solar radiation;
- the long-wave heat exchange with the surroundings, i.e. the environment and sky for exterior walls and the surrounding interior surfaces for interior walls, respectively.

The heat transport by conduction in the wall has been simplified to a one-dimensional heat transport. The wall has been modeled with a sequence of discrete resistances $R_i$ and capacitances $C_i$. The order of the model is defined by the number of capacitances. The model allows to take into account the temperature dependency of the thermal conductivity of the different materials.

#### Model extension for windows

The transient window model extends the transient wall model, but also includes:

- the absorption of solar irradiation by the glass panes;
- the heat transfer through the gas gaps between the different glass panes;
- the transmission of solar irradiation to the indoor zones.

The absorption and transmission properties are a function of the incidence angle of the solar irradiation.

#### Model extension for ground slabs

The heat transfer is similar to that of the heat transfer through walls, but it differs at the exterior surface: the heat transfer through the ground is

3-dimensional with a large time lag. As discussed in [246], the heat flow through the ground is approximated (based on ISO 13370).

### C.3.2 Transient zone model

The transient zone model consists of both the convective and radiative heat transfers, influencing the thermal zone comfort. This thermal response also influences the thermal response of the adjacent walls.

It is assumed that the air in a zone is well-mixed. Therefore, a uniform air temperature $T_{\text{air}}$ can be assumed and the thermal zone can be modeled as a thermal circuit.

Thermal energy enters and leaves the zone through air infiltration and ventilation. It is assumed that the resulting net air mass flow rate is zero and air leaves the zone at $T_{\text{air}}$. Corresponding to the low-energy standard, the building is supposed to be air-tight. A mechanical, continuous air-to-air heat recovery ventilation system is assumed to be present in the rooms, with an $n_{50}$ value of 0.3 and a heat recovery efficiency $\eta_{V,\text{rec}}$ of 0.84. The ventilation losses have been calculated as follows:

$$Q_V = 0.34 G_a (T_i - T_{\text{amb}})(1 - \eta_{V,\text{rec}}), \tag{C.1}$$

with $T_i$ the room air temperature, $T_{\text{amb}}$ the outside temperature and $G_a = n_{50} V_{\text{zone}}$. $n_{50}$ is the air tightness[1] of the building and $V_{\text{zone}}$ is the total zone air volume.

The internal gains due to the electrical loads, have been assumed to be 75 % of the electricity power demand. The internal heat gains due to the presence of people in the building have not been taken into account.

## C.4 Thermal building system models

The thermal comfort in a building can be achieved by making use of a heating system[2]. Here, heat is produced by means of a heat pump, including a thermal energy storage unit (water storage tank) for DHW. The heating system has been based upon the work in [19]. This section briefly discusses the modeling background.

[1] Air change rate at a pressure difference of 50 Pa.

[2] An active cooling system in a residential apartment building is neglected in this study.

## C.4.1 Heating system topology

A new apartment building has been considered that meets the latest energy performance regulations, i.e. a maximum K value of 40 [249]. Also, floor heating has been assumed to heat the building.

The hydraulic scheme of the heating system is shown in Fig. C.1. Heat is produced by means of a modulating air-to-water heat pump. A thermal energy storage (TES) unit (a storage tank) with internal heat exchanger is used as a buffer for DHW. Heat is emitted to the building interiors through a floor heating system[3]. Due to lower (heating) efficiencies, no TES has been considered for space heating. The losses to the environment have been taken into account[4].

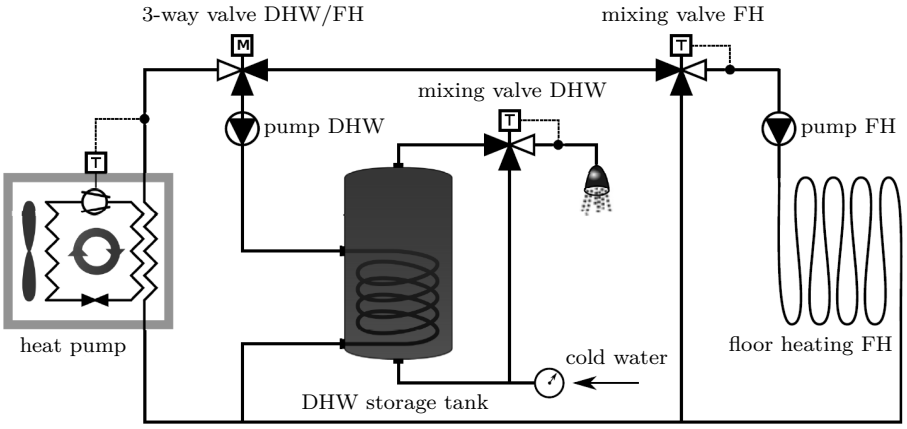


Figure C.1: Hydraulic scheme of the heating system [19].

## C.4.2 Modulating air-to-water heat pump

A dynamic heat pump model has been implemented [19], based on interpolation in a performance map to calculate the heating power $Q^{\mathrm{HP}}$ and the electric power $P^{\mathrm{HP}}$ [246] as a function of the condenser outlet temperature and the ambient temperature. The performance map has been obtained from manufacturers data [281][5]. The thermal losses to the environment have been taken into account.

[3]Embedded pipe emission system.

[4]The heat losses of the heater and all the pipes are connected to a central fix temperature.

[5]This heat pump has a thermal power of 3459 W at 2/35°C (air/water temperature). The nominal coefficient of performance (COP) is 3.17 and 2.44 at respectively 2/35°C and 2/45°C test conditions (full load).

Note that these losses have been compensated artificially. There is no minimal on or off time [246].

The heat pump can be modulated between 25 % and 100 % of the maximum thermal power $Q_{\max}$. $Q_{\max}$ is a function of the evaporator and condenser temperature. The heat pump is turned off when the modulation drops below 25 %. The modulation $f_{\mathrm{mod}}$ is calculated as follows:

$$f_{\mathrm{mod}} = \frac{Q_{\mathrm{dem}}}{Q_{\max}}, \tag{C.2}$$

with $Q_{\mathrm{dem}}$ the thermal power demand, which is calculated as:

$$Q_{\mathrm{dem}} = \dot{m} c_p (T_{\mathrm{set}} - T_i), \tag{C.3}$$

with $\dot{m}$ the condenser mass flow rate [kg/s] at the water side, $c_p$ the specific heat capacity of water[6] [J/kg s], $T_{\mathrm{set}}$ the condenser set temperature and $T_i$ the condenser inlet temperature.

The dynamic heat transfer in the condenser takes into account the water in the condenser, the dry capacity, the condensation heat, and the environmental heat losses.

### C.4.3 Domestic hot water production and storage tank

Only the DHW production makes use of the stratified water storage tank, including an internal heat exchanger [19, 245]. A thermostatic mixing valve is used to withdraw water at 45°C. The model has been calibrated to be used for different storage sizes [282].

The storage tank has been modeled as a one-dimensional multinode (vertical) storage tank. For each node $i$ (top node: $i = 1$), Eqns. (C.4) and (C.5) give the energy and mass balances, respectively, as also shown in Fig. C.2:

$$m_i c_p \frac{dT_i}{dt} = \sum_i c_p \dot{m}_i T_i + Q_{\mathrm{cond},i-1} + Q_{\mathrm{cond},i} + Q_{\mathrm{buo},i-1} + Q_{\mathrm{buo},i} + Q_{\mathrm{amb},i} + Q_{\mathrm{HX},i}, \tag{C.4}$$

$$\dot{m}_{i-1} + \dot{m}_{\mathrm{in},i} = \dot{m}_i + \dot{m}_{\mathrm{out},i}, \tag{C.5}$$

with $m_i$ and $T_i$ the mass and temperature of the water in node $i$. The water flowing in and out a node have been represented by $\dot{m}_i$. $Q_{\mathrm{cond}}$ is the conductive

[6] Assumed constant at 4177 J/kg K.

heat transfer with the adjacent nodes, $Q_{\text{amb}}$ the conductive heat losses to the environment, $Q_{\text{HX},i}$ the heat transfer from the internal heat exchanger to node $i$ and $Q_{\text{buo}}$ the natural convective heat transfer due to buoyancy effects in case of temperature inversion to the neighbouring nodes.

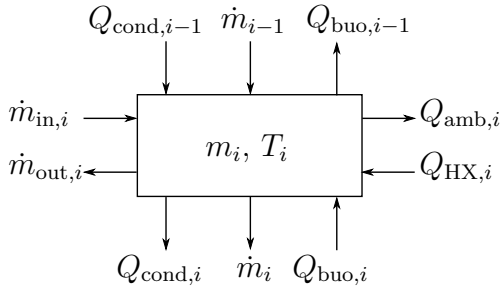


Figure C.2: Energy and mass balance for node $i$ in the energy storage tank [19].

The following heat exchanges occur through the internal heat exchanger:

- convection between the water in the heat exchanger and the coil wall;
- conduction through the coil wall;
- convection between the coil wall and the water in the storage tank.

The storage tank model contains two temperature sensors for control purposes, i.e. at the top and bottom layer, respectively. Heat losses to the surroundings have been taken into account.

### C.4.4 Control

Controllers have been implemented for:

- the on/off control of the pumps for floor heating and domestic hot water;
- the condenser set temperature.

The pumps for floor heating and DHW are controlled based on the zone thermostat (set temperature) and the temperatures in the storage tank, respectively. The temperature of the condenser is controlled when a flow rate occurs. The set point follows either the heating curve for space heating or DHW. A compensation for any distribution losses has been built in.

# Bibliography


[1] International Energy Agency, *Energy technology perspectives 2014: Harnessing Electricity's Potential*. Paris, France: IEA Publications, 2014.

[2] H. Hens and A. Janssens, *Energy Today and Tomorrow*. Leuven: ACCO, 2006, ch. Building, living and energy, pp. 133–151.

[3] The European Commission. (2014, Nov.) Reducing CO2 emissions from passenger cars. [Online]. Available: http://ec.europa.eu/clima/policies/transport/vehicles/cars/index_en.htm

[4] The European Commission. (2014, Nov.) The EU climate and energy package. [Online]. Available: http://ec.europa.eu/clima/policies/package/

[5] The European Commission. (2014, Nov.) 2030 framework for climate and energy policies. [Online]. Available: http://ec.europa.eu/clima/policies/2030/index_en.htm

[6] D. Stanway. (2014, Nov.) China, U.S. agree limits on emissions, but experts see little new. [Online]. Available: http://www.reuters.com/article/2014/11/12/us-china-usa-climatechange-idUSKCN0IW07Z20141112

[7] The European Parliament, "Directive 2002/91/EC of the European Parliament and the Council on 16 December 2002 on the energy performance of buildings (recast)," *Official J. of the European Union*, vol. 1, pp. 65–71, Jan. 2003.

[8] The European Parliament, "Directive 2010/31/EU of the European Parliament and the Council on 19 May 2010 on the energy performance of buildings (recast)," *Official J. of the European Union*, vol. 153, pp. 13–35, Jun. 2010.

[9] S. Pless and P. Torcellini, "Net-zero energy buildings: A classification system based on renewable energy supply options," National Renewable Energy Laboratory, Tech. Rep. NREL/TP-550-44586, 2010.

[10] A. Marszal, P. Heiselberg, J. Bourrelle, E. Musall, K. Voss, I. Sartori, and A. Napolitano, "Zero energy building: A review of definitions and calculation methodologies," *Energy and Buildings*, vol. 43, no. 4, pp. 971–979, Apr. 2011.

[11] E. Mlecnik, "Defining nearly zero-energy housing in Belgium and the Netherlands," *Energy Efficiency*, vol. 5, no. 3, pp. 411–431, Aug. 2012.

[12] I. Sartori, A. Napolitano, and K. Voss, "Net zero energy buildings: A consistent definition framework," *Energy and Buildings*, vol. 48, pp. 220–232, May 2012.

[13] S. Pless and P. Torcellini, "Getting to net zero," National Renewable Energy Laboratory, Tech. Rep., 2009.

[14] (2014, Nov.) Energieprestatieregelgeving (EPB) voor nieuwbouw en renovatie. [Online]. Available: http://www.vlaanderen.be/nl/bouwen-wonen-en-energie/bouwen-en-verbouwen/energienormen/energieprestatieregelgeving-epb-voor-nieuwbouw-en-renovatie

[15] The European Parliament, "Regulation (EC) No 715/2007 of the European Parliament and the Council of 20 June 2007 on type approval of motor vehicles with respect to emissions from light passenger and commercial vehicles (Euro 5 and Euro 6) and on access to vehicle repair and maintenance information," *Official J. of the European Union*, vol. 171, pp. 1–16, Jun. 2007.

[16] M. Duvall, E. Knipping, M. Alexander, L. Tonachel, and C. Clarc, "Environmental assessment of plug-in hybrid electric vehicles," Electric Power Research Institute, Tech. Rep. 1015325, 2007.

[17] K. Clement, E. Haesen, and J. Driesen, "The impact of charging plug-in hybrid electric vehicles on a residential distribution grid," *IEEE Trans. Power Syst.*, vol. 25, no. 1, pp. 371–380, Feb. 2010.

[18] G. Heydt, "The impact of electric vehicle deployment on load management strategies," *IEEE Power Eng. Rev.*, vol. 3, no. 5, pp. 41–42, May 1983.

[19] R. De Coninck, R. Baetens, D. Saelens, A. Woyte, and L. Helsen, "Rule-based demand-side management of domestic hot water production with heat pumps in zero energy neighbourhoods," *J. of Building Performance Simulation*, vol. 7, no. 4, pp. 271–288, Jul. 2014.

[20] D. Six, J. Desmedt, D. Van Houdt, and J. Van Bael, "Exploring the flexibility potential of residential heat pumps combined with thermal storage for smart grids," in *21st Int. Conf. and Exhibition on Electricity Distribution (CIRED)*, Frankfurt, Germany, Jun. 2011, pp. 1–4.

[21] T. Nuytten, B. Claessens, K. Paredis, J. Van Bael, and D. Six, "Flexibility of a combined heat and power system with thermal energy storage for district heating," *Appl. Energy*, vol. 104, pp. 583–591, Apr. 2013.

[22] International Energy Agency, *Energy technology perspectives 2012: Pathways to a clean energy system.* Paris, France: IEA Publications, 2012.

[23] D. Van Hertem and M. Ghandhari, "Multi-terminal VSC HVDC for the European supergrid: Obstacles," *Renewable and Sustainable Energy Reviews*, vol. 14, no. 9, pp. 3156–3163, Dec. 2010.

[24] (2014, Dec.) EMerge Alliance Standards. [Online]. Available: http://www.emergealliance.org/Standards/OurStandards.aspx

[25] (2014, Dec.) A Call for Participation: IEEE Plan for "DC in the Home". [Online]. Available: http://standards.ieee.org/email/2013_10_cfp_dchome_web.html

[26] "DPC for code of practice for low and extra low voltage direct current power distribution in buildings," IET, Tech. Rep. draft, Dec. 2014. [Online]. Available: http://www.theiet.org/resources/standards/dpc-cop-form-dcpower.cfm?utm_source=redirect&utm_medium=any&utm_campaign=dc-cop

[27] (2014, Mar.) Linear. [Online]. Available: http://www.linear-smartgrid.be/

[28] N. Leemput, F. Geth, J. Van Roy, A. Delnooz, J. Büscher, and J. Driesen, "Impact of electric vehicle on-board single-phase charging strategies on a Flemish residential grid," *IEEE Trans. on Smart Grid*, vol. 5, no. 4, pp. 1815–1822, Jul. 2014.

[29] B. Verbruggen, "Grid impact of active electricity systems in the residential environment," Ph.D. dissertation, KU Leuven, draft.

[30] International Energy Agency, *Technology roadmap: Electric and plug-in hybrid electric vehicles.* Paris, France: IEA Publications, Jun. 2011.

[31] FOD Economie. (2014, Feb.) Statbel: Directorate-general Statistics and Economic information. [Online]. Available: http://statbel.fgov.be

[32] M. Duvall, E. Knipping, M. Alexander, L. Tonachel, and C. Clarc, "Environmental assessment of plug-in hybrid electric vehicles," Electric Power Research Institute, Tech. Rep. 1015325, 2007.

[33] The European Commission. (2014, Dec.) The EU Emissions Trading System (EU ETS). [Online]. Available: http://ec.europa.eu/clima/policies/ets/index_en.htm

[34] X. Mosquet, M. Devineni, T. Mezger, H. Zablit, A. Dinger, G. Sticher, M. Gerrits, and M. Russo, "Powering autos to 2020: The era of the electric car," BCG, Tech. Rep. 80920, Jul. 2011. [Online]. Available: http://www.bcg.be/documents/file80920.pdf

[35] M. Book, M. Groll, X. Mosquet, D. Rizoulis, and G. Sticher, "The comeback of the electric car? How real, how soon, and what must happen next," BCG, Tech. Rep. 15404, Jul. 2009. [Online]. Available: http://www.bcg.be/documents/file15404.pdf

[36] (2014, Dec.) Hybrid cars: Auto alternatives for the 21st century. [Online]. Available: http://www.hybridcars.com/

[37] T. Devloo, N. Leemput, J. Van Roy, F. Geth, and J. Driesen, "Component improvements in the electrification of passenger vehicles drivetrains," in *IEEE Transportation Electrification Conf. and Expo (ITEC)*, Dearborn, Detroit, MI, USA, June 2013, pp. 1–6.

[38] M. Messagie, K. Lebeau, N. Omar, J.-M. Timmermans, J. Van Mierlo, C. Macharis, P. Van Den Boscche, J. Van Roy, N. Leemput, and J. Driesen, *Technologische verkenning: Elektrische voertuigen.* VEI, 2011.

[39] N. Jalil, N. Kheir, and M. Salman, "A rule-based energy management strategy for a series hybrid vehicle," in *Proc. of the Amer. Control Conf.*, Albuquerque, New Mexico, Jun. 1997.

[40] M. Salman and N. Schouten, "Control strategies for parallel hybrid vehicles," in *Proc. of the Amer. Control Conf.*, Chicago, IL, USA, Jun. 2010, pp. 524–528.

[41] (2014, Dec.) Toyota Prius. [Online]. Available: http://nl.toyota.be/modellen/Prius/

[42] J. Van Roy, S. De Breucker, and J. Driesen, "Analysis of the optimal battery sizing for plug-in hybrid and battery electric vehicles on the power consumption and V2G availability," in *16th Int. Conf. on Intelligent System Applicat. to Power Syst. (ISAP)*, Hersonissos, Crete, Greece, Sep. 2011, pp. 1–6.

[43] (2014, Dec.) Chevrolet Volt. [Online]. Available: http://www.chevrolet.com/volt-electric-car.html

[44] (2014, Dec.) Wikipedia - Fisker Karma. [Online]. Available: http://en.wikipedia.org/wiki/Fisker_Karma

[45] (2014, Dec.) Ford C-Max Energi. [Online]. Available: http://www.ford.com/cars/cmax/trim/energi/

[46] (2014, Dec.) Mitsubishi Outlander PHEV. [Online]. Available: http://www.mitsubishi-cars.co.uk/outlander/explore-phev.aspx

[47] (2014, Dec.) Volvo V60 Plug-in Hybrid. [Online]. Available: http://www.volvocars.com/uk/campaigns/v60-plugin-hybrid/Pages/default.aspx

[48] (2014, Dec.) BMW i3. [Online]. Available: http://www.bmw.com/com/en/newvehicles/i/i3/2013/showroom/

[49] (2014, Dec.) Ford Focus Electric. [Online]. Available: http://www.ford.com/cars/focus/trim/electric/

[50] (2014, Dec.) Kia Soul EV. [Online]. Available: http://www.kia.com/us/en/vehicle/soul-ev/2015/experience?story=hello

[51] (2014, Feb.) Mitsubishi i-MiEV. [Online]. Available: http://www.mitsubishi-motors.com/special/ev

[52] (2014, Feb.) Nissan Leaf. [Online]. Available: http://nl.nissan.be/BE/nl/vehicle/electric-vehicles/leaf.html

[53] (2014, Dec.) Renault Zoe. [Online]. Available: http://zoe.renault.fr

[54] (2014, Dec.) Volkswagen e-up! [Online]. Available: http://www.volkswagen.de/de/models/up/varianten.s9_trimlevel_detail.suffix.html/e-up~2Fe-up.html

[55] (2014, Dec.) Volkswagen e-Golf. [Online]. Available: http://www.volkswagen.de/de/models/golf_7/trimlevel_overview.s9_trimlevel_detail.suffix.html/der-e-golf~2Fe-golf.html

[56] (2014, Dec.) Volvo C30 eDrive. [Online]. Available: http://esd.volvocars.com/site/owners-information/MY12/C30_PEV/SUPPL_1146/C30_Electric_MY12_EN_tp14621.pdf

[57] (2014, Dec.) Tesla Model S. [Online]. Available: http://www.teslamotors.com/models

[58] "Factsheet Electric Vehicles," KU Leuven Energy Institute, Tech. Rep. 2014-03, Nov. 2014.

[59] Electric Vehicle Wiki. (2014, Dec.) Battery Capacity Loss. [Online]. Available: http://www.electricvehiclewiki.com/Battery_Capacity_Loss

[60] J. Dogger, B. Roossien, and F. Nieuwenhout, "Characterization of Li-ion batteries for intelligent management of distributed grid-connected storage," *IEEE Trans. Energy Convers.*, vol. 26, no. 1, pp. 256–263, Mar. 2011.

[61] M. Koller, T. Borsche, A. Ulbig, and G. Andersson, "Defining a degradation cost function for optimal control of a battery energy storage system," in *IEEE PowerTech*, Grenoble, France, 2013, pp. 1–6.

[62] P. Ramadass, B. Hara, R. White, and B. N. Popov, "Performance study of commercial LiCoO2 and spinel-based Li-ion cells," *J. of Power Sources*, vol. 111, pp. 210–220, Apr. 2002.

[63] F. Geth, "Battery energy storage systems and distribution grid support," Ph.D. dissertation, KU Leuven, Sep. 2014.

[64] H. Seljeseth, H. Taxt, and T. Solvang, "Measurement of network impact from electric vehicles during slow and fast charging," in *23rd Int. Conf. & Exhibition on Electricity Distribution (CIRED)*, Stockholm, Sweden, Jun. 2013, pp. 1–4.

[65] *Electric vehicle conductive charging system - Part 1: General requirements*, IEC Std. IEC 61 851-1, Nov. 2010.

[66] P. Van Den Bossche, "The electric vehicle: raising the standards," Ph.D. dissertation, ETEC, VUB, 2003.

[67] CEN-CENELEC, "Standardization for road vehicles and associated infrastructure," Tech. Rep., Oct. 2011. [Online]. Available: ftp://ftp.cen.eu/CEN/Sectors/List/Transport/Automobile/EVReportOctober.pdf

[68] Nationale plattform Elektromobilität, "The German standardization roadmap for electromobility," Tech. Rep., May 2013. [Online]. Available: http://www.elektromobilitaet.din.de

[69] ACEA, "ACEA position and recommendations for the standardization of the charging of electrically chargeable vehicles," Tech. Rep., May 2012. [Online]. Available: http://www.acea.be/uploads/publications/Updated_ACEA_position_on_charging_ECVs.pdf

[70] S. Luyten, "Standaardisatie van laadinfrastructuur voor elektrische voertuigen," Master's thesis, KU Leuven, 2012.

[71] The European Parliament, "M468 - Standardisation mandate to CEN, CENELEC and ETSI concerning the charging of electric vehicles," Jun. 2010. [Online]. Available: http://ec.europa.eu/energy/gas_electricity/smartgrids/doc/2010_06_04_mandate_m468_en.pdf

[72] S. Luyten, N. Leemput, F. Geth, J. Van Roy, J. Büscher, and J. Driesen, "Standardization of conductive AC charging infrastructure for electric vehicles,"

in *23rd Int. Conf. & Exhibition on Electricity Distribution (CIRED)*, Stockholm, Sweden, Jun. 2013.

[73] C. Ricaud and P. Vollet, "Connection system on the recharging spot: A key element for electric vehicles," White Paper, Schneider Electric. [Online]. Available: http://www.schneider-electric.com/sites/corporate/en/support/white-papers/recharging-spot-electric-vehicles.page

[74] J. John, "REstore: Balancing Europe's wind and solar with EVs, cold storage." [Online]. Available: http://www.greentechmedia.com/articles/read/restore-balances-european-load-with-evs-cold-storage

[75] Groen7.nl, "Amsterdam ArenA laadt elektrische auto op basis van vertrektijd." [Online]. Available: http://www.groen7.nl/amsterdam-arena-laadt-elektrische-auto-op-basis-van-vertrektijd/

[76] K. De Craemer, "Event-driven demand response for electric vehicles in multi-aggregator distribution grid settings," Ph.D. dissertation, KU Leuven, Jul. 2014.

[77] *Road vehicles - Vehicle to grid communication interface*, IEC Std. IEC 15 118, 2013.

[78] A. Mathoy, "Definition and implementation of a global EV charging infrastructure," Final report, Brusa Elektronik. [Online]. Available: http://www.park-charge.ch/documents/EV-infrastructureproject.pdf

[79] *Plugs, socket-outlets, vehicle connectors and vehicle inlets - Conductive charging of electric vehicles - Part 2: Dimensional compatibility and interchangeability requirements for a.c. pin and contact-tube accessories*, IEC Std. IEC 62 196-2, Oct. 2011.

[80] (2014, Nov.) CHAdeMO. [Online]. Available: http://www.chademo.com/

[81] (2014, Nov.) Tesla Motors - Supercharger. [Online]. Available: http://www.teslamotors.com/supercharger

[82] J. Pokrzywa and M. Reidy, "SAE's J1772 'combo connector' for ac and dc charging advances with IEEE's help." [Online]. Available: http://articles.sae.org/10128/

[83] A. Ulbig and G. Andersson, "On operational flexibility in power systems," in *IEEE PES General Meeting*, San Diego, CA, USA, Jul. 2012, pp. 1–8.

[84] G. Papaefthymiou, B. Hasche, and C. Nabe, "Potential of heat pumps for demand side management and wind power integration in the German electricity market," *IEEE Trans. Sustain. Energy*, vol. 3, no. 4, pp. 636–642, Oct. 2012.

[85] J. Van Roy, N. Leemput, S. De Breucker, F. Geth, P. Tant, and J. Driesen, "An availability analysis and energy consumption model for a Flemish fleet of electric vehicles," in *European Electric Vehicle Congr.*, Brussels, Belgium, Oct. 2011, pp. 1–12.

[86] N. Leemput, F. Geth, B. Claessens, J. Van Roy, R. Ponnette, and J. Driesen, "A case study of coordinated electric vehicle charging for peak shaving on a low

voltage grid," in *3rd IEEE PES Innovative Smart Grid Technologies Europe (ISGT)*, Berlin, Germany, Oct. 2012, pp. 1–7.

[87] K. Clement, E. Haesen, and J. Driesen, "The impact of vehicle-to-grid on the distribution grid," *Electric Power Syst. Research J.*, vol. 81, no. 1, pp. 185–192, Jan. 2011.

[88] K. Clement-Nyns, "Impact of plug-in hybrid electric vehicles on the electricity system," Ph.D. dissertation, KU Leuven, Oct. 2010.

[89] R. Passey, T. Spooner, I. MacGill, M. Watt, and K. Syngellakis, "The potential impacts of grid-connected distributed generation and how to address them: A review of technical and non-technical factors," *Energy Policy*, vol. 39, no. 10, pp. 6280–6290, Oct. 2011.

[90] (2013, Jun.) Flemish Regulator for the Energy and Gas markets (VREG). [Online]. Available: http://www.vreg.be

[91] Q. Gong, S. Midlam-Mohler, V. Marano, and G. Rizzoni, "Study of PEV charging on residential distribution transformer life," *IEEE Trans. Smart Grid*, vol. 3, no. 1, pp. 404–412, Mar. 2012.

[92] C. Dang, J. Parpal, and J. Crine, "Electrical aging of extruded dielectric cables: Review of existing theories and data," *IEEE Trans. Dielect. Elect. Insul.*, vol. 3, no. 2, pp. 404–412, Mar. 1996.

[93] J. Gomez and M. Morcos, "Impact of EV battery chargers on the power quality of distribution systems," *IEEE Trans. Power Del.*, vol. 18, no. 3, pp. 975–981, Jul. 2003.

[94] *IEEE Guide for Loading Mineral-Oil-Immersed Transformers and Step-Voltage Regulators*, IEEE Std. C57.91-2011, Mar. 2012.

[95] J. Lopes, F. Soares, and P. Almeida, "Integration of electric vehicles in the electric power system," *Proc. of the IEEE*, vol. 99, no. 1, pp. 168–183, Jan. 2011.

[96] S. Weckx, R. D'Hulst, B. Claessens, and J. Driesen, "Multiagent charging of electric vehicles respecting distribution transformer loading and voltage limits," *IEEE Trans. Smart Grid*, vol. 5, no. 6, pp. 2857–2867, Nov. 2014.

[97] E. Sortomme, M. Hindi, S. MacPherson, and S. Venkata, "Coordinated charging of plug-in hybrid electric vehicles to minimize distribution system losses," *IEEE Trans. Smart Grid*, vol. 2, no. 1, pp. 198–205, Mar. 2011.

[98] K. De Craemer, S. Vandael, B. Claessens, and G. Deconinck, "An event-driven dual coordination mechanism for demand side management of PHEVs," *IEEE Trans. Smart Grid*, vol. 5, no. 2, pp. 751–760, Mar. 2014.

[99] F. Ruelens, S. Vandael, W. Leterme, B. Claessens, M. Hommelberg, T. Holvoet, and R. Belmans, "Demand side management of electric vehicles with uncertainty on arrival and departure times," in *3rd IEEE PES Innovative Smart Grid Technologies Europe (ISGT)*, Berlin, Germany, Oct. 2012, pp. 1–8.

[100] F. Ruelens, S. Weckx, W. Leterme, S. Vandael, B. Claessens, and R. Belmans, "Stochastic portfolio management of an electric vehicles aggregator under price uncertainty," in *4th IEEE PES Innovative Smart Grid Technologies Europe (ISGT)*, Lyngby, Denmark, Oct. 2013, pp. 1–5.

[101] S. Vandael, B. Claessens, M. Hommelberg, T. Holvoet, and G. Deconinck, "A scalable three-step approach for demand side management of plug-in hybrid vehicles," *IEEE Trans. Smart Grid*, vol. 4, no. 2, pp. 720–728, Jun. 2013.

[102] N. Rotering and M. Ilic, "Optimal charge control of plug-in hybrid electric vehicles in deregulated electricity markets," *IEEE Trans. Power Syst.*, vol. 26, no. 3, pp. 1021–1029, Aug. 2011.

[103] S. Weckx, R. D'Hulst, and J. Driesen, "Primary and secondary frequency support by a multi-agent demand control system," *IEEE Trans. Power Syst.*, vol. PP, no. 99, pp. 1–11, 2014.

[104] S. Han, S. Han, and K. Sezaki, "Development of an optimal vehicle-to-grid aggregator for frequency regulation," *IEEE Trans. Smart Grid*, vol. 1, no. 1, pp. 65–72, Jun. 2010.

[105] S. Vandael, K. De Craemer, N. Boucké, T. Holvoet, and G. Deconinck, "Decentralized coordination of plug-in hybrid vehicles for imbalance reduction in a smart grid," in *Proc. of 10th Int. Conf. on Autonomous Agents and Multiagent Syst.*, Taipei, Taiwan, May 2011, pp. 803–810.

[106] B. Mathiesen and H. Lund, "Comparative analyses of seven technologies to facilitate the integration of fluctuating renewable energy sources," *IET Renew. Power Gen.*, vol. 3, no. 2, pp. 190–204, Jun. 2009.

[107] W. Leterme, F. Ruelens, B. Claessens, and R. Belmans, "A flexible stochastic optimization method for wind power balancing with PHEVs," *IEEE Trans. Smart Grid*, vol. 5, no. 3, pp. 1238–1245, May 2014.

[108] W. Kempton and J. Tomić, "Vehicle-to-grid power implementation: From stabilizing the grid to supporting large-scale renewable energy," *J. of Power Sources*, vol. 144, no. 1, pp. 280–294, Jun. 2005.

[109] A. Saber and G. Venayagamoorthy, "Plug-in vehicles and renewable energy sources for cost and emission reductions," *IEEE Trans. Ind. Electron.*, vol. 58, no. 4, pp. 1229–1238, Apr. 2011.

[110] M. D. Galus, R. La Fauci, and G. Andersson, "Investigating PHEV wind balancing capabilities using heuristics and model predictive control," in *IEEE PES General Meeting*, Minneapolis, MN, USA, Jul. 2010, pp. 1–8.

[111] N. Leemput, J. Van Roy, F. Geth, P. Tant, and J. Driesen, "Comparative analysis of coordination strategies for electric vehicles," in *IEEE PES Innovative Smart Grid Technologies (ISGT) Europe*, Manchester, United Kingdom, Dec. 2011, pp. 1–8.

[112] W. Kempton and J. Tomić, "Vehicle-to-grid power fundamentals: Calculating capacity and net revenue," *J. of Power Sources*, vol. 144, no. 1, pp. 268–279, Jun. 2005.

[113] D. Dallinger, D. Krampe, and M. Wietschel, "Vehicle-to-grid regulation reserves based on a dynamic simulation of mobility behavior," *IEEE Trans. Smart Grid*, vol. 2, no. 2, pp. 302–313, Jun. 2011.

[114] A. Bedir, B. Ozpineci, and J. E. Christian, "The impact of plug-in hybrid electric vehicle interaction with energy storage and solar panels on the grid for a zero energy house," in *IEEE PES Transmission and Distribution Conf. and Expo.*, New Orleans, LA, USA, Apr. 2010.

[115] K. Mets, T. Verschueren, W. Haerick, C. Develder, and F. De Turck, "Optimizing smart energy control strategies for plug-in hybrid electric vehicle charging," in *IEEE/IFIP Network Operations and Manage. Symp. Workshops*, Osaka, Japan, Apr. 2010, pp. 293–299.

[116] L. Jian, H. Xue, G. Xu, X. Zhu, D. Zhao, and Z. Shao, "Regulated charging of plug-in hybrid electric vehicles for minimizing load variance in household smart micro-grid," *IEEE Trans. Ind. Electron.*, vol. 60, no. 8, pp. 3218–3226, 2013.

[117] H. K. Nguyen and J. B. Song, "Optimal charging and discharging for multiple PHEVs with demand side management in vehicle-to-building," *J. of Commun. and Netw.*, vol. 14, no. 6, pp. 662–671, Dec. 2012.

[118] I. Momber, T. Gómez, G. Venkataramanan, M. Stadler, S. Beer, J. Lai, C. Marnay, and V. Battaglia, "Plug-in electric vehicle interactions with a small office building: An economic analysis using DER-CAM," in *IEEE PES General Meeting*, Minneapolis, MN, USA, Jul. 2010, pp. 1–8.

[119] C. Gamallo, R. Alvaro, J. Fraile-Ardanuy, and M. Fuentes, "Evaluation of the utilization of electric vehicles for building energy management in hotels," in *Int. Conf. on New Concepts in Smart Cities: Fostering Public and Private Alliances (SmartMILE)*, Gijón, Spain, Dec. 2013, pp. 1–6.

[120] D. Nguyen and L. B. Le, "Optimal energy trading for building microgrid with electric vehicles and renewable energy resources," in *IEEE PES Innovative Smart Grid Technologies Conference (ISGT)*, Washington, DC, USA, Feb. 2014, pp. 1–5.

[121] F. Fattori, N. Anglani, and G. Muliere, "Combining photovoltaic energy with electric vehicles, smart charging and vehicle-to-grid," *Solar Energy*, vol. 110, pp. 438–451, Dec. 2014.

[122] S. Derakhshandeh, A. Masoum, S. Deilami, M. Masoum, and M. Hamedani Golshan, "Coordination of generation scheduling with PEVs charging in industrial microgrids," *IEEE Trans. Power Syst.*, vol. 28, no. 3, pp. 3451–3461, Aug. 2013.

[123] M. Bozchalui and R. Sharma, "Analysis of electric vehicles as mobile energy storage in commercial buildings: Economic and environmental impacts," in *IEEE PES General Meeting*, San Diego, CA, USA, Jul. 2012, pp. 1–8.

[124] T. P. Lyon, M. Michelin, A. Jongejan, and T. Leahy, "Is "smart charging" policy for electric vehicles worthwhile?" *Energy Policy*, vol. 41, pp. 259–268, Feb. 2012.

[125] L. Jerram and J. Gartner, "Electric vehicle charging equipment," Navigant Research, London, United Kingdom, Tech. Rep., 2012.

[126] J. Van Roy, N. Leemput, F. Geth, R. Salenbien, J. Büscher, and J. Driesen, "Apartment building electricity system impact of operational electric vehicle charging strategies," *IEEE Trans. Sustain. Energy*, vol. 5, no. 1, pp. 264–272, Jan. 2014.

[127] J. Van Roy, N. Leemput, F. Geth, J. Büscher, R. Salenbien, and J. Driesen, "Electric vehicle charging in an office building microgrid with distributed energy resources," *IEEE Trans. Sustain. Energy*, vol. 5, no. 4, pp. 1389–1396, Oct. 2014.

[128] F. Geth, N. Leemput, J. Van Roy, J. Büscher, R. Ponnette, and J. Driesen, "Voltage droop charging of electric vehicles in a residential distribution feeder," in *IEEE PES Innovative Smart Grid Technologies Europe (ISGT)*, Berlin, Germany, Oct. 2012, pp. 1–8.

[129] R. Rei, F. Soares, P. Almeida, and J. Peças Lopes, "Grid interactive charging control for plug-in electric vehicles," in *13th Int. IEEE Conf. on Intelligent Transportation Systems (ITSC)*, Funchal, Portugal, Sep. 2010, pp. 386–391.

[130] D. Becker and B. Sonnenberg, "DC microgrids in buildings and data centers," in *IEEE 33rd Int. Telecommun. Energy Conf. (INTELEC)*, Amsterdam, The Netherlands, Oct. 2011, pp. 1–7.

[131] B. Williamson, M. Redfern, R. Aggarwal, J. Allinson, C. Harris, P. Bowley, and R. Hotchkiss, "Project Edison: SMART-DC," in *IEEE PES Innovative Smart Grids Technologies Europe (ISGT)*, Manchester, United Kingdom, Dec. 2011, pp. 1–10.

[132] C. Marnay, S. Lanzisera, M. Stadler, and J. Lai, "Building scale DC microgrids," in *IEEE Energytech*, Cleveland, OH, USA, May 2012, pp. 1–5.

[133] W. Li, X. Mou, Y. Zhou, and C. Marnay, "On voltage standards for DC home microgrids energized by distributed sources," in *7th Int. Power Electron. and Motion Control Conf.*, Harbin, China, Jun. 2012, pp. 2282–2286.

[134] M. Rodriguez-Otero and E. O'Neill-Carrillo, "Efficient Home Appliances for a Future DC Residence," in *IEEE Energy 2030 Conf.*, Atlanta, GA, USA, Nov. 2008, pp. 1–6.

[135] H. Kakigano, T. Hashimoto, Y. Matsumura, T. Kurotani, W. Iwamoto, Y. Miura, T. Ise, T. Momose, and H. Hayakawa, "Fundamental characteristics of laboratory scale model DC microgrid to exchange electric power from distributed generators installed in residential houses," *Elect. Eng. in Japan*, vol. 172, no. 3, pp. 28–41, May 2010.

[136] E. Cetin, A. Yilanci, H. K. Ozturk, M. Colak, I. Kasikci, and S. Iplikci, "A micro-DC power distribution system for a residential application energized by photovoltaic-wind/fuel cell hybrid energy systems," *Energy and Buildings*, vol. 42, no. 8, pp. 1344–1352, Aug. 2010.

[137] A. Goikoetxea, J. Canales, R. Sanchez, and P. Zumeta, "DC versus AC in residential buildings: Efficiency comparison," in *IEEE EUROCON*, Zagreb, Croatia, Jul. 2013, pp. 1–5.

[138] T. D. Mai, J. Tant, and J. Driesen, "Power flow efficiency of a DC distribution grid," in *3rd Int. Workshop on Integration of Solar Power into Power Syst.*, London, United Kingdom, Oct. 2013, pp. 1–6.

[139] K. Garbesi, V. Vosso, A. H. Sanstad, and G. Burch, "Optimizing energy savings from direct-DC in U.S. residential buildings," Lawrence Berkeley National Laboratory, Berkeley, CA, Tech. Rep. LBNL-5193E, Oct. 2011.

[140] H. Kakigano, M. Nomura, and T. Ise, "Loss evaluation of DC distribution for residential houses compared with AC system," in *Int. Power Electron. Conf. (IPEC)*, Sapporo, Japan, Jun. 2010, pp. 480–486.

[141] K. Engelen, E. Leung Shun, P. Vermeyen, I. Pardon, R. D'hulst, J. Driesen, and R. Belmans, "The feasibility of small-scale residential DC distribution systems," in *32nd IEEE Annu. Conf. on Ind. Electron. (IECON)*, Paris, France, Nov. 2006, pp. 2618–2623.

[142] H. Pang, E. Lo, and B. Pong, "Dc electrical distribution systems in buildings," in *2nd Int. Conf. on Power Electron. Syst. and Applicat.*, Hong Kong, Nov. 2006, pp. 115–119.

[143] J. Rekola, J. Jokipii, and T. Suntio, "Effect of network configuration and load profile on efficiency of LVDC distribution network," in *16th European Conf. on Power Electron. and Applicat.*, Lappeenranta, Finland, Aug. 2014, pp. 1–10.

[144] H. Kakigano, Y. Miura, and T. Ise, "Low-voltage bipolar-type DC microgrid for super high quality distribution," *IEEE Trans. Power Electron.*, vol. 25, no. 12, pp. 3066–3075, Dec. 2010.

[145] T. Kaipia, P. Salonen, J. Lassila, and J. Partanen, "Possibilities of the low voltage DC distribution systems," in *Nordic Distribution and Asset Manage. Conf.*, Stockholm, Sweden, Aug. 2006, pp. 1–10.

[146] H. Kakigano, Y. Miura, T. Ise, J. Van Roy, and J. Driesen, "Basic sensitivity analysis of conversion losses in a dc microgrid," in *Int. Conf. on Renewable Energy Research and Applicat. (ICRERA)*, Nagasaki, Japan, Nov. 2012, pp. 1–6.

[147] A. Sannino, G. Postiglione, and M. H. J. Bonno, "Feasibility of a DC network for commercial facilities," *IEEE Trans. Ind. Appl.*, vol. 39, no. 5, pp. 1499–1507, Sep. 2003.

[148] J. J. Justo, F. Mwasilu, J. Lee, and J.-W. Jung, "AC-microgrids versus DC-microgrids with distributed energy resources: A review," *Renewable and Sustainable Energy Reviews*, vol. 24, pp. 387–405, Aug. 2013.

[149] U. Boeke, R. Weiss, A. Mauder, L. Hamilton, and L. Ott, "Efficiency advantages of ±380 V DC grids in comparison with 230 V/400 V AC grids," Tech. Rep. White paper, May 2014.

[150] G. Van den Broeck, "Overall voltage stability with the presence of distributed energy resources in a low voltage DC network," Master's thesis, KU Leuven, 2014.

[151] P. Savege, R. Nordhaus, and S. Jamieson, *From silos to systems: Issues in clean energy and climate change*, 2010, ch. DC Microgrids: Benefits and Barriers, pp. 51–66.

[152] M. Starke, F. Li, L. Tolbert, and B. Ozpineci, "AC vs. DC distribution: Maximum transfer capability," in *IEEE PES General Meeting*, Pittsburgh, PA, USA, Jul. 2008, pp. 1–6.

[153] J. Tant, F. Geth, D. Six, and J. Driesen, "Multiobjective battery storage to improve PV integration in residential distribution grids," *IEEE Trans. Sustain. Energy*, vol. 4, no. 1, pp. 182–191, Jan. 2013.

[154] D. Salomonsson, "Modeling, control and protection of low-voltage dc microgrids," Ph.D. dissertation, KTH, 2008.

[155] T. D. Mai, G. Van den Broeck, and J. Driesen, "Modeling the dynamics of a DC distribution grid integrated by renewable energy sources," in *40th Annu. Conf. of the IEEE Ind. Electron. Soc.*, Dallas, TX, USA, Oct. 2014, pp. 1–6.

[156] B. Verbruggen and J. Driesen, "Grid impact indicators for active building simulations," *IEEE Trans. Sustain. Energy*, vol. 6, no. 1, pp. 43–50, Jan. 2015.

[157] *Voltage Characteristics of Electricity Supplied by Public Electricity Networks*, CENELEC Std. EN50 160, Jul. 2010.

[158] E. De Caluwé, "Potentieel van demand side management, piekvermogen en netondersteunende diensten geleverd door plug-in hybride elektrische voertuigen op basis van een beschikbaarheidsanalyse," Master's thesis, KU Leuven, 2008.

[159] J. Van Roy and K. Vogt, "Analyse van verschillende batterijcapaciteiten voor plug-in hybride elektrische voertuigen," Master's thesis, KU Leuven, 2010.

[160] D. Janssens, E. Moons, E. Nuyts, and G. Wets. (2013, Dec.) Onderzoek Verplaatsingsgedrag Vlaanderen 3 (2007-2008). [Online]. Available: http://www.mobielvlaanderen.be/ovg/

[161] M. Nanni, R. Trasarti, P. Cintia, B. Furletti, C. Renso, L. Gabrielli, S. Rinzivillo, and F. Giannotti, *Data Science and Simulation in Transportation Research.* Hershey, PA, USA: IGI Global, 2014, ch. 1: Mobility profiling, pp. 1–29.

[162] S. Cho, T. Bellemans, L. Creemers, L. Knapen, D. Janssens, and G. Wets, *Data Science and Simulation in Transportation Research.* Hershey, PA, USA: IGI Global, 2014, ch. 3: Synthetic population techniques in activity-based research, pp. 48–70.

[163] W. Do Lee, C.-H. Joh, S. Cho, and B. Kochan, *Data Science and Simulation in Transportation Research.* Hershey, PA, USA: IGI Global, 2014, ch. 4: Issues in FEATHERS application in the Seoul Metropolitan Area, pp. 71–85.

[164] A. Pirdavani, T. Bellemans, T. Brijs, B. Kochan, and G. Wets, *Data Science and Simulation in Transportation Research.* Hershey, PA, USA: IGI Global, 2014, ch. 7: Traffic safety implications of travel demand management policies: The cases of teleworking and fuel cost increase, pp. 115–140.

[165] M. Lützenberger, *Data Science and Simulation in Transportation Research*. Hershey, PA, USA: IGI Global, 2014, ch. 10: A driver's mind: Psychology runs simulation, pp. 182–205.

[166] Ministry of Infrastructure and Environment. (2014, Apr.) Mobiliteitsonderzoek Nederland. [Online]. Available: http://www.rijkswaterstaat.nl/zakelijk/innovatie/innovatieprogrammas/mobiliteitsonderzoek/

[167] P. S. Hu, T. Reuscher, R. L. Schmoyer, and S.-M. Chin, "Transferring 2001 National Household Travel Survey," Prepared by Oak Ridge National Laboratory, Managed by UT-Battelle, LLC for the U.S. Department of Energy Under Contract DE-AC-05-00OR22725, Tech. Rep. ORNL/TM-2007/013, May 2007.

[168] National Renewable Energy Laboratory (NREL). (2014, Dec.) Transportation Secure Data Center. [Online]. Available: http://www.nrel.gov/tsdc

[169] Bundesministerium für Verkehr und digitale Infrastruktur. (2014, May) Mobilität in Deutschland. [Online]. Available: http://www.mobilitaet-in-deutschland.de/

[170] "The United Kingdom 2000 time use survey," Office for National Statistics, United Kingdom, Tech. Rep., 2003.

[171] M. Kintner-Meyer, T. B. Nguyen, C. Jin, P. Balducci, and T. Secrest, "Impact assessment of plug-in hybrid vehicles on the U.S. power grid," in *The 25th World Battery, Hybrid and Fuel Cell Electric Vehicle Symp. & Exhibition*, Shenzhen, China, Nov. 2010, pp. 1–7.

[172] S. Huang and D. Infield, "The potential of domestic electric vehicles to contribute to power system operation through vehicle to grid technology," in *44th Int. Universities Power Eng. Conf.*, Glasgow, Scotland, Sep. 2009, pp. 1–5.

[173] K. Qian, C. Zhou, M. Allan, and Y. Yuan, "Modeling of load demand due to EV battery charging in distribution systems," *IEEE Trans. Power Syst.*, vol. 26, no. 2, pp. 802–810, May 2011.

[174] "Driving profile generator," Karlsruhe Institute of Technology, Tech. Rep., Jun. 2010.

[175] L. Knapen, B. Kochan, T. Bellemans, D. Janssens, and G. Wets, "Activity based models for countrywide electric vehicle power demand calculation," in *2011 IEEE 1st Int. Workshop on Smart Grid Modeling and Simulation (SGMS)*, Brusels, Belgium, Oct 2011, pp. 13–18.

[176] R. Álvaro, J. González, J. Fraile-Ardanuy, L. Knapen, and D. Janssens, "Nationwide impact and vehicle to grid application of electric vehicles mobility using an activity based model," in *Int. Conf. on Renewable Energy Research and Applicat. (ICRERA)*, Madrid, Spain, Oct. 2013, pp. 857–861.

[177] R. A. Verzijlbergh, Z. Lukszo, E. Veldman, J. Slootweg, and M. Ilic, "Deriving electric vehicle charge profiles from driving statistics," in *IEEE Power & Energy Soc. General Meeting*, San Diego, CA, USA, Jul. 2011, pp. 1–6.

[178] P. Grahn, J. Munkhammar, J. Widén, K. Alvehag, and L. Söder, "PHEV home-charging model based on residential activity patterns," *IEEE Trans. Power Syst.*, vol. 28, no. 3, pp. 2507–2515, Aug. 2013.

[179] M. ElNozahy and M. Salama, "A comprehensive study of the impacts of PHEVs on residential distribution networks," *IEEE Trans. Sustain. Energy*, vol. 5, no. 1, pp. 332–342, Jan. 2014.

[180] L. Kelly, A. Rowe, and P. Wild, "Analyzing the impacts of plug-in electric vehicles on distribution networks in British Columbia," in *IEEE Elect. Power Energy Conf.*, Montréal, Canada, Oct. 2009, pp. 1–6.

[181] K. Zhou and L. Cai, "Randomized PHEV charging under distribution grid constraints," *IEEE Trans. Smart Grid*, vol. 5, no. 2, pp. 879–887, Apr. 2014.

[182] J. Taylor, A. Maitra, M. Alexander, D. Brooks, and M. Duvall, "Evaluation of the impact of plug-in electric vehicle loading on distribution system operations," in *IEEE PES General Meeting*, Calgary, Canada, Jul. 2009, pp. 1–6.

[183] Z. Darabi and M. Ferdowsi, "Aggregated impact of plug-in hybrid electric vehicles on electricity demand profile," *IEEE Trans. Sustain. Energy*, vol. 2, no. 4, pp. 501–508, Oct. 2011.

[184] S. Shao, M. Pipattanasomporn, and S. Rahman, "Challenges of PHEV penetration to the residential distribution network," in *IEEE PES General Meeting*, Calgary, Canada, Jul. 2009, pp. 1–8.

[185] N. DeForest, J. Funk, A. Lorimer, B. Ur, I. Sidhu, P. Kaminsky, and B. Tenderich, "Impact of widespread electric vehicle adoption on the electrical utility business – Threats and opportunities," Center for Entrepreneurship & Technology, University of California, Tech. Rep. 2009.5.v.1.1, Aug. 2009.

[186] J. A. Peças Lopes, F. J. Soares, P. M. Almeida, and M. Moreira da Silva, "Smart charging strategies for electric vehicles: Enhancing grid performance and maximizing the use of variable renewable energy resources," in *The 24th World Battery, Hybrid and Fuel Cell Electric Vehicle Symp. & Exhibition*, Stavanger, Norway, May 2009, pp. 1–11.

[187] S. Bae and A. Kwasinski, "Spatial and temporal model of electric vehicle charging demand," *IEEE Trans. Smart Grid*, vol. 3, no. 1, pp. 394–403, Mar. 2012.

[188] N. Leemput, J. Van Roy, F. Geth, J. Driesen, and S. De Breucker, *Data Science and Simulation in Transportation Research.* Hershey, PA, USA: IGI Global, 2014, ch. 17: Grid and fleet impact mapping of EV charge opportunities, pp. 364–390.

[189] F. Geth, K. Willekens, K. Clement, J. Driesen, and S. De Breucker, "Impact-analysis of the charging of plug-in hybrid vehicles on the production park in belgium," in *15th IEEE Mediterranean Electrotechnical Conf.*, Valletta, Malta, Apr. 2010, pp. 425–430.

[190] N. Shah, B. Cho, F. Geth, K. Clement, P. Tant, and J. Driesen, "Electric vehicle impact assessment study based on data-logged vehicle and driver behavior," in *IEEE Vehicle Power and Propulsion Conf. (VPPC)*, Chicago, IL, USA, Sep. 2011, pp. 1–6.

[191] S. Vandael, N. Boucké, T. Holvoet, and G. Deconinck, "Decentralized demand side management of plug-in hybrid vehicles in a smart grid," in *Proc. of 9th Int. Conf. on Autonomous Agents and Multiagent Syst.*, Toronto, Canada, May 2010, pp. 67–74.

[192] B. Dupont, K. Dietrich, C. De Jonghe, A. Ramos, and R. Belmans, "Impact of residential demand response on power system operation: A Belgian case study," *Appl. Energy*, vol. 122, pp. 1–10, Jun. 2014.

[193] K. Mets, F. De Turck, and C. Develder, "Distributed smart charging of electric vehicles for balancing wind energy," in *IEEE 3rd Int. Conf. on Smart Grid Commun.*, Tainan, Taiwan, Nov. 2012, pp. 133–138.

[194] K. De Craemer and G. Deconinck, "Balancing trade-offs in coordinated PHEV charging with continuous market-based control," in *3rd IEEE PES Innovative Smart Grid Technologies Europe (ISGT)*, Berlin, Germany, Oct. 2012, pp. 1–8.

[195] S. Iacovella, K. Lemkens, P. Vingerhoets, F. Geth, G. Deconinck, R. D'Hulst, and K. Vanthournout, "Standalone LV distribution network voltage control mechanism," in *39th Annu. Conf. of the IEEE Ind. Electron. Soc. (IECON)*, Vienna, Austria, Nov. 2013, pp. 7493–7498.

[196] S. Iacovella, F. Geth, F. Ruelens, N. Leemput, P. Vingerhoets, G. Deconinck, and B. Claessens, "Double-layered control methodology combining price objective and grid constraints," in *IEEE Int. Conf. on Smart Grid Communications (SmartGridComm)*, Vancouver, Canada, Oct. 2013, pp. 25–30.

[197] S. Iacovella, K. Lemkens, F. Geth, P. Vingerhoets, G. Deconinck, R. D'Hulst, and K. Vanthournout, "Distributed voltage control mechanism in low-voltage distribution grid field test," in *4th IEEE PES Innovative Smart Grid Technologies Europe (ISGT)*, Lyngby, Denmark, Oct. 2013, pp. 1–5.

[198] K. De Craemer, S. Vandael, B. Claessens, and G. Deconinck, *Plug-In Electric Vehicles in Smart Grid: Management and Control Strategies*. Springer, 2014, ch. 6: Integration of distribution grid constraints in an event-driven control strategy for plug-in electric vehicles in a multi-aggregator setting, pp. 129–171.

[199] M. Strobbe, K. Mets, M. Tahon, M. Tilman, F. Spiessens, J. Gheerardyn, K. De Craemer, S. Vandael, K. Geebelen, B. Lagaisse, B. Clasessens, and C. Develder, "Smart and secure charging of electric vehicles in public parking spaces," in *Proc. 4th Int. Conf. Innovation for Sustainable Production (i-SUP)*, Bruges, Belgium, May 2012, pp. 1–5.

[200] N. Machiels, N. Leemput, F. Geth, J. Van Roy, J. Büscher, and J. Driesen, "Design criteria for electric vehicle fast charge infrastructure based on Flemish mobility behavior," *IEEE Trans. Smart Grid*, vol. 5, no. 1, pp. 320–327, Jan. 2014.

[201] N. Leemput, F. Geth, J. Van Roy, P. Rosell-Olivella, J. Driesen, and A. Sumper, "MV and LV residential grid impact of combined slow and fast charging of electric vehicles," *Energies (Submitted for review)*, vol. 99, pp. 1–8, Dec. 2014.

[202] C. Kopp, B. Kochan, M. May, L. Pappalardo, S. Rinzivillo, D. Schulw, and F. Simini, *Data Science and Simulation in Transportation Research.* Hershey, PA, USA: IGI Global, 2014, ch. 8: Evaluation of spatio-temporal microsimulation systems, pp. 141–166.

[203] (2014, Feb.) FEBIAC. [Online]. Available: http://www.febiac.be

[204] (2014, Feb.) FOD Mobiliteit en Vervoer. [Online]. Available: http://www.mobilit.belgium.be

[205] Vlaamse Milieumaatschappij, "Milieurapport vlaanderen: Achtergronddocument 2010, transport," Feb. 2011.

[206] A. Perujo and B. Ciuffo, "The introduction of electric vehicles in the private fleet: Potential impact on the electric supply system and on the environment. A case study for the Province of Milan, Italy," *Energy Policy*, vol. 38, no. 8, pp. 4549–4561, Aug. 2010.

[207] J. Widén, M. Lundh, I. Vassileva, E. Dahlquist, K. Ellegård, and E. Wackelgård, "Constructing load profiles for household electricity and hot water from time-use data-modelling approach and validation," *Energy and Buildings*, vol. 41, no. 7, pp. 753–768, Jul. 2009.

[208] E. Gutiérrez-i-Puigarnau and J. van Ommeren, "Welfare effects of distortionary company car taxation," Tinbergen Institute, Tinbergen Institute Discussion Papers 07-060/3, Aug. 2007.

[209] E. Cornelis, A. Malchair, T. Asperges, and K. Ramaekers, "COCA: Company cars analysis," FOD Mobiliteit en Vervoer, Tech. Rep., Apr. 2007.

[210] W. Labeeuw, "Characterisation and modelling of residential electricity demand," Ph.D. dissertation, KU Leuven, Dec. 2013.

[211] H. Jeeninga, M. Uyterlinde, and J. Uitzinger, "Energieverbruik van energiezuinige woningen," ECN, Tech. Rep. ECN-C-01-072, Oct. 2001.

[212] I. Mansouri, M. Newborough, and D. Probert, "Energy consumption in UK households: Impact of domestic electrical appliances," *Appl. Energy*, vol. 54, no. 3, pp. 211–285, Jul. 1996.

[213] A. Capasso, W. Grattieri, R. Lamedica, and A. Prudenzi, "A bottom-up approach to residential load modeling," *IEEE Trans. Power Syst.*, vol. 9, no. 2, pp. 957–964, May 1994.

[214] R. Yao and K. Steemers, "A method of formulating energy load profile for domestic buildings in the UK," *Energy and Buildings*, vol. 37, no. 6, pp. 663–671, Jun. 2005.

[215] M. D. Galus, R. Waraich, F. Noembrini, K. Steurs, G. Georges, K. Boulouchos, K. Axhausen, and G. Andersson, "Integrating power systems, transport systems

and vehicle technology for electric mobility impact assessment and efficient control," *IEEE Trans. Smart Grid*, vol. 3, no. 2, pp. 934–949, Jun. 2012.

[216] US Environmental Protection Agency (EPA). (2014, Feb.) Dynamometer Driver's Aid. [Online]. Available: http://www.epa.gov/nvfel/testing/

[217] "Fuel economy labeling of motor vehicles: Revisions to improve calculation of fuel economy estimates," US Environmental Protection Agency, Tech. Rep. EPA420-R-06-017, Dec. 2006.

[218] R. Baetens, R. De Coninck, J. Van Roy, B. Verbruggen, J. Driesen, L. Helsen, and D. Saelens, "Assessing electrical bottlenecks at feeder level for residential net zero-energy buildings by integrated system simulation," *Appl. Energy*, vol. 96, pp. 74–83, Aug. 2012.

[219] J. Van Roy, B. Verbruggen, and J. Driesen, "Ideas for tomorrow: New tools for integrated building and district modeling," *IEEE Power Energy Mag.*, vol. 11, no. 5, pp. 75–81, Sep. 2013.

[220] M. O'Malley and B. Kroposki, "Energy comes together: The integration of all systems," *IEEE Power Energy Mag.*, vol. 11, no. 5, pp. 18–23, Sep. 2013.

[221] M. Wetter and C. van Treeck. (2014, Feb.) IEA EBC Annex 60. [Online]. Available: http://iea-annex60.org

[222] Meteotest, "METEONORM Version 6.1 - Edition 2009," Bern, 2008.

[223] R. Baetens and D. Saelens, "Multi-criteria grid impact evaluation of heat pump and photovoltaic based zero-energy dwellings," in *13th Conf. of Int. Building Performance Simulation Assoc.*, Chambéry, France, Aug. 2013, pp. 3529–3536.

[224] B. Verbruggen, J. Van Roy, R. De Coninck, R. Baetens, L. Helsen, and J. Driesen, "Object-oriented electrical grid and photovoltaic system modelling in modelica," in *8th Int. Modelica Conf.*, Dresden, Germany, Mar. 2011, pp. 730–738.

[225] (2014, Aug.) Modelica and the Modelica Association. [Online]. Available: https://www.modelica.org/

[226] (2014, Aug.) Dymola Modelica Systems Engineering – Dassault Systèmes. [Online]. Available: http://www.3ds.com/products-services/catia/capabilities/systems-engineering/modelica-systems-simulation/dymola/

[227] P. Fritzson, *Principles of object-oriented modeling and simulation with Modelica 2.1.* Hoboken, NJ, USA: Wiley, 2004.

[228] M. Tiller. (2014, Dec.) Modelica by Example. [Online]. Available: http://book.xogeny.com

[229] J. Van Roy, R. Salenbien, and J. Driesen, "Modelica library for building and low-voltage electrical AC and DC grid modeling," in *10th Int. Modelica Conf.*, Lund, Sweden, Mar. 2014, pp. 301–309.

[230] H. Wiesmann. (2014, Aug.) SPOT library. [Online]. Available: https://github.com/modelica-3rdparty/SPOT

[231] Modelon. (2014, Aug.) Electric power library. [Online]. Available: http://www.modelon.com/products/modelica-libraries/electric-power-library

[232] H. Wiesmann, M. Otter, and R. Franke. (2015, Mar.) PowerSystems. [Online]. Available: https://github.com/Modelica/PowerSystems

[233] M. Bonvini, M. Wetter, and T. S. Nouidui, "A Modelica package for building-to-electrical grid integration," in *5th German-Austrian IBPSA Conf.*, Aachen, Germany, Sep. 2014, pp. 6–13.

[234] H. Lee Willis, *Power Distribution Planning Reference Book*. New York, USA: Marcel Dekker, Inc., 1997.

[235] L. Liu, F. Felgner, and G. Frey, "Comparison of 4 numerical solvers for stiff and hybrid systems simulation," in *IEEE Conf. on Emerging Technologies and Factory Automation*, Bilbao, Spain, Sep. 2010, pp. 1–8.

[236] P. Vovos, A. Kiprakis, and A. Wallace, "Centralized and distributed voltage control: Impact on distributed generation parameters," *IEEE Trans. Power Syst.*, vol. 22, no. 1, pp. 476–483, Feb. 2007.

[237] K. Büdenbender, M. Braun, T. Stetz, and P. Strauss, "Multifunctional PV systems offering additional functionalities and improving grid integration," *J. of Distributed Energy Resources*, vol. 7, no. 2, pp. 109–128, 2011.

[238] M. Braun, T. Stetz, R. Bründinger, C. Mayr, K. Ogimoto, H. Hatta, H. Kobayashi, B. Kroposki, B. Mather, M. Coddington, K. Lyon, G. Graditi, A. Woyte, and I. MacGill, "Is the distribution grid ready to accept large-scale photovoltaic deployment? State of the art, progress, and future prospects," *Progress in Photovoltaics: Research and Applicat.*, vol. 20, no. 6, pp. 681–697, Sep. 2012.

[239] *Erzeugungsanlagen am Niederspannungsnetz, Technische Mindestanforderungen für Anschluss und Parallelbetrieb von Erzeugungsanlagen am Niederspannungsnetz*, DIN VDE Std. VDE-AR-N 4105, Aug. 2011.

[240] W. De Soto, S. Klein, and W. Beckman, "Improvement and validation of a model for photovoltaic array performance," *Solar Energy*, vol. 80, no. 1, pp. 78–88, 2006.

[241] D. Sera, R. Teodorescu, and P. Rodriguez, "PV panel model based on datasheet values," in *IEEE Int. Symp. on Ind. Electron.*, Vigo, Spain, 2007, pp. 2392–2396.

[242] N. Machiels, "Ontwerpcriteria voor snellaadstations voor elektrische wagens gebaseerd op Vlaams mobiliteitsgedrag," Master's thesis, KU Leuven, 2012.

[243] ABB, "ABB EV charging infrastructure, ABB Highway DC Fast Charger Terra 100.2 Base Station," Tech. Rep. 4EVC200202-LFEN, Mar. 2012.

[244] R. De Coninck and G. Verbeeck, "Technisch-economische analyse van de rendabiliteit van energiebesparende investeringen," Brussels Instituut voor Milieubeheer, Tech. Rep. Energie/E04-154, Aug. 2005.

[245] (2014, Jul.) IDEAS v0.1. [Online]. Available: https://github.com/open-ideas/IDEAS

[246] R. Baetens, R. De Coninck, J. Van Roy, B. Verbruggen, J. Driesen, L. Helsen, and D. Saelens. (2014, Jun.) IDEAS: Specifications. [Online]. Available: https://github.com/open-ideas/IDEAS

[247] J. Ordòñez, E. Jadraque, J. Alegre, and G. Martínez, "Analysis of the photovoltaic solar energy capacity of residential rooftops in Andalusia (Spain)," *Renewable and Sustainable Energy Reviews*, vol. 14, no. 7, pp. 2122–2130, Sep. 2010.

[248] *Warmte-isolatieprestatie van gebouwen - Globaal warmte-isolatiepeil (K-peil) van een gebouw*, NBN Std. B 62-301, 2008.

[249] VEA - Vlaams Energieagentschap. (2014, Jul.) EPB-eisen vanaf 2014. [Online]. Available: http://www2.vlaanderen.be/economie/energiesparen/epb/doc/epbeisentabel2014.pdf

[250] A. Delnooz, D. Six, C. Mol, and E. Gielen, "State-of-the-art business models for charging services: The EVCITY approach," in *European Electric Vehicle Congr.*, Brussels, Belgium, Nov. 2012.

[251] *Kabels voor ondergrondse aanleg, met synthetische isolatie en versterkte mantel (Type 1* kV*)*, NBN Std. C 33-322, 1975.

[252] W. Labeeuw and G. Deconinck, "Residential electrical load model based on mixture model clustering and Markov models," *IEEE Trans. Ind. Informat.*, vol. 9, no. 3, pp. 1561–1569, Aug. 2013.

[253] (2014, Aug.) Sanyo. [Online]. Available: http://www.sanyo.be

[254] M. Valentini, A. Raducu, D. Sera, and R. Teodorescu, "PV inverter test setup for European efficiency, static and dynamic MPPT efficiency evaluation," in *11th Int. Conf. on Optimization of Elect. and Electron. Equipment*, Brasov, Romania, May 2008, pp. 433–438.

[255] (2014, Oct.) SMA - MLX 60. [Online]. Available: http://www.sma.de/en/products/solarinverters/mlx-60.html

[256] "Breaking the "heating barrier": Learning from the first houses without conventional heating," *Energy and Buildings*, vol. 36, no. 4, pp. 373–380, 2004.

[257] B. Oleson, "Control of floor heating and cooling systems," in *Clima 2000/Napoli 2001 World Congr.*, Naples, Italy, Sep. 2001, pp. 1–15.

[258] S. De Breucker, "Impact of dc-dc converters on Li-ion batteries," Ph.D. dissertation, KU Leuven, Dec. 2012.

[259] J. Everts, "Modeling and optimization of bidirectional dual active bridge ac-dc converter topologies," Ph.D. dissertation, KU Leuven, Mar. 2014.

[260] W. Yu, H. Wan, J.-S. Lai, H. Miwa, W.-H. Lai, N.-H. Tseng, C.-S. Lee, C.-H. Lin, and Y.-W. Shih, "High efficiency isolated DC-DC converter combining resonant and phase-shifted topologies for electrical vehicle chargers," in *1st Int. Future Energy Electron. Conf.*, Tainan, Taiwan, Nov. 2013, pp. 175–180.

[261] "Pv grid integration: Backgrounds, requirements, and SMA solutions," SMA, Tech. Rep. TechnologyCompendium 3.4, May 2012.

[262] (2014, Dec.) Laadstations witty - Loadmanagementmodule. [Online]. Available: http://www.hager.nl/producten/energiedistributiesystemen/e-mobility/e-mobility-laadstation/laadstations-witty/82456.htm

[263] P. Richardson, D. Flynn, and A. Keane, "Optimal charging of electric vehicles in low-voltage distribution systems," *IEEE Trans. Power Syst.*, vol. 27, no. 1, pp. 268–279, Feb. 2012.

[264] P. Richardson, D. Flynn, and A. Keane, "Local versus centralized charging strategies for electric vehicles in low voltage distribution systems," *IEEE Trans. Smart Grid*, vol. 3, no. 2, pp. 1020–1028, Jun. 2012.

[265] (2014, Sep.) Eandis. [Online]. Available: http://www.eandis.be/

[266] *Standard specification for standard nominal diameters and cross-sectional areas of AWG sizes of solid round wires used as electrical conductors*, ASTM International Std. B 258-02, 2002.

[267] (2014, Nov.) Wikipedia: American wire gauge. [Online]. Available: http://en.wikipedia.org/wiki/American_wire_gauge

[268] J. Van Roy, R. Salenbien, and J. Driesen, "Common dc bus for PV and EVs in buildings: Benefits for PV systems," in *29th European PV Solar Energy Conf. and Exhibition*, Amsterdam, The Netherlands, Sep. 2014, pp. 1–7.

[269] (2014, Nov.) Flemish Living Lab Electric Vehicles – Volt-Air Platform. [Online]. Available: http://www.livinglab-ev.be/content/volt-air-platform

[270] (2013, Jun.) COGEN Vlaanderen – Rekentools voor prehaalbaarheid. [Online]. Available: http://www.cogenvlaanderen.be

[271] J. Lu, F. Berkel, T. Nagel, D. Gorges, and S. Liu, "Integrated energy and parking management for parking areas with electric vehicles," in *IEEE Conf. on Control Applicat.*, Juan Les Antibes, France, Oct. 2014, pp. 1924–1929.

[272] (2014, Feb.) Smart fortwo electric drive. [Online]. Available: http://be.smart.com/be/nl/index/smart-fortwo-electric-drive.html

[273] (2014, Feb.) Toyota RAV4 EV. [Online]. Available: http://www.toyota.com/rav4ev/#!/Welcome

[274] (2009, Dec.) Greencar Congress – eRUF Stormster Electric SUV Debuts in Copenhagen. [Online]. Available: http://www.greencarcongress.com/2009/12/stormster-20091210.html

[275] E. Giakoumis and A. Alafouzos, "Study of diesel engine performance and emissions during a transient cycle applying an engine mapping-based methodology," *Appl. Energy*, vol. 87, no. 4, pp. 1358–1365, Apr. 2010.

[276] "Tires and passenger vehicle fuel economy: Informing consumers, improving performance," Transportation Research Board, Washington DC, USA, Tech. Rep. TRB Special Report 286, 2006.

[277] R. Barrero, X. Tackoen, and J. Van Mierlo, "Improving energy efficiency in public transport: Stationary supercapacitor based energy storage systems for a metro network," in *IEEE Vehicle Power and Propulsion Conf.*, Harbin, China, Sep. 2008, pp. 1–8.

[278] R. Farrington and J. Rugh, "Impact of vehicle air-conditioning on fuel-economy, tailpipe emissions and electric vehicle range," National Renewable Energy Laboratory, Tech. Rep. NREL/CP-540-28960, Oct. 2000.

[279] F. Geth, J. Tant, D. Six, P. Tant, T. De Rybel, and J. Driesen, "Techno-economical and life expectancy modeling of battery energy storage systems," in *21st Int. Conf. & Exhibition on Electricity Distribution (CIRED)*, Frankfurt, Germany, Jun. 2011, pp. 1–4.

[280] R. Baetens and D. Saelens, "Integrating occupant behaviour in the simulation of coupled electric and thermal systems in buildings," in *8th Int. Modelica Conf.*, March 20-22, Dresden, 2011.

[281] "Technical data Altherma ERYQ007A, EKHB007A / EKHBX007A, EKSWW150-300," Daikin Europe N.V., Oostende, Belgium.

[282] "Vitocell- 100-V, 390 liter, Datenblatt," Viessmann.

# Curriculum vitae

## Personal

**Juan Van Roy**
Born August 23, 1987 in Diest, Belgium
vanroy.juan@gmail.com

## Education

**1999 – 2005**
Secondary school
Amandinacollege, Sint-Martinusscholen, Herk-de-Stad, Belgium
Sciences – Mathematics

**2005 – 2010**
Master of Science in Engineering: Energy
Master thesis: *Analysis of different battery capacities for plug-in hybrid electric vehicles*
Graduated Cum laude
KU Leuven, Leuven, Belgium

**2010 – 2014**
Doctoral training in Engineering
KU Leuven, Leuven, Belgium

**2012 – 2015**
EIT-KIC InnoEnergy PhD School
CC Benelux: Energy efficient buildings and cities

## Research

**2010 – present**
Research assistant at KU Leuven, Leuven, Belgium
Department of Electrical Engineering (ESAT), Research Group Electa

**2012 – 2014**
PhD scholarship (2 years) with Vito, Mol, Belgium
Vito, Unit Energy Technology

**May 2013 – August 2013**
Visiting researcher at Lawrence Berkeley National Lab, Berkeley, CA, USA
Environmental Energy Technologies Division

**April 2014 – May 2014**
Visiting researcher at University College Dublin, Dublin, Ireland
Electricity Research Center

# List of publications

## Internationally reviewed academic journals


[1] J. Van Roy, P. Richardson, N. Leemput, A. Keane, and J. Driesen, "Local rule-based versus centralized optimal capacity charging coordination for EVs," *IEEE Trans. Smart Grid*, Mar. 2015, 8 pages, submitted for review.

[2] N. Leemput, F. Geth, J. Van Roy, J. Büscher, and J. Driesen, "Reactive power support in residential LV distribution grids through electric vehicle charging," *Sustainable Energy, Grids and Networks*, Feb. 2015, 22 pages, submitted for review.

[3] N. Leemput, F. Geth, J. Van Roy, P. Olivella-Rosell, J. Driesen, and A. Sumper, "MV and LV residential grid impact of combined slow and fast charging of electric vehicles," *Energies (Special Section on "Electrical Power and Energy Systems for Transportation Applications")*, vol. 8, no. 3, pp. 1760–1783, Mar. 2015.

[4] J. Van Roy, N. Leemput, F. Geth, J. Büscher, R. Salenbien, and J. Driesen, "Electric vehicle charging in an office building microgrid with distributed energy resources," *IEEE Trans. Sustain. Energy (Special Section on "Microgrids for Sustainable Energy Systems")*, vol. 5, no. 4, pp. 1389–1396, Oct. 2014.

[5] N. Leemput, F. Geth, J. Van Roy, A. Delnooz, J. Büscher, and J. Driesen, "Impact of electric vehicle on-board single-phase charging strategies on a Flemish residential grid," *IEEE Trans. Smart Grid*, vol. 5, no. 4, pp. 1815–1822, Jul. 2014.

[6] J. Van Roy, N. Leemput, F. Geth, R. Salenbien, J. Büscher, and J. Driesen, "Apartment building electricity system impact of operational electric vehicle charging strategies," *IEEE Trans. Sustain. Energy*, vol. 5, no. 1, pp. 264–272, Jan. 2014.

[7] N. Machiels, N. Leemput, F. Geth, J. Van Roy, J. Büscher, and J. Driesen, "Design criteria for electric vehicle fast charge infrastructure based on Flemish mobility behavior," *IEEE Trans. Smart Grids*, vol. 5, no. 1, pp. 320–327, Jan. 2014.

[8] J. Van Roy, B. Verbruggen, and J. Driesen, "Ideas for tomorrow: New tools for integrated building and district modeling," *IEEE Power Energy Mag.*, vol. 11, no. 5, pp. 75–81, Sep. 2013.

[9] R. Baetens, R. De Coninck, J. Van Roy, B. Verbruggen, J. Driesen, L. Helsen, and D. Saelens, "Assessing electrical bottlenecks at feeder level for residential net zero-energy buildings by integrated system simulation," *Appl. Energy*, vol. 96, pp. 74–83, Aug. 2012.

## Chapter in academic books

[1] N. Leemput, J. Van Roy, F. Geth, J. Driesen, and S. De Breucker, *Data Science and Simulation in Transportation Research*. Hershey, PA: IGI Global, 2014, ch. 17: Grid and fleet impact mapping of EV charge opportunities, pp. 364–390.

[2] J. Van Roy, N. Leemput, and J. Driesen, *Technologische verkenning - Elektrische voertuigen*. Vlaams Elektro Innovatiecentrum, 2011, ch. 9: Invloed van elektrische voertuigen op het elektriciteitsnet, pp. 100–121.

## Other academic journals

[1] J. Van Roy, and J. Driesen, "Elektriciteitsnetten en hun beperkingen: Geïntegreerd modelleren voor gebouwen en wijken," *TVVL-Magazine*, no. 10, pp. 22–24, Oct. 2014.

[2] D. Saelens, R. Baetens, R. De Coninck, J. Van Roy, B. Verbruggen, L. Helsen, and J. Driesen, "PV-panelen: de oplossing voor nul-energiegebouwen?" *Het Ingenieursblad*, vol. 80, no. 6, pp. 48–53, Dec. 2011.

## Conference papers

[1] J. Van Roy, R. Salenbien, and J. Driesen, "Common DC Bus for PV and EVs in Buildings: Benefits for PV Systems," in *European Photovoltaic Solar Energy Conf. (EU PVSEC)*, Amsterdam, The Netherlands, Sep. 2014, pp. 3671–3677.

[2] J. Van Roy, R. Salenbien, and J. Driesen, "Modelica library for building and low-voltage electrical AC and DC grid modeling," in *Proc. of the 10th Int. Modelica Conf.*, Lund, Sweden, Mar. 2014, pp. 301–309.

[3] J. Verveckken, F. Geth, J. Beerten, B. Hunyadi, N. Leemput, J. Van Roy, P. Tielens, V. De Smedt, S. Iacovella, H. Höschle, N. Koolen, H. De Clercq, J. Driesen, G. Gielen, R. Puers, S. Van Huffel, R. Belmans, G. Deconinck, and W. Dehaene, "Development of open-source interactive smart energy house for K12 engineering education on residential energy efficiency," in *41st SEFI Annu. Conf.*, Leuven, Belgium, Sept. 2013.

[4] F. Geth, J. Verveckken, N. Leemput, J. Van Roy, J. Beerten, P. Tielens, V. De Smedt, S. Iacovella, B. Hunyadi, N. Koolen, H. De Clerca, G. Gielen, B. Puers, S. Van Huffel, R. Belmans, G. Deconinck, W. Dehaene, and J. Driesen, "Development of an open-source smart energy house for K-12 education," in *Proc. IEEE Power & Energy Soc. Annu. Meeting*, Vancouver, Canada, Jul. 2013.

[5] J. Verveckken, F. Geth, B. Hunyadi, J. Beerten, N. Leemput, J. Van Roy, P. Tielens, V. De Smedt, S. Iacovella, N. Koolen, H. De Clercq, J. Driesen, G. Gielen, B. Puers, J. Vandewalle, S. Van Huffel, R. Belmans, G. Deconinck, and W. Dehaene, "Developing engineering-oriented educational workshops within a student branch," in *Proc. IEEE EUROCON 2013*, Zagreb, Croatia, Jul. 2013, pp. 933–939.

[6] J. Van Roy, R. Salenbien, D. Vanhoudt, J. Desmedt, and J. Driesen, "Thermal and electrical cover factors: Definition and application for net-zero energy buildings," in *CLIMA 2013*, Prague, Czech Republic, Jun. 2013, pp. 997–1007.

[7] T. Devloo, N. Leemput, J. Van Roy, F. Geth, and J. Driesen, "Component improvements in the electrification of passenger vehicles drivetrains," in *IEEE Transportation Electrification Conf & Expo*, Dearborn, Detroit, MI, Jun. 2013.

[8] S. Luyten, N. Leemput, F. Geth, J. Van Roy, J. Büscher, and J. Driesen, "Standardization of conductive AC charging infrastructure for electric vehicles," in *Int. Electricity Conf. & Exhibition*, Stockholm, Sweden, Jun. 2013.

[9] R. De Koster, J. Van Roy, and J. Driesen, "A profile-based identification of standby and useless electricity consumption in buildings," in *IEEE Green Technologies Conf.*, Denver, CO, Apr. 2013.

[10] H. Kakigano, Y. Miura, T. Ise, J. Van Roy, and J. Driesen, "Basic sensitivity analysis of conversion losses in a DC microgrid," in *Int. Conf. on Renewable Energy Research and Applicat.*, Nagasaki, Japan, Nov. 2012.

[11] F. Geth, N. Leemput, J. Van Roy, J. Büscher, R. Ponnette, and J. Driesen, "Voltage droop charging of electric vehicles in a residential distribution feeder," in *IEEE PES Innovative Smart Grid Technologies Conf. Europe (ISGT Europe)*, Berlin, Germany, Oct. 2012.

[12] N. Leemput, F. Geth, B. Claessens, J. Van Roy, R. Ponnette, and J. Driesen, "A case study of coordinated electric vehicle charging for peak shaving on a low voltage grid," in *IEEE PES Innovative Smart Grid Technologies Conf. Europe (ISGT Europe)*, Berlin, Germany, Oct. 2012.

[13] J. Tant, J. Zwysen, K. Engelen, N. Leemput, J. Van Roy, S. Weckx, and J. Driesen, "Power electronics for electric vehicles: A student laboratory platform," in *13th IEEE Workshop on Control and Modeling for Power Electron. (COMPEL)*, Kyoto, Japan, Jun. 2012.

[14] J. Van Roy, and J. Driesen, "Optimized energy flows and electric networks in nearly zero-energy buildings," in *6th IEEE Young Researchers Symp. in Elect. Power Eng.*, Delft, The Netherlands, Apr. 2012.

[15] N. Leemput, S. De Breucker, K. Engelen, J. Van Roy, F. Geth, and J. Driesen, "Electrification of trucks and buses in an urban environment through continuous charging," in *IEEE Int. Electric Vehicle Conf.*, Greenville, SC, Mar. 2012.

[16] B. Verbruggen, J. Van Roy, R. De Coninck, R. Baetens, L. Helsen, and J. Driesen, "Object-oriented electrical grid and photovoltaic system modelling in Modelica," in *8th Int. Modelica Conf.*, Dresden, Germany, Mar. 2011, pp. 730–738.

[17] N. Leemput, J. Van Roy, F. Geth, P. Tant, and J. Driesen, "Comparative analysis of coordination strategies for electric vehicles," in *IEEE PES Innovative Smart Grid Technologies Conf. Europe (ISGT Europe)*, Manchester, United Kingdom, Dec. 2011.

[18] J. Van Roy, N. Leemput, S. De Breucker, F. Geth, P. Tant, and J. Driesen, "An availability analysis and energy consumption model for a Flemish fleet of electric vehicles," in *European Electric Vehicle Congr. (EEVC)*, Brussels, Belgium, Oct. 2011.

[19] J. Van Roy, S. De Breucker, and J. Driesen, "Analysis of the optimal battery sizing for plug-in hybrid and battery electric vehicles on the power consumption and V2G availability," in *Int. Conf. on Intelligent Syst. Applicat. to Power Syst. (ISAP)*, Hersonissos, Crete, Greece, Sept. 2011.

## Other publications

[1] J. Van Roy, R. Salenbien, and J. Driesen, "Integration of electric vehicle charging in buildings and their interaction with thermal energy flows," abstract in *2nd KIC InnoEnergy Scientist Conf.*, Karlsruhe, Germany, Nov. 2013.

[2] J. Van Roy, R. Salenbien, J. Desmedt and J. Driesen, "Integration and interaction of electrical and thermal energy flows, storage and networks for net-zero energy buildings," abstract in *1st KIC InnoEnergy Scientist Conf.*, Leuven, Belgium, Nov. 2012.

[3] R. De Coninck, R. Baetens, B. Verbruggen, J. Van Roy, J. Driesen, D. Saelens, and L. Helsen, "Optimal energy networks for buildings," in *5th Strategic Energy Forum*, Brussels, Belgium, May 2011.

FACULTY OF ENGINEERING SCIENCE
DEPARTMENT OF ELECTRICAL ENGINEERING
ELECTA
Kasteelpark Arenberg 10, bus 2445
3001 Leuven
vanroy.juan@gmail.com
http://www.esat.kuleuven.be/electa